Author:
Nobbs, D. W

Title:
The effect of downward vapour velocity and inundation on the condensation rates on horizontal tubes and tube banks

University of Bristol

Department of Mechanical Engineering

THE EFFECT OF DOWNWARD VAPOUR VELOCITY AND INUNDATION ON THE CONDENSATION RATES ON HORIZONTAL TUBES AND TUBE BANKS

D.W. Nobbs

A Dissertation submitted to the University of Bristol for the Degree of Doctor of Philosophy

April, 1975.

MEMORANDUM

The accompanying dissertation entitled "The Effect of Downward Vapour Velocity and Inundation on the Condensation Rates on Horizontal Tubes and Tube Banks" is submitted in support of an application for the degree of Doctor of Philosophy in Engineering in The University of Bristol.

The dissertation is based on independent work by the candidate: all help received from others has been fully acknowledged in the dissertation itself.

None of the work described in the dissertation is being, nor has been, submitted for any other degree or diploma of this or any other university.

I hereby declare that the statements in this memorandum are true in all particulars.

D.W. Nobbs

April, 1975.

SUMMARY

The rate of steam condensation on a horizontal tube is well accounted for by Nusselt's simple theory, provided that the velocity of the steam across the tube is low, the tube is not inundated by condensate falling on it from above, and the steam is free from non-condensable gases. Of these effects the first tends to enhance the rate of condensation, and the latter two tend to reduce it. Although Nusselt developed a theory to account for inundation, and to account for vapour velocity on a flat plate, the assumptions made are not satisfied in practice, and measurements do not support Nusselt's predictions.

Although there exists some theoretical and experimental work on the various effects mentioned, the ranges of velocity and inundation rate covered are inadequate to establish the validity of any theory; moreover, the important aspect of simultaneous interaction of various effects has received little attention. The present work is concerned entirely with furthering our understanding of the effects of velocity and inundation, separately and acting together, but in the absence of non-condensable gases. Two tube bank arrangements were used, both with downward vapour flow; namely square and equilateral-triangle arrangements of tubes having a diameter of 19.05 mm and a pitch-diameter ratio of 1.25.

Although all the work was carried out with steam at pressures slightly above atmospheric, by using appropriate ranges of steam velocity and raised cooling water temperatures, conditions analogous in certain respects to typical vacuum condensers were covered.

Useful experimental results are presented, and it has also been possible to develop an adequate theory to account for velocity effects in the absence of inundation both for a single tube and for banks of tubes. Qualitatively the results can be summarised as follows: (i) Velocity enhances condensation rates, the effect being most marked when cooling water-steam temperature differences, and therefore heat fluxes, are high. (ii) Beyond a certain velocity, improvement in condensation rate becomes very small, the limiting velocity depending on the heat flux which governs the vapour flow separation. (iii) The usual method of design based on mean tube surface temperature is found to be unsatisfactory, and an improved procedure is proposed. (iv) Inundation almost always reduces condensation rates, but less so than predicted by Nusselt's theory; under certain conditions it may indeed increase condensation rates.

ACKNOWLEDGEMENTS

The author wishes to thank the many people who have given assistance of varying forms throughout the period of his research, and especially the following.

The National Engineering Laboratory, East Kilbride, for providing financial support for the project, and particularly Dr. W.H. Emerson for his general guidance.

I.C.I. Ltd. (Organics Division) for providing the author with the opportunity to perform the work and for their generous assistance throughout.

Dr. Y.R. Mayhew for the encouragement and advice that he has given in all phases of the project and Professor G.F.C. Rogers and other members of the academic staff in the Mechanical Engineering Department for their many constructive suggestions.

Messrs. S. Burke, M. Newman and J. Hooper who helped construct the test rig, and Mr. R. Boyd and other members of the Mechanical Engineering Workshops who gave welcome assistance.

Miss G.M. Davis whose patient efforts in typing this thesis are more than appreciated.

CONTENTS

NOTATION

a	A factor less than 1 in eqn. (2.24)
A	A dimensionless group ($= \mu k(T_s - T_w)/\rho^2 g h'_{fg} d^3$)
A_{HT}	Area of heat transfer
b	A factor less than 1 in eqn. (1.20) and eqn. (2.24)
B, B'	Constants in Appendix D
c	Momentum loss coefficient in Appendix G
c_p	Specific heat at constant pressure
C, C'	Constants in Appendices D and E
C_D	Discharge coefficient
C_L	A correction factor for thermal entry effects eqn. (2.64)
d	Tube outside diameter
d_i	Tube inside diameter
d_h	Orifice diameter
Dr	A dimensionless group ($= \rho \tau_F h'_{fg} H^2/\mu k \Delta T$)
E	A dimensionless group ($= c_p \Delta T/h_{fg}$)
F_d	Tube spacing parameter in eqn. (1.40)
Fr	The Froude number ($= U_\infty^2/gx$ or U_∞^2/gd)
g	The acceleration due to gravity
H	Height of the plate
h_{fg}	Enthalpy change associated with liquid-vapour change of phase at constant pressure
h'_{fg}	Value of h_{fg} corrected for sub-cooling of condensate $[= h_{fg} + 0.68\ c_p(T_s - T_w)]$
j	Condensation rate per unit area
J	A dimensionless group ($= c_p \Delta T/(Pr) h_{fg}$)
k	Thermal conductivity
k_w	Thermal conductivity of tube wall
K	A dimensionless group ($= \rho^2 H^3 g/\mu^2$ or $\rho^2 d^3 g/\mu^2$)
K_T	Tube bank arrangement factor in eqn. (1.36)
l	Width of test section
L	Length of condenser tube
LMTD	Log mean temperature difference
m	Mass flow rate of condensate per unit length; (mass flow rate of fluid in manifold in Appendix G)
m_{cw}, m_{cond}	Mass flow rates of cooling water and condensate

n	Power exponent; number of holes per unit length in Appendix F
n_o	Number of holes per unit length at manifold inlet
N	Number of tubes from the top of the column
Nu_d	Nusselt number: average value for condensation on a tube (= $\alpha d/k$)
Nu_H	Nusselt number: average value for condensation on a plate (= $\alpha H/k$)
Nu_{cw}	Nusselt number: for forced convection inside a tube (= $\alpha_{cw} d_i/k_w$)
Nu_{Nu}	Nusselt number: average value for condensation based on Nusselt eqns. (1.1a) and 1.1b)
p	Total pressure
p_o	Static pressure in free stream
P	Power dissipated
Pr	Prandtl number (= $c_p \mu/k$)
P_T	Tube pitch to diameter ratio
q	Heat flux
Q	Heat transfer rate; volumetric discharge rate in Appendix G
Q_o	Total volumetric flow rate into the manifold
r	Factor in eqn. (1.30)
R	A dimensionless group $(\rho\mu/\rho_v\mu_v)^{\frac{1}{2}}$
Re	Reynolds number
Re_{TP}	Two-phase Reynolds number ($\rho U_\infty d/\mu$ or $\rho U_\infty H/\mu$)
Re_v	Vapour Reynolds number (= $\rho_v U_\infty d/\mu_v$)
Sh	Sherwood number (= $\rho^2 g h'_{fg} H^3/4\mu k \Delta T$)
T	Temperature
T_{sub}	Bulk mean temperature of condensate
ΔT	Temperature difference across condensate layer (= $T_s - T_w$)
ΔT_{cw}	Temperature rise of cooling water corrected for entry length temperature change
$\Delta T'_{cw}$	Measured rise in cooling water temperature
ΔT_{EL}	Temperature drop in entry length
u	Velocity within condensate layer
$\bar{u}$	Weighted mean air velocity
U	Local value of steam velocity
U_∞	Free stream velocity
U_ϕ	Velocity at angle Φ at the outer edge of the vapour boundary layer
v	Suction velocity perpendicular to and at condensate-vapour interface
v_o	Mean value of suction velocity v for the tube
V	Anemometer voltage in Appendix D; fluid velocity in Appendix G

V_c	Anemometer voltage corrected for temperature variations
V_o	Anemometer voltage at zero velocity in Appendix D; fluid velocity at manifold inlet in Appendix G
w	Rate of condensation on a tube
w'	Rate of condensate collection in energy balance tests
W	Rate of inundation falling on to a tube
x	Co-ordinate parallel to plate or tube axis
X	Modified Wilson Plot coefficient defined by eqn. (2.61)
y	Co-ordinate perpendicular to tube wall
Y	Modified Wilson Plot coefficient defined by eqn. (2.60)
α	Mean value of the condensate h.t.c.
α_{cw}	Cooling water h.t.c. due to forced convection
α_D	Dirt coefficient
α_e	Combined inside and wall h.t.c. defined by eqn. (2.20)
α_i	Inside wall h.t.c.
α_{MGFP}	Theoretical value of α calculated using MGFP theory with variable separation and variable wall temperature
α_n	Mean value of condensate h.t.c. for the Nth tube in a column
α_N	Mean value of the condensate h.t.c. for a column of N tubes
α_{Nu}	Mean value of the condensate h.t.c. based on the Nusselt eqns. (1.1) or (1.2)
α_o	Overall h.t.c.
α_w	Tube wall h.t.c.
β	Coefficient for calculating T_r in eqn. (1.8)
β_1, β_2, β_3	Constants used for calculating β
γ	Constant in eqn. (2.57)
δ	Condensate film thickness
ε	Constant in eqn. (2.54)
ε_{fj}	Reynolds flux dependent on condensation rate j
ε_o	Reynolds flux with no condensation
ε_{AE}	Value of ε in eqn. (2.63) of Allen and Eckert
θ	Angle measured from the horizontal
μ	Dynamic viscosity
ν	Variable defined in eqn. (2.58)
ρ	Density
σ	Surface tension
τ	Shear stress in condensate layer
τ_F	Shear stress on a wall due to the flow of a non-condensing vapour

τ_M	Momentum transfer of condensing vapour per unit area
τ_S	Total shear stress at condensate-vapour interface
τ_{we}	Equivalent wall shear stress in eqn. (G.3)
χ	Variable defined in eqn. (1.35)
Φ	Angle measured from forward stagnation point
Ω	Variable defined in eqn. (2.54)

Subscripts

B	Bulk properties
cw	Cooling water
E	Surroundings
H	At distance H from leading edge
i	At inside of tube wall
IN	At inlet
L	Lower half of cylinder: point at which flow becomes laminar in Appendix G
m	Mean value
Nu	Assuming the Nusselt conditions outlined in section 1.2
OUT	At outlet
r	Reference value
s	At vapour-condensate interface
sat	Saturation conditions
SE	Sensor
st	Steam
u	Upper half of cylinder
un	Uninumdated
v	Vapour
w	At outside of wall
Φ	At angle Φ

Physical properties without a suffix refer to the condensate

LIST OF FIGURES

CHAPTER 1

INTRODUCTION

1.1 Condenser design problems

The physical operation of condensing a vapour into a liquid occurs in many fields, particularly in the chemical and process industries and in power generating plant. Condensers are often plant components of relatively large capital cost: for instance, the price of a steam condenser for a modern power station would be of the order of £1 000 000. It is therefore essential that information be available so that such components can be designed to meet their requirements as economically as possible.

There are many factors which influence the direct and indirect costs of a condenser. For example, the tube arrangement affects the cost of the condenser shell and that of the building to house it. The layout will also determine accessibility for cleaning and the cost of such an operation. The quality of the metal used will determine the total life, particularly in corrosive or erosive conditions.

The most important factor, however, is the total heat exchange surface area that must be provided, which depends on the overall h.t.c. (heat transfer coefficient) through the tube wall. Adequate information exists for the prediction of the inside, cooling water, h.t.c., except for the often important uncertainty about fouling factors. It is with the outside, condensation, h.t.c. that the present work is concerned.

In his classical paper (1) Nusselt solved the problem of laminar film condensation for flat surfaces and horizontal cylinders, and the assumptions underlying the solution are enumerated in some detail in section 1.2. Although there exist some more "exact" solutions they have not substantially modified Nusselt's final results which are still correct for some practical situations: it is worth remembering that condensation is one of the few instances of heat transfer where an assumption of laminar flow can lead to results of real practical interest.

There are, however, a number of conditions under which all the assumptions made are not valid, and the predictions of Nusselt's theory must then be modified to a lesser or greater degree. In particular, for single tubes, the two most important assumptions which may not be valid are as follows:

(i) The vapour velocity across the tube is sufficiently low for the shear stress exerted on the vapour-liquid interface to be negligible. The effect of vapour shear is to thin the condensate film and improve the h.t.c.

(ii) Non-condensable gases are absent from the vapour. When such gases are present even in small quantities they tend to accumulate on the condensate film, thus reducing the vapour-liquid interface temperature below the bulk vapour saturation temperature and thereby the effective temperature drop and h.t.c. across the condensate film.

For multi-tube condensers, an additional complication arises:

(iii) Inundation progressively increases down a column of horizontal tubes. Nusselt assumed that the condensate flows off a tube as a sheet on to the tube beneath it, and that the film, even on highly-inundated tubes, remains laminar. His prediction of progressively falling h.t.c. is qualitatively correct, but much too pessimistic; splashing, rippled films, and inundation in discrete drops rather than sheets, all conspire to moderate the reduction expected.

It will be appreciated that the interaction of the three effects presents a formidable theoretical and experimental problem. The present work is concerned foremost with velocity effects, and when velocities are high, presence of non-condensables is less serious because the gases are usually swept away by the flowing vapour. It was therefore decided to concentrate on pure steam condensation, but to study the effect of velocity and inundation separately and when acting simultaneously.

Prediction of velocity effects, even for a flat plate, are not as simple as might at first be expected. Firstly the "suction" effect of the vapour migrating to and condensing on the vapour-liquid interface invalidates the normal laws of friction drag. Moreover, around a cylinder, both flow separation, which itself depends on "suction", and pressure variations will modify forces acting on the condensate film. It will be seen that some definite progress has been made in understanding the phenomena involved.

An unexpected result emerged from some of the present analysis. Nusselt derived his theory on the basis of a "boundary condition" of uniform temperature on the surface of the tube. It has always been taken for granted previously, that substitution of an "area-mean" surface temperature would provide substantially correct predictions of h.t.c. It appears that

this is far from true. It should be remembered that the "independent" variables in the real situation are the cooling water temperature and velocity: the tube surface temperature is dependent on the "boundary conditions" prevailing inside and outside the tube.

The results with inundation, as was anticipated, are essentially empirical, but they are correlated in a manner that throws new light on the behaviour of tube arrays.

Unfortunately, velocities and inundation rates vary through a condenser. If one considers a horizontal tube condenser with vapour entering at the top and condensate and non-condensables leaving at the bottom, the inundation and concentration of non-condensables increase as the vapour flows through the condenser, whilst the vapour velocity decreases. Moreover, the cooling water temperature varies along each tube, and from tube to tube. It is therefore not possible to treat the condenser as a single unit for design purposes and a step by step method has to be used: knowing the inlet conditions, the condensation rate for the first row of tubes can be calculated; the conditions approaching the second row can then be obtained and the rate of condensation for this row calculated. The procedure is then repeated for subsequent rows. This method, which must also take account of pressure changes, is ideally suited to solution by computer. Whatever method is used, however, the basic information concerning the condensation rate on a tube under given conditions is still required. The more detailed and reliable such information is, the more accurate will be the prediction for a complete design. It is hoped that the work presented here adds a little to our present state of knowledge.

1.2 Literature survey

The first published work of significance on the prediction of condensation heat transfer coefficients was that of Nusselt (1) and this still provides a basis for most of the present day knowledge on condensation. Nusselt considered the cases of condensation on a vertical and inclined plane and on a horizontal tube, making the following assumptions:

1. the wall temperature is constant;
2. the flow is laminar in the condensate film;
3. heat transfer in the condensate is by conduction perpendicular to the condensate surface only and subcooling can be neglected;
4. fluid properties are constant within the condensate layer;
5. hydrostatic pressure, surface tension, inertia forces and vapour/liquid interfacial shear are negligible compared to viscous and gravitational forces;
6. the surrounding steam and vapour/liquid interface are at saturation temperature;
7. the film thickness is small compared with normal tube diameters and the effects of curvature can be ignored.

Nusselt's analysis led to the following equations for the average condensate h.t.c. (heat transfer coefficient):

for an inclined plate

$$\alpha_{Nu} = 0.943\left[\frac{k^3\rho(\rho - \rho_v)h_{fg}g\sin\Theta}{\mu H(T_s - T_w)}\right]^{\frac{1}{4}} \qquad (1.1)$$

for a horizontal cylinder

$$\alpha_{Nu} = 0.728\left[\frac{k^3\rho(\rho - \rho_v)h_{fg}g}{\mu d(T_s - T_w)}\right]^{\frac{1}{4}} \qquad (1.2)$$

The suffix Nu is used to distinguish these values of α from values used later to which the above conditions do not apply. The equations can be put into the usual dimensionless forms

$$Nu_{Nu} = \frac{\alpha_{Nu}H}{k} = 0.943\left[\frac{\rho(\rho - \rho_v)h_{fg}gH^3\sin\Theta}{k\mu(T_s - T_w)}\right]^{\frac{1}{4}} \qquad (1.1a)$$

and

$$Nu_{Nu} = \frac{\alpha_{Nu}d}{k} = 0.728\left[\frac{\rho(\rho - \rho_v)h_{fg}gd^3}{k\mu(T_s - T_w)}\right]^{\frac{1}{4}} \qquad (1.2a)$$

These equations have been shown to agree with data obtained from experiments performed under conditions which closely satisfy Nusselt's assumptions.

Nusselt went on to consider a vertical bank of horizontal tubes and examined the effect of condensate falling successively from one tube to the next. He arrived at a recursion formula for finding the film thickness at any angle Φ on the Nth tube but deduced the value of α only for the second tube in a column. Jakob (2) used Nusselt's formula to suggest the following equation for the mean heat transfer coefficient for a bank of N tubes

$$\alpha_N = 0.728 \left(\frac{k^3 h_{fg} \rho (\rho - \rho_v) g}{N d \mu (T_s - T_w)} \right)^{\frac{1}{4}} \qquad (1.3)$$

A rigorous proof of Jakob's formula is given by McKechan and Zeitlin (3). Experimental results (4 - 12) indicate that the above equation underestimates the heat transfer and this has been explained as being due to the presence of ripples, splashing and turbulent flow.

Nusselt considered the effect of vapour shear for the case of laminar flow on a flat plate. He assumed that the interface shear stress was of the form τ_s = constant x U_∞^2 leading to a quartic equation in δ, which he solved.

Rohsenow, Webber and Ling (13) examined the case where vapour shear is present for laminar and turbulent film condensation on a vertical plate. For the laminar case they perform a similar analysis to Nusselt but with an added term for vapour shear in the force-balance (momentum effects are neglected). For turbulent flow they assume that within the liquid film the velocity is given by the universal velocity profile and that within the turbulent layer the temperature is uniform. A Martinelli procedure is used for solving the equations and results are presented graphically in terms of Prandtl number and dimensionless forms of heat transfer coefficient, plate height, and vapour shear stress.

Sugawara et al (14) considered condensation on a horizontal tube with vapour drag. Assuming that the interfacial shear stress was the same as that outside a solid cylinder with a non-condensing vapour flowing past, i.e.

$$\tau_s = \tau_F \qquad (1.4)$$

they produced, by numerical methods, graphs indicating the variation of

film thickness and heat transfer around the cylinder. They assumed that separation took place at $\Phi = 83.3^{o}$ and that beyond this point skin friction was absent. Their results indicated that the overall heat transfer coefficient increases with increase in vapour velocity.

Mandelzweig (15) presented an analysis due to Le Fevre which is similar in approach to that of Sugawara et al (14), but includes variation of pressure and buoyancy effects.

Sparrow and Gregg (16, 17) used a boundary layer analysis for laminar film condensation on a vertical plate and horizontal tube. This included the effects of inertia forces and energy convection but made the assumption of zero vapour drag at the interface. Their method was to reduce the partial differential equations of the problem (the conservation laws) to ordinary differential equations and solve these numerically. Their results showed that inclusion of the inertia forces produced a dependence on Prandtl Number, but for Pr > 1 the effects were very small. Results are presented graphically as dimensionless heat transfer coefficient vs $(c_p \Delta T/h_{fg})$ for different Prandtl numbers. For the vertical plate their results for Pr > 1 agree with a formula derived by Rohsenow (18)

$$Nu_H = \frac{4}{3}\left[\frac{gc_p\rho(\rho - \rho_v)H^3}{4\mu k}\right]^{\frac{1}{4}} \left[\frac{1 + 0.68\ c_p\Delta T/h_{fg}}{c_p\Delta T/h_{fg}}\right]^{\frac{1}{4}} \qquad (1.5)$$

where $Nu_H = \alpha H/k$. For the horizontal tube, they show that for all values of Prandtl number and small values of $c_p\Delta T/h_{fg}$

$$Nu_d = 0.733\left[\frac{g\rho^2 h_{fg} d^3}{k\mu(T_s - T_w)}\right]^{\frac{1}{4}} \qquad (1.6)$$

which is within 1% of Nusselt's value.

Chen (19) went through an analysis similar to that of Sparrow and Gregg (16, 17) for the cases of laminar film condensation on a vertical surface and a horizontal tube in a stationary vapour. However, he did not assume zero vapour shear at the interface but instead chose as one of his boundary conditions zero vapour velocity at large distances from the interface. His results predicted lower heat transfer coefficients than those of Sparrow and Gregg, though for Pr > 10 there was little difference. However, for Pr < 0.03 much lower coefficients were predicted, though these were still somewhat higher than available experimental data in this range. Chen also looked at a bank of tubes and took into account condensation on the subcooled draining condensate between tubes which he showed increased the heat transfer on the lower tubes compared with that calculated using

Nusselt's approach. Satisfactory agreement was obtained with experimental results, even though the effects of splashing and ripples were ignored.

His results can be approximated by

$$\frac{\alpha_N}{\alpha_{Nu}} \cdot N = \left(1 + 0.2E(N - 1)\right) \left[\frac{1 + 0.68E + 0.02EJ}{1 + 0.95E - 0.15EJ}\right]^{\frac{1}{4}} \qquad (1.7)$$

where α_N = mean value of the condensate h.t.c. for a column of N tubes

$$E = c_p \Delta T / h_{fg} \qquad J = E/Pr$$

This equation applies provided that

$1 \geq Pr \geq 0.05$ for a single tube $\quad J \leq 0.1$ for multiple tubes

$E \leq 2 \quad J \leq 20 \qquad\qquad E(N-1) \leq 2$

Koh, Sparrow and Hartnett (20) used a boundary layer solution to account for the interface shear force due to the vapour flow induced by the flow of condensate down a vertical plate. They found that for Pr > 10 the effect of this is negligible and for Pr ≈ 1 it is quite small, but for liquid metals this shear-force can substantially reduce the heat transfer.

Poots and Miles (21) use boundary layer approximations and a similarity solution to solve the governing equations to the problem of laminar filmwise condensation on a vertical plate. They assume that far from the condensate the vapour velocity is zero but account for the shear stress at the interface due to the drag produced by the vapour on the condensate. Using the Runge-Kutta-Gill method for integrating the differential equations they produce numerical solutions for saturated steam at 100 ^{o}C condensing on a wall at 0, 10, 40, 70 and 90 ^{o}C. In these numerical solutions they take account of the variations in fluid properties. It was found that very close agreement was obtained with the expressions for heat transfer coefficients given by Nusselt (1), Rohsenow (18) and Chen (19) if all the properties in those expressions were calculated at a reference temperature given by

$$T_r = T_w + \beta(T_s - T_w) \qquad (1.8)$$

where

$$\beta = \beta_1 + \beta_2\left(\frac{\Delta T}{T_s}\right) + \beta_3\left(\frac{\Delta T}{T_s}\right)^2$$

For the case of saturated steam at 100 ^{o}C, β ranged from 0.33 - 0.26 as ΔT went from 100 ^{o}C to 10 ^{o}C.

A boundary layer analysis is used by Chung (22) to examine the influence of vapour shear at the liquid vapour interface on condensation on a vertical plate in a gravitational field. The inclusion of vapour shear requires a simultaneous study of the liquid layer and gas-phase boundary layer, which is achieved by obtaining solutions for each layer and matching the interface temperature, shear stress and mass transfer between the two solutions. It is shown that the major parameters controlling condensation of a pure vapour under these circumstances are the ratio of the product of the density and viscosity of the gas to that of the liquid $(\rho_v\mu_v/\rho\mu)^{\frac{1}{2}}$, the ratio of temperature potential to the heat of condensation $J\left[= c_p\Delta T/(Pr)h_{fg}\right]$ and the Froude Number $Fr_x(= U_\infty^2/gx)$.

A boundary layer analysis was also used by Koh (23) and Cess (24) for laminar film condensation on a flat plate in the absence of body forces. Cess neglected the inertia forces and convection terms, whereas Koh included these and also accounted for the interface velocity which Chung assumed to be negligible for the vapour boundary layer. Koh found that for low Pr, i.e. liquid metals, the parameters controlling condensation were the same as those obtained by Chung, namely $(\rho_v\mu_v/\rho\mu)^{\frac{1}{2}}$ and $\left[c_p\Delta T/(Pr)h_{fg}\right]$ (which Koh shows to be a dimensionless liquid film thickness), and his results agreed with those predicted by Cess. However, for Pr > 1 he found that Prandtl Number becomes an added parameter and energy transfer by convection within the liquid film cannot be neglected, as was assumed by Cess.

Condensation of steam flowing inside a horizontal tube bank was examined experimentally by Fuks (6). He used a staggered bundle of 19 mm o.d. tubes with steam flowing vertically downwards at saturation pressures of 0.05 to 1.05 bar and steam loadings of 0.3 to 2.9 kg/m^2 s. For the first row of tubes he found that experimental data satisfied

$$\frac{\alpha}{\alpha_{Nu}} = 28.3\left(\frac{U_\infty^2\rho_v\alpha_{Nu}}{gk\rho}\right)^{0.08}(Nu_{Nu})^{-0.58}$$

$$= 28.3\left(Fr\,\frac{\rho_v}{\rho}\right)^{0.08}(Nu_{Nu})^{-0.5} \qquad (1.9)$$

where U_∞ is the velocity at the widest section.

This equation does not reduce to the simple Nusselt expression when $U_\infty = 0$. To examine the effects of condensate drainage, data were obtained for tubes down to the 11th row of the bundle and this was

supplemented by information from tests conducted with an additional condensate flow which was provided by supplying saturated water to the top of the bundle. Fuks correlated these data by a power function in the form

$$\frac{\alpha_n}{\alpha_1} = \left(\frac{W + w}{w}\right)^{-0.07} \qquad (1.10)$$

where α_n = coefficient for the Nth tube
α_1 = coefficient for the 1st tube
W = condensate draining on to Nth tube per unit time
w = condensate forming on Nth tube per unit time.

Results are only reported for $(W + w)/w < 10$.

Isachenko and Glushkov (10) supplied inundation to a single tube in stagnant surroundings at rates of $(W + w)/w$ up to 15 and claimed good agreement with Fuks for the variation of α/α_{Nu} with the ratio of inundation to condensation rate. However, examination of their results indicates that a better fit of their data would be given by an exponent of - 0.125 in eqn. (1.10) rather than - 0.07 obtained by Fuks.

Agreement with Fuks was also obtained by Turek (11) for values of $(W + w)/w$ up to 8. Experiments were performed at just above atmospheric pressure on a small tube bank with steam approach velocities up to 10 m/s. Inundation could be supplied to the top of the tube bank to simulate conditions in a large condenser, with values of $(W + w)/w$ up to 70. For values of $(W + w)/w$ greater than 8 the results of Turek lie below those of Fuks. This is accounted for by amending the results to account for pressure drop, and, therefore, the temperature driving force, through the bank. Pressure drop was found to decrease with increase in heat flux and this was attributed to a delay in the point of separation with increase in the "suction" effect.

Berman and Tumanov (25) carried out experiments on a single horizontal tube placed in the fourth row of a bundle of diagonally arranged uncooled tubes. They were able to show that for $(Re_v)^{11.8/\sqrt{(Nu_{Nu})}} < 50$ the effect of steam velocity can be accounted for by using the following equation:-

$$\frac{\alpha}{\alpha_{Nu}} = 1 + 9.5 \times 10^{-3}(Re_v)^{11.8/\sqrt{(Nu_{Nu})}} \qquad (1.11)$$

where α = condensate h.t.c.

$$Nu_{Nu} = \frac{\alpha_{Nu} d}{k} \quad \text{and} \quad Re_v = \frac{\rho_v U_\infty d}{\mu_v}$$

Their experimental data indicated that under otherwise similar conditions, the increase of α with increasing steam velocity is greater, the greater is the temperature difference and steam pressure. They attributed the increase in α not only to the reduction in the film thickness but also to a change from laminar to ripply and turbulent flow with an associated change in the mechanism of heat transfer from conduction to conduction and convection.

The effects of inundation and vapour shear have been examined experimentally by Grant and Osment (7). They derived two equations for calculating the condensation heat transfer coefficient α_n on the Nth row of a tube bank. (Note the difference between α_n and α_N: the latter is the average h.t.c. for a column of N tubes):-

(i) they extended the Nusselt analysis (1, 2) for inundation using the data of Berman and Tumanov (25) for vapour shear, to produce

$$\frac{\alpha_n}{\alpha_{Nu}} = \left[N^{\frac{3}{4}} - (N-1)^{\frac{3}{4}}\right] \left[1 + 0.0095\ (Re_v)^{11.8/\sqrt{(Nu_{Nu})}}\right] \qquad (1.12)$$

(ii) they used the experimental data of Fuks (6) for inundation with the data of Berman and Tumanov for vapour shear to get

$$\frac{\alpha_n}{\alpha_{Nu}} = \left(\frac{W + w}{w}\right)^{-0.07} \left[1 + 0.0095\ (Re_v)^{11.8/\sqrt{(Nu_{Nu})}}\right] \qquad (1.13)$$

where W = amount of condensate falling on to Nth tube per unit time

w = amount of condensate forming on Nth tube per unit time.

Their results were higher than those predicted by (i) (indicating that the Nusselt analysis for inundation underestimates the condensate h.t.c.) but lower than those predicted by (ii). However, by changing the exponent of $(W + w)/w$ from - 0.07 to - 0.223 in eqn. (1.13) they were able to achieve agreement between their experimental and predicted results with a r.m.s. deviation of 13%.

$$\frac{\alpha_n}{\alpha_{Nu}} = \left(\frac{W + w}{w}\right)^{-0.223} \left[1 + 0.0095\ (Re_v)^{11.8/\sqrt{(Nu_{Nu})}}\right] \qquad (1.14)$$

Mayhew et al (26) looked at the effect of vapour drag on laminar film condensation on a vertical surface. The drag on the liquid film is

considered to be equal to the sum of the "dry" frictional force plus the momentum change due to condensation. Thus

$$\tau_s = \tau_F + \tau_M \tag{1.15}$$

where τ_s = total shear stress at the condensate-vapour interface

τ_F = shear stress produced by a non-condensing vapour flowing past the surface

τ_M = shear stress due to the total momentum transfer of the condensing vapour

The first term on the r.h.s. of eqn. (1.15) was accounted for by using the Blasius Law and the second term by assuming that the condensed mass retains the velocity of the mainstream.

$$\tau_M = j(U_\infty - u_s) \simeq jU_\infty \tag{1.16}$$

where j = rate of condensation per unit area

U_∞ = free stream velocity of vapour

u_s = velocity at condensate-vapour interface

Constant properties are assumed though a reference temperature T_r, eqn. (1.8), is used for evaluating the viscosity, where β varies from 0.25 at zero shear to 0.33 at high shear.

The theory provides a quartic equation

$$(Sh)\left(\frac{\delta_H}{H}\right)^4 + \frac{1}{3}(Dr)\left(\frac{\delta_H}{H}\right)^3 + \frac{1}{4}(Re_{TP})\left(\frac{\delta_H}{H}\right)^2 - 1 = 0 \tag{1.17}$$

to be solved for the ratio of the film thickness at the bottom of the plate δ_H to the plate height H, in terms of the three non-dimensional parameters

Sherwood number	$Sh = \rho^2 g h'_{fg} H^3/4\mu k\Delta T$	gravity term
	$Dr = \rho \tau_F h'_{fg} H^2/\mu k\Delta T$	dry friction term
Two-phase Reynolds Number	$Re_{TP} = \rho U_\infty H/\mu$	momentum term

(Note: Re_{TP} contains the properties of the condensate but the velocity of the vapour)

The real positive root of eqn. (1.17) was found by trial and error and substituted into

$$Nu_H = \frac{4}{3}(Sh)\left(\frac{\delta_H}{H}\right)^3 + \frac{1}{2}(Dr)\left(\frac{\delta_H}{H}\right)^2 + \frac{1}{2}(Re_{TP})\left(\frac{\delta_H}{H}\right) \tag{1.18}$$

to find the average Nusselt number for the plate. The limited experimental results obtained agreed well with the theory.

Further work with condensation on flat horizontal and vertical surfaces was done by Mayhew and Aggarwal (27). The results for the horizontal plate confirmed the view that the shear stress could be allowed for by simply adding the Blasius and momentum terms, whilst for the vertical plate it was found that

$$\tau_s = \tau_F + 0.75\ \tau_M \qquad (1.19)$$

gave better agreement with experimental results.

Aggarwal et al (28) also performed experiments to examine the effect on the wall shear stress of sucking air out of a stream of air, flowing through a porous tube. Assuming that the shear stress could be represented by

$$\tau_s = \tau_F + b\tau_M \qquad (1.20)$$

where $\tau_M = \rho_v v\bar{u}$

$\bar{u}$ = local weighted mean air velocity

ρ_v = air density

v = suction velocity at and perpendicular to the wall

b = a factor less than unity

they found that, though b was a function of Re_v, x/d_i and suction rate, a value of 0.75 was sufficiently accurate for most design purposes. (Note $\rho_v v$ is analogous to j introduced previously.)

Shekriladze and Gomelauri (29, 30) considered the case where the effect of friction due to vapour drag can be neglected as being small compared with the momentum transferred and assumed

$$\tau_s = \tau_M = j(U_\infty - u_s) \simeq jU_\infty \qquad (1.21)$$

They considered the cases of a flat plate with T_w = constant and q_w = constant under conditions where gravity could be ignored and showed that the effects of inertia and convection were negligible. Their theoretical results were compared with experimental data of Jakob and agreement was within the scatter of the experimental results.

For T_w = constant

$$Nu_H = \sqrt{\left(\frac{Re_{TP}}{J + 1}\right)} \qquad (1.22)$$

q_w = constant

$$Nu_H = 1.41\sqrt{(Re_{TP})} \qquad (1.23)$$

where $J = k\Delta T/h_{fg}\mu$ $\qquad$ $Re_{TP} = \rho U_\infty H/\mu$

For the case of a vertical plate in a gravity field they obtained

$$Nu_H = \sqrt{(Re_{TP})} \quad \frac{\sqrt{2}}{3} \frac{\left[2 + \sqrt{(1 + 16/(Fr_H)J)}\right]}{\sqrt{\left[1+ \sqrt{(1 + 16/(Fr_H)J)}\right]}} \tag{1.24}$$

where $Fr_H = \dfrac{U_\infty^2}{gH}$

They then considered condensation on a horizontal cylinder in a transverse flow assuming:-

(1) that the effect of pressure gradient around the cylinder periphery could be neglected in comparison to the momentum transferred

(2) outside the vapour boundary layer the velocity field is that due to potential flow around a cylinder ($U_\phi = 2U_\infty \sin\phi$)

(3) the vapour boundary layer is laminar up to the point of separation

(4) inertia forces can be neglected.

It is possible with high rates of phase change to have flow around a cylinder without separation even with high approach velocities (c.f. boundary layer suction) and this case was considered first. In the absence of body forces Shekriladze and Gomelauri's results predict

$$\alpha = 0.9\sqrt{\left(\frac{k^2 \rho U_\infty}{\mu d}\right)} \tag{1.25}$$

$$Nu_d = 0.9\sqrt{(Re_{TP})} \tag{1.26}$$

In a gravitational field they found it impossible to obtain an explicit solution but, with approximation, arrived at

$$\alpha = 0.64 \sqrt{\left(\frac{k^2 \rho U_\infty}{\mu d}\right)} \; x \sqrt{\left[1 + \sqrt{\left(1 + \frac{1.69 dg}{U_\infty^2 J}\right)}\right]} \tag{1.27}$$

$$Nu_d = 0.64\sqrt{(Re_{TP})} \; x \sqrt{\left[1 + \sqrt{\left(1 + \frac{1.69}{(Fr)J}\right)}\right]} \tag{1.28}$$

It appears from this that the greater the temperature difference the greater is the effect of the vapour velocity on the h.t.c. compared with the value at zero velocity, which agrees with the experimental evidence of Fuks (6) but not with the theoretical work of Sugawara (14).

To account for separation at the minimum angle of 82° it was assumed that there was no heat transfer beyond the separation point and that up to this point the heat transfer was the same as in the case with no separation

$$Nu_d = 0.42\sqrt{(Re_{TP})} \times \sqrt{\left[1 + \sqrt{\left(1 + \frac{1.69}{(Fr)J}\right)}\right]} \qquad (1.29)$$

It was then argued that when separation occurs between 82° and 180° the overall heat transfer coefficient will lie somewhere between that predicted for the two extremes and this was shown to agree with experimental evidence from (25).

Silver (31, 32) uses a Reynolds flux model to predict surface shear stresses and introduces these values in place of the assumption of zero shear stress at the interface. The effect of this is to predict a heat transfer coefficient given by the Nusselt coefficient multiplied by a factor r, where r is obtained from

$$r^2 = \frac{1}{r} + \frac{3(\varepsilon_{fj} + j)U_\infty \alpha_{Nu}}{2gk\rho} \qquad (1.30)$$

where α_{Nu} is the Nusselt coefficient
ε_{fj} is a Reynolds flux dependent on the condensation rate
j is the condensation rate

Wallis (33) also uses a Reynolds flux model to account for the vapour shear stress acting on the condensate layer and shows that

$$\tau_s = \tau_F + \tfrac{1}{2}\tau_M \quad \text{for } j < 2\varepsilon_o \qquad (1.31)$$

$$\tau_s = \tau_M \quad \text{for } j > 2\varepsilon_o \qquad (1.32)$$

where ε_o = Reynolds flux ($= \tau_F/U_\infty$)
τ_M = interfacial shear stress due to momentum transfer of condensing vapour
$= j(U_\infty - u_s)$

Nicol and Wallace (34) examined theoretically and experimentally the effect of vapour velocity on condensation on a single horizontal cylinder, for both upward and downward flow. In their theoretical approach, they take the vapour shear stress as

$$\tau_s = \tau_F + b\tau_M \qquad (1.20)$$

where $0 < b < 1$.

They assume that the frictional shear stress term is given by the Blasius power series predicting separation at an angle of 108.8° and that beyond

the point of separation Nusselt conditions prevail. The wall temperature was assumed constant and pressure effects ignored. The experimental results were lower than those predicted using b = 0 and it was concluded that the momentum term could be neglected. During the tests at high velocity in the downward flow case, a line of discontinuity was observed at an angle of 95^{o}, which was attributed to separation of the vapour flow. A further point of interest was that at high velocities the overall measured coefficient was higher in the upward vapour flow case than in the downward flow case, as had also been predicted from their theoretical work.

The combined effect of body force and forced convection resulting from vapour flow on laminar filmwise condensation on a vertical plate was examined by Jacobs (35). Neglecting the effects of inertia and convection in the condensate layer he used an integral method to solve the two-phase boundary layer equations. Unfortunately he appears to have used an invalid boundary condition, but his method has been corrected by Fujii and Uehara (36). Their results, at the limiting cases of body force only and forced convection only, agree with the solutions of Nusselt (1) and Cess (24). They find that the average Nusselt number can be expressed by

$$Nu_H = \left[0.656\left(1.2 + \frac{1}{RJ}\right)^{4/3} \times (Re_{TP})^2 + 0.79\,\frac{K}{J}\right] \qquad (1.33)$$

where $R = \left(\frac{\rho\mu}{\rho_v\mu_v}\right)^{\frac{1}{2}}$ $\qquad J = \frac{c_p\Delta T}{Pr\ h_{fg}}$

$$K = \frac{\rho^2 H^3 g}{\mu^2} \qquad Re_{TP} = \frac{\rho U_\infty d}{\mu}$$

and this agrees to within 4% of their integrated values. Predicted results are compared with experimental data from various sources for water and organic substances. Reasonable agreement is achieved within stated limits to the range of Nu_H and ΔT.

Fujii et al (37) use a similar analysis for the case of a horizontal cylinder in a saturated vapour flowing vertically downwards. They assume that outside the vapour boundary layer the flow is a potential one and can be expressed as $2U_\infty \sin\phi$. At low vapour velocity the results tend towards Nusselt's prediction (eqn. 1.2a) and for large vapour velocities towards

$$Nu_d = 0.90\left(1 + \frac{1}{RJ}\right)^{1/3} (Re_{TP})^{\frac{1}{2}} \qquad RJ < 10 \qquad (1.34)$$

A general expression which satisfied both limiting cases is proposed

$$Nu_d = \chi\left[1 + \frac{0.276}{\chi^4(Fr)J}\right]^{\frac{1}{4}} (Re_{TP})^{\frac{1}{2}} \qquad (1.35)$$

where $\chi = 0.90\left[1 + \frac{1}{RJ}\right]^{1/3}$ and $Fr = \frac{U_\infty^2}{gd}$

The maximum difference between results predicted by this equation and the numerical results is 5%. The authors found that the overall heat transfer coefficient calculated using their analysis for a typical case was larger than that predicted by both Sugawara (14) and Shekriladze and Gomelauri (29). They attributed this to the fact that Sugawara assumed that separation occurs and, in the particular case they compared, Shekriladze and Gomelauri ignored gravitation.

Most of the experimental results of Berman and Tumanov (25) were predicted from eqn. (1.35) to within ± 20% as were the authors' own experimental results which were for a horizontal tube in a horizontal flow perpendicular to the tube axis.

Fujii et al (38) use the same parameters as obtained for a single tube for correlating data for a bank of tubes. They performed experiments on a bank of horizontal tubes with 15 columns and 5 rows using steam at a pressure of 0.01 - 0.07 bar flowing horizontally at oncoming velocities of 10 - 40 m/s. They proposed that for the first three columns of tubes (beyond the third column the amount of air present influenced the heat transfer) the mean Nusselt number for a column is given by

$$Nu_d = K_T\chi\left[1 + \frac{.276}{\chi^4(Fr)J}\right]^{\frac{1}{4}} (Re_{TP})^{\frac{1}{2}} \qquad (1.36)$$

where the velocity is taken as that at the maximum flow area

K_T = 0.8 for an in-line arrangement

= 1.0 for a staggered arrangement.

The data of Berman and Tumanov (25) for vertical flow over a staggered bank of horizontal tubes was also correlated, but with $K_T = 1.1 \pm 0.1$. The authors attributed the difference in K_T to a systematic error in measuring heat flux.

Denny and Mills (39) developed a computer program for solving the conservation equations, in boundary layer form, of laminar film condensation on a vertical surface. They used a finite difference analogue involving a technique developed by Patankar and Spalding (40). They compared this solution with analytical solutions obtained using the basic

Nusselt assumptions which were extended to include a non-isothermal wall and vapour drag. The latter was accounted for using an asymptotic solution of the vapour boundary layer under strong suction as in (29) in which the local shear stress is equal to the momentum given up by the condensing vapour. From the comparison of the two solutions they were able to propose a reference temperature T_r for the liquid film defined as

$$T_r = T_w + \beta(T_s - T_w) \qquad (1.8)$$

which accounts for the effects of variable properties in the liquid film and of the convection and inertia terms which were omitted in the analytical solution. The authors suggest that this reference temperature be used with the Nusselt assumptions to analyse the liquid film in other condensation problems where an analytical solution would be difficult to obtain otherwise. For a given liquid the value of β was a weak function of all parameters and it is of interest to note that the average value quoted for water of 0.33 agrees quite well with that of Minkowycz and Sparrow 0.31 (41), Poots and Miles 0.26 - 0.33 (21) and Mayhew et al 0.25 - 0.33 (26).

The same authors considered the problem of laminar film condensation of a flowing vapour on a horizontal cylinder in a gravity field (42). This is the same problem as that considered by Shekriladze and Gomelauri (29) who obtained eqns. (1.28) and (1.29) by an approximate method. Denny and Mills obtained an explicit analytical solution by using integral mean values for coefficients in the governing differential equations. The analysis produced a complicated expression for the film thickness at any point and solution requires reference to tables of the functions which were averaged. As in (39), comparison is made with results predicted by a general computer program. The concept of a reference temperature is applied again, and by using the same values of β as for the vertical plate, agreement was within 2% up to an angle of $\Phi = 140^{o}$. It would appear that beyond this point the Nusselt assumptions, particularly that of negligible inertia effects, are invalid. A point of interest arising from this analysis is that the film thickness increases from the forward stagnation point and does not go through a minimum at 5^{o} as predicted by Nusselt. This was also found by McKechan and Zeitlin (3) who attributed the discrepancy to the fact that Nusselt performed the necessary integration using a planimeter and probably used quite large intervals, which could account for the apparent inaccuracy, whereas they had used relatively small intervals and integrated by numerical methods using a computer.

Denny et al have extended their computer program to include the effect of non-condensable gases in a forced vapour flow on laminar film

condensation on a vertical plate and horizontal tube (43, 44, 45). The results of this show that the decrease in heat transfer coefficient due to the presence of non-condensables, which can be significant even with very low concentrations at low vapour velocities, is reduced with increase in vapour velocity. They suggest that the interfacial shear can be predicted using a formula of the form

$$\tau_s = (\tau_F^n + \tau_M^n)^{1/n} \qquad (1.37)$$

and found that a value of n = 1.375 gave good agreement with numerical results for a flat plate and stagnation flow on a horizontal tube.

It is well-known that suction can delay the point of separation. Prandtl (46a) uses a simple boundary layer analysis to show that to prevent separation occurring at all around a cylinder with uniform suction

$$\frac{v}{U_\infty}\sqrt{(Re_v)} > 4.36 \qquad (1.38)$$

where v is the suction velocity.

The process of condensation is very similar to suction and it has been postulated (29, 47) that, because of this, boundary layer separation is delayed by condensation.

Drummond (47) carried out tests with air flow across a small tube bank and suction into the sintered bronze tube walls. He measured the overall pressure drop, and found that, as the rate of mass extraction was increased, the pressure drop was reduced. A further decrease in pressure drop was found when Thwaites flaps were fitted along the rear stagnation line of the cylinders. It was suggested that condensate falling from one tube to the next acted in the same way as the flaps, reducing circulation and improving pressure recovery.

A detailed study of the effect of suction on a cylinder in cross-flow has been made by Morsey (48). Using a perforated cylinder, he measured the variation of pressure and shear stress around the periphery of a single cylinder and a cylinder at various positions in a triangular pitch tube bank. For the single cylinder, he found that the wall shear stress increased with increase in suction rate and that at the highest suction rates ($v\sqrt{(Re_v)}/U_\infty = 25$) it was about three times the no-suction value. The point of separation moved further back with increasing suction but, although the suction rates were very much higher than those predicted by Prandtl to prevent separation, the maximum point of separation occurred

at $\phi = 130^{o}$. Similar results were found when the tube bank was used, with separation being further delayed to angles of up to 160^{o} for all but the first and last rows.

Experimental tests were performed by Eissenberg (8, 9) to examine the effects of steam temperature, steam velocity, inundation rate and non-condensable gas fraction on the condensate h.t.c. for a vertical column of 5 tubes, located in a triangular arrayed horizontal tube bank, with horizontal steam flow. The steam temperature range was 60 ^{o}C to 120 ^{o}C, the steam flowrate 500 kg/h m^2 to 12 500 kg/h m^2 and the maximum temperature difference across the condensate layer about 7.5 K. An increase in condensate h.t.c. was found with increase in velocity. This was attributed to the fact that condensate was carried away from the top tubes and did not subsequently drop on to the tubes below. The amount of condensate entrained was found to be related to the kinetic energy of the steam flow. The values of α obtained from inundation were well above those predicted by Nusselt, which was in agreement with other authors. A "side-drainage" model was developed to account for this increase in condensate h.t.c. This model assumes that some drainage occurred from tube bottom to tube side, Fig. 1, in triangular tube banks, with the result that only part of the tube is inundated and the condensate h.t.c. for the whole tube is increased. If all the drainage was in this fashion, Eissenberg showed that

$$\frac{\alpha_N}{\alpha_{Nu}} = 0.6 + \frac{0.5}{N^{\frac{1}{4}}} \qquad (1.39)$$

and found that his experimental results lay between this curve and the Nusselt prediction. He recommended the design equation

$$\frac{\alpha_n}{\alpha_{Nu}} = 0.6\ F_d + (1 - 0.58\ F_d)(N^{0.75} - (N - 1)^{0.75}) \qquad (1.40)$$

where F_d is a tube bundle spacing parameter

= 0.8 for triangular staggered arrangement with $P_T = 1.33$ and d = 25.4 mm

= 0 for in-line arrangement.

A small number of experiments, on quite a large tube bank of 162 tubes of 19.05 mm dia. x 1 m long on a 25 mm equilateral triangle tube pitch, were made by Takahashi and Soda (12). For the tube bank as a whole they found that the condensate h.t.c. approximately doubled with a change of Re_v from 2 x 10^3 to 8 x 10^3, and that it was reduced by about 20% when the amount of condensate recycled to the top of the bank was increased by

$2\frac{1}{2}$ times,

i.e. $\alpha \propto Re_v^{\frac{1}{2}}$

$\alpha \propto W^{-0.25}$.

1.3 Purpose of present research

The main aim of the research programme was to investigate the combined effects of downward vapour velocity and condensate inundation on the condensation rates in horizontal tube banks. It was anticipated that it would be impossible to obtain a direct theoretical approach to the problem for comparison with experimental data and, therefore, a basic understanding of the physical processes involved was sought in the hope that the data could be correlated using general parameters.

The initial part of the programme dealt with the case of an uninundated single tube, with the intention of comparing the experimental data with new and existing theories, so that the principal "velocity-effect" parameters involved could be identified. Tests with a single tube in a bank of dummy tubes were then performed to examine the effect of the proximity of other tubes on the uninundated condensation process and to try and relate the results to those from the single tube tests. Finally, tests on an artificially inundated tube bank were made to measure the combined effects of condensate inundation and vapour velocity.

Throughout the programme evidence was sought to explain some of the discrepancies amongst previous reported work.

Steam was the most convenient condensing fluid to use for the tests. The number of parameters investigated was reduced by restricting the work to the study of the condensation of pure vapours and the effects of non-condensable gases were not included. The saturation pressure in the experimental work was maintained, therefore, slightly in excess of atmospheric to prevent ingress of air into the rig. In order to make the experimental conditions somewhat comparable to those found in practice, the test rig was designed to give a similar range of mass velocity ($\rho_v U_\infty$) as is found in a power station condenser, where the saturation pressure is typically 50 mmHg, and the geometrical details of the tube and tube bank were made characteristic of those found in commercial condensers.

The remainder of this thesis is divided into three sections, the first dealing with the single tube, the second with tube banks and the third with recommendations for further work.

CHAPTER 2

SINGLE TUBE

2.1 Theory

Following some simple assumptions a general differential equation is derived for predicting the variation of condensate film thickness around a horizontal tube with a saturated vapour flowing vertically downwards over it. Suitable boundary conditions are chosen and the equation is solved to give the value of the mean condensate h.t.c. for the tube under certain conditions. In particular the effects of separation, different theories for predicting the interfacial shear stress, the peripheral variation of tube wall temperature and the distribution of vapour pressure are examined.

2.1.1 Derivation of general equation for predicting local film thickness

Consider a saturated vapour at a temperature T_{sat} and pressure p_{sat} flowing vertically downwards with a free-stream velocity U_∞ past a horizontal cylinder of external diameter d. Let the tube wall temperature be T_w and the shear stress at the interface between condensate and vapour be τ_s. In general both T_w and τ_s will vary peripherally with the angle Φ measured from the forward stagnation point, viz.

$$T_w = f(\Phi) \tag{2.1}$$

$$\tau_s = f(\Phi) \tag{2.2}$$

A force balance on the shaded element shown in Fig. 2 gives

$$(\tau - \tau_s)\,\frac{d}{2}\,d\Phi + \left(p + \frac{dp}{d\Phi}\,.\,d\Phi\right)(\delta - y) - p(\delta - y) =$$

$$(\rho - \rho_v)g\sin\Phi(\delta - y)\,\frac{d}{2}\,d\Phi \tag{2.3}$$

where the following assumptions have been made:

(a) momentum changes within the liquid film and surface tension forces can be neglected;

(b) the thickness δ of the condensate layer is small compared with the tube diameter (i.e. $\delta \ll d$). (Note that at $\Phi = \pi$, $\delta \to \infty$ and this assumption is no longer valid, but its effect on the predicted value of the mean condensate h.t.c. will be small.)

The following assumptions are also made:

(a) buoyancy effects can be neglected ($\rho_v << \rho$);

(b) the flow within the condensate is laminar

$$\tau = \mu \frac{du}{dy} \tag{2.4}$$

(c) hydrostatic pressure changes within the condensate in a radial direction can be neglected, and the pressure at any angle Φ is given by the potential flow solution

$$p = p_o + \frac{\rho_v U_\infty^2}{2} (1 - 4 \sin^2\Phi) \tag{2.5}$$

where p_o = static pressure in the free stream.

Note that the above assumptions, with the exception of (c), were also made by Nusselt (1) as outlined in section 1.2.

Differentiating eqn. (2.5) w.r.t. Φ

$$\frac{dp}{d\Phi} = - 2\rho_v U_\infty^2 \sin 2\Phi \tag{2.6}$$

and then combining this with eqn. (2.3), eqn. (2.4) can be written as

$$\tau = \mu \frac{du}{dy} = \rho g \sin\Phi(\delta - y) + \frac{4\rho_v U_\infty^2}{d} \sin 2\Phi(\delta - y) + \tau_s \tag{2.7}$$

Integrating between y = 0 and y = y with the boundary condition u = 0 at y = 0 the velocity distribution across the condensate layer is given by:

$$u = \left(\frac{\rho g \sin\Phi}{\mu} + \frac{4\rho_v U_\infty^2}{\mu d} \sin 2\Phi\right)\left(\delta y - \frac{y^2}{2}\right) + \frac{\tau_s y}{\mu} \tag{2.8}$$

The mass flow rate of condensate m per unit length of tube at angle Φ is given by:

$$m = \int_o^\delta \rho u dy \tag{2.9}$$

and hence

$$\begin{aligned} m &= \int_o^\delta \left[\left(\frac{\rho^2 g \sin\Phi}{\mu} + \frac{4\rho\rho_v U_\infty^2}{\mu d} \sin 2\Phi\right)\left(\delta y - \frac{y^2}{2}\right) + \frac{\rho \tau_s y}{\mu}\right] dy \\ &= \left(\frac{\rho^2 g \sin\Phi}{\mu} + \frac{4\rho\rho_v U_\infty^2}{\mu d} \sin 2\Phi\right) \frac{\delta^3}{3} + \frac{\tau_s \rho \delta^2}{2\mu} \end{aligned} \tag{2.10}$$

If it is assumed that heat transfer through the condensate layer is by conduction only, we can write for unit length of tube, Fig. 3,

$$dQ = \frac{k(T_s - T_w)d}{2\delta} d\Phi = h'_{fg} dm = \alpha_\phi (T_s - T_w) \frac{d}{2} d\Phi \tag{2.11}$$

where dQ is the heat transfer rate through the element

T_s is the interface temperature of condensate and vapour ($= T_{sat}$)

α_ϕ is the local condensate h.t.c.

h'_{fg} is the latent heat of vaporisation corrected to include subcooling of the condensate ($= h_{fg} + 0.68\, c_p(T_s - T_w)$)

(Note: The heat transferred to the wall is the sum of the energy released at the interface due to change of phase plus the enthalpy reduction due to the condensate layer being at a mean temperature less than the saturation value. By imagining this subcooling of the condensate to be equivalent to an additional energy release at the interface, the total enthalpy change can be accounted for by modifying h_{fg}. The value of the coefficient applied to the subcooling term depends on the refinement of the analysis and the condensation conditions, but it is not too critical as this term is generally small when compared with h_{fg}. The factor 0.68 is that obtained by Rohsenow (18)).

Differentiating eqn. (2.10) w.r.t. Φ, we obtain

$$\frac{dm}{d\Phi} = \left(\frac{\rho^2 g \sin\Phi}{\mu} + \frac{4\rho\rho_v U_\infty^2 \sin 2\Phi}{\mu d}\right)\delta^2 \frac{d\delta}{d\Phi} + \left(\frac{\rho^2 g \cos\Phi}{\mu} + \frac{8\rho\rho_v U_\infty^2 \cos 2\Phi}{\mu d}\right)\frac{\delta^3}{3} + \frac{\tau_s \rho\delta}{\mu}\frac{d\delta}{d\Phi} + \frac{\rho\delta^2}{2\mu}\frac{d\tau_s}{d\Phi} \qquad (2.12)$$

From eqn. (2.11)

$$\frac{dm}{d\Phi} = \frac{k(T_s - T_w)d}{2\delta h'_{fg}} \qquad (2.13)$$

Equating eqn. (2.12) and eqn. (2.13) and re-arranging terms

$$\frac{d\delta}{d\Phi} = \frac{\dfrac{k(T_s - T_w)d}{2h'_{fg}} - \left(\dfrac{\rho^2 g\cos\Phi}{\mu} + \dfrac{3\rho_v \rho U_\infty^2 \cos 2\Phi}{\mu d}\right)\dfrac{\delta^4}{3} - \dfrac{\rho\delta^3}{2\mu}\dfrac{d\tau_s}{d\Phi}}{\left(\dfrac{\rho^2 g\sin\Phi}{\mu} + \dfrac{4\rho\rho_v U_\infty^2 \sin 2\Phi}{\mu d}\right)\delta^3 + \dfrac{\rho\tau_s\delta^2}{\mu}} \qquad (2.14)$$

Let $$A = \frac{J}{K} = \frac{\mu k(T_s - T_w)}{\rho^2 g h'_{fg} d^3}$$

$$Fr = \frac{U_\infty^2}{gd} \qquad (2.15)$$

(Note the similarity between A and the expression for Nu_{Nu} given by the Nusselt analysis eqn. (1.2a). Equation (2.14) becomes

$$\frac{d\delta}{d\Phi} = \frac{\frac{Ad^4}{2} - \left(\cos\Phi + 8\left(\frac{\rho_v}{\rho}\right)Fr\cos 2\Phi\right)\frac{\delta^3}{3} - \frac{\delta^3}{2\rho g}\frac{d\tau_s}{d\Phi}}{\left(\sin\Phi + 4\left(\frac{\rho_v}{\rho}\right)Fr\,\sin 2\Phi\right)\delta^3 + \frac{\tau_s\delta^2}{\rho g}} \qquad (2.16)$$

Provided that T_w and τ_s are known functions of Φ or δ, eqn. (2.16) can be integrated numerically starting from the boundary condition at

$$\Phi = 0 : \quad \frac{d\delta}{d\Phi} = 0 \qquad (2.17)$$

2.1.2 Variation of tube outer surface temperature

Previous workers have usually taken T_w as constant, or worked in terms of an average value; there can, however, be a large variation in temperature around the tube. A physically meaningful alternative to assuming T_w = constant is to assume the inside surface h.t.c. α_i, defined in terms of the difference between the inside temperature of the tube wall and the bulk mean temperature of the coolant $(T_i - T_B)$, is uniform. Because the local value of the condensation h.t.c. varies around the tube, it follows from this latter assumption that the outside wall temperature of the tube is also a variable. A consequence of this wall temperature variation is that there will be peripheral conduction within the tube wall. Although the heat flux in the circumferential direction is not always insignificant as compared to that in the radial direction, particularly in the region $\Phi = \pi$, the heat transfer will be assumed to be one-dimensional to simplify the mathematical solution which would otherwise require an iterative procedure. We can then write the heat transferred dQ per unit length of the segment $d\Phi$, Fig. 3, as

$$dQ = \alpha_\phi(T_s - T_w)\frac{d}{2}d\Phi = \frac{k_w(T_w - T_i)}{\ln\left(\frac{d}{d_i}\right)}d\Phi = \alpha_i(T_i - T_B)\frac{d_i}{2}d\Phi$$

$$= \alpha_e(T_w - T_B)\frac{d}{2}d\Phi = \alpha_{o\phi}(T_s - T_B)\frac{d}{2}d\Phi \qquad (2.18)$$

where α_ϕ is the local condensate h.t.c. which from eqn. (2.11), is

$$\alpha_\phi = \frac{k}{\delta} \qquad (2.19)$$

α_e is the combined inside and wall heat transfer coefficient referred to unit outside tube surface area and can be shown to be given by

$$\frac{1}{\alpha_e} = \frac{d}{d_i \alpha_i} + \frac{d \ln\left(\frac{d}{d_i}\right)}{2 k_w} \qquad (2.20)$$

($1/\alpha_e$ is constant if α_i is, as suggested, assumed constant) and $\alpha_{o\phi}$ is the local value of the overall h.t.c. which is given by

$$\frac{1}{\alpha_{o\phi}} = \frac{1}{\alpha_e} + \frac{1}{\alpha_\phi} \qquad (2.21)$$

Re-arranging eqn. (2.18) and substituting from equations (2.21) and(2.19) we obtain

$$(T_s - T_w) = \frac{\alpha_{o\phi}}{\alpha_\phi}(T_s - T_B) = \frac{\alpha_e \delta}{k + \alpha_e \delta}(T_s - T_B) \qquad (2.22)$$

Thus, $(T_s - T_w)$ is known as a function of δ and can be substituted into eqn. (2.15) to give

$$A = \frac{\mu k (T_s - T_B)\alpha_e \delta}{\rho^2 g h'_{fg} d^3 (k + \alpha_e \delta)} = f(\Phi) \qquad (2.23)$$

Note that for a constant wall temperature solution $(T_s - T_w)$ = constant and yields a constant value of A from eqn. (2.15).

2.1.3 Liquid-vapour interfacial shear stress

A number of simple methods of accounting for the shear stress τ_s at the condensate-vapour interface have been proposed as outlined in section 1.2.

The more important methods have been incorporated into solutions derived here and are as follows:

(a) Dry Friction Model

The shear stress is assumed to be that on a cylinder with no condensation (14)

$$\tau_s = \tau_F \qquad (1.4)$$

(b) Friction and Momentum Model

An extra term is included to account for the increase in shear stress due to the momentum transferred by the condensing vapour (26, 34)

$$\tau_s = \tau_F + \tau_M \qquad (1.15)$$

(c) Reynolds Flux Model

This is similar in concept to the Friction and Momentum model but differs in the degree to which the momentum transfer and dry friction terms

affect the interfacial shear stress under different conditions (33)

$$\tau_s = \tau_F + \tfrac{1}{2}\tau_M \qquad \tau_M < 2\tau_F \tag{1.31}$$

$$\tau_s = \tau_M \qquad \tau_M > 2\tau_F \tag{1.32}$$

(d) Power Law

This model recognises the fact that at high rates of condensation the shear stress will approach that given by the momentum term alone, and at low rates that given by the friction term. It is suggested (45) that the entire range of condensation rate can be covered by taking

$$\tau_s = \left(\tau_F^n + \tau_M^n\right)^{1/n} \tag{1.37}$$

The first three methods can be accounted for mathematically by assuming

$$\tau_s = a\tau_F + b\tau_M \tag{2.24}$$

$$\frac{d\tau_s}{d\Phi} = a\frac{d\tau_F}{d\Phi} + b\frac{d\tau_M}{d\Phi} \tag{2.25}$$

where the values of a and b are given below.

Model	a	b
Friction	1	0
Friction + Momentum	1	1
Reynolds Flux: $\tau_M > 2\tau_F$	0	1
$\tau_M < 2\tau_F$	1	½

The Blasius (46b) solution will be used for predicting the dry friction term

$$\tau_F = \frac{\rho_v U_\infty^2}{2\sqrt{Re_v}}\left(9.861\Phi - 3.863\Phi^2 + 0.413\Phi^5 - 0.0259\Phi^7 + 0.00061\Phi^9 - 0.000163\Phi^{11}\right) \tag{2.26}$$

$$\frac{d\tau_F}{d\Phi} = \frac{\rho_v U_\infty^2}{2\sqrt{Re_v}}\left(9.861 - 11.589\Phi^2 + 2.065\Phi^4 - 0.1813\Phi^6 + 0.00055\Phi^8 - 0.00179\Phi^{10}\right) \tag{2.27}$$

The Blasius solution is consistent with separation at $\Phi = 108.8^\circ$.

The momentum term is given by

$$\tau_M = j_\phi(U_\phi - u_s) \tag{2.28}$$

where j_ϕ = local rate of condensation.

It will be assumed that $u_s << U_\phi$ and that the velocity at the outside edge of the vapour boundary layer is given by the potential flow solution

$$U_\phi = 2U_\infty \sin\Phi \tag{2.29}$$

Substituting into eqn. (2.28)

$$\tau_M = j_\phi 2U_\infty \sin\Phi$$

From a mass balance and eqn. (2.11) it can be shown that

$$j_\phi = \frac{2}{d}\frac{dm}{d\Phi} = \frac{2}{d}\frac{k(T_s - T_w)d}{2\delta h'_{fg}}$$

$$= \frac{k(T_s - T_w)}{\delta h'_{fg}} \tag{2.30}$$

Thus

$$\tau_M = \frac{2U_\infty k(T_s - T_w)\sin\Phi}{\delta h'_{fg}} \tag{2.31}$$

For the variable temperature solution one obtains by differentiating eqn. (2.31)

$$\frac{d\tau_M}{d\Phi} = \frac{2U_\infty k}{h'_{fg}}\left[\frac{(T_s - T_w)\cos\Phi}{\delta} + \frac{\sin\Phi}{\delta}\frac{d(T_s - T_w)}{d\Phi} - \frac{\sin\Phi(T_s - T_w)}{\delta^2}\frac{d\delta}{d\Phi}\right]$$

Differentiating eqn. (2.22) w.r.t. Φ

$$\frac{d(T_s - T_w)}{d\Phi} = \frac{\alpha_e k(T_s - T_B)}{(k + \alpha_e\delta)^2}\frac{d\delta}{d\Phi} = \frac{k(T_s - T_w)}{\delta(k + \alpha_e\delta)}\frac{d\delta}{d\Phi} \tag{2.32}$$

and substituting into the above equation

$$\frac{d\tau_M}{d\Phi} = \frac{2U_\infty k(T_s - T_w)\cos\Phi}{h'_{fg}\delta} + \frac{2U_\infty k\sin\Phi(T_s - T_w)}{h'_{fg}\delta^2}\left(\frac{k}{k + \alpha_e\delta} - 1\right)\frac{d\delta}{d\Phi} \tag{2.33}$$

For the constant temperature solution

$$\frac{d\tau_M}{d\Phi} = \frac{2U_\infty k(T_s - T_w)\cos\Phi}{h'_{fg}\delta} - \frac{2U_\infty k\sin\Phi(T_s - T_w)}{h'_{fg}\delta^2}\frac{d\delta}{d\Phi} \tag{2.34}$$

Substituting τ_F and τ_M in eqn.(2.24) and $d\tau_F/d\Phi$ and $d\tau_M/d\Phi$ in eqn.(2.25) and then substituting for τ_s and $d\tau_s$ in eqn. (2.16) we obtain:

(i) for the variable outside tube wall temperature case

$$\frac{d\delta}{d\Phi} =$$

$$\frac{\frac{Ad^4}{2} - \left(\cos\Phi + 8\left(\frac{\rho_v}{\rho}\right) Fr\cos 2\Phi\right)\frac{\delta^4}{3} - \frac{a\delta^3}{2\rho g}\frac{d\tau_F}{d\Phi} - bARe_{TP}d^2\delta^2\cos\Phi}{\left(\sin\Phi + 4\left(\frac{\rho_v}{\rho}\right) Fr\sin 2\Phi\right)\delta^3 + \frac{a\tau_F\delta^2}{\rho g} + bARe_{TP}\sin\Phi\left(1 + \frac{k}{(k + \alpha_e\delta)}\right)d^2\delta} \qquad (2.35)$$

(ii) for the constant outside tube wall temperature case

$$\frac{d\delta}{d\Phi} =$$

$$\frac{\frac{Ad^4}{2} - \left(\cos\Phi + 8\left(\frac{\rho_v}{\rho}\right) Fr\cos 2\Phi\right)\frac{\delta^4}{3} - \frac{a\delta^3}{2\rho g}\frac{d\tau_F}{d\Phi} - bARe_{TP}d^2\delta^2\cos\Phi}{\left(\sin\Phi + 4\left(\frac{\rho_v}{\rho}\right) Fr\sin 2\Phi\right)\delta^3 + \frac{a\tau_F\delta^2}{\rho g} + bARe_{TP}\sin\Phi d^2\delta} \qquad (2.36)$$

It is emphasized here that A = f(Φ) for the variable temperature case, whereas A = constant for the constant temperature solution.

A similar procedure, though mathematically more complex, can be carried out for the power law approximation for the interfacial shear stress. This is shown in detail in Appendix A, the relevant equations for substitution into eqn. (2.16) for the variable temperature case are:

$$\tau_s = \left(\tau_F^n + \tau_M^n\right)^{1/n}$$

$$\frac{\delta^3}{\rho g}\frac{d\tau_s}{d\Phi} = \tau_s^{1-n}\left[\tau_M^{n-1} ARe_{TP}d^2\delta^2\cos\Phi + \frac{\delta^3\tau_F^{n-1}}{2\rho g}\frac{d\tau_F}{d\Phi}\right].$$

$$+ \tau_s^{1-n}\left[\tau_M^{n-1} ARe_{TP}d^2\delta\sin\Phi\left(\frac{k}{(\alpha_e\delta + k)} - 1\right)\right]\frac{d\delta}{d\Phi} \qquad (2.37)$$

2.1.4 Vapour flow separation

Beyond the point at which separation of the vapour boundary layer occurs, the interfacial shear stress will be reduced to almost zero, it may even become negative due to the presence of recirculating eddies, and the pressure becomes approximately constant. The only forces acting on the condensate may be taken to be the internal viscous forces and gravity,

which is the situation assumed in the basic Nusselt solution. It will be assumed, therefore, that beyond the separation point the local condensation rate is given by the Nusselt solution for which eqn. (2.16) reduces to

$$\frac{d\delta}{d\Phi} = \frac{\frac{Ad^4}{2} - \frac{\delta^4 \cos\Phi}{3}}{\delta^3 \sin\Phi} \tag{2.38}$$

The solution of this equation starts with the appropriate boundary conditions at the point of separation.

There is ample evidence (47, 48) to suggest that suction delays separation, and that the greater the suction, the closer the point of separation moves to the rear stagnation point. The only theoretical method of predicting the point of separation of a fluid flowing past a two-dimensional body with suction through its surface is that of Prandtl (46a). Starting from the two-dimensional boundary layer equations for laminar flow, and applying the appropriate boundary conditions, Prandtl was able to show that, in order to prevent separation, the suction velocity v had to satisfy the following condition

$$v > 2.18\sqrt{\left(-\frac{\mu_v}{\rho_v}\frac{dU}{dx}\right)} \tag{2.39}$$

where U is the local velocity at the edge of the vapour boundary layer. For a cylinder, from eqn. (2.29),

$$U = U_\phi = 2U_\infty \sin\Phi$$

$$\therefore \quad \frac{dU}{dx} = \frac{2}{d}\frac{dU_\phi}{d\Phi} = \frac{4U_\infty \cos\Phi}{d} \tag{2.40}$$

Substituting eqn. (2.40) into eqn. (2.39) and re-arranging, one obtains the following criterion for predicting that separation has not occurred at angle Φ

$$\frac{v_\phi}{U_\infty}\sqrt{(Re_v)} > 4.36\sqrt{(-\cos\Phi)} \tag{2.41}$$

where v_ϕ is the local suction velocity.

Note that this relation is only applicable for $\Phi > \pi/2$.

In the condensation process v_ϕ will vary around the cylinder with the local condensation rate

$$v_\phi = \frac{j_\phi}{\rho_v} \tag{2.42}$$

From a local energy balance - see eqn. (2.11) and eqn. (2.30) -

$$j_\phi = \frac{\alpha_\phi (T_s - T_w)}{h'_{fg}} \tag{2.43}$$

Substituting back into eqn. (2.41) for v_ϕ,

$$\frac{\alpha_\phi (T_s - T_w)\sqrt{(Re_v)}}{\rho_v h'_{fg} U_\infty} > 4.36\sqrt{(-\cos\Phi)} \qquad \Phi > \frac{\pi}{2} \tag{2.44}$$

becomes the criterion that will be used for predicting that separation has not occurred in the author's solution.

2.2 Numerical solutions

2.2.1 Method of solution

The differential equations (2.35) and (2.36) were integrated numerically using a Runge-Kutta method on an I.C.L.475 computer. The initial value of δ at $\Phi = 0$ was obtained from the boundary condition (2.17)

$$\frac{d\delta}{d\Phi} = 0 \qquad \text{at} \quad \Phi = 0$$

and this was calculated using the Newton-Raphson method of successive approximation for finding the roots of an equation. An integration step size of 0.04 radian was used. (It had been first established that the difference in the solution obtained for the average condensate h.t.c. using a step size of 0.04 radian and one of 0.01 radian was of the order of 0.2%.)

Physical property data were calculated from polynomials in terms of temperature which were obtained from a least-squares fit of the data in (49) over the temperature range used in the author's experiments. The only exceptions to this were the viscosity and Prandtl number of water where it was found more convenient to express the reciprocal of these quantities as a polynomial in terms of temperature. For details see Appendix B.

The saturation temperature was used for calculating the vapour properties and the reference temperature concept of Poots and Miles (21) for the condensate properties.

Having obtained the initial value of δ at $\Phi = 0$, the local value of the condensate h.t.c. was calculated from eqn. (2.19)

$$\alpha_{\phi=0} = \frac{k}{\delta_o}$$

and, in the variable wall temperature solutions, the local temperature

difference across the condensate layer was calculated from eqn. (2.22)

$$\Delta T_{\phi=0} = T_s - T_{w\phi} = \frac{\alpha_e \delta_o (T_s - T_B)}{\alpha_e \delta_o + k}$$

The local wall temperature $T_{w\phi}$ is then given by

$$T_{w\phi} = T_s - \Delta T_\phi \qquad (2.45)$$

and the local heat flux q_ϕ by

$$q_\phi = \alpha_\phi \Delta T_\phi \qquad (2.46)$$

The next value of δ (i.e. at $\Phi = 0.04$ radian) was then calculated using the Runge-Kutta method (50), and the above calculations repeated. This procedure was continued up to $\Phi = \pi$, or to the point of separation. When the latter effect was included in the analysis, the inequality (2.44)

$$\text{i.e.} \quad \frac{\alpha_\phi (T_s - T_{w\phi})}{\rho_v h'_{fg} U_\infty} \sqrt{(Re_v)} > 4.36 \sqrt{(-\cos\Phi)}$$

was tested for values of $\Phi > \pi/2$. If the inequality was found to be false (i.e. separation had occurred) then the differential equation for δ, either eqn. (2.35) or (2.36), was replaced by that of eqn. (2.38) and the solution, in other respects, was continued as before.

In the Dry Friction Model separation is predicted to occur at a fixed angle of 108.8° and therefore, beyond this angle, eqn. (2.38) was automatically substituted in place of eqn. (2.35) or (2.36).

The total rate of heat transfer per unit length of tube, Q/L, and the mean temperature difference across the condensate layer, ΔT_m, were obtained by applying the Trapezoidal Rule to the local values of heat flux and temperature difference.

The mean condensate h.t.c. was then calculated from

$$\alpha = \frac{Q}{\pi d L \Delta T_m} \qquad (2.47)$$

This was put in a non-dimensionalised form by dividing by the "Nusselt coefficient", α_{Nu}, deduced from eqn. (1.2) for a constant value of $(T_s - T_w)$ equal to the mean temperature difference ΔT_m. Results of α/α_{Nu} were plotted against the vapour velocity U_∞ made dimensionless in the form of the two-phase Reynolds number $Re_{TP} (= \rho U_\infty d/\mu)$.

2.2.2 Effect of interfacial shear stress term

The differential equation for the variable wall temperature case, eqn. (2.35), was solved without the pressure terms (i.e. the terms involving $Fr\rho_v/\rho$) for the following theories of interfacial shear:

(a) $\tau_s = \tau_F + \tau_M$ (this will be referred to as the M + G + F case, where M denotes inclusion of the momentum term, G the gravity term and F the "dry" friction term).

(b) $\tau_s = \tau_F$ (the G + F case).

In both these models the "dry" friction term can only be included up to an angle of 108.8^o.

Model (a) represents the highest value of interfacial shear stress expected. Model (b) represents the lowest value, with the possible exception of some cases when the predicted point of separation is at an angle less than 108.8^o.

The results for four sets of conditions are shown in Figs. 4 - 7, the first three representing different waterside conditions with steam at just above atmospheric pressure, and the fourth, conditions more typical of a power station condenser. The three different waterside conditions with the same saturation pressure correspond to different heat fluxes, and, for the purposes of identification within this thesis, will be referred to as the "high", "medium" and "low" heat flux conditions. The range of steam velocity covered in the first three figures is 0 - 10 m/s and the fourth 0 - 100 m/s, the corresponding mass velocities ($\rho_v U_\infty$) being 6 kg/m^2 s and 13 kg/m^2 s.

It is apparent that the effect of the vapour shear force is to produce a significant increase in the condensate h.t.c.. However, there is a substantial difference between the M + G + F and G + F theories, the former predicting much higher heat transfer coefficients than the latter. Comparison of Figs. 4 - 6 shows that the ratio α/α_{Nu} increases with heat flux according to the M + G + F theory (the line numbered 4 in Figs. 4 - 7), whilst it is almost independent of heat flux for the G + F theory (line number 10). This is to be expected as the momentum term is proportional to the local rate of condensation j_ϕ.

It should be noted that at zero velocity there is very good agreement with the Nusselt solution, even though a variable wall temperature has been assumed.

2.2.3 Effect of the pressure term

The differential equation for δ was solved for the same two cases as before, under identical conditions, but with the pressure terms included. These two cases will be referred to as the M + G + F + P (line number 6) and G + F + P (line number 11), P denoting inclusion of the pressure term. (In the G + F + P case the pressure term is only included as far as the separation point.)

The results are shown in Figs. 4 - 7. Comparison of the results with and without the pressure term (lines 6 and 4, and 11 and 10) show that at low velocity there is very little difference between them, but as the velocity increases the pressure terms reduce the value of α/α_{Nu}. The pressure probably has little effect over the forward half of the cylinder where the shear stress terms are high. However, beyond the point $\Phi = \pi/2$ the shear stress terms are becoming smaller, whilst the pressure is not only increasing but acting in the opposite direction to both the gravitational and shear forces. This will cause a thickening of the condensate layer in this region and the local and overall h.t.c.'s will be reduced.

Eventually a velocity is reached at which the pressure gradient is theoretically steep enough to prevent the condensate flowing away. The solution of the differential equation breaks down at this point as the denominator of eqn.(2.35) becomes equal to zero, $d\delta/d\Phi = \infty$, and thus δ becomes infinite. In practice this is obviously impossible, though there probably would be a sudden thickening of the liquid film. The point at which this phenomenon occurs moves forward from the rear stagnation point as the velocity is increased, and this is shown in Fig. 8 for the M + G + F + P theory by the lines marked "$\delta = \infty$". The curves (numbers 6 and 11) in Figs. 4 - 7 have been terminated at the point at which this phenomenon first occurs.

2.2.4 Effect of separation

The G + F theory, which is based on the Blasius solution for the shear stress, implies a constant angle of separation which has been included in the previous solutions already discussed in sub-section 2.2.2. Criterion (2.44) for predicting a variable point of separation was, therefore, just included in the M + G + F and M + G + F + P theories. The solutions are shown in Figs. 4 - 7 and the variation of separation angle in Fig. 8 by the lines marked "separation".

The solutions with and without the pressure terms (line number 5) are virtually identical. This is because, under the particular conditions

for which the equation was solved, separation occurs at an angle earlier than that at which the pressure term seriously affects the thickness of the condensate. Beyond the point of separation the pressure has been assumed constant and, therefore, has no effect. (Note: if separation occurs δ will not become infinite.)

At low velocities separation is close to the rear stagnation point and the reduction of α/α_{Nu} is small, but as the velocity is increased, the point of separation moves forward and produces quite a large reduction in α/α_{Nu}. This is particularly shown in Fig. 7, where for $Re_{TP} > 2.0 \times 10^5$ ($U_\infty > 60$ m/s) there is virtually no increase in the condensate h.t.c., in fact at higher values of Re_{TP} there is a slight decrease, and there is a large difference between the solutions with (line 5) and without (line 4) separation. This would appear surprising, as a large proportion of the heat transfer occurs before separation. The change in the mean condensate h.t.c. is not so much due to the reduction in the mean rate of heat transfer as to an increase in the mean temperature difference. A simplified example illustrates this fact.

Consider a cylinder of diameter d with an inside h.t.c $\alpha_i = 10$ kW/m^2 K and coolant temperature $T_B = 20\ ^oC$. Let the mean condensate h.t.c. for the upper half of the cylinder, $\alpha_u = 50$ kW/m^2 K and that for the lower half, $\alpha_L = 30$ kW/m^2 K. Assuming a saturation temperature of 60 ^oC and the tube wall thickness to be negligible, one finds for the upper half of the cylinder

$$T_s - T_w = \frac{\alpha_i}{\alpha_i + \alpha_u}(T_s - T_B) = \frac{10}{10 + 50}(60 - 20) = 6.67 \text{ K}$$

$$\therefore \quad Q_u = \alpha_u \frac{\pi d}{2}(T_s - T_w) = 50 \frac{\pi d}{2} 6.67 = 333 \frac{\pi d}{2} \text{ kW/m}$$

for the lower half

$$T_s - T_w = \frac{10}{10 + 30}(60 - 20) = 10 \text{ K}$$

$$Q_L = 30 \frac{\pi d}{2} 10 = 300 \frac{\pi d}{2} \text{ kW/m}$$

Total heat transfer rate

$$Q = Q_u + Q_L = 633 \frac{\pi d}{2} \text{ kW/m}$$

Mean temperature difference

$$\Delta T_m = \tfrac{1}{2}(10 + 6.67) = 8.33 \text{ K}$$

$$\therefore \quad \text{Mean condensate h.t.c.} \alpha = \frac{Q}{\pi d \Delta T_m}$$

$$= \frac{633}{2 \times 8.33} = 38 \text{ kW/m}^2 \text{ K}$$

Now assume that separation occurs and the mean condensate h.t.c. for the lower half of the cylinder is reduced to 10 kW/m^2 K.

Then for the lower half

$$T_s - T_w = \frac{10}{10 + 10} \quad (60 - 20) = 20 \text{ K}$$

$$Q_L = 10 \times \frac{\pi d}{2} \times 20 = 200 \frac{\pi d}{2} \text{ kW/m}$$

$$Q = Q_L + Q_u = 533 \frac{\pi d}{2} \text{ kW/m}$$

$$\Delta T_m = \tfrac{1}{2}(20 + 6.67) = 13.33 \text{ K}$$

$$\alpha = \frac{533}{2 \times 13.33} = 20 \text{ kW/m}^2 \text{ K}$$

Thus, although the mean rate of heat transfer has only been reduced by about 16% the condensate h.t.c. has been approximately halved because of the increase in the mean temperature difference across the condensate layer.

2.2.5 Constant wall temperature solutions

The differential equation (2.36), which assumes a constant wall temperature, was solved for the following cases:-

(1) M + G + F + P with and without separation

(2) M + G + F without separation

(3) G + F

To obtain a valid comparison in each case with the variable wall temperature solution, the mean wall temperature obtained from the corresponding variable wall temperature solution was used. The results are shown in Figs. 4 - 7.

Note that the phrase "constant wall temperature" only applies to the fact that there is no variation of wall temperature with angle and does not mean that along the curve shown the wall temperature is constant for all values of Re_{TP}. Moreover, any constant wall temperature solution can only be compared with the relevant variable wall temperature solution and not with another constant wall temperature solution, because different wall temperatures at a given value of Re_{TP} have been used,
i.e. $T_w \neq f(\Phi)$

$T_w = f(Re_{TP})$

$T_w = f$ (method of solution, i.e. G + F etc.)

In all cases the constant temperature solution is greater than the variable temperature solution, the difference increasing with increase in velocity. The greatest differences occur in the use of the M + G + F + P solution with variable separation (lines numbers 1 and 5), which is the solution with the largest variations in condensate h.t.c. and wall temperature around the cylinder periphery.

Consider the simplified examples of section 2.2.4 and,merely as an illustration,apply a constant wall temperature analysis to them.

Without separation:

$\Delta T_m = 8.33$ K

$\therefore \quad Q_u = \alpha_u \frac{\pi d}{2} \Delta T_m = 50 \times \frac{\pi d}{2} \times 8.33$

$= 416 \frac{\pi d}{2}$ kW/m

$Q_L = 30 \times \pi d \, \Delta T_m = 250 \frac{\pi d}{2}$ kW/m

$Q = 666 \frac{\pi d}{2}$ kW/m

$\therefore \quad \alpha = \frac{666}{2 \times 8.33} = 40.1$ kW/m^2 K

which is an increase of 5.5% over the variable temperature solution.

With separation:

$\Delta T_m = 13.33$ K

$Q_u = 50 \times \frac{\pi d}{2} \times 13.33 = 666 \frac{\pi d}{2}$ kW/m

$Q_L = 10 \times \frac{\pi d}{2} 13.33 = 133 \frac{\pi d}{2}$ kW/m

$Q = 799 \frac{\pi d}{2}$ kW/m

$\alpha = \frac{799}{2 \times 13.3} = 29.9$ kW/m^2 K

which is an increase of almost 50% over the variable temperature solution.

Thus where the ratio of the minimum temperature difference (i.e. at the forward stagnation point) to the mean temperature difference is close to unity, the constant wall temperature theory gives good agreement with the variable temperature solution; as this ratio decreases, the discrepancy between the two results increases.

2.2.6 Remaining shear stress theories

The shear stress terms predicted by the two remaining theories, viz. the Reynolds Flux Model and the Power Law, were substituted into the differential equation (2.16) and solved for the most general case i.e. with variable wall temperature, the inclusion of the pressure term and variable separation.

The Power Law solution for α was very similar to the corresponding M + G + F + P solution, being up to 3% less. This was to be expected as the maximum difference between these two methods of solution occurs when

$$\tau_F = \tau_M$$

and then the difference in the predicted total shear stress is only

$$= \frac{2 - 2^{1/1.375}}{2} \times 100 = 17.2\%$$

The difference in the h.t.c. would be less than this. For the particular conditions for which the equation was solved, τ_M was in general greater than τ_F and one would expect little difference between the two solutions, but, even for the cases where $\tau_M \simeq \tau_F$, the difference between the solutions did not justify the extra numerical effort required for the Power Law solution.

The Reynolds Flux Model solutions are shown in Figs. 4 - 7 as the M + G + P and 0.5 M + G + F + P curves (number 7 and 8). These are seen to lie below the corresponding M + G + F + P curve (number 5) as would be expected, the difference between the solutions depending entirely on the relative values of the M and F terms. At low velocities the 0.5 M + G + F + P solution is greater than that of the M + G + P theory, but as the velocity increases the F term ($\propto U_\infty^{3/2}$) starts to outweigh the M term ($\propto U_\infty$) and the solutions cross, except in Fig. 4, the "high" heat flux case, when the M term is still dominant due to the high value of the condensation rate j. According to the model of Wallis (33) one should use the 0.5 M + G + F + P solution for $\tau_F > 0.5\ \tau_M$ and the M + G + P solution for $\tau_F < 0.5\ \tau_M$. Only local values of τ_F and τ_M can be compared but at the intersection of the two solutions the effect of the F term on the condensate h.t.c. is equivalent to that of 0.5 M. Wallis's Reynolds Flux Model case, therefore, can be regarded as being approximately represented by the upper envelope of these two curves (numbers 7 and 8).

Experimental tests have been performed at conditions closely relating to those used in obtaining the theoretical results which have been discussed in this section and shown in Figs. 4 - 6. The experimental

results will be outlined and discussed, with reference to the various theoretical approaches taken, in section 2.5. A description of the experimental apparatus and the programme of tests will be given first.

2.3 Experimental apparatus

Several factors had to be considered in designing the experimental apparatus, the most important of which were:-

(1) a mass velocity of at least 3 kg/m^2 s,equivalent to that of saturated steam at a pressure of 50 mm Hg and velocity of 60 m/s, had to be achieved;

(2) The condenser tube outside diameter had to be typical of commercial condensers, i.e. 19 mm;

(3) tests were to be made with a small tube bank of which the minimum width would be three tubes with two half-tubes on the walls;

(4) the rise in the cooling water temperature had to be sufficient to ensure acceptable experimental accuracy, but small enough to keep the heat flux along the tube reasonably constant;

(5) a range of heat flux conditions was necessary;

(6) non-condensables were to be kept to a minimum.

In order to satisfy (6) the saturation pressure was to be kept slightly in excess of atmospheric, so that any leaks were of steam out rather than air in. The maximum steam mass flow rate was limited by the supply and equipment already available for condensing it. This fact together with points (1) to (4) above fixed the linear dimensions of the rig to within certain limits.

A photograph of the test rig is shown in Fig. 9. A line diagram of the experimental apparatus is shown in Fig. 10, which also shows the inundation system for tube bank tests which will be covered in more detail in section 3.2.

2.3.1 Steam line

Steam flowed from a main at approximately 10 bar through one of two sets of valves each comprising a gate valve, strainer, pressure control valve and pressure relief valve. One set of valves was used for the lower range of steam flow rates of 0 - 0.15 kg/s, and the other for steam flow rates of 0.17 - 0.25 kg/s. The steam pressure was reduced to between 1 and 1.2 bar at a point just upstream of the test section, depending on the mass flow rate required. The pipework from the valve trains to the test section was 7.6 mm nominal bore. A desuperheater which consisted of a 0.73 m length of 15.2 mm nominal bore pipe, with spray nozzles pointing in

the opposite direction to the steam flow, was inserted immediately after the valves. However, it was found that although the superheat was reduced, this was accompanied by drops of unvaporised water in the test section. These drops were very much larger in diameter than the spray size and it is thought that the small drops were deposited on the outside of bends in the pipework, coalesced, and were then either re-entrained into the steam flow or ran down the pipe wall. It was decided not to use the desuperheater and thus the steam was superheated by as much as 35 K when it entered the test section. (Superheat has been shown experimentally by Provan (51) to have little influence on the rate of condensation for condensation on a horizontal tube in static surroundings; and the same conclusion was reached by Ferreira (52) from a theoretical analysis of condensation on a horizontal tube in a moving vapour stream.) The steam entered the test section through a diffuser and flowed vertically over the condenser tube. Only a portion of the steam was condensed, the excess being required to achieve the desired value of approach velocity. On leaving the test section the steam turned through a sharp angled bend, Fig. 11, thus depositing most of the condensate in a collecting vessel. The steam finally flowed into a dump condenser where it was condensed and the condensate collected in a weigh tank before going to drain.

2.3.2 Cooling water system

The cooling water was taken from a softened water supply (but see section 2.4.5.2). It was desirable to have control over the mean cooling water temperature level and this was achieved by regulating the steam flow to a steam preheater, through which the cooling water was passed. The water then flowed through a globe valve, used for fine control, and the flow rate measured using a rotameter. Immediately preceding the test section was an entry length of 50 tube diameters to allow the fully developed velocity profile to be attained and thus minimize entry effects. Each end of the copper condenser tube, which was 19.05 mm o.d. and 15.875 mm i.d., was thermally insulated from the condenser walls by nylon bushes. On leaving the test section, the water flowed into a mixing chamber, Fig. 12, so that a uniform outlet temperature was obtained, and then through a Saunders valve,used to keep a back pressure within the condenser tube, to drain.

2.3.3 Test section

A diagram of the test section is shown in Fig. 13. Steam flowed in through the diffusing section, which was vaned to prevent channelling of

the flow. At the top of each vane was a small flap which could be adjusted to control the amount of steam flowing between each pair of vanes. At the exit from the diffuser there was an aluminium honeycomb followed by a brass gauze of 0.38 mm diameter wire on a 0.8 mm pitch which straightened the flow, damped out any large eddies and improved the flow distribution across the section.

The steam flow cross-section after the diffuser was 500 mm x 95.25 mm which at maximum flow rates gave an approach mass velocity of 5.25 kg/m^2 s (equivalent to a velocity of 8.8 m/s with steam at 1 bar).

The tapering parts at the top and bottom were made from stainless steel, while the central section was made from mild steel which was then cadmium plated (but note early unsatisfactory mode of construction discussed in detail in sub-section 2.4.2).

There were four windows in the test section so that observations could be made.

2.3.4 Instrumentation

2.3.4.1 Flow rates

The cooling water flow rate was measured using a Fischer and Porter rotameter, which was calibrated in position at three cooling water temperatures using a weigh tank and stopwatch. A calibration equation (Appendix C), incorporating a temperature correction factor, was then obtained using a least-squares fit.

The steam mass flow rate was obtained by measuring the time for a known mass of condensate to flow from the dump condenser into the weigh tank. The small amount of condensate overflowing from the condensate collecting vessel during this time was also included. With knowledge of the steam mass flow rate, the flow area, steam temperature and pressure, the steam approach velocity could be calculated.

2.3.4.2 Pressure

A Bourdon pressure gauge was fitted just downstream of each pressure control valve.

The static pressure of the steam in the test section was taken through a tapping in the side wall and measured with a mercury manometer. The lines, between the point at which the pressure was measured and the manometer, were made to slope downwards to a condensate collecting pot so

that they were not blocked with water.

2.3.4.3 Temperature

The majority of the temperature measurements were made using 0.18 mm diameter copper/constantan enamelled and glass wound thermocouples. The thermocouple wire was calibrated in an oil bath over the range 20 °C to 100 °C using NPL calibrated mercury-in-glass thermometers. The calibration is given in Appendix C.

Three thermocouples were used to measure each of the following temperatures:

(a) steam temperature in the test section,
(b) cooling water temperature at inlet to the entry length,
(c) cooling water temperature at outlet from the mixing chamber,

and were connected generally as shown in Fig. 14.

The condenser tube wall temperature was measured by three thermocouples set at 83.3 mm, 250 mm and 417.7 mm from the inlet of the working tube. These thermocouples were laid in slots 10 mm long, 1 mm deep and 0.8 mm wide which were spark eroded in the tube wall (Fig. 15).

The thermocouple wires passed through a 1 mm hole drilled at one end of each slot into the inside of the tube, inside which they then ran along before leaving through the side of the mixing chamber. The thermocouples were held in position by filling the slot with a conducting cement, Eccobond Solder 57C, which cures at room temperature. The tube could be rotated about its axis and thus the peripheral variation of tube wall temperature could be obtained.

The cooling water temperatures at inlet to the entry length and exit from the mixing chamber were also measured by two Rosemount Type BSE 712-F4 resistance thermometers. These were supplied with Rosemount Type E32015 matched linear temperature transmitters, which gave a linear output of 1 mV per °C measured. The cooling water temperature rise was measured by connecting the temperature transmitters (Fig. 16) so that the individual outputs from the two thermometers and the difference between them could be read.

The thermocouple e.m.f.s and the voltage output from the resistance thermometer transmitters were measured using a Solartron A200 digital voltmeter with a sensitivity of 1 μV.

2.4 Experimental work on single tube

2.4.1 Experimental procedure

The procedure for starting up the rig and carrying out an experimental test was as follows:-

(a) the working tube was cleaned with wet-and-dry paper and washed to ensure that the surface was fully wetted;

(b) the cooling water supplies to the working tube and dump condensers were turned on;

(c) the steam supply was turned on, with the vent on the dump condenser open, and steam allowed to flow through the rig for a few minutes. The vent was then closed and the steam supply was set to the desired value;

(d) the cooling water flow rate was adjusted and steam allowed into the cooling water preheater. The steam flow to the preheater was adjusted until the mean of the cooling water inlet and outlet temperatures was within ± 0.5 K of the required temperature level;

(e) once the cooling water inlet temperature reached a steady level, a few minutes were allowed before results were taken;

(f) the valve on the weigh tank was closed and whilst the condensate from the dump condenser was being collected, three sets of readings of all the individual temperatures, cooling water temperature rise and flow rate, and steam pressure were taken;

(g) provided that the three sets of readings were consistent within acceptable limits, another set of test conditions was then set up;

(h) the three sets of readings for each test were averaged for calculating the results.

2.4.2 The presence of dropwise condensation

Dropwise condensation is often encountered during the initial stages of condensation experiments. This is generally attributed to dirt or grease either on the condensation surface or within the apparatus. However, with careful cleaning of the condensation surface and continued running of the apparatus, in effect steam cleaning it, the mode of condensation changes from dropwise to filmwise.

The early behaviour in the tests reported here was completely opposite to this. On practically every occasion on which the rig was run, the mode of condensation started off as filmwise. After a period of time,

which varied from a few minutes to two hours or more, patches of dropwise condensation started to form and these gradually increased in size until the entire tube surface was covered. This situation was maintained until the rig was shut down.

At first it was thought that the method of cleaning the tubes was not thorough enough. Various cleaning methods were tried including combinations of the following:-

(a) wet-and-dry paper;
(b) use of solvents;
(c) washing with soap and water;
(d) washing with demineralised water or tap water.

The tube was always finally washed with either demineralised or tap water to check that the surface wetted completely, i.e. the water ran over the surface as a film and did not tend to run into drops. It was concluded that the best method of cleaning was the use of wet-and-dry paper with plenty of water, followed by a final wash with tap water. The surface did not wet as well when either solvents or soap and water were used. Although great care had been taken in cleaning the tubes, the problem of dropwise condensation persisted. When the tubes were removed from the condenser and washed with tap water the surface no longer wetted as before, but the water ran off the tube rather like that off a duck's back indicating a change in the nature of the surface.

Contamination of the steam supply, possible causes of which could have been carry over of impurities from the boiler or a leaking feed pump gland, could have accounted for the occurrence of dropwise condensation. The steam is raised at a nearby hospital and their engineering staff confirmed that every precaution was taken to ensure the purity of the steam supply. The steam has to travel a distance of about 600 metres from the boiler-house and it was thought that, if there was a source of contamination in this line, its effect would be reduced by taking large steam flows. The rig was therefore run with a very large by-pass flow of steam but this did not noticeably change the onset of dropwise condensation.

One basic difference between this rig and other condensation rigs at Bristol University was the nature of the internal surface. The rig had been constructed primarily of mild steel and to prevent corrosion it had been dipped in a zinc phosphate bath and then the internal surfaces had been coated with either aluminium or a two component neoprene paint (Adcora Neoprene P6, manufactured by E. & F. Richardson Ltd., Buckingham).

It was possible that the steam was leaching something out of either or both of these paints and this was affecting the condensation process. The Surface Chemistry Department at the University was consulted, and agreed that this was a possibility. As a preliminary test to check this theory, samples of condensate were taken from the rig and from points immediately before and after the rig. The surface tension of each was measured and found to agree with the value for double distilled water of 72 x 10^{-3} N/m at room temperature.

A small condensation rig was built to obtain further information on the effect of the two paints on the mode of condensation. This consisted of a QVF glass tube 105 mm dia. x 1 m long, and placed axially within this was a 19 mm o.d. copper tube through which cooling water passed. Steam was supplied at 1 bar through equally spaced holes drilled in the side of another copper tube, which ran the length of the condenser and was orientated so that the holes faced away from the condensation tube, Fig. 17. The steam for the small condenser was taken from a point immediately upstream of the main test rig so that any contamination of the supply would be included.

The condensation tube was cleaned in exactly the same manner as the tubes for the main condensation rig. When steam was first admitted to the rig the condensation started off as an apparent mixture of filmwise and dropwise. The droplets were, however, much flatter than those that had appeared in the main experimental rig and they did not run off the tube so easily. This is in line with previous experience at Bristol University and it is suspected that this is not a true representation of dropwise condensation but merely an unstable form of filmwise condensation. To ensure that condensation started off in the filmwise mode, the rig was flooded with water until the tube was submerged, steam was then admitted and the water level gradually reduced. The rig was run for several hours and the condensation was filmwise throughout.

A strip 150 mm x 25 mm of thin mild steel sheet was coated with the neoprene paint and this was suspended inside the QVF tube. The rig was started as before and soon after admitting steam, dropwise condensation began to appear immediately beneath the paint sample. This gradually spread until a length of about 300 mm of the condenser tube beneath and to either side of the paint sample was covered with dropwise condensation. The remaining 700 mm of the tube was covered with filmwise condensation and this situation remained for about five hours, after which the rig was shut down. This test was repeated with the same result, and thus provided

evidence that the neoprene paint was the probable cause of the dropwise condensation.

A similar strip of mild steel was coated with the aluminium paint and tested in the same manner. This also promoted a small area of dropwise condensation but not to the same extent as the neoprene sample. The only other materials used in the experimental rig were nylon and neoprene sheet,both of these were tested but were found to have no effect.

Two further strips 300 mm x 25 mm of mild steel were coated with neoprene and aluminium paints and then boiled in water. The vapour produced was condensed and the surface tension measured and found to be 54×10^{-3} N/m for the neoprene and 62×10^{-3} N/m for the aluminium compared with 72×10^{-3} N/m for water. This again indicated that both the paints could cause dropwise condensation, and confirmed the observations made previously that the neoprene paint was more likely to do so than the aluminium paint. It should be remembered, though, that the concentration of impurity in the experimental rig was not high enough to have produced a detectable fall in the surface tension of the condensate.

A brass tube and an aluminium tube were tested separately in the original neoprene painted condenser. Both tubes were cleaned in exactly the same way as the copper tubes had been. Condensation started as filmwise on both tubes but soon changed to dropwise on the brass tube. However, the condensation remained filmwise on the aluminium tube for the duration of three days testing. The aluminium tube would presumably have formed an outside layer of aluminium oxide, which would not have combined so readily with any impurity as would the copper or brass tube. This evidence led to the conclusion that the dropwise condensation was caused by a change in nature of the tube surface, due to an impurity in the condensate originating from the neoprene paint.

As neoprene sheet had been shown to have no effect on the mode of condensation, it was thought likely that the source of the trouble was some additive in the paint, such as a plasticiser or solvent. A brief outline of the problem was sent to the paint manufacturers and their help requested in identifying any such additive. They replied that there were traces of aromatic hydrocarbons and chlorinated paraffins in the paint.

They thought that the substance most likely to be causing the trouble was Vulcafor B.A. which is believed to be a condensation product of an aromatic amine and an aldehyde. It is well known that long chain

aliphatic amines are sometimes added to steam systems to promote dropwise condensation. The polar amine group attaches itself to the copper surface, leaving the hydrophobic hydrocarbon chain sticking out, thus giving a surface which is not easily wetted. It is probable that other compounds with one end of the molecule polar and the other hydrocarbon, would act in a similar manner.

As a result of this investigation the following modifications were made to the rig:

(a) the top and bottom diffuser sections were replaced with similar ones made of stainless steel;

(b) the central part of the test section was thoroughly cleaned and cadmium plated;

thus all traces of the aluminium and neoprene paint were removed. After these changes, apart from an occasional localised patch of dropwise condensation, there was no difficulty in obtaining and maintaining filmwise condensation.

2.4.3 Energy balance

The analysis of the experimental results was primarily based on the amount of heat transferred from the steam to the cooling water and it was, therefore, important that this quantity could be calculated to within a known accuracy. Either the heat lost by the steam or the heat gained by the cooling water could be measured, but only the latter method was suitable for all test conditions. However, it was decided to carry out a series of tests where the heat transferred was calculated using both methods, so that an energy balance could be made in order to verify the calibration of the instrumentation.

Before this was done some preliminary tests were made so that the error due to heat loss along the entry length could be accounted for. The cooling water was to be heated to temperatures of up to 65 ^{o}C at entry and, though the entry length was lagged, the temperature drop along this length would not be entirely negligible compared with the temperature rise in the test section. Thg mixing chamber with the outlet resistance thermometer and thermocouples was connected to the downstream end of the entry length. Tests were run at various water flow rates and temperatures and the drop in temperature, as measured by the difference in reading of the resistance thermometers, was recorded. The results are shown in Fig.18.

The measured temperature loss appeared to depend on the cooling water inlet temperature and to be independent of the flow rate. The temperature loss along the entry length was, therefore, correlated as follows:

$$\Delta T_{EL}/K = 0.00197\ T_{IN}/^{o}C + 0.0267 \qquad (2.48)$$

The correction for any difference in calibration of the two resistance thermometers is also incorporated in this equation.

The only modification to be made to the experimental apparatus for the energy balance tests was the provision of a tray for collecting the condensate. This was done by placing a copper tube, the top quarter of which had been milled away, directly beneath the condensation tube. One end of the collecting tube was closed and the condensate drained away through a pipe leading from the other end, through a valve to a collecting vessel, Fig. 19.

The steam velocity was kept very low to reduce the possibility of entrainment of the condensate. The cooling water flow rate and inlet temperature were adjusted to the required values and the valve in the condensate line set so that steam was not blowing through. When conditions were steady, the condensate was collected for a measured length of time.

In all, 70 energy balances were made, covering the following ranges:

Cooling water mass flowrate	0.137 - 0.517	kg/s
" " inlet temperature	23.4 - 51.2	^{o}C
" " temperature rise	3.33 - 11.68	K
Heat flux	1.76 - 3.38	kW/m^2

Heat lost by steam = heat gained by cooling water

$$Q_{st} = Q_{cw}$$

where

$$Q_{cw} = m_{cw}\ c_{p_{cw}}\ \Delta T_{cw} \qquad (2.49)$$

$$Q_{st} = w\left[h_{fg} + c_{p_{st}}(T_{st} - T_s) + c_p(T_s - T_{sub})\right] \qquad (2.50)$$

where

w = rate of condensation on the tube

T_{sub} = bulk mean temperature of condensate

As the condensate is subcooled when it falls into the collecting tray, further condensation will take place in the collecting tube and the measured

rate of condensate flowing into the collecting vessel will be greater than that flowing from the condenser tube.

An analysis of the heat transfer to the condensate collection tube shows,

$$(w' - w)\left[h_{fg} + c_{p_{st}}(T_{st} - T_s)\right] \leq w(T_s - T_{sub})c_p \qquad (2.51)$$

where w' is the flow rate of condensate into the collecting vessel, and if it is assumed that the two sides of (2.51) are in fact equal, i.e. all of the subcooling is compensated for by further condensation in the collecting tube, eqn. (2.50) can be re-written as

$$Q_{st} = w'\left[h_{fg} + c_{p_{st}}(T_{st} - T_s)\right] \qquad (2.52)$$

The maximum error in calculating Q_{st} due to the above assumption would occur if there was no further condensation in the collection tube. Making use of the method outlined in section (2.1.1) for allowing for subcooling, together with the facts that the maximum value of $(T_s - T_w)$ in the energy balance tests was calculated to be 40 K and the superheat was negligible, the maximum error, defined as the (predicted-actual)/(actual value of Q_{st}), can be estimated as follows:

$$\% \text{ Error} = \frac{-c_p(T_s - T_{sub}) \times 100}{h_{fg} + c_p(T_s - T_{sub})} = \frac{-0.68\ c_p(T_s - T_w) \times 100}{h_{fg} + 0.68\ c_p(T_s - T_w)}$$

$$= \frac{-0.68 \times 4.18 \times 40 \times 100}{2257 + 0.68 \times 4.18 \times 40}$$

$$= -4.8\%$$

The error in the energy balances was calculated from

$$\frac{Q_{st} - Q_{cw}}{Q_{cw}} \times \frac{100}{1}$$

where Q_{st} was obtained from eqn. (2.52) and Q_{cw} from eqn. (2.49), and was found to range from - 5.04% to + 0.88% with a mean value of - 2.3%. The largest negative errors occurred when the effect of subcooling was at a maximum i.e. large $(T_s - T_w)$. It seems likely, therefore, that some of this error can be attributed to the assumption made earlier about the compensation for subcooling. However, apart from this there was good agreement between the quantity of heat calculated from the measurements on the steam and cooling water sides. The error in measuring the cooling water flow is estimated as ± 1.5% and in measuring the temperature difference

± 2%, thus giving a maximum probable error in the calculation of the heat transferred to the cooling water of ± 2.5%.

2.4.4 Measurement of velocity profile across the test section

The variation of steam velocity across the test section had to be measured to check that the velocity distribution was reasonably uniform so that, if required, adjustment could be made to the flaps on the leading edges of the diffuser vanes.

The original intention was to use a pitot tube to measure the variation of stagnation pressure across the duct and to measure the static pressure from the tapping in the wall of the duct. The variation in velocity head, and hence velocity, could then be calculated. Unfortunately, no sensible readings were taken using this method due to condensation in the line from the pitot tube to the inclined manometer.

The pitot tube was replaced with a stainless steel pitot-static tube, the horizontal limb of which was wrapped with electrical heating tape. This assembly was covered with a stainless steel tube to provide a surface suitable for an O-ring seal so that it could be moved across the rig without leaking. A thermocouple was inserted between the heating tape and the pitot-static tube so that the outside surface temperature of the latter could be kept at 190 ^{o}C. This was the limiting temperature of the heating tape and was significantly higher than the saturation temperature of the steam. Even with this system, there was still condensation occurring, particularly in the pitot line. An attempt was made to try and keep the lines free from condensation by allowing steam to flow through the pressure lines until just before a reading was to be taken, when this steam purge was shut off. There was still insufficient time for a reading to be taken before one of the lines was blocked by condensate. Therefore, some alternative method of measuring velocity was sought.

A DISA type 55D01 anemometer unit was used in conjunction with a type 55P13 right angled probe and a 55D30 digital DC voltmeter. The anemometer probe was traversed across the centre line of the test section at the same point at which the condenser tube was to be positioned. A thermocouple was attached to the probe support to measure the local steam temperature so that variations in temperature across the duct could be compensated for.

Tests were performed over a range of total steam flows, and as only relative velocities were required, a non-dimensional velocity profile across

the duct was calculated as shown in Appendix D. The initial tests were performed without the honeycomb and it was found that the diffuser was directing the flow out to the sides of the duct. The honeycomb overcame this problem and then the flaps on the diffuser vanes were adjusted to obtain the flattest profile possible. The results of the tests, Fig. 20, indicated that there was little change in the profile at different velocities. Most of the profile fell within ± 10% of the mean velocity and the maximum variations were + 13.6% and - 18.2%. The mean value of the non-dimensionalised velocity for each of the five sections formed by drawing vertical lines from the base of each diffuser vane, was approximately one (i.e. the mean value of the velocity was the same in all the sections) and it was thought that this was probably the best profile that could be achieved.

2.4.5 Calculation of waterside heat transfer coefficient using a modified Wilson Plot

2.4.5.1 Calculations for clean tube

The condensate h.t.c. can be obtained in two different ways:

(a) from measurement of the tube wall temperature;

(b) by subtracting the reciprocal of the waterside and wall h.t.c.'s from that of the overall h.t.c.

The measurement of the tube wall temperature is time-consuming, and indeed difficult to perform reliably; therefore most of the tests were run without wall thermocouples and the condensate h.t.c. calculated using the second of the above methods. This requires knowledge of the waterside h.t.c., for which there are many published data, but because of the variation of coefficient predicted by the various methods, a check was made using a modified Wilson Plot (53).

The overall h.t.c. is given by:

$$\frac{1}{\alpha_o} = \frac{1}{\alpha} + \frac{1}{\alpha_w} + \frac{d}{d_i \alpha_i} \qquad (2.53)$$

In the absence of fouling the inside h.t.c. α_i is equal to the waterside h.t.c., α_{cw}, which is generally expressed in the form

$$Nu_{cw} = \frac{\alpha_{cw} d_i}{k_{cw}} = \varepsilon \, \Omega \qquad (2.54)$$

where ε = constant

$\Omega = f(Re_{cw}, Pr_{cw}, \text{geometry})$.

For tests at zero steam velocity the condensate h.t.c. can be written using the Nusselt equation (1.2).

$$\alpha = 0.728 \left(\frac{k^3 \rho^2 g h'_{fg}}{\mu d \ (T_s - T_w)} \right)^{\frac{1}{4}} \tag{2.55}$$

Substituting for $(T_s - T_w)$ from

$$Q = \pi \ dL\alpha \ \ (T_s - T_w) \tag{2.56}$$

into eqn. (2.55) we can write

$$\alpha = \gamma \nu^{1/3} \tag{2.57}$$

where $$\nu = \frac{k^3 \rho^2 g h'_{fg}}{\mu} \frac{\pi L}{Q} \tag{2.58}$$

and γ = constant

$\gamma_{Nu} = 0.655$

Thus substituting (2.57) and (2.54) into (2.53) and re-arranging,

$$\nu^{1/3} \left(\frac{1}{\alpha_o} - \frac{1}{\alpha_w} \right) = \frac{1}{\gamma} + \frac{d\nu^{1/3}}{\varepsilon \Omega d_i} \qquad \backslash k_{cw} \tag{2.59}$$

Let $$Y = \nu^{1/3} \left(\frac{1}{\alpha_o} - \frac{1}{\alpha_w} \right) \tag{2.60}$$

$$X = \frac{d\nu^{1/3}}{\Omega d_i} \qquad \backslash k_{ow} \qquad \begin{matrix} YCM \\ 28.4.76 \end{matrix} \tag{2.61}$$

Eqn. (2.59) becomes

$$Y = \frac{1}{\gamma} + \frac{X}{\varepsilon} \tag{2.62}$$

By plotting Y against X a straight line should be obtained with slope $(1/\varepsilon)$ and intercept on the Y axis of $(1/\gamma)$.

Tests were run at a low steam velocity (< 0.5 m/s) with different waterside conditions, and a plot of Y against X made using the equations for predicting the waterside h.t.c. of Hausen, Dittus-Boelter, Everett and Allan and Eckert. The data were correlated best using the equation of Allan and Eckert,

$$Nu_{cw} = 0.00123 \ C_L \ Re_{cw} \ Pr_{cw}^{0.42} \left(1 + 25 Re_{cw}^{-0.27} \right) \left(\frac{\mu_{cw}}{\mu_i} \right)^n \tag{2.63}$$

where the correction C_L for the thermal entry effect is

$$C_L = 1 + \frac{0.96(7/Pr_{cw})^{0.42}}{(L/d_i)} \tag{2.64}$$

Re_{cw}, Pr_{cw} and μ_{cw} are all calculated at the bulk mean temperature of the cooling water, and

$$n = \left(\frac{Re_{cw}}{8.7 \times 10^5}\right)^{0.84} \qquad Re_{cw} \leqslant 6.25 \times 10^4$$

$$n = 0.11 \qquad Re_{cw} > 6.25 \times 10^4$$

The plot of Y versus X is shown in Fig. 21, from which the values of $\gamma = 0.662$ and $\varepsilon = 0.00124$ were obtained. These compare well with the theoretical values of $\gamma_{Nu} = 0.655$ and $\varepsilon_{AE} = 0.00123$ from eqns. (2.55) and (2.63) respectively. It had been expected that the value of γ may well have been higher as, although the tests were run at the lowest steam flow possible, this was still theoretically high enough to produce a rise in the condensation h.t.c. above that predicted by Nusselt.

2.4.5.2 Correction for dirt coefficient

It was suspected during the initial tests with inundation on the square tube bank that there could have been some fouling of the inside of the working tube. It was not immediately apparent from visual inspection whether this was the case, and so the inside of the tube was cleaned using wet-and-dry paper, and a further set of tests run to establish another modified Wilson Plot. This is shown in Fig. 22, and gives values of $\gamma = 0.69$ and $\varepsilon = 0.00127$. Comparing these with the theoretical values γ_{Nu} and ε_{AE}, we obtain

$$\frac{\gamma}{\gamma_{Nu}} = 1.052$$

$$\frac{\varepsilon}{\varepsilon_{AE}} = 1.032$$

Thus, as expected, there was a slight increase in the condensate h.t.c. due to the small vapour velocity, and the agreement between the experimental and predicted waterside h.t.c.'s was within 3.5%.

The value of the dirt h.t.c. during the previous Wilson Plot tests was evaluated by comparing Fig. 21 and Fig. 22. Re-writing eqn. (2.53) to include the dirt coefficient α_D, we obtain

$$\frac{1}{\alpha_o} = \frac{1}{\alpha} + \frac{1}{\alpha_w} + \frac{d}{d_i \alpha_{cw}} + \frac{d}{d_i \alpha_D} \quad , \qquad (2.65)$$

where the substitution

$$\frac{1}{\alpha_i} = \frac{1}{\alpha_{cw}} + \frac{1}{\alpha_D}$$

has been made. Eqn. (2.65) becomes, on making the substitutions from eqn. (2.61) and (2.60) for X and Y

$$Y = \frac{1}{\gamma} + \frac{X}{\varepsilon} + \frac{d\nu^{1/3}}{d_i \alpha_D} \tag{2.66}$$

The value of $d\nu^{1/3}/d_i\alpha_D$ is the difference between the two values of Y at a given value of X. The two Wilson Plots are not parallel because ν is a variable, dependent on the heat flux. The value of $d\nu^{1/3}/d_i\alpha_D$ was evaluated at each end of the Wilson Plot and, using the corresponding values of ν, it was found that

$$0.0057 < \frac{d}{d_i \alpha_D} < 0.0069$$

$$212 > \alpha_D > 174 \text{ kW/m}^2 \text{ K}$$

This only indicates the value of the dirt coefficient at the start of the test programme and there was probably an increase in the dirt coefficient as the tests proceeded. Tests from different parts of the programme which had been completed, including tests on a single tube and on the square tube bank with and without inundation, were repeated. A comparison was then made, Fig. 23, between the reciprocal of the overall h.t.c. with the clean tube and that of the dirty tube under similar test conditions, the relation between them being

$$\frac{1}{\alpha_{o_{dirty}}} = \frac{1}{\alpha_{o_{clean}}} + \frac{d}{d_i \alpha_D} \tag{2.67}$$

If the dirt coefficient had remained constant, then the points on Fig. 23 should all lie on a straight line with a slope of 45^o, and if there had been a gradual increase in the dirt coefficient, the later tests should have shown a larger difference between $1/\alpha_{o_{dirty}}$ and $1/\alpha_{o_{clean}}$ than the earlier tests. Examination of Fig. 23 shows that the results are scattered about the line

$$\frac{1}{\alpha_{o_{dirty}}} = \frac{1}{\alpha_{o_{clean}}} + 0.01 \tag{2.68}$$

and, although there was a tendency for the earliest tests to show a lower value of dirt coefficient than the later tests, it was difficult to correlate this. This was probably due to the fact that the differences between $1/\alpha_{o_{dirty}}$ and $1/\alpha_{o_{clean}}$ are of the same order as the experimental error.

All the results up to the point at which the tube was cleaned were, therefore, calculated from eqn. (2.65), using eqn. (2.63) for the waterside coefficient, but with the constant 0.00127 as obtained from the Wilson Plot instead of 0.00123, and a constant value of $d/d_i\alpha_D = 0.01$ m^2K/kW.

The maximum error expected in the calculation of α/α_{Nu} as a result of assuming a constant value for the dirt coefficient, will be at the highest values of the condensate h.t.c., i.e. for tests at high velocity without inundation. It was calculated that a variation of ± 0.005 m^2 K/kW from the assumed value of $d/d_i\alpha_i$ would result in an error of up to 11% in the predicted value of α/α_{Nu}.

2.4.6 Programme of experimental test conditions

As all the tests were to be run at approximately the same saturation conditions, the vapour and condensate properties cannot be regarded as true variables. Examination of eqns. (2.14), (2.26) and (2.31) shows that the two parameters which will determine the condensate h.t.c. are the steam velocity, U_∞, and the temperature difference across the condensate, $(T_s - T_w)$. It would have been desirable to have kept one of these quantities constant and varied the other. However, as most of the tests were to be run without wall thermocouples it would not be possible to obtain the value of $(T_s - T_w)$ directly. It was decided, therefore, to maintain the same cooling water conditions (i.e. constant α_i and T_B) and to vary the steam velocity. Three sets of tests were made with mean cooling water bulk temperatures of 36.5 °C, 48 °C and 68.5 °C. The inside coefficient was kept at the maximum that could possibly be maintained at these temperatures, to reduce the error in the calculation of the condensate h.t.c.

Two sets of tests were run with wall thermocouples. It was possible with these tests to obtain some indication and control of the value of $(T_s - T_w)$, and this was maintained at around 27.5 K and 14.5 K, while the steam velocity was varied through the full range.

During the initial tests with wall thermocouples, temperature readings were made at 0°, 30°, 60°, 90°, 120°, 150°, 180° and at 0°, 45°, 90°, 135°, 180°; as there were three wall thermocouples, this gave a total of 21 and 15 temperatures respectively from which the mean tube wall temperature was calculated. A comparison was made between the mean wall temperatures obtained from the two sets of readings, Fig. 24, and they are seen to be within ± 0.6 K. The minimum steam/tube wall temperature

difference to be measured was expected to be about 10 K and so this represents an error of 6%. It was decided that the time involved in taking wall temperature measurements did not warrant taking any more than 21 readings, but to obtain reasonable accuracy, readings were taken at 0^{o}, 30^{o}, 60^{o}, 90^{o}, 120^{o}, 150^{o} and 180^{o} in all further tests.

The method of calculating the experimental results is outlined in Appendix E, and a summary of the experimental readings is given in Appendix H.

2.5 Discussion of experimental results from single tube tests

2.5.1 The effect of vapour velocity and heat flux on the mean condensate h.t.c.

The results from the experimental tests on a single tube are shown as graphs of α/α_{Nu} plotted against Re_{TP} in Figs. 25 and 26. It should be noted that α_{Nu} was calculated separately for each point from Nusselt's formula using the particular saturated steam/wall temperature difference for that test.

Fig. 25 shows the results obtained under three different sets of cooling water conditions, where the condensate h.t.c. was calculated using the method without wall thermocouples described in Appendix E. The range of temperature differences across the condensate layer for each set of results is also shown. Fig. 26 shows the results for tests performed with an approximately constant wall temperature, where the condensate h.t.c. was obtained directly from the measured mean wall temperature and overall h.t.c.. The two sets of figures show the same trends and where the conditions (saturated steam/wall temperature difference and steam velocity) are similar there is good agreement between them.

i.e. For $T_s - T_w = 27$ K $\quad Re_{TP} = 0.7 \times 10^5$

From Fig. 26 $\alpha/\alpha_{Nu} = 1.3$

From Fig. 25 $1.26 < \alpha/\alpha_{Nu} < 1.34$

For $T_s - T_w = 14.5$ K $\quad Re_{TP} = 4.64 \times 10^5$

From Fig. 26 $\alpha/\alpha_{Nu} = 1.66$

Fig. 25 $\alpha/\alpha_{Nu} = 1.57$

Figs. 25 and 26 indicate that, compared with the value at zero velocity, there is a significant rise in the condensate h.t.c. with increase in steam velocity and that the amount by which the ratio α/α_{Nu} increases is strongly influenced by the heat flux, i.e. the greater the heat flux (or $(T_s - T_w)$) the greater the effect of increase in vapour velocity.

The same result was found experimentally by Fuks (6) and Berman and Tumanov (25). Unfortunately, almost all the present experimental data lay outside the narrow limits imposed by Berman and Tumanov on the use of their correlation, eqn. (1.11), but for the few points which were within the limits, the values of α/α_{Nu} were much less than those predicted by eqn. (1.11). The same problem arose in comparing the experimental data with Fuk's equation (1.9) as the range of temperature differences, steam velocity and pressure were somewhat different to his. The only experimental data for which some comparison can be made with Fuks' equation are shown in Fig. 29. The agreement over the limited velocity range is within 10%. It should be noted that these tests are those at the lowest heat fluxes. At the higher heat fluxes, which were outside the limits imposed by Fuks on the use of his equation, the experimental results were consistently higher than those predicted by eqn. (1.9).

The equations of Shekriladze and Gomelauri (29), eqns. (1.27) and (1.29), and Fujii et al (37), eqn. (1.35), along with some of the numerical solutions from section 2.2 are shown compared with the experimental data in Figs. 27 - 29. It should be remembered that the numerical solutions are based on the experimental cooling water conditions from which a theoretical wall temperature distribution is obtained, whereas the curves for the equations of Fuks, Fujii et al, and Shekriladze and Gomelauri, are all based on the mean wall temperatures calculated from the test results.

Shekriladze and Gomelauri's equation is an approximation to the M + G theory with constant wall temperature. Equation (2.36) was solved for velocities of 0 - 10 m/s and constant steam/wall temperature differences of 14.5 K and 27 K with $\tau_S = \tau_M$ (i.e. the M + G theory). The pressure terms and separation were excluded, and the results compared with eqn. (1.27). Agreement was within 1.5% which validates the approximate mathematical approach used by Shekriladze (30) in obtaining eqn. (1.27). The equation of Fujii is a mathematical approximation to numerical data obtained from solution of the boundary layer equations, assuming a constant wall temperature and no separation. Comparing the values of α/α_{Nu} from Fujii's equation as shown in Figs. 27 - 29 with the numerical solutions shown in Figs. 4 - 6, it would appear that at low velocities Fujii's equation approaches the G + F theory, whilst at higher velocities it approaches the M + G + F theory with constant wall temperature.

Examination of Figs. 27 - 29 shows that the experimental results do not follow any one predicted solution. In Fig. 27 and Fig. 28 the

experimental results lie close to the M + G + F + P solution at low velocities and then, as the velocity increases, the value of α/α_{Nu} flattens out before beginning to rise again at even higher velocities. This flattening out could be attributable to a sudden movement of the point of separation instead of the steady change in its position predicted by eqn. (2.44) and used in the M + G + F + P theory. However, one would expect that at higher velocities, as the predicted point of separation moved further forward, the experimental results would again begin to approach the predicted solution. There is some evidence to suggest that this does occur to an extent, but over the velocity range covered there is still quite a large difference between the experimental and predicted values at the highest velocities. Fig. 8 shows that at these high velocities the predicted point of separation has already moved round as far as $\Phi = 120^{o}$ and the discrepancy between the predicted and experimental results cannot be accounted for by suggesting that separation is actually occurring at $\Phi = 109^{o}$ (as predicted by the Blasius equation).

The rise in the experimental results after they had flattened out could be due to a change in the way in which the condensate left the tube. At low velocities the condensate formed into discrete drops along the rear stagnation line of the tube, the drops gradually growing in size until they fell from the tube due to the force of gravity overcoming surface tension. However, as the velocity was increased, it was noticed that the way in which the drops formed became less orderly, the drops being buffetted from side to side by the vapour flowing past the cylinder. At the highest velocities it was not very clear whether or not drops actually formed and grew at the rear stagnation line. The condensate appeared to be stripped off the tube by the vapour flowing past and the size of droplet in the vapour stream was very much smaller than the droplet size under stagnant conditions. It is possible that condensate was in fact dragged off the tube before $\Phi = 180^{o}$ and this would produce an increase in condensate h.t.c. due to the thinner layer of condensate. This effect would produce experimental values of α/α_{Nu} greater than those theoretically predicted, but at the higher velocities the experimental results fall significantly below those predicted using the M + G + F + P theory. It is concluded, therefore, that as the velocity is increased beyond a certain point the interfacial shear stress is less than that predicted by eqn. (1.15), i.e. the addition of the condensing vapour momentum term to the "dry" friction term.

In the theoretical analysis it was assumed that after the point of separation the interfacial shear stress was zero. It is well-known, though, that there are slowly recirculating eddies formed in this area and these would produce a small shear stress acting in the opposite direction to the condensate flow. This would cause an extra thickening of the condensate layer in this region, and thus a reduction in the h.t.c., compared with that obtained by assuming that Nusselt conditions prevailed. However, it is not thought that this could account for the full difference between the experimental and theoretical results.

Fig. 29 does not fall in line with Figs. 27 and 28. Even at low velocities the experimental results are much less than those predicted using the M + G + F + P theory, and agree best with the G + F theory and the equation of Fuks, as has already been mentioned. This suggests that under these conditions, which were the lowest rates of heat flux covered, the momentum term has little effect. (The magnitude of the momentum is directly proportional to the heat flux and, therefore, it becomes less significant as the heat flux is reduced, but it is still of the same order of magnitude as the Blasius stress under all the test conditions, as can be seen by comparing the M + G + F solutions with those of the G + F.)

2.5.2 Peripheral variation of the outside tube wall temperature

In Figs. 30 and 31 comparison is made between the measured temperature profile around the tube wall and the profiles predicted using the M + G + F + P theory with variable separation, and the G + F theory for two mean wall/saturated steam temperature differences. The measured temperatures shown have not been corrected to compensate for the fact that the thermocouples lay slightly beneath the surface of the tube. The maximum correction to be made was calculated to be 0.7 K. (A correction was applied in calculating the condensate h.t.c..) For both temperature differences the agreement between the experimental profile and that predicted by the M + G + F + P theory is good at the lower velocities, except in the region of the rear stagnation point. Some discrepancy is expected here as the theoretical model predicts that at $\Phi = 180^{o}$ the thickness of the condensate layer is infinite and, therefore, the wall temperature becomes equal to the cooling water temperature. No account is made either of peripheral heat conduction, which would smooth out the cusp in the predicted temperature profile at the rear stagnation point and bring it closer to the measured profile. It was assumed that this would have little effect on the mean condensate h.t.c. for the tube, because the heat transfer rate in this region is low.

As the steam velocity is increased, the experimental points begin to migrate from the M + G + F + P profile towards the G + F profile. This is in agreement with the results without wall thermocouples, Figs. 27 - 29, and tends to confirm the view that, under otherwise similar conditions, as the vapour velocity is increased, the influence of the momentum term is reduced. If the reduction in heat transfer coefficient had been entirely due to the point of separation being earlier than expected or due to the effect of the reversed flow beyond the point of separation, one would have expected the measured and predicted temperature profiles to have been the same up to the point of separation and then to have diverged.

2.5.3 Effect of the suction parameter

A method of accounting for the effect of the heat flux on the condensate h.t.c. was sought. The heat flux is directly proportional to the rate of condensation and, therefore, to the rate of "suction", so it was decided to make use of the suction parameter $v_o\sqrt{(Re_v)}/U_\infty$. This parameter can, in fact, be shown to be proportional to the ratio of the momentum shear stress to the dry frictional shear stress, i.e.

$$\tau_M \propto \rho_v v_o U_\infty$$

$$\tau_F \propto \frac{\rho_v U_\infty^2}{2\sqrt{(Re_v)}}$$

$$\therefore \quad \frac{\tau_M}{\tau_F} \propto \frac{v_o}{U_\infty}\sqrt{(Re_v)}$$

The experimental results from all the single tube tests, both with and without thermocouples, were plotted as a function of the experimental condensate h.t.c., divided by the condensate h.t.c. from the M + G + F + P theory with variable separation and wall temperature, against the suction parameter, Fig. 32. For values of $v_o\sqrt{(Re_v)}/U_\infty > 4.2$, the majority of the results lie within the range $0.9 < \alpha/\alpha_{MGFP} < 1.1$, i.e. the M + G + F + P theory with variable wall temperature and separation predicts the condensate h.t.c. to within ± 10%. For values of $v_o\sqrt{(Re_v)}/U_\infty < 4.2$, there is a steady decrease in the value of α/α_{MGFP}. This suggests that the interfacial shear stress can be represented by

$$\tau_S = \tau_F + b\tau_M \qquad (1.20)$$

where for $\dfrac{v_o\sqrt{(Re_v)}}{U_\infty} > 4.2$ $\quad b = 1$

< 4.2 $\quad b = f\left(\dfrac{v_o\sqrt{(Re_v)}}{U_\infty}\right) < 1$

It is of interest to note that Nicol and Wallace (34) who found that their experimental results could not be accounted for by including the momentum term, were working in the range $1 < v_o\sqrt{(Re_v)}/U_\infty < 2$. Their results were even lower than those predicted using a dry friction model (i.e. G + F), but they were based on the assumption of constant wall temperature. It has been shown in section 2.2.5 that the assumption of a constant wall temperature rather than a constant inside h.t.c. overestimates the predicted condensate h.t.c. and this could account for the difference between their results and the G + F theory.

The range of experimental conditions covered by Fuks was $0.5 < v_o\sqrt{(Re_v)}/U_\infty < 5.3$, with most of his results having a value of the suction parameter less than 4, i.e. less than that thought necessary for the M + G + F + P theory to apply. In Fig.29 where there is agreement between the experimental data, the equation of Fuks and the G + F theory, the value of the suction parameter varies from 5.3 at the lowest velocity to 1.2 at the highest. (Note: the value of the suction parameter at $Re_{TP} = 0.7 \times 10^5$ has already fallen to 2.8 for these tests.) Following this interpretation of the author's results and those of (34), it is tentatively suggested that for values of $v_o\sqrt{(Re_v)}/U_\infty < 2$ the value of b in eqn. (1.20) should be taken as zero.

In Refs. (26) and (27) there was satisfactory agreement between experimental results for condensation on horizontal and vertical plates and the corresponding M + G + F theories. However, in all cases the condensation rates were high (i.e. $(T_s - T_w) > 23$ K and $p_{sat} = 1$ bar) and, although no direct comparison can be made with the suction parameter as calculated for the case of the horizontal cylinder, these conditions suggest that the momentum term would indeed be significant. Examination of Fig. 2 in Ref. (27) shows a similar trend to that of Figs. 27 and 28, that is, as the vapour velocity increases the experimental results begin to fall consistently below the predicted values.

The effect of suction on the surface shear stress for flow in a tube was studied in Ref. (28). It was shown that the effect of the momentum term on the shear stress increased with the increase of v/U_∞, except at very low values of suction. This is in general agreement with the conclusion reached here, though it was found in (28) that the fraction of the momentum term to be used in eqn. (1.20) reached a maximum of about 0.7 and not 1.0.

2.6 Conclusions from single tube work

The following conclusions are to be drawn from the theoretical and experimental investigations that have been made for the case of a downward flowing vapour condensing on a horizontal tube:-

(i) the assumption that the outside tube wall temperature is uniform leads to an over-estimation of the condensate h.t.c. and this can be large, particularly if there is a wide temperature distribution around the tube, i.e. if the vapour approach velocity is high or separation occurs. A more accurate solution is obtained by defining the inside wall boundary conditions in terms of the bulk temperature of the coolant and a constant inside h.t.c.;

(ii) separation reduces the condensate h.t.c., although with present knowledge it is difficult to be sure of the exact point of separation;

(iii) the pressure forces acting on the condensate layer cannot be ignored, as they can produce a further thickening of the condensate layer beyond $\Phi = 90^{o}$ which reduces the condensate h.t.c.. However, using existing theories, separation is generally predicted to occur before the point at which the pressure forces would otherwise significantly affect the thickness of the condensate layer; thus, if separation takes place the effect of the pressure terms is reduced;

(iv) at high condensation rates ($v_o\sqrt{(Re_v)}/U_\infty > 4.2$) the condensate h.t.c. is quite accurately predicted by assuming that the interfacial shear stress is given by the sum of the Blasius type shear stress for flow of a non-condensing vapour, plus the momentum exchanged by the condensing vapour. As the condensation rate is reduced, not only does the momentum term become numerically less significant, but so does its contribution to the total shear stress. For $v_o\sqrt{(Re_v)}/U_\infty < 2$, the momentum term appears to have no effect on the interfacial shear stress.

(v) at high vapour velocity the flow of condensate towards the rear stagnation point becomes unsteady, drops no longer fall from $\Phi = 180^{o}$ but condensate appears to be torn off before this point, resulting in an increase in condensate h.t.c. which is difficult to predict by a realistic model.

CHAPTER 3

TUBE BANK

3.1 Analysis of Problem

The main differences between condensation on a tube within a large condenser and on a single tube are the presence of surrounding tubes and condensate falling from tubes above.

The main effect of the surrounding tubes is on the vapour velocity distribution, which will depend on the spacing between the tubes and their configuration. For a given vapour mass flux, ρU_∞ approaching a bank, the closer the tubes are packed together, the greater will be the mean velocity around them and the greater the shear stress. The vapour velocity in most previous work has been calculated using the maximum flow area, but this takes no account of the tube spacing and the effect this must have on the interfacial shear. To enable a comparison with the single tube case to be made, it was decided to base the velocity on the mean flow area, as shown in Fig. 33.

The vapour flow pattern around a tube will depend on the particular tube arrangement employed. For instance, one would expect that for a square in-line arrangement there would be an area of low velocity around the forward and rear "stagnation" points, with a high velocity, and thus high interfacial shear, around the sides of the tube, the range over which the high velocity is effective depending on the point of separation. The sudden divergence of flow after the narrowest section might encourage separation earlier than on an isolated tube. With a triangular arrangement, the velocity distribution would be more akin to that on a single tube and, because in the expected region of separation the flow channel is converging, the point of separation could even be delayed.

The local condensate h.t.c. for a single tube is inversely proportional to the thickness of the condensate layer. Inundation with condensate from tubes above thickens the condensate layer and it is, therefore, to be expected that the condensate h.t.c. would decrease with increasing inundation. However, the single tube analysis assumed laminar flow within the condensate layer, whereas in practice the condensate flow on an inundated tube is wavy and at high inundation rates probably turbulent. The dependence of the condensate h.t.c. on the condensate

layer thickness is, therefore, likely to be reduced under inundation, and this has been reported (4) to (12).

The combined effects of vapour velocity and inundation on the condensation process on a tube within a tube bank are seen to be complex. In Appendix F an attempt at analysing this problem is shown, but it leads to an unrealistic conclusion and it is merely included for interest. It was expected that the experimental results could be correlated using the same variables as those for a single tube, based on a mean velocity, with an additional parameter to account for the inundation rate and perhaps tube bank geometry.

Before presenting and discussing the results obtained with tube banks, the modifications made to the rig, described in section 2.3, will be outlined.

3.2 Experimental apparatus

Two additions were made to the rig used for the single tube tests; these were the tube bank itself and a system to provide uniform condensate inundation of the working tube. The line diagram shown in Fig. 10 is again being referred to here.

3.2.1 Tube banks

Two tube banks were used, one a square in-line arrangement and the other an equilateral-triangle arrangement, Fig. 34. Each consisted of three complete columns with half-columns on the walls, and there were six and seven rows in the in-line and triangular arrangements respectively. The pitch-to-diameter ratio was 1.25 with a nominal tube i.d. of 19.05 mm as for the single tube. All but four of the tubes were dummy tubes, which simply consisted of lengths of copper tube with the ends sealed. Three of the tubes were inundation tubes which were supplied with water at one end, and sealed at the other. A series of holes was drilled along the forward stagnation line of each of these tubes from which the water flowed, thus simulating inundation. The remaining tube was the working tube as outlined in section 2.3.2, and was the only tube on which condensation took place.

The tubes were kept in position by two tube plates at either end of the test section. The half tubes were held against the wall by screws which passed through a clearance hole in the wall into tapped holes in semi-cylindrical blocks which were soldered into the half-tubes, Fig. 35.

3.2.2 Inundation system

The major part of the inundation water was continuously recirculated within the system. Having fallen from the inundation tube and through the tube bank, it was separated from the vapour flow along with the condensate by the separation bend, Fig. 11, and collected in the condensate collecting vessel. However, part of the inundation was entrained in the steam flow and swept into the dump condenser. The rate of entrainment increased with increase in vapour velocity. The water level in the condensate collecting vessel was kept constant by pumping water into it from the dump condenser weigh tank at a sufficient rate to have an overflow through the float valve. This overflow was collected for subsequent weighing.

The inundation water was pumped from the collecting vessel, using a low N.P.S.H. (net positive suction head) pump, through one of three rotameters. The flowrate through each rotameter was controlled by a globe valve. The water then flowed from the rotameters to the inundation tubes via a steam-heater. This consisted of a steam chest with three coils inside, through which passed the inundation water streams. The temperature of the inundation water was measured by a thermocouple at the entrance to each of the inundation tubes and was controlled by varying the steam supply to the inundation water heater.

3.2.3 Inundation tubes

The basic design requirement of the inundation tubes was to produce a uniform distribution of inundation along the length of the working tube, over as wide a range of inundation rates as possible.

A small rig, shown in Fig. 36, was built to measure the distribution of inundation. The inundation tube was placed at the top of a column of four tubes and on the same pitch to diameter ratio as used in the rig. Water was pumped into the inundation tube through a rotameter and was collected in a tray with six compartments as it fell from the lowest tube. Beneath each compartment there was a measuring cylinder, and the amount of water collected in each cylinder during a measured time was used to calculate the distribution of inundation. On the basis of this, a tube could either be modified by increasing the size of certain holes or blocking them off, or, if necessary, another tube could be designed.

For inundation rates < 0.064 kg/s, a tube with 125 1 mm holes drilled on a 4 mm pitch was found to give a fairly uniform distribution

of inundation. The 7th, 111th and 119th holes were blocked off and the 21st - 45th holes drilled out to 1.05 mm diameter (the first hole being taken as that nearest to the inlet). The distribution of inundation for different flow rates is shown in Fig. 37(a).

At higher inundation rates, the pressure distribution within the tube becomes significant and to achieve a uniform distribution of inundation the hole diameter or pitch, or both, have to be changed along the length of the inundation tube. The design method used was that of Van Der Hegge Zijnen (54) with some modifications, Appendix G, but is summarised as follows:

(a) calculate the pressure variation along the length of the inundation tube, assuming that the velocity within the tube decreases linearly with length and accounting for the pressure loss due to wall friction and the pressure rise due to the decrease in momentum;

(b) knowing the pressure distribution and assuming a discharge coefficient, calculate the size and spacing of the discharge holes.

However, for inundation rates > 0.085 kg/s, inundation tubes designed in this way did not produce a very uniform distribution. This could be accounted for by the fact that:

(a) the flow of water out of the inundation tube affects the pressure distribution within the manifold and, although this was accounted for in three different ways, there is very little information available on the subject;

(b) the discharge coefficient was taken as that from a sharp edged orifice, which was not a very good approximation because:
(i) the height of the jet of water from the holes in the inundation tube was kept to a minimum (< 5 mm), and was of the same order as the wall thickness of the tube (1.6 mm);
(ii) the jet of water did not flow vertically upwards out of the hole, but was inclined in the direction of the flow of water within the inundation tube, Fig. 38, i.e. it was retaining some of its forward momentum.

An attempt to even out the distribution of inundation was made by designing a tube of smaller diameter, using the above method, and inserting it inside an inundation tube with uniform holes on a uniform pitch, Fig. 39. It was thought that this would produce a uniform pressure within the space between the two tubes. Though this system produced a more uniform

distribution of inundation than the plain tube, it was still not regarded as satisfactory.

If the velocity of water within the inundation tube was kept constant by using an insert, the pressure increase due to the slowing up of the water would be eliminated and, provided that the wall friction forces were small, an inundation tube with constant diameter holes on a fixed pitch could be used. Two inserts were tried:

(a) a tapered cone, Fig. 40(a);

(b) a diagonally cut cylinder, Fig. 40(b);

in an inundation tube with 5 mm diameter holes on a 10 mm pitch. The distribution of inundation from the tube with the tapered cone insert is shown in Fig. 37(b). That from the diagonally cut cylinder was similar but showed slightly greater scatter at the higher flow rate. In view of the difficulty experienced using other tube designs, it was decided to use the tapered cone insert for the central inundation tube and diagonally cut cylinders for the two outer inundation tubes.

3.3 Experimental work on tube banks

3.3.1 Experimental procedure

The experimental procedure for tests with inundation was very similar to that with the single tube tests. The tube was cleaned before each test and steam and cooling water supplies switched on as before, with the exception that the steam flow was set at about ¼ of maximum (items a - c of 2.4.1). The following procedure was then adopted:

(d) the cooling water flow rate was adjusted to the required level and steam allowed into the cooling water preheater;

(e) the inundation make-up pump was switched on and the flow adjusted to ensure an adequate overflow from the condensate collection vessel;

(f) the low N.P.S.H. pump was switched on and the valves opened to allow water at the rate required to flow into the inundation tubes;

(g) the steam valve to the inundation heater was opened and time allowed for the recirculating inundation water to reach a temperature in excess of 80 ^{o}C;

(h) the steam flow was adjusted to the required rate;

(i) the flow of steam to the cooling water preheater was set to give the correct mean cooling water temperature, and the flow of steam to the inundation water heater set so that the temperature of the inundation water was within 3 K of the saturation

temperature (see Note at end of section). These two operations were performed simultaneously as the flow of steam to one heater affected the flow to the other;

(j) a few minutes were allowed, to ensure that the temperature levels and flow rates were stable;

(k) the valve on the weigh tank was closed and at the same time collection of the overflow from the condensate collecting vessel was started;

(l) three sets of readings of temperatures, cooling water and inundation flow rates and steam pressure were taken;

(m) the amount collected in the weigh tank and from the overflow were measured and added together to give the total condensate flow rate, and thus the steam flow rate;

(n) provided that the three sets of results were consistent, they were averaged for calculating the results and the test conditions were changed;

(o) as the working tube was not easily visible in the tube bank, it was removed at the end of each set of tests, washed in water and the mode of wetting examined. Occasionally the tube showed signs that dropwise condensation might have occurred at the ends, but the area affected never amounted to more than two or three per cent of the total.

(Note: As the inundation water falls through the tube bank it will rise in temperature due to condensation of steam. A preliminary set of tests was run to examine the effect of the inundation water inlet temperature on the actual temperature of the inundation water when it reached the working tube. The working tube with thermocouples laid in the wall was put in the rig, but no cooling water was passed through the tube. Steam was passed through the rig at almost the lowest rate used in the tests ($\simeq$ 0.022 kg/s) and inundation water was pumped through at the highest flow rate ($\simeq$ 0.14 kg/s). It was thought that under these conditions the temperature of the inundation water would be at its lowest when it reached the working tube for any given inlet temperature. For an inlet temperature of 10 K below the saturation temperature it was found that by the time the inundation water reached the working tube it was only 0.5 K below T_{sat}, and for an inlet temperature 3K below, the corresponding temperature difference at the working tube was about 0.25 K.)

3.3.2 Programme of experimental tests with tube banks

Experimental tests were performed on the square in-line tube arrangement, without and then with inundation; similar tests were then run with the triangular pitch arrangement. Only two sets of cooling water conditions were generally used, these being the same as for the single tests with a bulk mean temperature of 36.5 ^{o}C and 68.5 ^{o}C, omitting the intermediate heat flux condition. For each cooling water condition, six inundation rates were used, and the steam mass-velocity approaching the bank varied through the full range used in the single tube tests.

A few supplementary tests were made on the square tube bank, without inundation, with:

(a) a condenser tube with wall thermocouples;

(b) cooling water at a bulk mean temperature of 48 ^{o}C

The experimental results were calculated in the same way as those for the single tube experiments, and plotted as α/α_{Nu} versus Re_{TP}, with an additional parameter, (W/w) to account for inundation.

A summary of the experimental readings is given in Appendix H.

3.4 Discussion of experimental results from tube bank tests

3.4.1 Tests without inundation

The results for the square in-line and triangular arrangements have been plotted together in Figs. 41 - 43. Comparison of the three figures shows that vapour velocity and heat flux have exactly the same effects as with the single tube, i.e. the ratio α/α_{Nu} increases with increase in velocity and is the greater, the greater the heat flux.

At the high heat flux, Fig. 41, the results for the two tube arrangements are in good agreement (Note: Re_{TP} is based on the velocity calculated for the mean cross-sectional area of flow, see Fig. 33), although at low velocities the square tube bank results are slightly lower than the triangular arrangement results, and at high velocities the reverse is the case. This situation is repeated at the low heat flux, Fig. 43, though the agreement between the two arrangements is not so good. Both sets of results at the low heat flux exhibit the "flattening out" found with the single tube tests, but beyond this point the value of α/α_{Nu} for the square pitch tests increases much more quickly than those for the triangular pitch tests. The reverse situation had been expected, as the "flattening out" of the curve is believed to be due to the separation point moving forward round the cylinder. It had been thought that in the case of the triangular arrangement, the negative pressure gradient caused by the decrease in width of the flow channel towards $\Phi = 150^{o}$ would limit the point of separation. One explanation that can be given to account for this discrepancy is that at high velocities the h.t.c. in the areas of highest shear will tend to dominate the overall h.t.c. and that, because of this, Re_{TP} would be more representative if it were based on the maximum value of the flow velocity, i.e. that in the smallest flow area. This would move the square tube bank results to the right with respect to the triangular bank results, and bring the two sets of results closer together at the high velocities; though, it would, of course, move them further apart at the low velocities. However, if this were the primary reason for the difference between the two sets of results, it would be expected that the effect would be more noticeable at the higher heat flux, because of the increased effect of vapour velocity on the h.t.c. with increase in heat flux.

It was observed during the tests with the square tube bank that at high velocities the condensate fell at approximately equal rates from all three tubes in the bottom row of the bank, although condensation was only occurring on the one tube in the middle column of the row above. This

indicates that the condensate does not flow from the base of one tube to the top of the next, as assumed by Nusselt, but that there is a high degree of lateral transfer, particularly at high velocities.

The predicted results of Fujii, eqn. (1.36), the M + G + F + P and G + F theories have been plotted with the experimental results, and, for the low heat flux case, the equation of Fuks, eqn. (1.9), has also been plotted. The M + G + F + P values were obtained by solving the differential equation (2.35) for the single tube, taking the approach velocity as being equal to the mean velocity through the tube bank. The same criterion (2.44) as before was used for predicting separation. Comparing the experimental results with those predicted by the M + G + F + P theory, it can be seen that there is good agreement at the highest heat flux, Fig. 41, but as the heat flux is reduced, Fig. 43, the experimental results generally lie beneath the predicted line and in the case of the triangular bank, approach the G + F theory at high velocity. This is similar to the single tube results, with the significant exception that, except for the triangular tube bank at low heat flux, the results for the tube banks at high velocity are much higher in comparison to the M + G + F + P theory than were those for the single tube. For the single tube it was shown, Fig. 32, that there appeared to be a relation between the ratio of the experimental and predicted results and the suction parameter. A similar plot was made for the tube bank tests, Fig. 44. (Note: the ordinate has been plotted as $(\alpha/\alpha_{Nu})/(\alpha_{MGFP}/\alpha_{Nu})$ which is not the same as α/α_{MGFP} because the two values of α_{Nu} have each been based on the corresponding mean value of ΔT. The maximum discrepancy between the plotted parameter and α/α_{MGFP} occurs either at the maximum or minimum value of α/α_{MGFP} and was calculated to be 9%. If α/α_{MGFP} had been used for plotting Fig. 44, it would have appeared similar, with the exception that values of the ordinate greater than 1 would have been slightly larger and values less than 1 slightly smaller.)

It can be seen from Fig. 44 that almost all the experimental results lie within ± 20% of the predicted value of α/α_{Nu} but there is not such an obvious correlation of the results with the suction parameter as there was with the single tube. There is some evidence, though, to suggest that the value of α/α_{MGFP} does fall with a decrease in the suction parameter, and there is no reason to suppose that the value of the local h.t.c. is related to the local suction parameter in the case of a single tube and not in the case of the tube bank. The following reasons are, therefore, suggested to account for this apparent discrepancy:

(a) the tube bank results have been compared with a single tube theory. The distribution of shear stres, pressure and, therefore, of condensate h.t.c. around a tube in a bank, will not be all that similar to that around a single tube;

(b) the point of separation will be affected by the presence of other tubes;

(c) the effect of condensate being dragged off the tube before $\Phi = 180^{o}$ at high velocites increases the h.t.c. in some of the tube bank tests (Note: the maximum velocity in the tube bank tests was about four times higher than that in the single tube tests).

The experimental results do not correlate very well with the equations of Fujii et al, being well above the predicted values in all cases, except for the triangular tube bank at low heat flux. Fujii's experiments were performed in the pressure range 0.01 to 0.07 bar, the maximum temperature difference between steam and tube wall was around 3.5 K with steam approach velocities of 10 - 40 m/s. The value of the suction parameter is, therefore, approximately in the range 0.6 to 1.3 (i.e. a low suction value as compared with the present tests), and, therefore, it would be expected that his results would be closer to the G + F theory than the M + G + F + P. Fujii's experimental results were taken as the mean value of a column of five tubes, which would produce a lower h.t.c. than that for a single tube in a bank. However, the difference in h.t.c. between square and triangular tube banks noted by Fujii was not repeated.

In Fig. 43 the only data which can be compared with the equation of Fuks are all seen to lie well above his predicted results. Fuks obtained his data from the first row in a tube bank, and found little difference from that obtained from a single tube using the same approach velocity. This was not found to be the case here, where even basing the results for a tube in a bank on the mean velocity, and not the approach velocity, has produced values generally about equal to, or greater than, the corresponding single tube results. It is not reasonable to assume that all of the difference, between Fuks' equation and the experimental results, can be attributed to the difference in flow pattern around the first row and that around any subsequent row. Fuks' equation does show a similar shape to the experimental results, that is a steep rise in α/α_{Nu} at low velocities and a gradual flattening out as the velocity increases, but α/α_{Nu} does not approach 1 as Re_{TP} approaches zero, which would appear to be incorrect.

The minimum value of Re_v used by Fuks in his tests was 500, therefore eqn. (1.9) should not be used for values less than this. However, even at this minimum value the condensate h.t.c. predicted by eqn. (1.9) is less than the corresponding Nusselt value, which suggests that there may have been some error in calculating the experimental value of α.

Some further tests were made with the square tube bank, using a condenser tube with wall thermocouples attached, so that peripheral temperature profiles could be obtained. Profiles for two different sets of cooling water conditions are shown in Figs. 45 and 46. It was noted during the tests that the temperature at any one point was not as steady as it had been during the single tube tests. This could be due to waves being formed on the condensate film caused by the unsteady nature of the flow around the tubes. Extra thermocouple readings were taken at 195, 225, 255, 285, 315, 345 and 360°, to supplement those at 0, 30, 60, 90, 120, 150 and 180°. In order to reduce the size of the diagrams the former values have been plotted at 0, 15, 45, 75, 105, 135 and 165°. The temperature profiles shown in Figs 45 and 46 show one particular difference to those obtained with the single tube and that is that they are a lot flatter over the front half of the tube. In fact, in some cases, the maximum wall temperature measured was not at the forward stagnation point but in the region $30^{\circ} < \Phi < 60^{\circ}$. This is due to the fact that the vapour does not flow completely round the tubes, and so the foremost part of each tube is shielded from the vapour flow by the tube above. As the condensate moves from $\Phi = 0^{\circ}$ to $\Phi = 90^{\circ}$, the amount of condensate increases but, because the vapour velocity is also increasing, the shear stress increases even more rapidly than in the equivalent single tube case, and thus maintains a thin condensate layer and high condensate h.t.c.

This difference in the shape of the temperature profile emphasises the point that only limited agreement between tube bank results and single tube theories can be expected, due to the different flow patterns.

3.4.2 Tests with inundation

The results for the inundation tests for the two different tube bank arrangements and two sets of cooling water conditions are shown in Figs. 47 - 50. (Note: w_{Nu} is the condensation rate on an uninundated tube with the same cooling water conditions, but with the condensate h.t.c. calculated from Nusselt's equation (1.2).) The corresponding results for tests without inundation are included for comparison. It can be seen that there are similar increases in the h.t.c. with increase in velocity for the

tests with inundation as there were for those without. It is not the case, however, that, under otherwise similar conditions, the greater the rate of inundation the lower the heat flux. This can be seen in Figs. 51 - 54, where α/α_{Nu} has been plotted against W/w_{Nu} for constant values of Re_{TP} (Note: the points shown in these diagrams do not correspond to particular experimental tests but have been obtained by interpolation from the results shown in Figs. 47 - 50).

For the square tube bank, Figs. 51 and 52, as the inundation rate is increased, the value of α/α_{Nu} falls quickly at first, then starts to level out and increases at the highest inundation rates for the lower values of Re_{TP}. This is thought to be due to an increase in the value of the condensate film Reynolds Number, accompanied by a transition from laminar to turbulent flow of the condensate. At the higher values of Re_{TP} (increase in steam velocity) the flow within the condensate layer is probably turbulent even at low inundation rates.

A similar situation exists for the triangular bank, Figs. 53 and 54, but the increase in h.t.c. at the higher inundation rates is much more marked. In fact up to a value of Re_{TP} of 5×10^5 the value of α/α_{Nu} is greater for inundation rates of 0.093 kg/s than it is for those of 0.018 kg/s. This can be seen best in Figs. 49 and 50, where for values of W/w_{Nu} of 22.2 and 47.6 respectively, which correspond to an inundation rate of 0.093 kg/s, the value of α/α_{Nu} decreases very sharply at Re_{TP} equal to 4×10^5 before beginning to rise again at about 7×10^5. It was at first thought that there had been some experimental error during these tests, so the tests at high heat flux, which were carried out first, were repeated. The results were consistently repeatable and similar results were obtained with the low heat flux tests. These effects are due to the way in which the condensate flows from one tube row to the next. For the two highest rates of inundation on the triangular tube bank, it had been noted that with the inundation tubes in the positions shown in Fig. 34(b), most of the inundation was falling down the walls at the bottom of the tube bank and not from the last row of tubes. In order to combat this, the inundation tubes were moved two rows further down the tube bank so that they were only two rows above the working tube. This resulted in much more of the inundation falling from the last tube row, but there was still a tendency for the inundation to flow diagonally, as shown in Fig. 1, rather than vertically, and therefore much of the inundation could have been by-passing the working tube.

It had been noted during the tests on measuring the distribution of flow from the inundation tubes, section 3.2.3, that, even at the lowest inundation rates, a drop would grow at the bottom of one tube and would elongate until it touched the top of the tube below, i.e. drops did not actually fall from one tube to the next. With the triangular tube bank arrangement, because there is no tube immediately beneath another one, the drops would either have to fall from the tube or form a diagonal "bridge" with one of the tubes in the row below. Thus, the local transfer from one tube row to the next is likely to be by diagonal flow and, as can be seen from Fig. 1, it is possible for one tube to receive no inundation. It would not have been expected that this situation would be stable. The fact that the results were repeatable led to the assumption that for this one particular flow rate, the inundation flowed from the distribution tubes diagonally towards the walls at low steam velocities. As the steam velocity was increased the drag forces exerted by the steam on the inundation were sufficient to draw the inundation through the tube bank.

The results have been plotted, Fig. 55, on a logarithmic scale as α/α_{un} against $(W + w)/w$ for several constant values of Re_{TP} where

α = condensate h.t.c. with inundation W,

w = condensation rate " " ",

α_{un} = condensate h.t.c., as found from experiment, with no inundation but otherwise for the same steam and waterside conditions.

The equations of Fuks, eqn. (1.10), Grant and Osment, eqn. (1.14), and Nusselt, eqn. (1.3), are also shown. (Note that eqn. (1.3) cannot be written in terms of the two parameters α/α_{un} and $(W + w)/w$, but corresponding values can be obtained by calculation.) As has been found in almost all previous work, the experimental values lie well above those predicted by Nusselt. Both Fuks, and Grant and Osment were able to correlate their data in the form

$$\frac{\alpha}{\alpha_1} = \left(\frac{W + w}{w}\right)^n \qquad (3.1)$$

where α_1 = condensate h.t.c. for top tube row

n = - 0.07 for Fuks

= - 0.233 for Grant and Osment.

(Note: the experimental data have been compared with the h.t.c. for an uninundated tube within the bank, whereas Fuks, and Grant and Osment compare their data with the h.t.c. for the top tube row, so there is some disparity between the two.)

The scatter of the results shown in Fig. 55, is such that no such general correlation can be applied. However, the scatter of the results for any one value of Re_{TP} is much less than the scatter of the results as a whole and it is, therefore, suggested that the value of n in equation (3.1) is a function of velocity (or Re_{TP}). One possible reason for this is that, as the velocity is increased, there is a greater amount of inundation entrained in the steam flow and, therefore, the actual amount of inundation falling on the tube is less than predicted; and another possible reason is the increase in the turbulence of the vapour flow and condensate with increase in velocity.

The relationship between n and Re_{TP} is shown in Fig. 56, and it can be seen that n varies from - 0.22 to - 0.095 as Re_{TP} increases from 1×10^5 to 9×10^5. At the low velocity end, there is very good agreement with the value of - 0.223 reported by Grant and Osment. The value of n is always smaller than the value of - 0.07 reported by Fuks, though the maximum value of Re_{TP} in his experiments at atmospheric pressure was only 3.1×10^5.

One explanation of the low value of the exponent obtained by Fuks arises out of the fact that he used a triangular bank of tubes. He appears only to have added extra inundation at the top of the column in which he was taking measurements. In view of the points made earlier and in Ref. (9) about side drainage, it is likely that a high proportion of his inundation did not reach the working tubes.

The two-phase Reynolds number is probably not the best parameter to use for accounting for the changes in n due to entrainment. Eissenberg (8) was able to show a relation between the amount of condensate carried over, in a horizontal tube condenser with horizontal flow, and the kinetic energy of the steam ($\rho_v U_\infty^2$). The surface tension of the condensate, σ, will have some effect on the rate of entrainment and the present author suggests that a suitable non-dimensional group could be $\rho_v U_\infty d/\sigma$. Tests using liquids with different surface tensions would be needed to confirm this.

3.5 Conclusions from tube bank work

The following conclusions are drawn from the experimental work on the two tube bank arrangements and the comparison made with single tube theories:-

(1) vapour velocity increases the condensate h.t.c. on both inundated and uninundated tubes in a tube bank; the increase, as compared

with the coefficient at zero velocity, is greater, the greater the heat flux;

(2) correlating the data using the mean velocity through the tube banks reduces the difference in results between the two configurations used and produces some agreement with single tube data;

(3) the effect of inundation is generally to reduce the condensate h.t.c., the rate of reduction with increase in inundation rate being smaller as the vapour velocity is increased. Although at very low vapour velocities an increase in inundation rate can produce an increase in the condensate h.t.c.;

(4) the condensate drainage path, particularly in triangular tube banks, is often not vertically downwards but in a diagonal direction, and this can lead to some tubes receiving no inundation, and others receiving more than their proper share.

CHAPTER 4

RECOMMENDATIONS FOR FURTHER WORK

The experimental work has been restricted to one saturation condition and to fairly high heat fluxes, which has been a major limitation when comparing data with the theoretical analyses. It has been concluded that for a single tube the condensate h.t.c. can be accurately predicted by the M + G + F + P theory, with variable wall temperature and separation, provided that the suction parameter $v_o\sqrt{(Re_v)}/U_\infty > 4.2$ (i.e. $\alpha\Delta T_m\sqrt{(Re_v)}/\rho_v h'_{fg} U_\infty > 4.2$). For values of the suction parameter less than this the contribution of the momentum term appears to be reduced, possibly to zero for $v_o\sqrt{(Re_v)}/U_\infty < 2$. Although some comparison has been made with the data of other authors it would be beneficial to examine further the relationship between the effect of the transfer of momentum by the condensing vapour and the condensate h.t.c. for $v_o\sqrt{(Re_v)}/U_\infty < 4.2$, particularly as this is the range within which most commercial condensers operate.

The flat plate work (26, 27), which has been carried out with rather high heat fluxes, should be repeated to cover the lower ranges. This appears important because this arrangement avoids the interaction of other factors, such as separation and pressure variation.

Although an improvement in accounting for the combined effects of inundation and velocity has been suggested, i.e. that the exponent in eqn. (3.1) should be taken as variable, this is by no means the ultimate answer. Further experimental work is required and the problems of side-drainage, resulting in an unpredictable flow pattern, should be considered, particularly for triangular pitch tube banks. It is recommended that at least three consecutive tubes in a horizontal row are instrumented so that errors due to uneven distribution of inundation can be evaluated. This will impose limitations on the minimum height and width of the tube bank required to ensure that conditions on the instrumented tubes are representative of conditions in a larger bank. Some indication of the expected differences in inundation rates on tubes at similar positions in a tube bank could be found from tests with air and water where visual and photographic evidence could be obtained.

CHAPTER 5

REFERENCES

1. Nusselt, W. 'Die Oberflächen-Kondensation des Wasserdampfes', Z. VD.I., 60, 541-546 and 569-575, 1916.
2. Jakob, M. 'Heat Transfer', Vol. 1, J. Wiley & Sons Inc., 1949.
3. McKechan, A. and Zeitlin, D.J. 'Vapour condensation on horizontal tubes with intermediate film drainage', Report for B.Sc., Bristol University, 1971.
4. Laing, F.L. and Wohlenberg, W.J. 'Condensation of saturated freon-12 vapour on a bank of horizontal tubes,' Trans. ASME, 64, 789, 1942.
5. Katz, D.L. and Geist, J.M. 'Condensation on six finned tubes in a vertical row', Trans. ASME, 70, 907, 1948.
6. Fuks, S.N. 'Heat transfer with condensation of steam flowing in a horizontal tube bundle', Teploenergetika, 4(1), 35-39, 1957; English translation NEL 1041, National Engineering Laboratory, East Kilbride.
7. Grant, I.D.R. and Osment, B.D.J. 'The effect of condensate drainage on condenser performance', NEL Report No. 350, 1968.
8. Eissenberg, D.M. and Bogue, D. 'Tests of an enhanced horizontal tube condenser under conditions of horizontal steam cross-flow'. 4th Int. Ht. Transf. Conf., Paris, Paper HE 2.1.
9. Eissenberg, D.M. 'An investigation of the variables affecting steam condensation on the outside of a horizontal tube bundle', Office of Saline Water ORNL-TM-4036, 1972.
10. Isachenko, V.P. and Glushkov, A.F. 'Heat transfer with steam condensing on a horizontal tube and with a flow of condensate from above', Teploenergetika, 16(6), 79-81, 1969.
11. Turek, K. 'Heat transfer and pressure losses in film condensation of flowing saturated steam on horizontal nests of tubes', Chemie. Ing. Techn. 44(5), 280-5, 1972.
12. Takahashi, Y. and Soda, M. 'Fundamental study on steam surface condenser', Mitsubishi Heavy Industries Ltd., Tech. Review, 183-190, Oct. 1973.
13. Rohsenow, W.M., Webber, J.H. and Ling, A.T. 'Effect of vapour velocity on laminar and turbulent film condensation', Trans. ASME, 78, 1637-43, 1956.

14. Sugawara. S., Michiyoshi, T. and Minamiyona, T. 'The condensation of vapour flowing normal to a horizontal pipe', Proc. 6th Japan. Nat. Congr. Appl. Mech. 385-388, 1956.

15. Mandelzweig, S.I. 'The effect of vertically downward velocity on the heat transfer from a steam-nitrogen mixture condensing on a horizontal cylinder', M.Sc. Thesis, London University, 1960.

16. Sparrow, E.M. and Gregg, J.L. 'A boundary layer treatment of laminar film condensation', Trans. ASME 81C, 13-18, 1959.

17. Sparrow, E.M. and Gregg, J.L. 'Laminar condensation heat transfer on a horizontal cylinder,' Trans. ASME 81C, 291-296, 1959.

18. Rohsenow, W.M. 'Heat transfer and temperature distribution in laminar film condensation', Trans. ASME 78, 1645-48, 1956.

19. Chen, M.M. 'An analytical study of laminar film condensation,' Trans. ASME 83C, 48-60, 1961.

20. Koh, J.C.Y., Sparrow, E.M. and Hartnett, J.P., 'The two-phase boundary layer in laminar film condensation', Int. J. Heat Mass Transfer,2, 69-82, 1961.

21. Poots, G. and Miles, R.G. 'Effects of variable physical properties on laminar film condensation of saturated steam on a vertical flat plate', Int. J. Heat Mass Transfer, 10, 1677-1692, 1967.

22. Chung, P.M. 'Film condensation with and without body force in boundary layer flow of vapour over a flat plate', NASA Tech. Note, D790, 1961.

23. Koh, J.C.Y. 'Film condensation in a forced-convection boundary layer flow', Int. J. Heat Mass Transfer, 5, 941-954, 1962.

24. Cess, R.D. 'Laminar film condensation on a flat plate in the absence of a body force', Z. Agnew Math. Phys. 11, 426-433, 1960.

25. Berman, L.D. and Tumanov, Yu.A. 'Investigation of the heat transfer in the condensation of moving steam on a horizontal tube', Teplo-energetika, 9(10), 77-83, 1967; English translation RTS 2593, National Lending Library.

26. Mayhew, Y.R., Griffiths, D.J. and Phillips, J.W. 'Effect of vapour drag on laminar film condensation on a vertical surface', Proc. Instn. Mech. Engrs 180(3J), 280-289, 1965-66.

27. Mayhew, Y.R. and Aggarwal, J.K. 'Laminar film condensation with vapour drag on a flat surface', Int. J. Heat Mass Transfer, 16, 1944-49, 1973.

28. Aggarwal, J.K., Hollingsworth, M.A. and Mayhew, Y.R. 'Experimental friction factors for turbulent flow with suction in a porous tube', Int. J. Heat Mass Transfer, 15, 1585-1602, 1972.

29. Shekriladze, I.G. and Gomelauri, V.I. 'Theoretical study of laminar film condensation of flowing vapour', Int. J. Heat Mass Transfer, 9, 581-591, 1966.
30. Shekriladze, I.G. 'Theory of laminar film condensation of flowing vapour', Ht. Transfer, Soviet Research 4(4), 99-112, 1972.
31. Silver, R.S. 'An approach to a general theory of surface condensers', Proc. Instn. Mech. Engrs, 178(1), 339-376, 1963-64.
32. Silver, R.S. and Wallis, G.B. 'A simple theory for longitudinal pressure drop in the presence of lateral condensation', Proc. Instn. Mech. Engrs, 180(1), 36-42, 1965-66.
33. Wallis, G.B. 'Use of Reynolds flux concept for analysing one-dimensional two-phase flow', Int. J. Heat Mass Transfer, 11, 445-458, 1968.
34. Nicol, A.A. and Wallace D.J. 'The influence of vapour shear force on condensation on a cylinder', I.Mech.E. and I.Chem.E. Symposium on Multi-Phase Flow Systems, April, 1974.
35. Jacobs, H.R. 'An integral treatment of combined body force and forced convection in laminar film condensation', Int. J. Heat Mass Transfer, 15, 217-233, 1972.
36. Fujii, T. and Uehara, H., 'Laminar filmwise condensation on a vertical surface', Int. J. Heat Mass Transfer, 15, 217-233, 1972.
37. Fujii, T., Uehara, H. and Kurata, C. 'Laminar filmwise condensation of flowing vapour on a horizontal cylinder', Int. J. Heat Mass Transfer, 15, 236-246, 1972.
38. Fujii, T., Uehara, H., Hirata, K. and Oda, K. 'Heat transfer and flow resistance in condensation of low pressure steam flowing through tube banks', Int. J. Heat Mass Transfer, 15, 247-260, 1972.
39. Denny, V.E. and Mills, A.F. 'Non-similar solutions for laminar film condensation on a vertical surface', Int. J. Heat Mass Transfer, 12, 965-979, 1969.
40. Patankar, S.V. and Spalding, D.B. 'A finite difference procedure for solving the equations of the two-dimensional boundary layer', Int. J. Heat Mass Transfer, 10, 1389-1411, 1967.
41. Minkowycz, W.J. and Sparrow, E.M. 'Condensation heat transfer in the presence of non-condensables, interfacial resistance, superheating, variable properties and diffusion', Int. J. Heat Mass Transfer, 9, 1125-1144, 1966.
42. Denny, V.E. and Mills, A.F. 'Laminar film condensation of a flowing vapour on a horizontal cylinder at normal gravity', J. Heat Transfer, 91, 495-501, 1969.

43. Denny, V.E., Mills, A.F. and Jusionis, V.J. 'Laminar film condensation from a steam-air mixture undergoing forced flow down a vertical surface', J. Heat Transfer, 93, 297-304, 1971.

44. Denny, V.E. and Jusionis, V.J. 'Effects of non-condensable gas and forced flow on laminar film condensation', Int. J. Heat Mass Transfer, 15, 315-326, 1972.

45. Denny, V.E. and South, V. 'Effects of forced flow, non-condensables and variable properties on film condensation of pure and binary vapors at the forward stagnation point of a horizontal cylinder', Int. J. Heat Mass Transfer, 15, 2133-42, 1972.

46. Schlichting, H. 'Boundary Layer Theory', 6th Ed., McGraw-Hill, 1968. (a) p.376; (b) p.160; (c) p.561; (d) p.78.

47. Drummond, G. 'Steam-side pressure gradients in surface condensers', Proc. Instn. Mech. Engrs, 186, 117-124, 1972.

48. Morsey, M.G. 'Skin friction and form pressure loss in tube bank condensers', Ph.D. Thesis Faculty of Engineering, University of Glasgow, 1973.

49. 'U.K. Steam Tables in S.I. Units 1970', Arnold, E., 1970.

50. Kreyszig,E. 'Advanced engineering mathematics', 2nd ed. J. Wiley & Sons, p.89, 1968.

51. Provan, T.F. 'Effect of vapour superheat and non-condensable gas on the performance of a horizontal single-tube condenser', N.E.L. Report No. 219, East Kilbride, 1966.

52. Ferreira, S.M. 'Forced convection condensation of vapour flowing around a circular cylinder: Effect of the presence of inert gas, gravitational field and superheating', Chem. Eng. Jnl., 6, 81-90, 1973: 'Effect of form drag reduction', Chem. Eng. Jnl., 7, 253-256, 1974.

53. Newson, I.H. and Hodgson, T.D. 'The development of enhanced heat transfer condenser tubing', AERE, R7318, 1973.

54. Van Der Hegge Zijnen, B.G. 'Flow through uniformly tapped pipes', Appl. Sci. Res. Vol. A3, 144-162.

55. King, L.V. 'On the convection of heat from small cylinders in a stream of fluid', Phil. Trans. Roy. Soc. London, Ser. A., Vol. 214, 1914.

APPENDIX A

DERIVATION OF EQUATIONS FOR POWER LAW REPRESENTATION OF SHEAR STRESS

The interfacial shear stress is given by eqn. (1.37)

$$\tau_S = \left(\tau_F^n + \tau_M^n\right)^{1/n} \tag{1.37}$$

which can be differentiated w.r.t. Φ to give

$$\frac{d\tau_S}{d\Phi} = \frac{1}{n}\left(\tau_F^n + \tau_M^n\right)^{1-n/n}\left(n\tau_M^{n-1}\frac{d\tau_M}{d\Phi} + n\tau_F^{n-1}\frac{d\tau_F}{d\Phi}\right)$$

$$= \tau_S^{1-n}\left(\tau_M^{n-1}\frac{d\tau_M}{d\Phi} + \tau_F^{n-1}\frac{d\tau_F}{d\Phi}\right) \tag{A.1}$$

τ_F and $d\tau_F/d\Phi$ are given by eqn. (2.26) and (2.27) respectively and are functions of Φ only.

τ_M and $d\tau_M/d\Phi$ are functions of Φ, δ and the temperature difference and therefore the solution for the constant and variable wall temperature cases are different. Only the more general case of variable wall temperature will be considered.

Substituting from eqn. (2.33) for $d\tau_M/d\Phi$ into (A.1) and re-arranging:

$$\frac{\delta^3}{2\rho g}\frac{d\tau_S}{d\Phi} = \tau_S^{1-n}\left[\tau_M^{n-1}A(Re_{TP})d^2\delta^2\cos\Phi + \delta^3\frac{\tau_F^{n-1}}{2\rho g}\frac{d\tau_F}{d\Phi}\right]$$

$$+ \tau_S^{1-n}\left[\tau_M^{n-1}A(Re_{TP})d^2\delta\sin\Phi\left(\frac{k}{(\alpha_e\delta + k)} - 1\right)\right]\frac{d\delta}{d\Phi} \tag{A.2}$$

Substituting (A.2) into eqn. (2.16)

$$\frac{d\delta}{d\Phi} = \tag{A.3}$$

$$\frac{\frac{Ad^4}{2} - \left[\cos\Phi + 8\left(\frac{\rho_v}{\rho}\right)(Fr)\cos 2\Phi\right]\frac{\delta^4}{3} - \tau_S^{1-n}\delta^2\left(\tau_M^{n-1}A(Re_{TP})d^2\cos\Phi + \frac{\delta\tau_F^{n-1}}{2\rho g}\frac{d\tau_F}{d\Phi}\right)}{\left[\sin\Phi + 4\left(\frac{\rho_v}{\rho}\right)(Fr)\sin 2\Phi\right]\delta^3 + \tau_S\delta^2/\rho g + \tau_S^{1-n}\left[\tau_M^{n-1}A(Re_{TP})d^2\delta\sin\Phi\left(\frac{k}{(\alpha\delta + k)} - 1\right)\right]}$$

From eqn. (2.17) the boundary condition is $d\delta/d\Phi = 0$ at $\Phi = 0$, which can be expressed as

$$f(\delta_o) = \frac{Ad^4}{2} - \left[1 + 8\left(\frac{\rho_v}{\rho}\right)(Fr)\right]\frac{\delta^4}{3} - \tau_S^{1-n}\ \tau_M^{n-1}\ A(Re_{TP})\,d^2\delta^2 -$$

$$\tau_S^{1-n}\ \tau_F^{n-1}\ \frac{\delta^3}{2\rho g}\frac{d\tau_F}{d\Phi} = 0 \qquad (A.4)$$

But at $\Phi = 0$ $\quad \tau_S = \tau_M = \tau_F = 0$

and as $n > 1$ $\quad \tau_S^{1-n} = \infty$

$$\tau_M^{n-1} = \tau_F^{n-1} = 0$$

therefore the last two terms of (A.4) are indeterminate.

However,

$$\tau_S^{1-n}\ \tau_M^{n-1} = \left(\tau_M^n + \tau_F^n\right)^{1-n/n}\ \tau_M^{n-1}$$

$$= \left(1 + \left(\frac{\tau_F}{\tau_M}\right)^n\right)^{1-n/n}$$

similarly

$$\tau_S^{1-n}\ \tau_F^{n-1} = \left[1 + \left(\frac{\tau_M}{\tau_F}\right)^n\right]^{1-n/n}$$

Substituting from eqn. (2.26) and (2.31) and taking the limit as $\phi \to 0$

$$\left(\frac{\tau_M}{\tau_F}\right) = \frac{2k(T_s - T_w)U_\infty \sin\Phi \,.\, 2\sqrt{(Re_v)}}{\delta h'_{fg}\rho_v U_\infty^2(9.861\Phi - 3.863\Phi + \ldots)}$$

$$\lim_{\Phi\to 0}\left(\frac{\tau_M}{\tau_F}\right) = \frac{4k(T_s - T_w)\sqrt{(Re_v)}}{\rho_v U_\infty h'_{fg}} \qquad (A.5)$$

$\lim_{\phi\to 0}(\tau_F/\tau_M)$ can be similarly found and together with eqn. (A.5) can be substituted into eqn. (A.4). A further substitution for $(T_s - T_w)$ from eqn. (2.22) can also be made. Equation (A.4) can now be expressed solely in terms of δ_o and can therefore be solved using the Newton-Raphson method.

Numerical integration of eqn. (A.3) can then proceed as outlined in section 2.2.

APPENDIX B

POLYNOMIALS FOR PREDICTING PROPERTIES OF STEAM AND WATER

Water

Prandtl Number

$$\frac{1}{Pr} = 7.588 \times 10^{-2} + 0.2839 \times 10^{-2}\left(\frac{T}{^oC}\right) + 2.934 \times 10^{-5}\left(\frac{T}{^oC}\right)^2 - 8.15 \times 10^{-8}\left(\frac{T}{^oC}\right)^3 \qquad (B.1)$$

$$0.01 < \frac{T}{^oC} < 100$$

Viscosity

$$\frac{1/\mu}{ms/kg} = 560.4 + 19.21\left(\frac{T}{^oC}\right) + 0.139\left(\frac{T}{^oC}\right)^2 - 3.382 \times 10^{-4}\left(\frac{T}{^oC}\right)^3 \qquad (B.2)$$

$$0.01 < \frac{T}{^oC} < 100$$

Specific heat

$$\frac{c_p}{kJ/kg\ K} = 4.215 - 2.229 \times 10^{-3}\left(\frac{T}{^oC}\right) + 3.772 \times 10^{-5}\left(\frac{T}{^oC}\right)^2 - 1.536 \times 10^{-7}\left(\frac{T}{^oC}\right)^3 \qquad (B.3)$$

$$0.01 < \frac{T}{^oC} < 100$$

Thermal conductivity

$$\frac{k}{kW/m\ K} = 5.707 \times 10^{-4} + 1.78 \times 10^{-6}\left(\frac{T}{^oC}\right) - 6.781 \times 10^{-9}\left(\frac{T}{^oC}\right)^2 \qquad (B.4)$$

$$30 < \frac{T}{^oC} < 100$$

Density

$$\frac{\rho}{kg/m^3} = 1003.7 - 0.174\left(\frac{T}{^oC}\right) - 0.00277\left(\frac{T}{^oC}\right)^2 \qquad (B.5)$$

$$30 < \frac{T}{^oC} < 100$$

Steam

Saturation temperature

$$\frac{T_s}{^oC} = 55.9 + 63.97\left(\frac{p_{sat}}{bar}\right) - 24.73\left(\frac{p_{sat}}{bar}\right)^2 + 4.497\left(\frac{p_{sat}}{bar}\right)^3 \qquad (B.6)$$

$$0.9 < \frac{p_{sat}}{bar} < 1.5$$

Latent heat of vaporisation

$$\frac{h_{fg}}{kJ/kg} = 2526.6 - 2.7\left(\frac{T_{sat}}{^{o}C}\right) \qquad (B.7)$$

Specific heat along saturated vapour line

$$\frac{c_{pv}}{kJ/kg\ K} = 1.932 - 1.902 \times 10^{-3}\left(\frac{T}{^{o}C}\right) + 2.937 \times 10^{-5}\left(\frac{T}{^{o}C}\right)^{2} \qquad (B.8)$$

$$40 < \frac{T}{^{o}C} < 140$$

Viscosity along saturated vapour line

$$\frac{\mu_{v}}{kg/m\ s} = 8.06 + 0.04159\left(\frac{T}{^{o}C}\right) - 1.579 \times 10^{-5}\left(\frac{T}{^{o}C}\right)^{2} \qquad (B.9)$$

$$40 < \frac{T}{^{o}C} < 140$$

APPENDIX C

CALIBRATION OF ROTAMETERS AND THERMOCOUPLES

Cooling water rotameter

The rotameter used was a Fischer and Porter type FP1½ -27-G-10/33 with float GUSVT-814. The flow rate was given by:-

$$\underset{kg/s}{\overline{m_{cw}}} = \underset{\%}{\overline{FLP}} \cdot \underset{kg/(s\%)}{\overline{GRAD}} \cdot \overline{COR}$$

where FLP = % flow reading from rotameter

GRAD = mean gradient of calibration curve at operating temperature $T_{IN}(^{o}C)$

COR = correction for non-linearity of calibration curve

$$\frac{GRAD}{kg/(s\%)} = 9.504 \times 10^{-3} - 7.115\left(\frac{T_{IN}}{^{o}C}\right) \times 10^{-6} + 5.233\left(\frac{T_{IN}}{^{o}C}\right)^{2} \times 10^{-8}$$

$$COR = 1 - 0.013 + 0.0026\left(\frac{FLP}{\%}\right) - 1.09\left(\frac{FLP}{\%}\right)^{2} \times 10^{-4} + 1.23\left(\frac{FLP}{\%}\right)^{3} \times 10^{-6}$$

$$\frac{FLP}{\%} < 55 \qquad 10 < \frac{T_{IN}}{^{o}C} < 50$$

Inundation rotameters

Three Fischer and Porter type FP1-35-G-10/55 rotameters were used and the difference in the calibration of the mass flow rates between them was less than 4%. The inundation rate was taken as that from the central tube and the calibration for the corresponding rotameter was:

with float GUSVT-611

$$\frac{W}{kg/s} = 0.00214 + 1.041\left(\frac{FLP}{\%}\right) \times 10^{-3} + 5.79\left(\frac{FLP}{\%}\right)^{2} \times 10^{-7}$$

where W = mass flow rate of inundation water

FLP = % flow reading from rotameter

$$10 < \frac{FLP}{\%} < 100 \qquad \frac{T}{^{o}C} \approx 85$$

with float GSVGT-69

$$\frac{W}{kg/s} = -0.00145 + 6.01\left(\frac{FLP}{\%}\right) \times 10^{-2} - 1.13\left(\frac{FLP}{\%}\right)^{2} \times 10^{-6}$$

$$15 < \frac{FLP}{\%} < 40 \qquad \frac{T}{^oC} \approx 80$$

Thermocouples

$$\frac{T}{^oC} = 0.638 + 25.17\left(\frac{MV}{mV}\right) - 0.4367\left(\frac{MV}{mV}\right)^2$$

where T = measured temperature

MV = millivolt reading from thermocouple

$$20 < \frac{T}{^oC} < 100$$

APPENDIX D

DETERMINATION OF VELOCITY PROFILE USING AN ANEMOMETER

The equation relating the power dissipated by a hot wire anemometer to the velocity of the fluid flowing past it is King's Law (55) and is as follows:

$$P^2 = \left[C' + B'(\rho_v U)^{1/n}\right](T_{SE} - T_E) \qquad (D.1)$$

where P = power dissipated
U = fluid velocity
T_{SE} = temperature of the anemometer wire
T_E = fluid temperature
C', B' = constants depending on fluid properties
n = constant (usually about 2)

For a constant current device

$$p^2 \propto V^2 \qquad (D.2)$$

where V is the voltage across the anemometer.

Therefore, eqn. (D.1) can be re-written as

$$V^2 = \left(C + B(\rho_v U)^{1/n}\right)(T_{SE} - T_E) \qquad (D.3)$$

where C and B are new constants.

C and B are usually obtained by calibration, but a non-dimensionalised velocity profile was all that was required and, therefore, this calibration was not necessary. The temperature of the anemometer wire was calculated from the characteristics of the probe and the anemometer bridge. The fluid temperature was measured by a thermocouple attached to the probe support and n was assumed to be 2.

The output voltage at zero velocity V_o is given by

$$V_o^2 = C(T_{SE} - T_E) \qquad (D.4)$$

A set of tests at different steam temperatures was performed to establish the relationship between V_o^2 and T_E. The steam temperature in the rig increased with increase in velocity, and the variation in steam temperature was achieved by allowing a high flow rate of steam through the rig for a while and then restricting it to a minimum. The steam temperature then gradually reduced and readings of output voltage and temperature taken. To ensure that the probe was in stagnant surroundings

it was placed inside a close fitting cylinder, which had its axis perpendicular to the steam flow and was only open at one end.

Equation (D.3) can now be written as

$$V^2 = V_o^2 + B(\rho_v U)^{\frac{1}{2}}(T_{SE} - T_E) \qquad (D.5)$$

where V_o is the output voltage at zero velocity and fluid temperature T_E. Re-arranging terms

$$U = \rho_v \left(\frac{V^2 - V_o^2}{(T_{SE} - T_E)B} \right)^2 \qquad (D.6)$$

During the velocity tests the variation of V and T_E was measured across the section. T_E was found to vary by up to 4 K during any one test, which was not insignificant as the steam temperature was about 120 ^oC and the anemometer wire about 210 ^oC.

However, the variation of T_E was small enough for variations in ρ_v to be ignored.

i.e. $$U \propto \left(\frac{V^2 - V_o^2}{T_{SE} - T_E} \right)^2$$

The procedure for calculating the non-dimensionalised velocity profile was as follows:

(1) calculate the mean steam temperature $\overline{T}_E$ and the zero velocity value of V_o^2 corresponding to $\overline{T}_E$;

(2) correct the local values of E^2 for temperature variation

$$V_c^2 = V^2 \frac{(T_{SE} - \overline{T}_E)}{(T_{SE} - T_E)}$$

Where V_c is the output that would have been obtained for a local temperature of $\overline{T}_E$ instead of T_E.

In effect this now means that

$$U \propto (V_c^2 - V_o^2)^2$$

(3) calculate local values of $(V_c^2 - V_o^2)^2$ and sum them to obtain mean value

$$\overline{U} \propto \frac{1}{n} \sum_{1}^{n} (V_c^2 - V_o^2)^2$$

where n = number of points at which readings were taken;

(4) calculate non-dimensionalised velocities

$$\frac{U}{\overline{U}} = \frac{(V_c^2 - V_o^2)^2}{\frac{1}{n}\sum_{1}^{n}(V_c^2 - V_o^2)^2}$$

APPENDIX E

NUMERICAL EXAMPLE OF METHOD OF CALCULATING CONDENSATE h.t.c. FROM EXPERIMENTAL DATA

1. Experimental data

Cooling water mass flow rate m_{cw} = 0.468 kg/s

" " inlet temperature T_{IN} = 33.68 ^{o}C

" " outlet " T_{OUT} = 38.91 ^{o}C

" " temperature rise $\Delta T'_{cw}$ = 5.238 K

Steam pressure p_{st} = 1.04 bar

Steam temperature T_{st} = 110.4 ^{o}C

Total condensate flow (from dump condenser plus overflow) m_{cond} = 0.0429 kg/s

Length of condenser tube L = 0.500 m

Outside diameter of condenser tube d = 19.05 mm

Inside diameter of condenser tube d_i = 15.8 mm

Width of test section l = 0.09525 m

2. Calculation of overall h.t.c.

Temperature drop along entry length from eqn. (2.48) is

$$\Delta T_{EL} = 0.00197\ T_{IN} + 0.0267 = 0.093 \text{ K}$$

Thus, the corrected cooling water temperature rise becomes

$$\Delta T_{cw} = \Delta T'_{cw} + \Delta T_{EL} = 5.331 \text{ K}$$

The saturation temperature of the steam is obtained from p_{st} together with eqn. (B.6) and is equal to the vapour-condensate interface temperature

$$T_S = T_{sat} = 100.74\ ^{o}\text{C}$$

The log-mean-temperature difference between the steam and cooling water can be calculated from

$$\text{LMTD} = \frac{\Delta T_{cw}}{\ln\left(1 + \frac{\Delta T_{cw}}{(T_S - T_{OUT})}\right)} = \frac{5.331}{\ln\left(1 + \frac{5.331}{(100.74 - 38.91)}\right)} = 64.46 \text{ K}$$

and the reference bulk temperature of the cooling water is defined as

$$T_B = T_{cw} = T_S - \text{LMTD} = 36.28\ ^{o}\text{C}$$

The properties of the cooling water are given by eqn. (B.1) to eqn. (B.5). The heat transferred to the cooling water is

$$Q_{cw} = m_{cw}\, c_{p_{cw}}\, \Delta T_{cw} = 0.468 \times 4.178 \times 5.331$$
$$= 10.41 \text{ kW}$$

and the area of heat transfer

$$A_{HT} = \pi dL = \pi \times 0.01905 \times 0.500 = 0.0299 \text{ m}^2$$

Thus, the overall h.t.c. can finally be calculated from

$$\alpha_o = \frac{Q_{cw}}{A_{HT} LMTD} = \frac{10.41}{0.0299 \times 64.46} = 5.4 \text{ kW/m}^2 \text{ K}$$

3. Calculation of tube wall h.t.c.

For one-dimensional heat transfer through the wall

$$\alpha_w = \frac{2k_w}{d \ln(d/d_i)} = \frac{2 \times 0.381}{0.01905 \ln(1.905/1.58)} = 214 \text{ kW/m}^2 \text{ K}$$

4. Calculation of inside h.t.c.

The cooling water h.t.c. is given by the modified form of eqn. (2.63)

$$\alpha_{cw} = 0.00127 \frac{k_{cw}}{d_i} C_L (Re_{cw})(Pr_{cw})^{0.42} \left[1 + 25(Re_{cw})^{0.27}\right] \left(\frac{\mu_{cw}}{\mu_i}\right)^n$$

where $C_L = 1 + \dfrac{0.96(7/Pr_{cw})^{0.42}}{(L/d_i)} = 1 + \dfrac{0.96(7/4.666)^{0.42}}{(0.5/0.0158)} = 1.036$

$$n = \left(\frac{Re_{cw}}{8.7 \times 10^5}\right)^{0.84} \quad \text{for } Re_{cw} \leqslant 6.25 \times 10^4$$

$$= 0.11 \qquad Re_{cw} > 6.25 \times 10^4$$

$$Re_{cw} = \frac{4m_{cw}}{\pi d_i \mu_{cw}} = \frac{4 \times 0.468}{\pi \times 0.0158 \times 0.7 \times 10^{-3}} = 5.36 \times 10^4$$

Thus

$$n = \left(\frac{5.36 \times 10^4}{8.7 \times 10^5}\right)^{0.84} = 0.0962$$

and

$$\alpha_{cw} = 0.00127 \times \frac{0.627 \times 10^{-3}}{0.0158} \times 1.036 \times 5.36 \times 10^4 \times 1.91 \times \left(1 + \frac{25}{18.92}\right)\left(\frac{\mu_{cw}}{\mu_i}\right)^{0.0962}$$

$$= 12.4 \left(\frac{\mu_{cw}}{\mu_i}\right)^{0.0962} \text{ kW/m}^2 \text{ K}$$

The value of the viscosity of the water at the inside tube wall cannot be calculated without knowing the temperature at that point. As a first approximation, assume

$$\mu_i = \mu_{cw}$$

then

$$\alpha_{cw} = 12.4 \text{ kW/m}^2 \text{ K}$$

The temperature of the water at the wall can then be calculated from

$$T_i = T_{cw} + \frac{Q_{cw}}{\alpha_{cw}\pi d_i L} = 36.28 + \frac{10.41}{12.4\pi \times 0.0158 \times 0.5} = 36.28 + 33.9$$

$$= 70.2 \ ^{o}C$$

and the value of μ_i can be calculated from eqn. (B.2).

Thus,

$$\left(\frac{\mu_{cw}}{\mu_i}\right)^{0.0962} = 1.055$$

and a second approximation of α_{cw} is obtained

$$\alpha_{cw} = 12.4 \times 1.055 = 13.1 \text{ kW/m}^2 \text{ K}$$

Re-calculating T_i using this value of α_{cw},

$$T_i = 36.28 + \frac{33.9}{1.055} = 68.4 \ ^{o}C$$

another value of μ_i can be obtained. Then

$$\left(\frac{\mu_{cw}}{\mu_i}\right)^{0.0962} = 1.053$$

and a third approximation of α_{cw} calculated

$$\alpha_{cw} = 1.053 \times 12.4 = 13.05 \text{ kW/m}^2 \text{ K}$$

This is close enough to the second approximation to be taken as correct, and the final of T_i is, therefore

$$T_i = 36.28 \frac{+33.9}{1.053} = 68.5 \ ^{o}C$$

The total inside h.t.c α_i is given by

$$\frac{1}{\alpha_i} = \frac{1}{\alpha_{cw}} + \frac{1}{\alpha_D}$$

where the dirt coefficient is calculated from eqn. (2.68) as

$$\alpha_D = \frac{d}{0.01\ d_i} = 120.5\ kW/m^2\ K$$

Thus,

$$\frac{1}{\alpha_i} = \frac{1}{13.05} + \frac{1}{120.5} = 0.08493$$

$$\alpha_i = 11.78\ kW/m^2\ K$$

5. Calculation of condensate h.t.c.

From eqn. (2.53)

$$\frac{1}{\alpha} = \frac{1}{\alpha_o} - \frac{1}{\alpha_w} - \frac{d}{d_i \alpha_i}$$

$$= 0.1852 - 0.00467 - 0.1024 = 0.0781$$

$\therefore$ $\alpha = 12.8\ kW/m^2\ K$

6. Calculation of Nusselt coefficient

The temperature difference across the condensate layer is calculated from

$$T_s - T_w = \frac{Q_{cw}}{\alpha \pi d L} = \frac{10.41}{12.8\pi \times 0.01905 \times 0.5}$$

$$= 27.2\ K$$

The reference temperature for calculating the condensate properties is given by eqn. (1.8)

$$T_r = T_w + \beta(T_s - T_w) = T_s - (1 - \beta)(T_s - T_w)$$

where, from a least squares fit to the data of Poots and Miles (21) for $(T_s - T_w) < 40\ K$,

$$\beta = 0.23 + 3.33 \times 10^{-3}(T_s - T_w) - 3.33 \times 10^{-5}(T_s - T_w)^2$$

$$= 0.296$$

Thus,

$$T_r = 100.74 - 0.704 \times 27.2 = 81.6^{o}$$

The condensate properties μ, k, ρ can now be calculated from eqns. (B.2), (B.4) and (B.5).

The reference temperature for calculating the specific heat of the steam from eqn. (B.8) was taken as

$$T_r = T_s + 0.5(T_{st} - T_s)$$

$$= 100.74 + 0.5(110.4 - 100.74) = 105.6\ ^{o}C$$

The specific enthalpy of vaporisation of the steam was calculated from eqn. (B.7) using the saturation temperature and the equivalent value of h_{fg} obtained from

$$h'_{fg} = h_{fg} + 0.68\ c_p(T_s - T_w) + c_{p_{st}}(T_{st} - T_s)$$

$$= 2255 + 0.68 \times 4.2 \times 27.2 + 2.03 \times 9.66 = 2352\ \text{kJ/kg}$$

From eqn. (1.2)

$$\alpha_{Nu} = 0.728 \left(\frac{k^3\rho^2 g h'_{fg}}{d\mu(T_s - T_w)}\right)^{\frac{1}{4}}$$

$$= 0.728\left(\frac{3.02 \times 10^{-10} \times 0.942 \times 10^6 \times 9.81 \times 2352}{0.01905 \times 3.44 \times 10^{-4} \times 27.2}\right)^{\frac{1}{4}}$$

$$= 10.1\ \text{kW/m}^2\ \text{K}$$

$$\frac{\alpha}{\alpha_{Nu}} = \frac{12.8}{10.1} = 1.27$$

7. <u>Calculation of two-phase Reynolds number</u>

The free stream velocity of the steam is

$$U_\infty = \frac{m_{cond}}{\rho_{st} L l}$$

The density of the steam is obtained from the perfect gas law

$$\rho_{st} = \frac{p_{st} \times 10^2}{0.4561(T_{st} + 273)} = \frac{1.04 \times 10^2}{0.4561 \times 383.4} = 0.595\ \text{kg/m}^3$$

(Note that the specific gas constant for steam was taken as 0.4561 kJ/kg K, as this value produced the best fit of tabulated data in the region close to the saturation line at p_s = 1 bar.)

Thus

$$U_\infty = \frac{0.0429}{0.595 \times 0.500 \times 0.09525} = 1.514\ \text{m/s}$$

and

$$Re_{TP} = \frac{\rho U_\infty d}{\mu} = \frac{970.8 \times 1.514 \times 0.01905}{3.44 \times 10^{-4}}$$

$$= 0.812 \times 10^5$$

APPENDIX F

THE COMBINED EFFECT OF CONDENSATE INUNDATION AND VAPOUR VELOCITY ON THE CONDENSATE h.t.c.

As has been mentioned in section 1.2 Nusselt (1) and Jakob (2) examined the effect of inundation on a column of tubes in a gravity field, and, though their predicted results underestimate the heat transfer coefficients found in practice, they have been a useful basis for comparison. A similar analysis was sought for the combined effects of inundation and vapour velocity. A general solution was required, rather than one which relied upon numerical integration, therefore, the following assumptions had to be made:

(i) the tube wall is isothermal;

(ii) the condensation rate is high enough to prevent separation of the vapour boundary layer;

(iii) the pressure force is negligible compared with the transfer of momentum of the condensing vapour, as is the "dry" frictional shear stress, i.e. $\tau_S = \tau_M$;

(iv) the gravity force is absent.

These conditions are the same as those assumed by Shekriladze and Gomelauri (29) in obtaining their solution - eqn. (1.25) - for an isolated uninundated tube.

The differential equation for δ, eqn. (2.36), with a constant tube wall temperature now reduces to

$$\frac{d\delta}{d\Phi} = \frac{d^2/2 - \delta^2(Re_{TP})\cos\Phi}{\delta(Re_{TP})\sin\Phi} \qquad (F.1)$$

which can be re-written as

$$\frac{d\delta^2}{d\Phi} + 2\delta^2\cot\Phi = \frac{\delta^2}{(Re_{TP})\sin\Phi}$$

and, after multiplying through by $\sin^2\Phi$, integrated to yield

$$\delta = \frac{1}{\sin\Phi}\left(C - \frac{d^2\cos\Phi}{Re_{TP}}\right)^{\frac{1}{2}} \qquad (F.2)$$

where C is a constant.

Under the assumed conditions eqn. (2.10) for the mass flow rate of condensate at angle Φ, reduces to

$$m = \frac{\tau_S \rho \delta^2}{2\mu} = \frac{\tau_M \rho \delta^2}{2\mu} \tag{F.3}$$

and substituting from eqn. (2.31) for τ_M eqn. (F.3) can be written as

$$m = \frac{\rho U_\infty k(T_s - T_w)\sin\Phi\delta}{\mu h'_{fg}} \tag{F.4}$$

Replacing δ from eqn. (F.2) the local condensate flow rate is given by

$$m = \frac{(Re_{TP})k(T_s - T_w)}{h'_{fg}d}\left(C - \frac{d^2\cos\Phi}{Re_{TP}}\right)^{\frac{1}{2}} \tag{F.5}$$

If it is now assumed that the tube we are considering is the Nth tube in the column and is being inundated at a rate of W per unit length, we can write the boundary condition:

$$\text{at } \Phi = 0 \quad m = \frac{W}{2}$$

(Note: half the inundation flows down each side of the tube.)
Substituting for $\Phi = 0$ in eqn. (F.5) and making use of this boundary condition, the value of the constant C is given by

$$C = \left(\frac{Wh'_{fg}d}{2(Re_{TP})k\Delta T}\right)^2 + \frac{d^2}{Re_{TP}}$$

and eqn. (F.5) becomes

$$m = \left[\left(\frac{W}{2}\right)^2 + Re_{TP}\left(\frac{k\Delta T}{h'_{fg}}\right)^2(1 - \cos\Phi)\right]^{\frac{1}{2}} \tag{F.6}$$

From a mass balance, the condensation rate w per unit length of tube is

$$w = 2(m_{\Phi=\pi} - m_{\Phi=0}) \tag{F.7}$$

and from an energy balance

$$wh'_{fg} = \pi d\alpha_n \Delta T \tag{F.8}$$

where α_n is the mean condensate h.t.c. for the Nth tube, which is being inundated at rate W.
Thus, from eqns.(F.6),(F.7) and (F.8) the value of the condensate h.t.c. is given by

$$\alpha_n = \frac{wh'_{fg}}{\pi d\Delta T} = \left[\left(\frac{Wh'_{fg}}{\pi d\Delta T}\right)^2 + 8(Re_{TP})\left(\frac{k}{\pi d}\right)^2\right]^{\frac{1}{2}} - \frac{Wh'_{fg}}{\pi d\Delta T} \tag{F.9}$$

The mean condensate h.t.c. α_{N-1} for the N-1 tubes above the Nth tube is obtained from an energy balance as

$$\alpha_{N-1} = \frac{Wh'_{fg}}{(N-1)\pi d\Delta T} \tag{F.10}$$

and the condensate h.t.c. for the top tube in the column (i.e. an uninundated tube) is from eqn. (1.25)

$$\alpha_1 = \frac{2\sqrt{2}}{\pi} \cdot \frac{k}{d} \sqrt{(Re_{TP})} \tag{F.11}$$

(Note: the coefficient $2\sqrt{(2)}/\pi$ comes from the exact solution.)

Substituting from eqns.(F.10) and (F.11) into eqn. (F.9) the condensate h.t.c. for the Nth tube is

$$\alpha_n = \left[\left((N-1)\alpha_{N-1}\right)^2 + \alpha_1^2\right]^{\frac{1}{2}} - (N-1)\alpha_{N-1} \tag{F.12}$$

The mean condensate h.t.c. for the column of N tubes is given by

$$\alpha_N = \frac{1}{N}\left(\alpha_n + (N-1)\alpha_{N-1}\right) \tag{F.13}$$

which after substitution from eqn. (F.12) can be re-written as

$$\alpha_N = \frac{1}{N}\left[\left((N-1)\alpha_{N-1}\right)^2 + \alpha_1^2\right]^{\frac{1}{2}} \tag{F.14}$$

Replacing N by (N - 1) in eqn. (F.14) we find

$$\alpha_{N-1} = \frac{1}{N-1}\left[\left((N-2)\alpha_{N-2}\right)^2 + \alpha_1^2\right]^{\frac{1}{2}}$$

which can be substituted into eqn. (F.14) to give

$$\alpha_N = \frac{1}{N}\left[\left((N-2)\alpha_{N-2}\right)^2 + \alpha_1^2 + \alpha_1^2\right]^{\frac{1}{2}} \tag{F.15}$$

The successive replacement of N by (N - 2), (N - 3) ... N - (N - 1) in eqn. (F.14) together with the corresponding substitution into eqn. (F.15) eventually leads to

$$\alpha_N = \frac{1}{N}\left(N\alpha_1^2\right)^{\frac{1}{2}} = \frac{\alpha_1}{\sqrt{N}} \tag{F.16}$$

and substituting into eqn. (F.12)

$$\alpha_n = \alpha_1\left(N^{\frac{1}{2}} - (N-1)^{\frac{1}{2}}\right) \tag{F.17}$$

In the analysis of Nusselt (1), extended by Jakob (2), which is similar to the above, except that the effect of gravity is included and vapour shear is

not, the equation equivalent to eqn. (F.16) is, from eqns.(1.2) and (1.3),

$$\alpha_N = \frac{\alpha_1}{N^{\frac{1}{4}}} \qquad \text{(F.18)}$$

As N is greater than one, eqn. (F.16) predicts a more rapid decrease of condensate h.t.c. with increase in the number of tubes than eqn. (F.18). Experimental data show that eqn. (F.18) underestimates the value of α_N and, therefore, eqn. (F.16) appears to have little practical significance.

APPENDIX G

DESIGN OF INUNDATION TUBES

The design of a manifold to achieve a uniform discharge rate along its whole length depends primarily on the way the pressure within the manifold varies. There are two main factors which control this pressure distribution:

(a) friction forces at the wall;

(b) pressure recovery due to deceleration of the fluid.

If the pressure distribution can be predicted, there are a number of ways of obtaining a uniform discharge rate, i.e.

(a) varying the spacing between discharge holes;

(b) varying the size of the holes;

(c) changing the effective diameter of the manifold by using inserts.

The simplest type of tube to manufacture is one with uniform diameter holes on a varying pitch, and the design method used is outlined below.

If the discharge rate is uniform, then the bulk velocity V at discance x from the inlet is given by

$$V = V_o \left(1 - \frac{x}{L}\right) \qquad (G.1)$$

when V_o = velocity at manifold inlet

L = overall length of manifold.

$$\therefore \quad \frac{dV}{dx} = - \frac{V_o}{L} \qquad (G.2)$$

Note that this is an idealised situation as it assumes that the fluid velocity V is a continuous function of the distance x from the manifold entrance, whereas in practice there will be a step change in velocity at each of the holes in the manifold.

The momentum relation from boundary layer theory is:

$$\frac{d}{dx}(mV) = - \frac{\pi d_i^2}{4} \frac{dp}{dx} - \pi d_i \tau_{we} \qquad (G.3)$$

where m = mass flow rate at x,

τ_{we} = local equivalent shear stress which includes the wall shear stress and axial momentum losses due to the flow through the wall.

From experiments with a porous tube it was suggested (28) that

$$\tau_{we} = \tau_F + cVv_w\rho \tag{G.4}$$

where v_w = suction velocity at the wall,

c = momentum loss coefficient,

τ_F = wall shear stress without suction.

From mass continuity

$$\pi d_i \rho v_w = -\frac{dm}{dx} = -\frac{\pi d_i^2}{4}\rho\frac{dV}{dx} \tag{G.5}$$

$$v_w = -\frac{d_i}{4\rho V}\frac{d}{dx}\left(\frac{\rho V^2}{2}\right) \tag{G.6}$$

Substituting into (G.4)

$$\tau_{we} = \tau_F - \frac{c\,d_i}{4}\frac{d}{dx}\left(\frac{\rho V^2}{2}\right) \tag{G.7}$$

Substituting (G.7) into (G.3)

$$\frac{d}{dx}\left(p + \left(1 - \frac{c}{2}\right)\rho V^2\right) = -\frac{4}{d_i}\tau_F \tag{G.8}$$

This is the same form as arrived at by Van Der Hegge Zijnen (54), except that the coefficient of ρV^2 is given as k/2, where k accounts for the rate of pressure recovery. The value of k was quoted as being expected to be almost constant and somewhat less than unity due to the effect of branching. This would appear to be wrong, as k could take values as high as 2, and substituting for c = 0.7 (28), k becomes equal to 1.3.

For turbulent flow in a pipe the wall shear stress is given by Blasius (46c) as

$$\tau_F = 0.0791\ Re^{-\frac{1}{4}}\frac{\rho V^2}{2} \tag{G.9}$$

Substituting eqn. (G.9) into eqn. (G.8) and integrating between 0 and x the pressure distribution in the turbulent flow region is given by

$$p = p_o + \frac{\rho V_o^2}{2}\left[(2 - c)\frac{x}{L}\left(2 - \frac{x}{L}\right) + 0.115\ Re_o^{-\frac{1}{4}}\frac{L}{d}\left(\left(1 - \frac{x}{L}\right)^{1\frac{1}{4}} - 1\right)\right] \tag{G.10}$$

where p_o = static pressure at inlet.

For Re < 2300 the flow becomes laminar and the wall shear stress is given by the Hagen-Poiseuille (46d) equation

i.e. for $\frac{x}{L} > \left(1 - \frac{2300}{Re_o}\right)$

$$\tau_F = \frac{16}{Re} \frac{\rho V^2}{2} \qquad (G.11)$$

Substituting (G.11) into (G.8) and integrating between the point at which the flow becomes laminar, ($x = x_L$), and $x = L$

$$p = p_{xL} + \left| \frac{x_L}{L} \left(2 - \frac{x_L}{L}\right) - \frac{x}{L}\left(2 - \frac{x}{L}\right) \right| \frac{\rho V_o^2}{2} \left(\frac{32L}{d_i Re_o} - (2 - c)\right) \qquad (G.12)$$

where P_{xL} = static pressure at the point at which the flow becomes laminar and is calculated from (G.10) with $x = x_L$

The volumetric discharge rate Q from a single orifice is

$$Q = C_D \frac{\pi d_h^2}{4} \sqrt{\left(\frac{2p}{\rho}\right)} \qquad (G.13)$$

where C_D = discharge coefficient,

d_h = orifice diameter

For a single sharp edged orifice, C_D is 0.63, and this value was used in the design of the inundation tubes as there is little available data for orifice coefficients in manifolds. This was thought to be the greatest cause of inaccuracy.

For a uniform discharge rate Q_o/L, the number of discharge holes per unit length n is given by

$$n = \frac{Q_o}{LQ} = \frac{4Q_o}{\pi C_D d_h^2 L} \sqrt{\left(\frac{\rho}{2p}\right)} \qquad (G.14)$$

The solution can proceed once values have been assigned to the inlet pressure p_o and the orifice diameter d_h. The choice of these will determine the height of the jets of fluid from the orifices and the relative spacing of the orifices. Bearing in mind the fact that the inundation tubes were required to simulate condensate flow, both the jet height and orifice spacing were kept to a minimum.

The inlet pressure was calculated to give a jet height no greater than the distance between tubes in the tube bank, i.e.

$$P_o = \frac{(P_T - 1) dg\rho}{C_D^2} \qquad (G.15)$$

where P_T = pitch-to-diameter ratio.

The product of the hole diameter and initial spacing of the orifices is now fixed by the required discharge rate

$$\frac{\pi d_h^2 n_o v_o}{4} = \frac{Q_o}{L} \qquad (G.16)$$

where v_o = discharge velocity from the first hole ($= C_D\sqrt{(2p_o/\rho)}$)

n_o = number of orifices per unit length at x = 0

$$\text{i.e.} \quad d_h^2 n_o = \frac{4Q_o}{\pi L v_o} \qquad (G.17)$$

n_o was chosen to be a suitable function of the orifice diameter to ensure that the orifices were reasonably close together, i.e.

$$1.5\ d_h < \frac{1}{n_o} < 5\ d_h \qquad (G.18)$$

The method of solution is therefore:-

(a) calculate p_o using eqn. (G.15);

(b) choose a value for n_o and calculate d_h from eqn. (G.17);

(c) calculate the position of the second orifice from $1/n_o$;

(d) calculate pressure at that orifice using either eqn. (G.10) if the flow is turbulent, or eqn. (G.12) if the flow is laminar;

(e) calculate new value of n from eqn. (G.14), and thus the position of the next orifice;

(f) repeat (d) and (e) until the end of the tube is reached;

(g) if the spacing between orifices exceeds the desired limits at any point, choose new values of p_o and/or n_o and repeat steps (a) to (f).

Values of c = 1, 0.7 and 0 were used; these correspond to the values of (54), (28) and the assumption that the flow from the orifices does not affect the pressure distribution, respectively. However, for flow rates > 0.085 kg/s none of these coefficients were successful in producing a tube which would give a uniform distribution of inundation, and for flow rates < 0.064 kg/s, a slightly modified tube with uniform size orifices with a uniform spacing was found to suffice.

APPENDIX H

SUMMARY OF EXPERIMENTAL READINGS

The experimental readings are given in Tables 1 - 4. Each line of data is the average of three sets of readings obtained as explained in sections 2.4.1 and 3.3.1. The following points should be noted:

(a) the cooling water inlet and outlet temperatures, T_{IN} and T_{OUT}, are the actual measured values, but the cooling water temperature rise, ΔT_{CW}, has been corrected for temperature loss in the entry length as discussed in section 2.4.3;

(b) for all the single tube tests and for some of the tests on the square tube bank (as noted in Table 3), a dirt coefficient of 120 kW/m^2 K needs to be included when calculating the tube inside h.t.c. (see section 2.4.5);

(c) the quoted inundation rate, W, is that from one inundation tube, and so the inundation for the bank as a whole is three times this value.

TABLE 1

DATA FOR SINGLE TUBE TESTS WITHOUT WALL THERMOCOUPLES

$\frac{m_{cw}}{kg/s}$	$\frac{T_{IN}}{^oC}$	$\frac{T_{OUT}}{^oC}$	$\frac{\Delta T_{cw}}{K}$	$\frac{P_{st}}{bar}$	$\frac{T_{st}}{^oC}$	$\frac{U_\infty}{m/s}$
0.467	34.0	39.7	5.79	0.995	126.0	4.22
0.468	33.6	39.4	5.79	0.995	126.2	3.82
0.468	33.4	39.1	5.77	0.991	125.1	3.66
0.468	33.5	39.1	5.75	0.993	125.0	3.30
0.468	33.5	39.0	5.61	0.997	122.2	2.57
0.468	33.6	39.1	5.66	0.999	121.8	2.77
0.467	33.8	39.4	5.68	1.018	121.2	2.65
0.468	33.7	39.3	5.64	1.024	121.0	2.46
0.467	33.5	39.0	5.57	1.024	117.0	1.70
0.468	33.3	38.6	5.42	1.024	116.1	1.24
0.468	33.7	38.9	5.30	1.031	108.0	1.00
0.468	33.7	38.9	5.30	1.014	116.1	1.69
0.468	33.8	39.1	5.46	1.018	117.7	1.75
0.468	33.6	39.0	5.49	1.021	118.7	1.78
0.468	33.5	39.2	5.76	1.013	125.7	3.59
0.468	33.7	39.4	5.83	1.018	128.2	3.69
0.468	33.9	39.9	6.00	1.037	131.6	4.71
0.468	33.5	39.4	6.07	1.031	131.8	4.74
0.466	34.1	39.9	5.85	1.039	129.2	3.44
0.467	33.6	39.0	5.57	1.039	116.3	2.26
0.467	33.9	39.3	5.55	1.040	120.1	2.28
0.468	33.3	38.6	5.46	1.050	120.9	1.64
0.468	33.5	38.9	5.43	1.050	117.0	1.62
0.468	33.3	38.4	5.27	1.046	110.5	1.08
0.468	33.1	38.3	5.29	1.044	108.5	1.08
0.468	33.5	39.4	5.93	1.046	130.7	4.58
0.468	33.6	39.5	5.98	1.027	132.8	4.65
0.468	33.8	38.2	4.43	1.099	105.9	0.07
0.468	33.7	38.7	5.14	1.051	105.7	0.91
0.467	33.8	38.8	5.16	1.052	105.4	0.92
0.468	33.7	38.7	5.04	1.059	102.8	0.61
0.468	33.2	38.1	5.06	1.055	102.2	0.60
0.469	33.1	37.9	4.96	1.091	102.3	0.29
0.468	33.7	38.9	5.33	1.040	110.4	1.51
0.466	33.5	39.0	5.61	1.034	116.1	2.44
0.467	34.0	40.4	6.50	1.116	134.4	8.74
0.468	33.7	40.2	6.49	1.116	135.6	8.77
0.469	33.8	40.2	6.50	1.109	136.7	8.77
0.323	44.8	51.4	6.73	1.109	137.8	8.69
0.326	44.6	51.1	6.65	1.103	138.4	8.65
0.326	44.6	50.8	6.23	1.059	131.9	5.44
0.326	44.5	50.7	6.28	1.061	134.3	5.15
0.326	44.6	50.6	6.08	1.022	130.8	3.90
0.325	45.0	50.2	5.36	1.169	129.6	0.06
0.325	45.1	50.5	5.46	1.155	104.2	0.05
0.326	44.3	49.9	5.69	1.015	108.3	1.22
0.328	44.0	49.5	5.69	1.021	107.9	1.19
0.325	44.7	50.4	5.88	1.049	113.0	1.75

$\frac{m_{cw}}{kg/s}$	$\frac{T_{IN}}{^oC}$	$\frac{T_{OUT}}{^oC}$	$\frac{\Delta T_{cw}}{K}$	$\frac{P_{st}}{bar}$	$\frac{T_{st}}{^oC}$	$\frac{U_\infty}{m/s}$
0.326	44.9	50.7	5.89	1.049	114.2	1.79
0.326	44.4	50.3	5.95	1.036	118.8	2.48
0.324	45.3	51.1	5.92	1.037	122.9	2.56
0.326	44.7	50.6	6.03	1.050	126.1	2.89
0.326	44.8	50.7	5.96	1.038	126.1	2.87
0.319	44.1	50.2	6.28	1.050	131.0	4.35
0.326	44.4	50.4	6.14	1.050	131.8	4.39
0.325	45.1	50.6	5.50	1.117	109.1	0.41
0.323	44.7	50.1	5.53	1.110	103.0	0.38
0.326	44.5	49.9	5.52	1.033	105.0	0.94
0.326	44.0	49.4	5.53	1.032	106.2	0.94
0.325	45.2	51.3	6.27	1.074	137.7	6.66
0.327	45.1	51.3	6.23	1.073	137.9	6.71
0.468	32.5	38.7	6.20	1.070	138.3	6.77
0.468	32.5	38.6	6.18	1.069	138.6	6.78
0.228	66.4	71.2	4.93	1.042	138.3	6.99
0.231	66.2	71.0	4.89	1.070	138.3	6.81
0.230	66.2	71.1	4.99	1.088	138.8	7.54
0.231	65.8	70.7	5.05	1.061	138.9	7.77
0.325	46.0	52.2	6.32	1.086	138.9	7.59
0.326	44.9	51.3	6.40	1.088	138.8	7.58
0.467	35.0	41.0	6.16	1.086	139.3	7.56
0.231	66.3	70.7	4.56	1.032	130.3	4.01
0.231	66.0	70.5	4.59	1.033	132.1	3.94
0.231	66.2	70.7	4.81	1.048	135.3	5.34
0.231	66.8	71.2	4.63	1.048	135.3	5.32
0.231	66.6	71.0	4.57	1.033	135.1	5.07
0.231	66.4	70.9	4.60	1.037	135.6	5.06
0.231	66.3	70.7	4.57	1.056	126.6	2.05
0.231	66.1	70.5	4.53	1.056	125.1	2.09
0.232	66.3	70.6	4.56	1.025	130.9	3.42
0.232	66.5	70.9	4.53	1.025	131.3	3.35
0.231	66.2	70.4	4.41	1.049	121.1	1.12
0.231	65.7	70.2	4.61	1.092	114.7	1.18
0.230	66.0	70.3	4.54	1.096	107.3	0.36
0.231	65.8	70.2	4.49	1.088	103.8	0.35

TABLE 2

DATA FOR SINGLE TUBE TESTS WITH WALL THERMOCOUPLES

$\frac{m_{cw}}{kg/s}$	$\frac{T_{IN}}{^oC}$	$\frac{T_{OUT}}{^oC}$	$\frac{\Delta T_{cw}}{K}$	$\frac{P_{st}}{bar}$	$\frac{T_{st}}{^oC}$	$\frac{U_\infty}{m/s}$	$\frac{\Delta T}{K}$
0.427	24.9	32.0	7.16	1.024	116.0	3.69	26.7
0.431	15.6	22.8	7.19	1.035	115.7	3.30	27.7
0.445	11.6	19.4	7.81	0.989	127.4	4.53	27.9
0.447	13.3	21.0	7.75	0.987	127.6	4.60	28.0
0.407	15.0	22.8	7.90	0.982	125.8	3.92	27.0
0.407	16.4	24.2	7.82	0.981	125.5	3.71	26.7
0.396	17.7	25.5	7.88	1.002	125.0	3.44	26.9
0.377	18.9	26.8	7.96	1.018	123.0	3.04	26.6
0.377	19.4	27.1	7.74	1.005	119.0	2.37	27.0
0.338	19.6	27.5	7.93	1.001	115.6	1.63	26.7
0.508	10.7	18.1	7.45	1.026	130.7	6.29	29.4
0.507	13.1	20.5	7.41	1.027	130.3	6.32	28.4
0.508	15.2	22.5	7.36	1.027	130.2	6.39	28.3
0.508	18.6	25.7	7.16	1.030	132.1	6.46	27.6
0.363	20.1	27.5	7.41	1.011	115.8	1.97	27.3
0.379	20.6	27.8	7.27	1.020	115.9	2.06	27.5
0.396	21.1	28.2	7.17	1.023	116.8	2.41	27.6
0.403	21.6	28.7	7.20	1.032	118.0	2.57	27.4
0.346	21.9	29.2	7.41	1.028	111.4	1.31	27.3
0.309	21.7	29.2	7.54	1.037	111.3	0.64	27.4
0.486	17.1	24.9	7.79	1.086	135.5	7.89	28.1
0.487	20.4	27.9	7.56	1.086	136.1	7.94	27.6
0.487	23.6	30.9	7.34	1.086	136.5	7.91	26.2
0.496	60.8	64.9	4.36	1.086	135.3	7.96	15.2
0.303	58.1	63.1	5.22	1.017	130.9	4.00	13.6
0.323	56.8	61.9	5.22	1.014	131.6	3.84	14.6
0.371	57.9	62.5	4.79	1.023	130.3	4.42	15.4
0.373	59.3	63.8	4.71	1.031	131.8	4.59	15.0
0.382	58.2	62.7	4.64	1.007	129.9	3.24	15.0
0.373	58.6	63.1	4.68	1.031	127.3	2.49	15.4
0.498	15.1	22.5	7.41	1.057	135.1	7.62	26.8
0.499	17.5	24.8	7.33	1.057	135.0	7.76	26.6
0.490	58.9	63.2	4.48	1.057	134.4	7.82	15.4
0.498	13.6	21.0	7.39	1.049	132.6	6.13	27.9
0.490	61.8	65.8	4.10	1.049	134.6	6.21	15.4
0.428	61.1	65.4	4.44	1.029	134.1	5.34	14.5
0.410	62.0	66.2	4.31	1.018	134.3	5.04	13.6
0.376	61.8	65.6	3.92	1.015	110.8	0.58	15.0
0.362	61.7	65.5	4.00	1.010	102.8	0.58	14.7
0.361	59.7	63.9	4.32	1.014	108.9	1.46	14.5
0.380	58.8	63.0	4.34	1.023	116.2	2.03	15.3
0.372	56.9	61.4	4.62	1.039	126.0	2.76	15.2

TABLE 3

DATA FOR SQUARE TUBE BANK TESTS

$\frac{m_{cw}}{kg/s}$	$\frac{T_{IN}}{^oC}$	$\frac{T_{OUT}}{^oC}$	$\frac{\Delta T_{cw}}{K}$	$\frac{P_{st}}{bar}$	$\frac{T_{st}}{^oC}$	$\frac{U_\infty}{m/s}$	$\frac{W}{10^{-2}\ kg/s}$
0.468	33.2	39.6	6.48	1.007	133.1	8.39	0.00
0.468	33.1	39.6	6.50	1.007	133.2	8.39	0.00
0.468	33.0	39.6	6.73	1.043	134.5	10.24	0.00
0.468	32.8	39.5	6.73	1.039	134.7	10.43	0.00
0.468	33.1	39.6	6.61	1.015	134.4	9.59	0.00
0.468	33.5	39.8	6.36	1.026	130.6	7.44	0.00
0.468	33.1	39.3	6.38	1.027	130.7	6.86	0.00
0.468	32.9	39.1	6.33	1.028	129.9	6.17	0.00
0.468	33.2	39.2	6.14	1.019	125.5	4.83	0.00
0.467	33.2	39.1	6.03	1.015	125.6	4.18	0.00
0.467	33.1	38.8	5.83	1.012	120.8	2.95	0.00
0.468	33.0	38.6	5.64	1.030	134.2	2.48	0.00
0.468	33.4	38.7	5.44	1.028	130.7	1.60	0.00
0.326	44.7	51.1	6.46	1.040	132.0	7.91	0.00
0.325	43.8	50.3	6.60	1.053	132.9	8.66	0.00
0.326	44.5	50.9	6.49	1.013	132.3	8.63	0.00
0.326	44.6	51.0	6.58	1.025	133.2	9.71	0.00
0.326	44.6	51.0	6.47	1.013	132.3	9.03	0.00
0.324	44.9	51.1	6.30	1.051	127.3	5.39	0.00
0.326	44.7	50.4	5.80	1.036	119.0	2.24	0.00
0.326	45.1	50.6	5.58	1.023	131.8	1.67	0.00
0.325	44.9	51.1	6.37	1.004	131.0	7.65	0.00
0.325	45.1	51.3	6.33	1.016	130.7	7.20	0.00
0.326	45.0	51.2	6.29	1.016	129.9	6.33	0.00
0.326	44.5	50.6	6.22	1.017	128.1	5.35	0.00
0.326	45.1	51.0	6.06	1.009	126.1	4.80	0.00
0.326	45.1	51.0	6.00	1.009	123.5	4.16	0.00
0.326	45.1	50.8	5.93	1.021	123.6	3.26	0.00
0.326	45.0	50.7	5.79	1.020	118.7	2.63	0.00
0.326	45.0	50.6	5.66	1.024	113.6	2.06	0.00
0.325	45.2	50.5	5.42	1.020	107.2	1.08	0.00
0.468	33.7	38.7	5.13	1.010	105.7	1.17	0.00
0.468	33.4	38.6	5.25	1.025	106.1	1.37	0.00
0.468	33.4	38.8	5.44	1.021	110.5	1.94	0.00
0.231	65.3	70.1	5.04	1.009	131.4	6.68	0.00
0.231	65.7	70.5	5.00	1.017	131.2	6.51	0.00
0.231	66.1	71.0	4.97	1.017	129.2	5.90	0.00
0.231	65.8	70.6	4.94	1.014	127.2	4.96	0.00
0.231	66.1	70.8	4.88	1.017	125.9	4.51	0.00
0.231	65.9	70.6	4.77	1.015	122.2	3.24	0.00
0.231	65.8	70.4	4.72	1.015	118.4	2.72	0.00
0.230	66.1	70.6	4.64	1.023	114.9	2.10	0.00
0.230	66.0	70.4	4.58	1.029	109.2	1.41	0.00
0.468	33.0	40.1	7.11	1.065	136.2	15.03	0.00
0.326	45.0	52.0	7.03	1.067	138.0	14.99	0.00
0.326	44.1	51.2	7.09	1.060	139.6	15.05	0.00
0.326	44.1	51.0	7.01	1.039	139.6	14.30	0.00
0.326	44.2	51.0	6.90	1.026	139.4	13.40	0.00
0.326	44.1	50.9	6.84	1.019	139.0	12.62	0.00

$\frac{m_{cw}}{kg/s}$	$\frac{T_{IN}}{^oC}$	$\frac{T_{OUT}}{^oC}$	$\frac{\Delta T_{cw}}{K}$	$\frac{P_{st}}{bar}$	$\frac{T_{st}}{^oC}$	$\frac{U_\infty}{m/s}$	$\frac{W}{10^{-2}\ kg/s}$
0.231	66.1	71.1	5.18	1.019	139.1	12.54	0.00
0.231	65.5	70.7	5.31	1.030	139.5	13.50	0.00
0.231	65.6	71.0	5.50	1.053	139.8	14.73	0.00
0.231	66.7	72.1	5.46	1.073	139.0	15.76	0.00
0.231	65.2	70.8	5.74	1.079	139.6	15.72	0.00
0.230	65.7	70.5	5.00	1.009	131.3	7.17	0.00
0.232	65.3	70.2	5.03	1.015	131.7	7.96	0.00
0.232	66.2	71.1	5.07	1.033	134.6	10.38	0.00
0.231	65.7	70.7	5.13	1.034	135.6	10.52	0.00
0.467	33.8	40.2	6.48	1.047	134.4	9.48	0.00
0.466	33.3	39.8	6.53	1.047	136.3	9.55	0.00
0.467	33.5	40.1	6.66	1.067	137.7	11.23	0.00
0.468	33.4	40.2	6.90	1.087	138.1	13.29	0.00
0.468	33.8	40.7	6.95	1.090	138.7	14.30	0.00
0.468	33.4	40.4	7.11	1.101	139.1	15.51	0.00
0.468	33.6	40.5	7.02	1.074	139.0	14.93	0.00
0.467	33.6	40.4	6.81	1.053	139.1	13.01	0.00
0.467	34.0	38.6	4.70	1.035	128.2	4.73	5.75
0.468	33.7	38.3	4.68	1.017	127.6	5.28	4.96
0.466	34.0	38.9	4.90	1.011	125.4	5.27	3.77
0.469	34.0	39.1	5.18	1.011	126.1	5.70	2.69
0.469	33.9	39.0	5.19	1.026	128.6	5.66	2.83
0.468	33.9	39.3	5.58	1.034	129.5	6.04	1.79
0.468	33.6	37.1	3.56	1.069	105.7	1.26	6.15
0.467	34.1	37.6	3.56	1.069	105.1	1.24	4.47
0.470	33.6	37.3	3.83	1.075	104.9	1.23	2.83
0.466	34.0	38.1	4.19	1.075	105.0	1.29	1.77
0.468	33.6	37.2	3.71	1.062	112.1	2.18	6.09
0.467	33.9	37.5	3.75	1.062	111.9	2.21	4.47
0.467	33.6	37.7	4.11	1.065	112.8	2.21	2.85
0.468	33.6	38.1	4.65	1.066	113.1	2.23	1.79
0.466	33.6	38.0	4.49	1.067	113.0	2.22	1.79
0.470	33.6	37.6	4.01	1.062	118.4	3.44	6.09
0.468	33.7	37.8	4.11	1.061	118.8	3.27	4.44
0.468	33.6	38.0	4.48	1.046	118.0	3.31	2.87
0.468	33.6	38.4	4.90	1.042	118.2	3.37	1.74
0.466	33.8	38.1	4.40	1.039	123.6	4.88	6.06
0.467	33.3	37.6	4.36	1.038	123.3	4.59	6.08
0.469	33.1	37.7	4.65	1.036	123.3	4.60	4.42
0.467	33.4	38.2	4.95	1.034	123.1	4.63	2.83
0.467	33.9	39.1	5.29	1.032	123.2	4.64	1.76
0.467	33.3	38.8	5.53	1.036	124.8	5.62	1.77
0.467	33.9	39.0	5.20	1.036	125.2	5.63	2.83
0.469	33.6	38.4	4.81	1.039	125.4	5.57	4.42
0.469	33.5	37.9	4.48	1.048	125.6	5.52	6.06
0.468	33.4	39.1	5.84	1.066	132.0	9.64	6.11
0.467	33.3	39.2	6.02	1.057	132.6	9.98	4.45
0.467	33.5	39.5	6.17	1.044	131.8	10.08	2.80
0.468	33.5	39.8	6.37	1.059	131.8	10.17	1.77
0.470	33.0	38.3	5.46	1.045	130.9	8.71	6.04
0.469	33.2	38.8	5.68	1.045	130.9	8.86	4.45
0.466	33.2	39.1	5.98	1.051	131.1	8.82	2.78
0.468	33.0	39.1	6.20	1.051	131.3	8.97	1.79

$\frac{m_{cw}}{kg/s}$	$\frac{T_{IN}}{^oC}$	$\frac{T_{OUT}}{^oC}$	$\frac{\Delta T_{cw}}{K}$	$\frac{P_{st}}{bar}$	$\frac{T_{st}}{^oC}$	$\frac{U_\infty}{m/s}$	$\frac{W}{10^{-2}\ kg/s}$
0.468	33,3	38.3	5.01	1.041	129.1	7,14	6.04
0.469	33.2	38.4	5.28	1.037	129.1	7.27	4.44
0.468	33.5	39.0	5.63	1.037	129.5	7.28	2.83
0.468	33.2	39.1	5.96	1.037	129.7	7.48	1.81
0.230	65.5	70.2	4.83	1.051	133.1	10.27	6.11
0.229	65.9	70.5	4.81	1.046	132.3	9.93	4.47
0.230	66.1	70.9	4.89	1.043	132.8	9.97	2.87
0.229	66.1	71.0	4.99	1.041	132.3	9.68	1.79
0.231	65.9	70.3	4.54	1.053	132.0	8.15	6.11
0.231	65.7	70.1	4.57	1.046	131.2	8.19	4.49
0.231	66.1	70.7	4.72	1.043	130.7	8.20	2.85
0.232	66.0	70.8	4.89	1.043	131.1	8.36	1.79
0.231	66.3	70.4	4.29	1.058	130.0	6.65	6.08
0.229	66.1	70.4	4.36	1.044	129.2	6.64	4.47
0.231	65.8	70.5	4.93	1.046	129.5	6.77	1.77
0.231	66.3	70.2	4.00	1.068	125.1	5.04	6.05
0.230	66.0	70.1	4.25	1.073	126.1	4.97	4.53
0.231	66.2	70.5	4.42	1.073	127.0	4.98	2.87
0.232	65.9	70.4	4.69	1.070	127.1	4.93	1.79
0.232	66.3	69.8	3.60	1.059	121.4	3.73	6.11
0.231	66.1	69.6	3.63	1.059	121.0	3.73	6.11
0.231	66.2	69.8	3.74	1.063	120.5	3.44	4.47
0.231	66.3	70.1	3.95	1.061	120.1	3.44	2.85
0.231	66.4	70.2	3.97	1.068	120.1	3.63	2.87
0.230	66.0	70.1	4.25	1.056	120.4	3.67	1.79
0.231	66.0	69.3	3.47	1.048	113.6	2.40	6.17
0.231	66.3	69.6	3.51	1.051	113.2	2.39	4.47
0.231	66.4	70.0	3.74	1.051	113.6	2.40	2.85
0.231	66.2	70.1	4.06	1.051	113.6	2.40	1.79
0.230	66.1	69.3	3.39	1.074	101.6	1.00	6.09
0.231	65.9	69.2	3.45	1.074	101.6	0.99	4.49
0.230	66.0	69.4	3.57	1.077	101.7	0.99	2.88
0.231	65.7	69.3	3.78	1.075	101.7	0.99	1.79
0.232	65.7	70.2	4.70	1.049	129.2	6.61	2.85
0.467	33.1	39.8	6.67	1.107	136.7	16.70	6.06
0.468	33.2	39.8	6.71	1.113	136.9	16.46	4.47
0.468	32.8	39.5	6.89	1.107	136.9	16.56	2.85
0.469	32.9	39.8	6.97	1.107	137.6	16.44	1.79
0.467	33.7	39.9	6.29	1.060	137.4	14.85	6.08
0.231	65.5	70.4	5.07	1.067	137.3	14.67	6.06
0.231	65.3	70.3	5.12	1.067	137.1	14.52	4.49
0.231	65.4	70.5	5.16	1.067	137.6	14.39	2.87
0.231	64.4	69.5	5.30	1.060	138.2	14.35	1.79
0.469	33.2	39.5	6.35	1.086	136.0	14.44	6.15
0.468	32.9	39.3	6.45	1.086	136.5	14.46	4.50
0.469	33.0	39.6	6.60	1.086	137.3	14.41	2.83
0.468	33.4	40.1	6.79	1.086	133.6	14.28	1.84
0.469	32.9	39.4	6.61	1.053	137.6	13.50	1.79
0.231	65.5	70.3	4.90	1.059	136.8	13.27	6.11
0.230	65.5	70.3	4.98	1.060	137.0	13.19	4.47
0.231	65.4	70.3	5.06	1.060	137.2	13.12	2.85
0.231	65.4	70.4	5.17	1.060	137.2	13.03	1.81
0.231	65.5	70.5	5.12	1.115	136.5	15.85	6.14
0.231	65.5	70.5	5.17	1.115	136.7	15.44	4.49
0.231	65.5	70.6	5.19	1.115	137.1	15.03	2.85

$\frac{m_{cw}}{kg/s}$	$\frac{T_{IN}}{^oC}$	$\frac{T_{OUT}}{^oC}$	$\frac{\Delta T_{cw}}{K}$	$\frac{P_{st}}{bar}$	$\frac{T_{st}}{^oC}$	$\frac{U_\infty}{m/s}$	$\frac{W}{10^{-2}\ kg/s}$
0.231	65.7	70.7	5.20	1.115	137.5	14.69	1.79
0.468	32.6	39.2	6.66	1.076	136.5	13.13	1.77
0.468	32.8	39.2	6.50	1.076	136.4	13.05	2.85
0.468	32.6	38.9	6.32	1.076	136.3	13.05	4.49
0.468	33.1	39.2	6.25	1.076	136.3	12.98	6.08
0.231	65.6	70.8	5.33	1.107	136.4	16.81	6.04
0.231	65.9	71.0	5.34	1.107	136.3	16.74	4.47
0.231	66.1	71.2	5.32	1.107	136.9	16.76	2.85
0.231	66.0	71.3	5.41	1.107	137.2	16.70	1.77

For all tests above, the dirt coefficient needs to be included; for tests below, it can be taken to be zero.

0.469	33.9	38.3	4.48	1.083	125.4	4.65	14.03
0.468	34.0	38.0	4.18	1.072	125.6	4.56	9.02
0.467	34.3	38.5	4.38	1.085	122.4	3.47	14.21
0.466	34.5	38.4	3.99	1.089	122.4	3.46	9.32
0.468	33.3	39.1	5.84	1.074	133.8	10.00	13.80
0.466	33.4	39.1	5.75	1.066	133.8	10.07	9.32
0.468	34.0	39.2	5.34	1.043	132.8	9.07	14.09
0.467	34.0	39.3	5.40	1.041	133.3	9.10	9.32
0.467	33.8	38.4	4.72	1.079	129.5	7.11	14.21
0.467	34.0	38.5	4.67	1.072	129.3	6.79	9.14
0.467	34.4	39.1	4.86	1.078	131.1	7.73	14.04
0.467	34.2	39.2	5.08	1.071	131.2	8.00	9.44
0.468	34.0	38.5	4.60	1.084	129.0	6.18	14.33
0.468	34.1	38.5	4.50	1.094	128.8	6.31	9.32
0.467	34.3	38.6	4.45	1.094	126.8	5.05	14.21
0.467	34.4	38.6	4.29	1.094	126.7	5.28	9.32
0.231	66.3	70.7	4.65	1.066	133.8	10.00	9.14
0.231	66.1	69.7	3.78	1.096	115.3	2.24	12.84
0.230	66.1	69.6	3.61	1.096	114.8	2.24	8.72
0.231	66.5	69.9	3.60	1.089	102.3	0.86	12.84
0.231	66.7	70.1	3.46	1.083	102.7	0.83	8.67
0.229	66.6	71.1	4.61	1.075	132.3	10.09	12.61
0.230	66.4	70.9	4.66	1.070	133.4	10.24	8.43
0.231	66.2	70.4	4.35	1.079	132.7	8.54	12.90
0.229	66.5	70.7	4.36	1.079	132.7	8.47	8.67
0.230	66.7	70.8	4.24	1.114	132.6	7.29	12.90
0.231	66.4	70.6	4.30	1.113	132.7	7.10	8.43
0.231	66.3	70.2	4.05	1.102	128.8	5.94	12.61
0.231	66.3	70.1	3.95	1.099	128.7	5.49	8.85
0.231	66.8	70.8	4.20	1.089	129.7	7.03	12.90
0.231	66.6	70.7	4.25	1.084	129.7	6.87	8.96
0.231	67.1	70.9	3.94	1.089	127.4	5.49	12.90
0.231	66.5	70.3	3.96	1.089	127.7	5.56	8.67
0.231	66.3	70.0	3.92	1.060	120.6	4.26	12.90
0.230	66.6	70.1	3.66	1.054	121.0	3.82	8.73
0.231	66.6	70.2	3.74	1.061	118.9	3.11	12.61
0.231	66.8	70.2	3.56	1.065	118.9	3.03	8.73
0.467	34.7	38.5	3.87	1.046	102.9	1.08	13.80

$\frac{m_{cw}}{kg/s}$	$\frac{T_{IN}}{^oC}$	$\frac{T_{OUT}}{^oC}$	$\frac{\Delta T_{cw}}{K}$	$\frac{P_{st}}{bar}$	$\frac{T_{st}}{^oC}$	$\frac{U_\infty}{m/s}$	$\frac{W}{10^{-2}\ kg/s}$
0.468	34.7	38.3	3.69	1.054	103.6	0.96	9.44
0.468	33.4	40.1	6.81	1.122	136.8	15.83	14.04
0.467	33.4	40.1	6.80	1.121	137.6	16.02	9.32
0.468	33.6	39.9	6.41	1.087	136.6	14.88	14.09
0.468	33.3	39.6	6.46	1.085	136.8	14.27	9.26
0.468	33.5	39.5	6.10	1.069	136.5	13.30	14.21
0.469	33.2	39.3	6.16	1.067	136.6	13.09	9.44
0.231	66.5	71.1	4.70	1.069	136.6	13.07	13.14
0.232	66.0	70.6	4.81	1.072	136.8	12.08	8.37
0.231	66.6	70.0	3.56	1.079	106.7	1.25	12.90
0.230	66.4	69.8	3.50	1.077	106.9	1.20	8.84
0.467	34.4	33.2	3.95	1.064	106.4	1.22	14.09
0.468	34.4	38.0	3.74	1.068	106.0	1.26	9.44
0.467	34.3	38.3	4.11	1.063	112.4	2.21	14.21
0.466	34.5	38.2	3.78	1.064	113.6	2.25	9.44
0.232	66.4	69.8	3.55	1.057	114.2	2.27	13.02
0.231	66.5	69.8	3.45	1.061	114.3	2.07	8.73
0.231	66.0	71.2	5.33	1.118	124.5	16.03	12.84
0.230	65.3	70.7	5.48	1.123	137.5	14.22	8.37
0.232	65.0	70.4	5.54	1.125	135.8	13.38	12.84
0.232	65.7	71.0	5.46	1.127	135.2	13.53	13.02

TABLE 4

DATA FOR TRIANGULAR TUBE BANK TESTS

$\frac{m_{cw}}{kg/s}$	$\frac{T_{IN}}{^oC}$	$\frac{T_{OUT}}{^oC}$	$\frac{\Delta T_{cw}}{K}$	$\frac{P_{st}}{bar}$	$\frac{T_{st}}{^oC}$	$\frac{U_\infty}{m/s}$	$\frac{W}{10^{-2}\ kg/s}$
0.467	32.6	40.4	7.87	1.107	129.6	21.90	0.00
0.467	33.1	40.7	7.67	1.073	131.3	20.53	0.00
0.468	32.8	40.3	7.61	1.059	133.7	19.62	0.00
0.468	32.6	40.1	7.54	1.047	134.3	18.82	0.00
0.468	32.7	40.1	7.51	1.041	134.2	18.10	0.00
0.468	33.3	40.6	7.34	1.031	134.0	16.84	0.00
0.468	33.7	41.0	7.37	1.031	132.9	17.06	0.00
0.469	33.0	40.2	7.33	1.021	134.7	16.02	0.00
0.469	33.1	40.3	7.31	1.019	134.0	16.04	0.00
0.468	33.8	40.0	5.23	1.062	102.3	0.88	0.00
0.467	32.9	39.8	6.99	1.035	130.0	11.72	0.00
0.468	32.9	39.8	6.99	1.042	130.5	11.40	0.00
0.468	33.1	40.0	6.97	1.038	131.3	11.20	0.00
0.467	33.1	39.9	6.86	1.024	130.4	10.06	0.00
0.467	32.9	39.7	6.88	1.035	129.6	8.96	0.00
0.468	33.4	40.0	6.74	1.031	126.7	6.72	0.00
0.467	33.6	40.4	6.89	1.052	126.3	8.00	0.00
0.468	32.9	39.3	6.57	1.032	121.8	3.66	0.00
0.231	65.0	70.9	6.00	1.118	131.4	21.04	0.00
0.231	66.3	72.0	5.89	1.118	131.3	20.71	0.00
0.231	66.4	71.9	5.68	1.090	133.0	20.22	0.00
0.231	65.7	71.3	5.71	1.076	134.3	19.42	0.00
0.231	65.8	71.3	5.64	1.064	134.9	18.35	0.00
0.231	65.5	71.0	5.64	1.056	135.1	17.71	0.00
0.232	65.5	70.8	5.54	1.050	135.3	16.85	0.00
0.231	66.1	71.4	5.45	1.043	134.1	16.20	0.00
0.231	66.2	71.4	5.40	1.036	134.2	15.59	0.00
0.231	66.0	71.2	5.36	1.062	121.0	4.85	0.00
0.231	66.2	71.2	5.16	1.106	107.8	1.00	0.00
0.231	66.0	71.1	5.22	1.079	106.8	1.70	0.00
0.232	65.8	70.9	5.26	1.071	111.1	2.61	0.00
0.231	66.5	71.6	5.26	1.078	117.2	4.17	0.00
0.231	65.9	70.9	5.23	1.024	120.2	4.98	0.00
0.231	66.4	71.6	5.34	1.064	124.8	7.31	0.00
0.468	33.7	40.4	6.79	1.059	122.5	6.51	0.00
0.468	33.6	39.1	5.59	1.059	106.5	1.05	0.00
0.468	33.4	39.2	5.96	1.062	105.3	1.81	0.00
0.468	33.5	39.7	6.30	1.062	109.1	2.77	0.00
0.468	33.1	39.7	6.75	1.055	116.6	4.34	0.00
0.467	33.1	40.0	7.02	1.054	123.4	6.31	0.00
0.468	33.1	40.0	6.96	1.050	122.6	5.28	0.00
0.467	32.6	39.9	7.29	1.031	130.2	9.45	0.00
0.231	66.3	71.5	5.39	1.062	130.4	11.60	0.00
0.231	66.4	71.6	5.39	1.056	131.4	11.88	0.00
0.231	66.1	71.3	5.28	1.040	131.2	11.08	0.00
0.231	66.2	71.3	5.33	1.045	130.9	10.40	0.00
0.230	66.1	71.2	5.28	1.042	130.0	9.17	0.00
0.231	66.0	71.1	5.27	1.050	128.0	7.55	0.00
0.232	66.3	71.4	5.29	1.056	125.0	5.65	0.00

$\frac{m_{cw}}{kg/s}$	$\frac{T_{IN}}{^oC}$	$\frac{T_{OUT}}{^oC}$	$\frac{\Delta T_{cw}}{K}$	$\frac{P_{st}}{bar}$	$\frac{T_{st}}{^oC}$	$\frac{U_\infty}{m/s}$	$\frac{W}{10^{-2}\ kg/s}$
0.231	66.3	71.2	4.99	1.058	111.3	1.30	0.00
0.469	33.7	39.3	5.73	1.037	105.0	1.41	0.00
0.468	33.1	39.1	6.10	1.045	105.8	2.02	0.00
0.468	33.5	39.8	6.40	1.044	110.6	2.94	0.00
0.468	33.3	39.9	6.68	1.070	114.4	4.02	0.00
0.471	33.7	39.0	5.30	1.033	120.6	4.43	5.97
0.468	34.0	39.2	5.32	1.035	120.9	4.39	6.09
0.467	33.8	38.9	5.18	1.036	120.9	4.42	4.50
0.466	33.9	39.0	5.19	1.035	120.6	4.42	4.47
0.467	34.1	39.1	5.14	1.029	121.3	4.54	2.87
0.468	33.5	38.8	5.44	1.033	120.4	4.46	1.79
0.467	33.6	40.3	6.76	1.067	131.3	12.06	6.06
0.465	33.1	39.7	6.73	1.046	131.9	12.20	4.44
0.470	33.2	39.9	6.76	1.042	132.2	12.42	2.83
0.469	33.1	39.9	6.86	1.040	132.8	12.45	1.77
0.469	33.6	40.1	6.50	1.036	130.3	10.03	1.77
0.470	32.9	39.4	6.57	1.036	130.8	10.04	1.79
0.468	33.5	39.8	6.38	1.036	130.2	10.03	2.85
0.468	33.5	39.7	6.35	1.035	130.8	10.10	4.44
0.467	33.4	39.6	6.32	1.032	130.3	10.16	6.06
0.469	33.8	39.2	5.48	1.042	125.7	6.04	6.08
0.467	33.9	39.3	5.48	1.047	125.9	6.40	4.47
0.468	33.6	39.0	5.47	1.044	125.7	6.18	2.91
0.468	33.5	39.2	5.82	1.042	125.0	6.14	1.77
0.468	32.7	40.1	7.56	1.150	134.1	18.08	6.09
0.468	32.8	40.3	7.55	1.150	134.6	18.36	4.45
0.467	32.8	40.4	7.61	1.148	135.0	18.72	2.88
0.466	32.9	40.5	7.72	1.144	134.9	19.35	1.81
0.472	32.8	40.2	7.44	1.094	134.7	18.02	1.79
0.468	33.2	40.4	7.28	1.086	135.3	16.81	2.83
0.469	32.8	40.0	7.24	1.088	135.4	16.43	4.49
0.469	33.2	40.3	7.19	1.090	135.1	15.80	6.09
0.467	34.1	38.9	4.83	1.071	102.1	0.74	1.77
0.467	34.3	38.5	4.29	1.062	101.9	0.93	2.85
0.468	34.8	38.9	4.24	1.064	101.7	1.08	4.44
0.472	34.1	38.7	4.66	1.066	101.8	1.48	6.00
0.467	34.2	39.0	4.87	1.043	103.3	1.72	6.04
0.467	34.2	38.5	4.39	1.042	103.3	1.72	4.47
0.467	34.4	38.6	4.32	1.042	103.4	1.72	2.85
0.467	34.1	38.9	4.90	1.040	102.9	1.72	1.79
0.467	34.0	39.1	5.15	1.028	109.6	2.77	1.79
0.469	34.2	38.7	4.55	1.027	111.9	2.79	2.82
0.467	34.6	39.1	4.58	1.027	112.4	2.81	4.47
0.467	34.3	39.3	5.07	1.026	112.4	2.78	6.15
0.468	33.8	39.3	5.68	1.043	127.7	6.87	6.09
0.468	34.1	39.6	5.62	1.043	128.3	7.24	4.45
0.467	33.9	39.6	5.72	1.044	129.0	7.46	2.85
0.229	65.6	71.4	5.94	1.158	132.9	18.62	6.00
0.231	65.2	71.1	5.98	1.158	132.9	18.62	4.50
0.232	65.6	71.4	5.92	1.148	133.1	18.32	2.83
0.234	66.0	71.7	5.89	1.150	134.1	19.29	1.79
0.231	65.9	71.4	5.70	1.097	135.0	17.81	1.79
0.231	65.7	71.2	5.61	1.102	135.1	16.89	2.85
0.233	65.7	71.1	5.65	1.102	135.1	16.30	4.42
0.232	65.9	71.3	5.57	1.105	135.2	15.84	6.08
0.231	66.5	70.8	4.42	1.066	119.1	3.85	6.06

$\frac{m_{cw}}{kg/s}$	$\frac{T_{IN}}{^oC}$	$\frac{T_{OUT}}{^oC}$	$\frac{\Delta T_{cw}}{K}$	$\frac{P_{st}}{bar}$	$\frac{T_{st}}{^oC}$	$\frac{U_\infty}{m/s}$	$\frac{W}{10^{-2}\ kg/s}$
0.230	66.7	70.8	4.23	1.074	120.0	3.93	4.47
0.232	66.5	70.6	4.19	1.073	120.1	4.07	2.83
0.234	66.3	70.6	4.46	1.069	121.3	4.19	1.79
0.231	66.9	70.9	4.25	1.070	114.9	2.12	1.79
0.233	66.9	70.6	3.89	1.074	112.0	2.17	2.85
0.234	66.8	70.6	3.93	1.073	112.2	2.09	4.42
0.231	66.2	70.4	4.31	1.065	112.6	2.01	6.14
0.231	66.1	71.1	5.16	1.061	131.2	11.99	6.11
0.230	66.5	71.5	5.18	1.061	132.2	12.28	4.45
0.231	66.0	71.0	5.15	1.052	131.6	11.84	2.83
0.233	65.7	70.8	5.18	1.043	130.9	11.66	1.79
0.232	66.2	71.0	4.93	1.064	130.3	9.21	2.83
0.231	65.9	70.6	4.91	1.060	129.2	8.75	4.47
0.232	66.2	70.9	4.90	1.057	129.4	9.33	6.06
0.233	66.5	70.9	4.55	1.073	124.7	6.04	6.06
0.232	66.8	71.1	4.49	1.073	125.5	6.29	4.45
0.232	66.5	70.9	4.55	1.071	125.6	6.41	2.85
0.231	66.8	71.4	4.70	1.069	125.3	6.72	1.79
0.231	66.4	70.9	4.58	1.061	124.5	5.73	1.81
0.231	66.3	70.5	4.39	1.069	122.6	4.86	2.85
0.231	66.6	70.7	4.33	1.069	122.4	4.88	4.42
0.231	66.4	70.8	4.47	1.069	122.6	4.77	6.11
0.465	32.5	39.1	6.70	1.075	135.6	14.13	14.51
0.467	33.3	39.8	6.54	1.068	134.7	13.84	14.33
0.468	33.2	39.4	6.37	1.056	134.2	13.54	9.26
0.468	33.7	39.6	5.96	1.034	133.0	11.56	9.44
0.468	33.4	39.3	6.01	1.033	129.9	10.06	14.21
0.467	33.3	39.1	5.81	1.022	130.5	9.82	9.02
0.468	33.5	39.3	5.82	1.035	129.5	9.00	9.44
0.467	34.0	39.7	5.84	1.049	129.6	8.93	14.21
0.467	33.5	39.1	5.63	1.039	127.5	7.44	14.21
0.474	33.8	39.9	6.19	1.031	127.2	7.39	9.14
0.468	33.5	39.7	6.38	1.058	121.9	4.91	9.56
0.469	33.7	39.1	5.45	1.059	121.1	4.86	14.09
0.467	34.2	39.3	5.16	1.037	113.3	3.68	14.04
0.468	33.6	39.4	5.91	1.034	115.1	3.70	9.14
0.468	33.6	39.1	5.68	1.033	111.8	2.48	9.32
0.468	34.0	39.0	5.19	1.036	109.5	2.47	13.61
0.468	34.2	38.9	4.79	1.045	101.4	1.23	13.61
0.468	34.0	39.1	5.21	1.050	101.3	1.28	9.32
0.468	32.9	40.0	7.18	1.152	127.1	17.03	14.21
0.467	32.9	39.9	7.10	1.140	125.3	16.89	9.26
0.470	33.2	39.8	6.63	1.088	130.0	14.78	9.14
0.468	33.5	40.1	6.69	1.092	130.5	14.33	14.09
0.231	67.1	72.1	5.12	1.091	130.7	14.01	14.21
0.231	66.8	71.8	5.21	1.095	131.7	14.42	14.21
0.231	65.9	71.0	5.29	1.096	131.8	14.91	9.32
0.231	65.7	71.2	5.67	1.149	126.9	16.90	9.44
0.232	66.2	71.7	5.64	1.155	127.1	16.52	13.92
0.230	66.6	71.2	4.71	1.093	130.6	7.20	14.21
0.230	66.4	71.3	5.10	1.093	131.6	7.54	9.26
0.231	66.9	71.8	5.02	1.084	137.0	13.29	9.02
0.231	65.8	71.0	5.30	1.088	137.5	13.17	14.09

$\frac{m_{cw}}{kg/s}$	$\frac{T_{IN}}{^oC}$	$\frac{T_{OUT}}{^oC}$	$\frac{\Delta T_{cw}}{K}$	$\frac{P_{st}}{bar}$	$\frac{T_{st}}{^oC}$	$\frac{U_\infty}{m/s}$	$\frac{W}{10^{-2}\ kg/s}$
0.463	34.1	40.0	5.95	1.127	130.0	7.53	14.21
0.468	33.5	39.6	6.20	1.130	131.6	7.86	9.32
0.468	33.5	39.9	6.43	1.079	129.7	6.74	9.44
0.469	33.6	39.2	5.68	1.079	129.7	6.65	14.21
0.463	33.9	39.3	5.43	1.074	125.1	4.68	14.21
0.468	33.2	39.4	6.33	1.070	124.2	4.72	9.44
0.469	34.0	39.8	5.93	1.072	120.2	3.20	9.32
0.467	34.2	39.5	5.36	1.063	116.9	3.10	14.21
0.467	34.0	38.6	4.79	1.055	101.7	1.13	13.62
0.466	34.0	39.2	5.23	1.054	101.3	1.13	9.32
0.230	66.2	71.3	5.22	1.084	124.9	5.23	9.32
0.231	65.9	70.5	4.70	1.082	125.9	5.21	14.21
0.232	66.8	71.0	4.43	1.075	120.1	2.92	14.21
0.231	66.4	71.1	4.90	1.070	117.3	2.90	9.44
0.231	65.8	70.4	4.69	1.067	105.3	0.97	9.56
0.231	66.6	70.7	4.30	1.068	103.1	1.21	14.09
0.231	66.2	71.1	5.10	1.082	134.2	11.16	14.21
0.231	65.9	70.8	5.01	1.078	135.4	11.67	9.32
0.226	65.5	71.1	5.79	1.156	138.4	17.37	14.04
0.231	65.1	70.8	5.76	1.156	138.4	17.61	9.44
0.469	33.0	40.1	7.14	1.155	138.7	17.73	9.32
0.472	33.1	40.2	7.18	1.155	138.7	17.56	14.09

FIG. 1

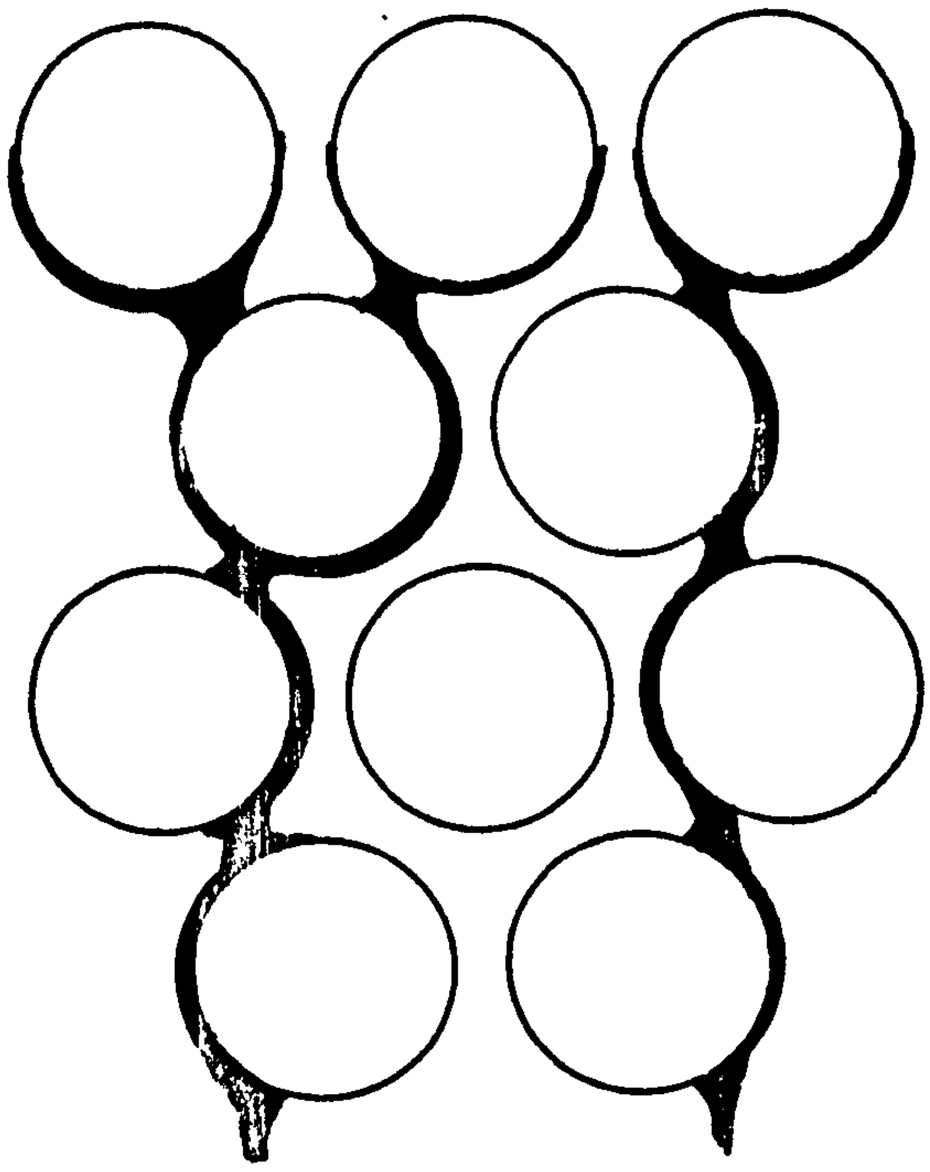

NOTE THAT ONE TUBE RECEIVES
NO INUNDATION

FIG. 1 SIDE DRAINAGE IN TRIANGULAR PITCH TUBE BANKS

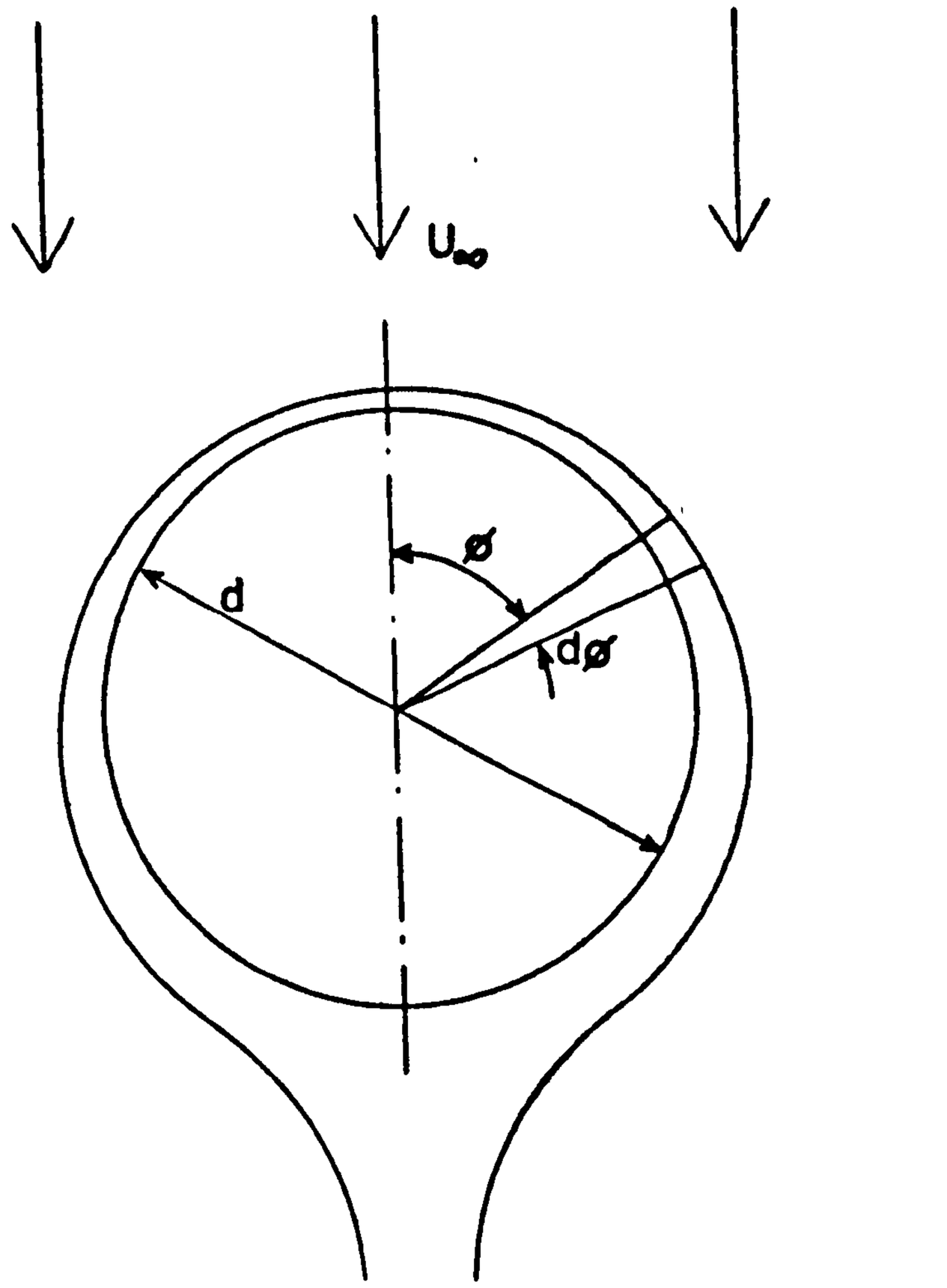

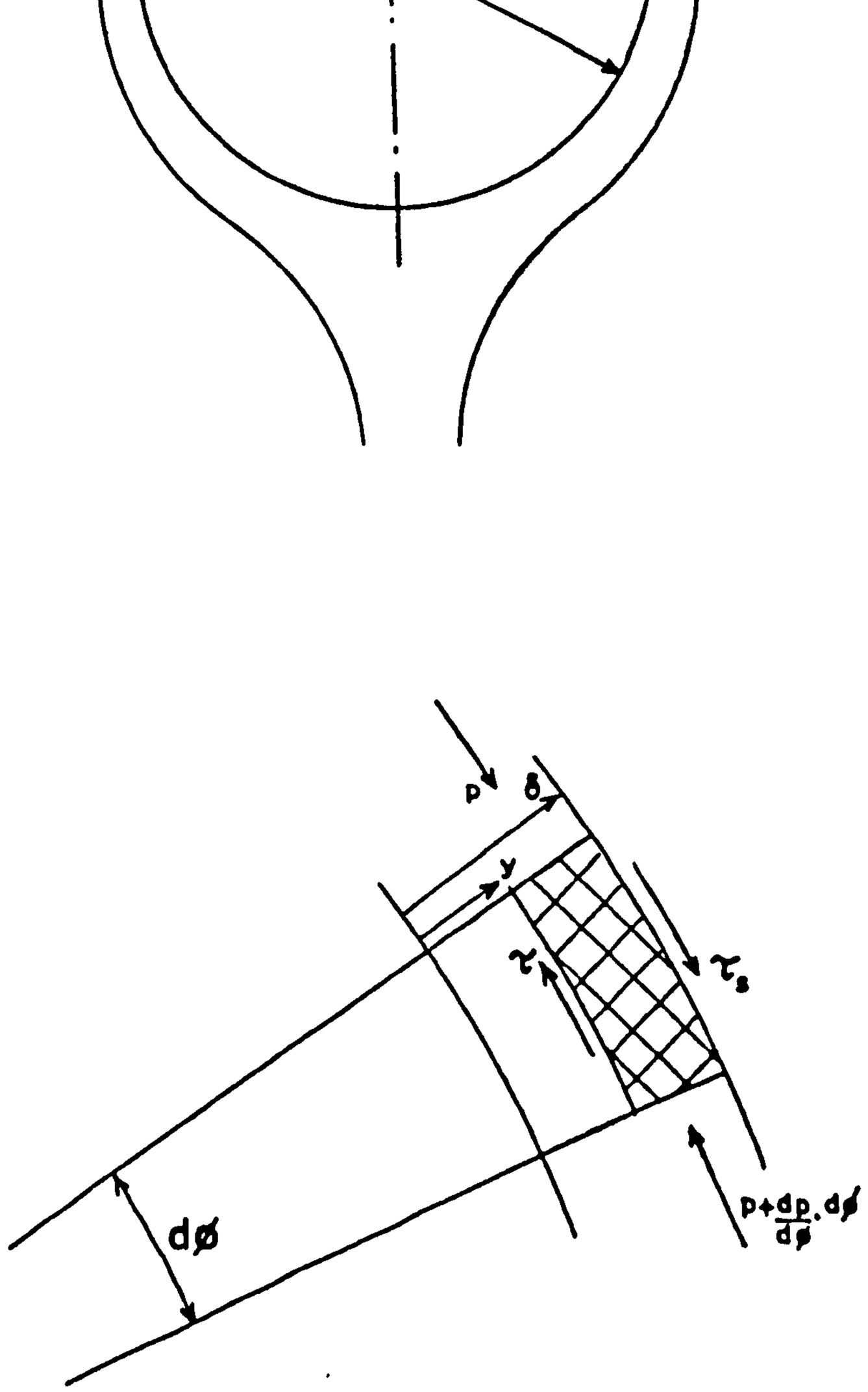

FIG. 2 PHYSICAL MODEL FOR SINGLE TUBE ANALYSIS

FIG. 3

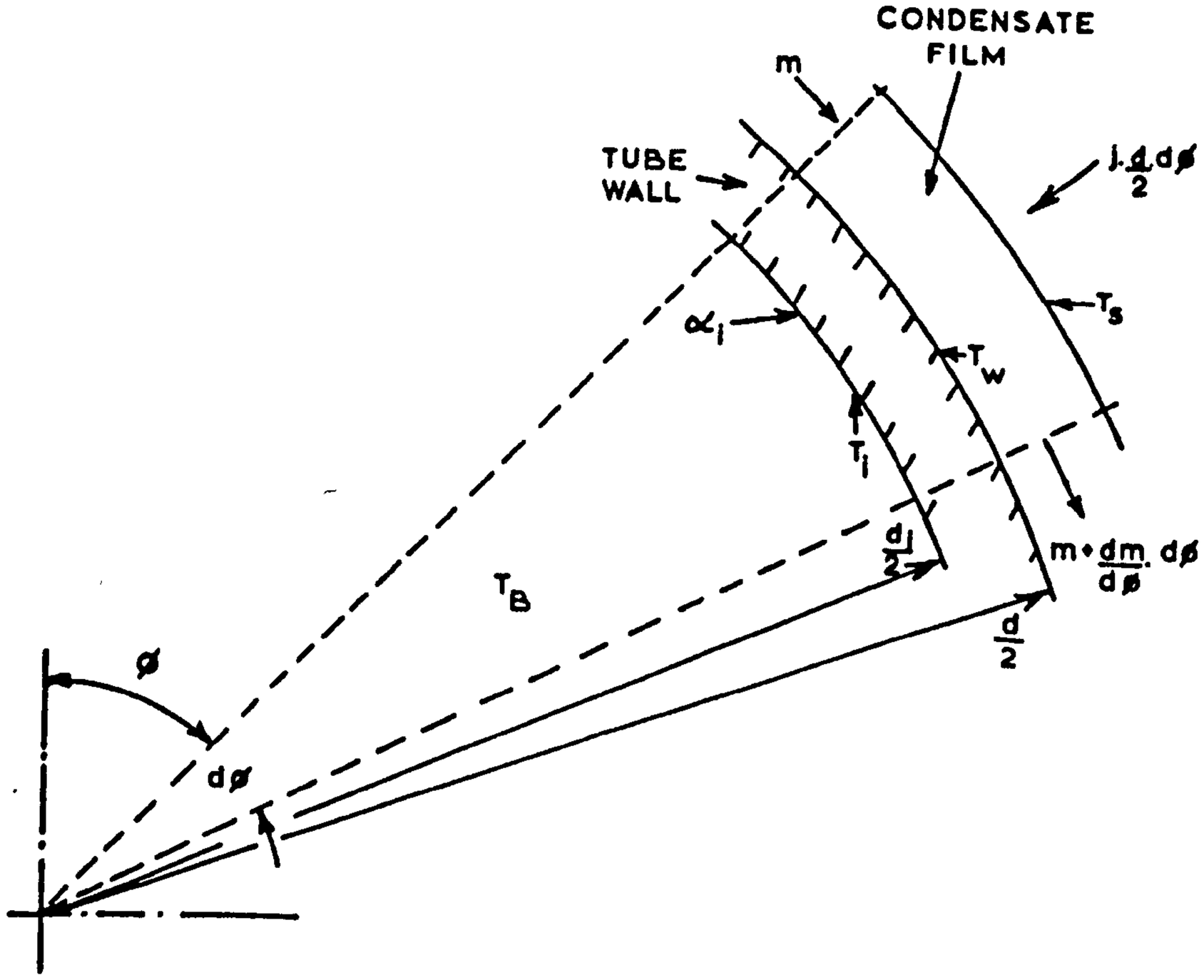

FIG. 3 MODEL FOR ENERGY BALANCE

FIG. 4

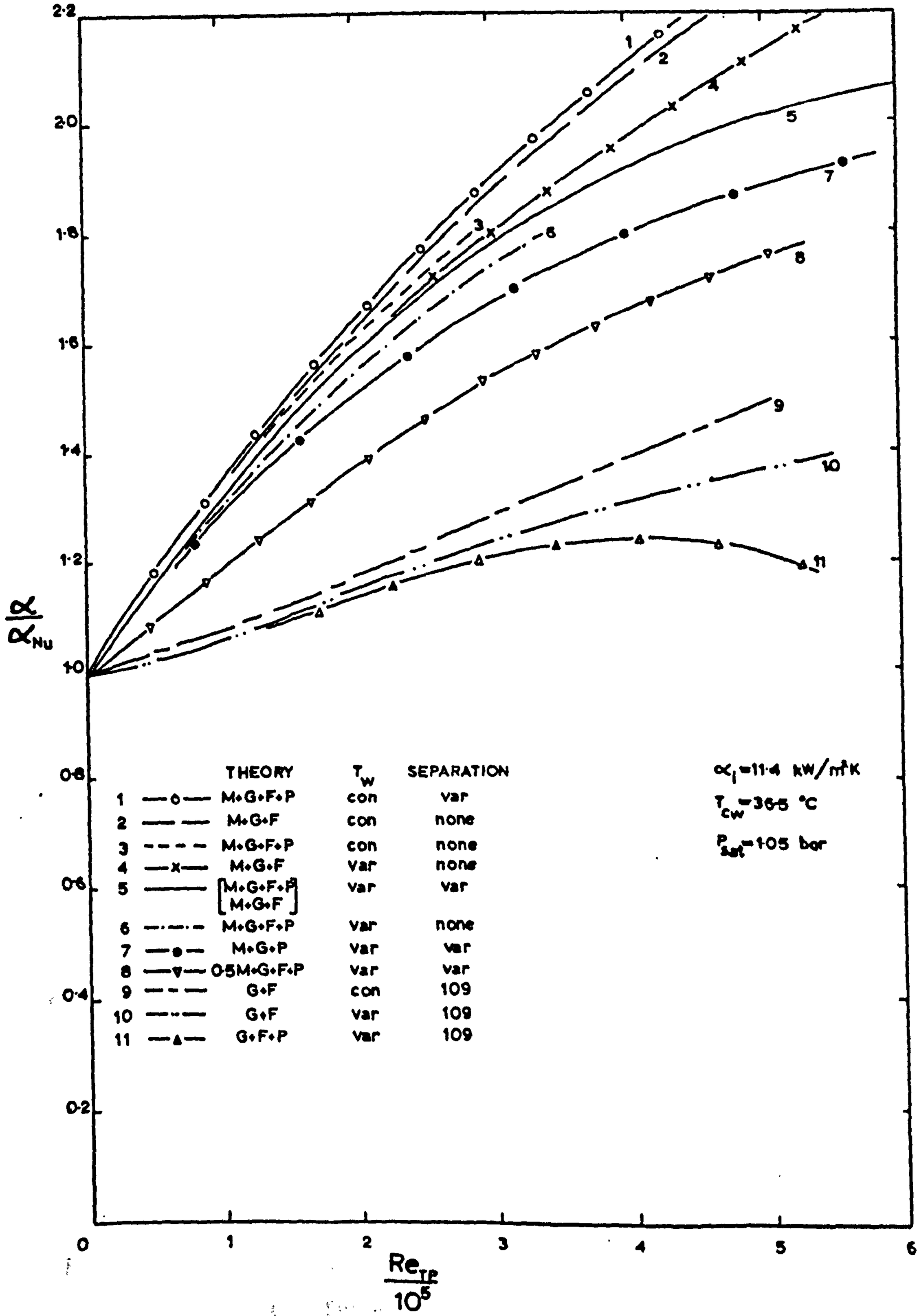

FIG. 4 NUMERICAL SOLUTIONS FOR SINGLE TUBE THEORIES (HIGH HEAT FLUX)

FIG. 5

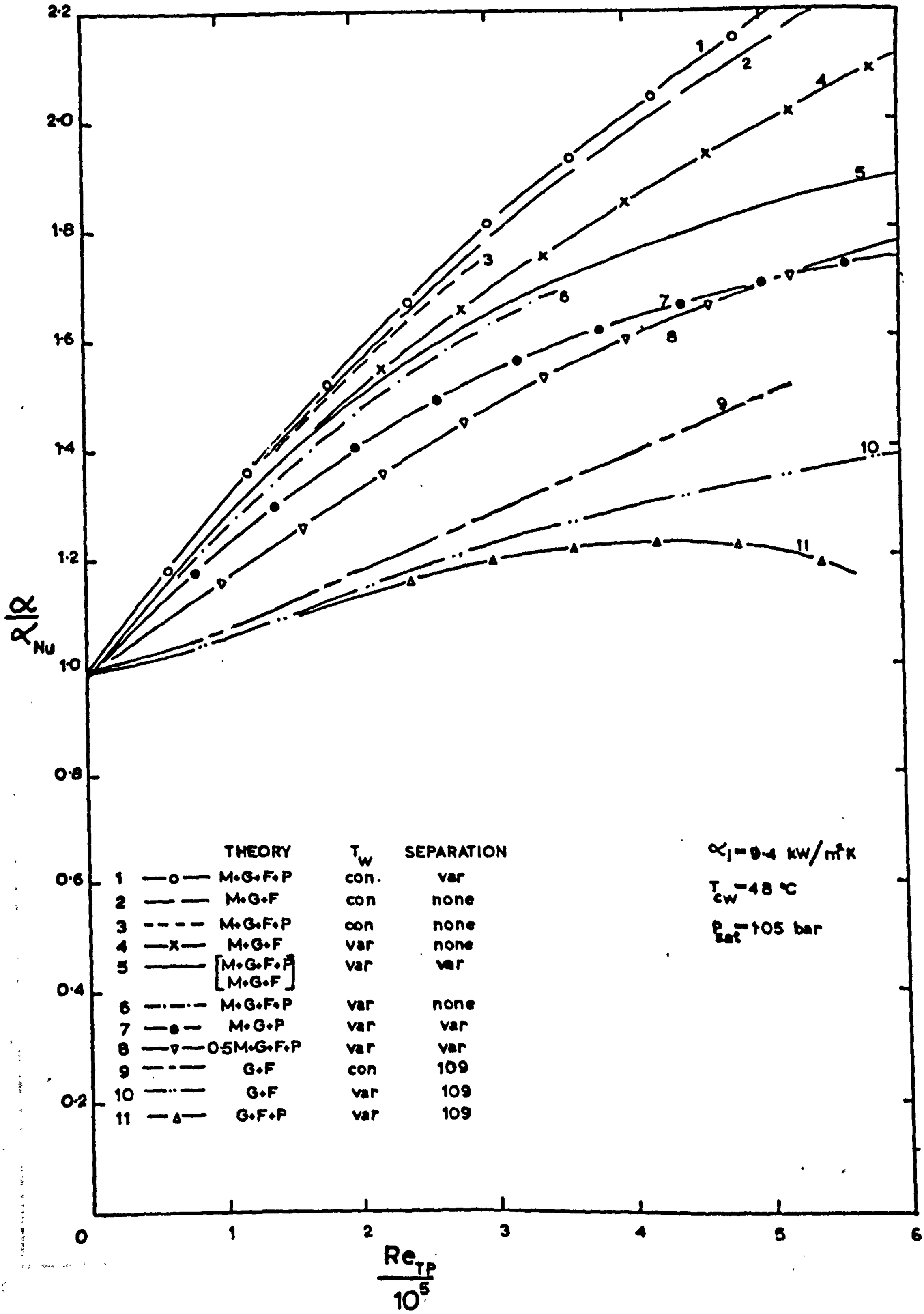

FIG. 5 NUMERICAL SOLUTIONS FOR SINGLE TUBE THEORIES
(MEDIUM HEAT FLUX)

FIG. 6

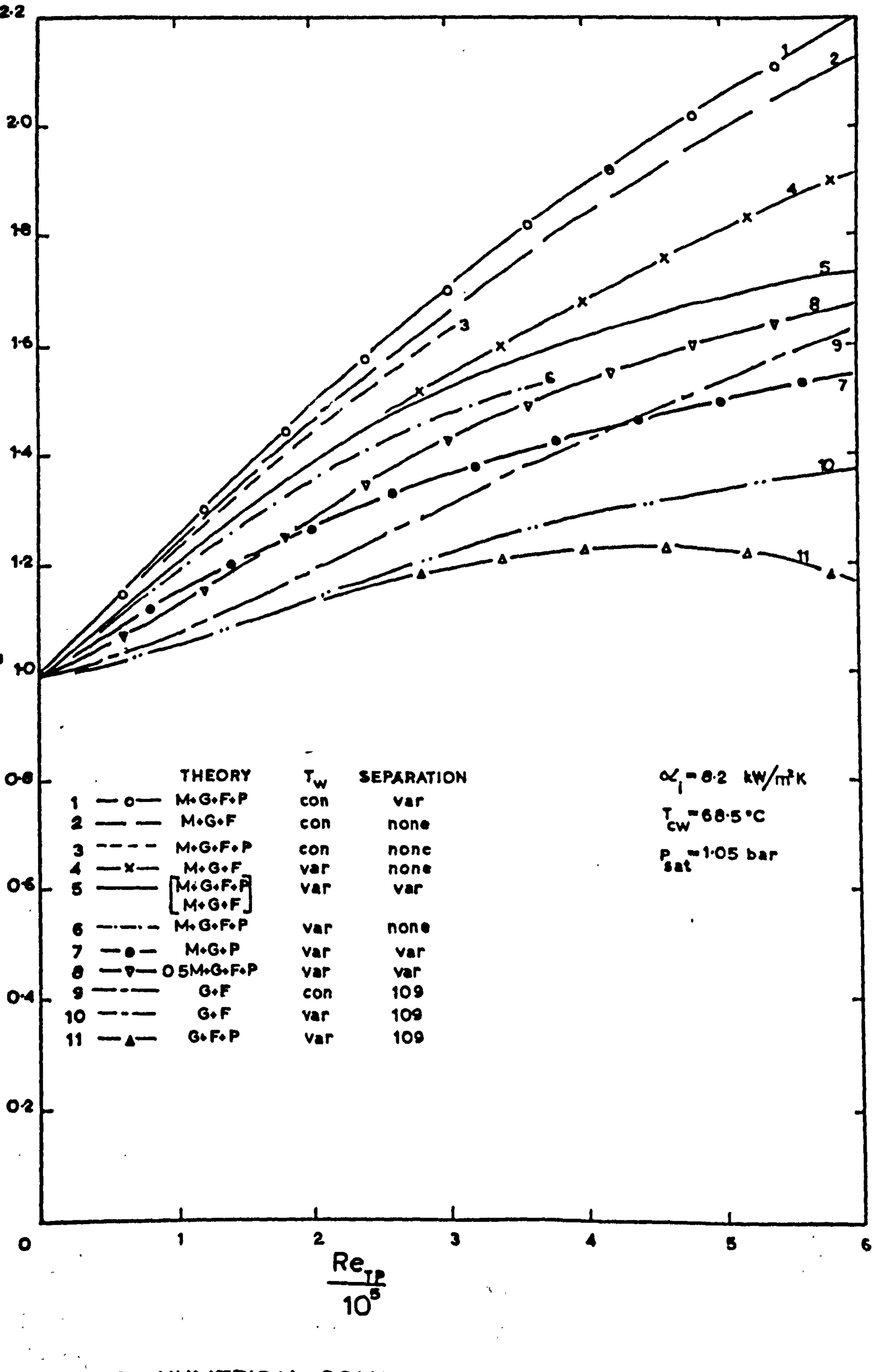

FIG. 6 NUMERICAL SOLUTIONS FOR SINGLE TUBE THEORIES
(LOW HEAT FLUX)

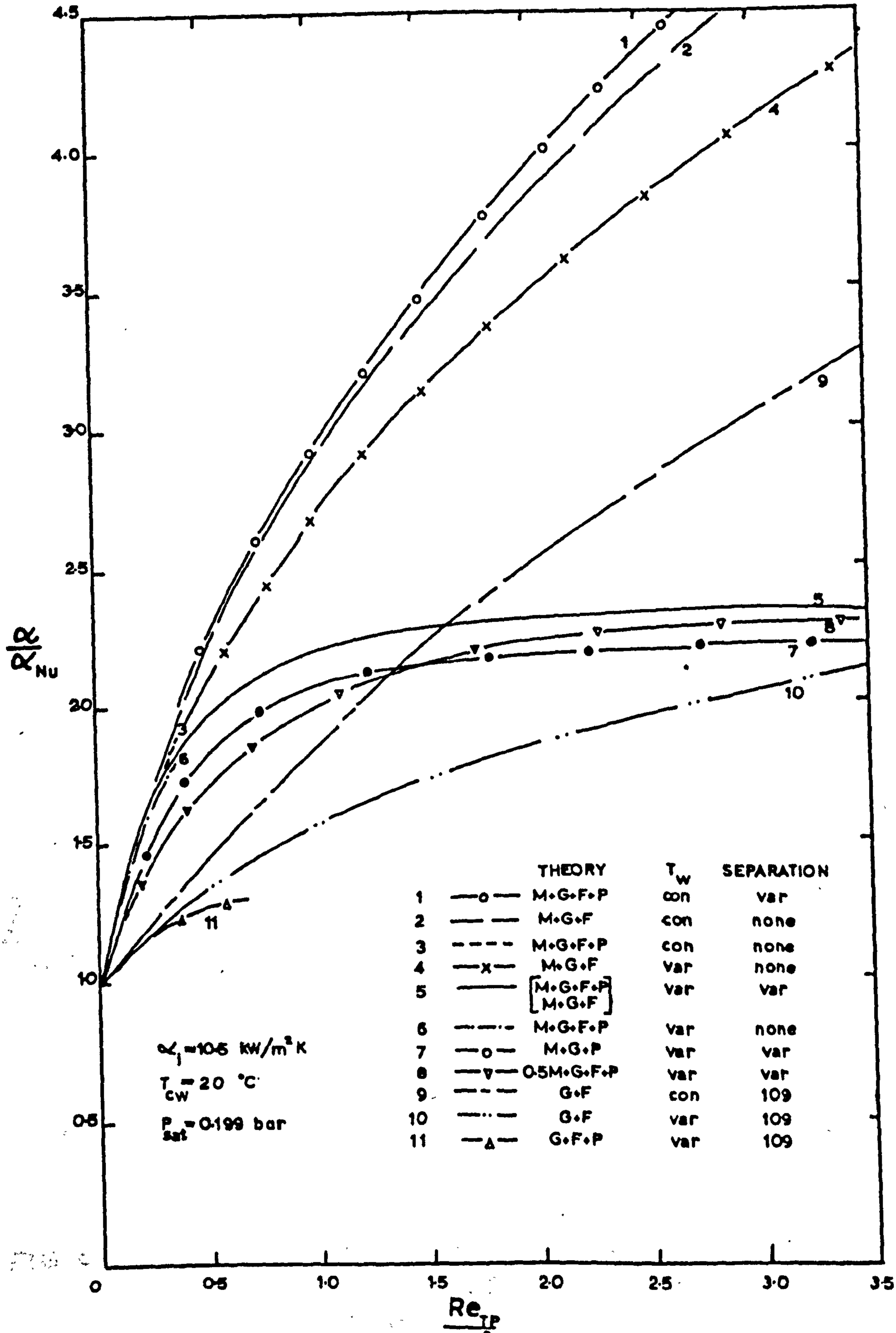

FIG. 7 NUMERICAL SOLUTIONS FOR SINGLE TUBE THEORIES

FIG. 8

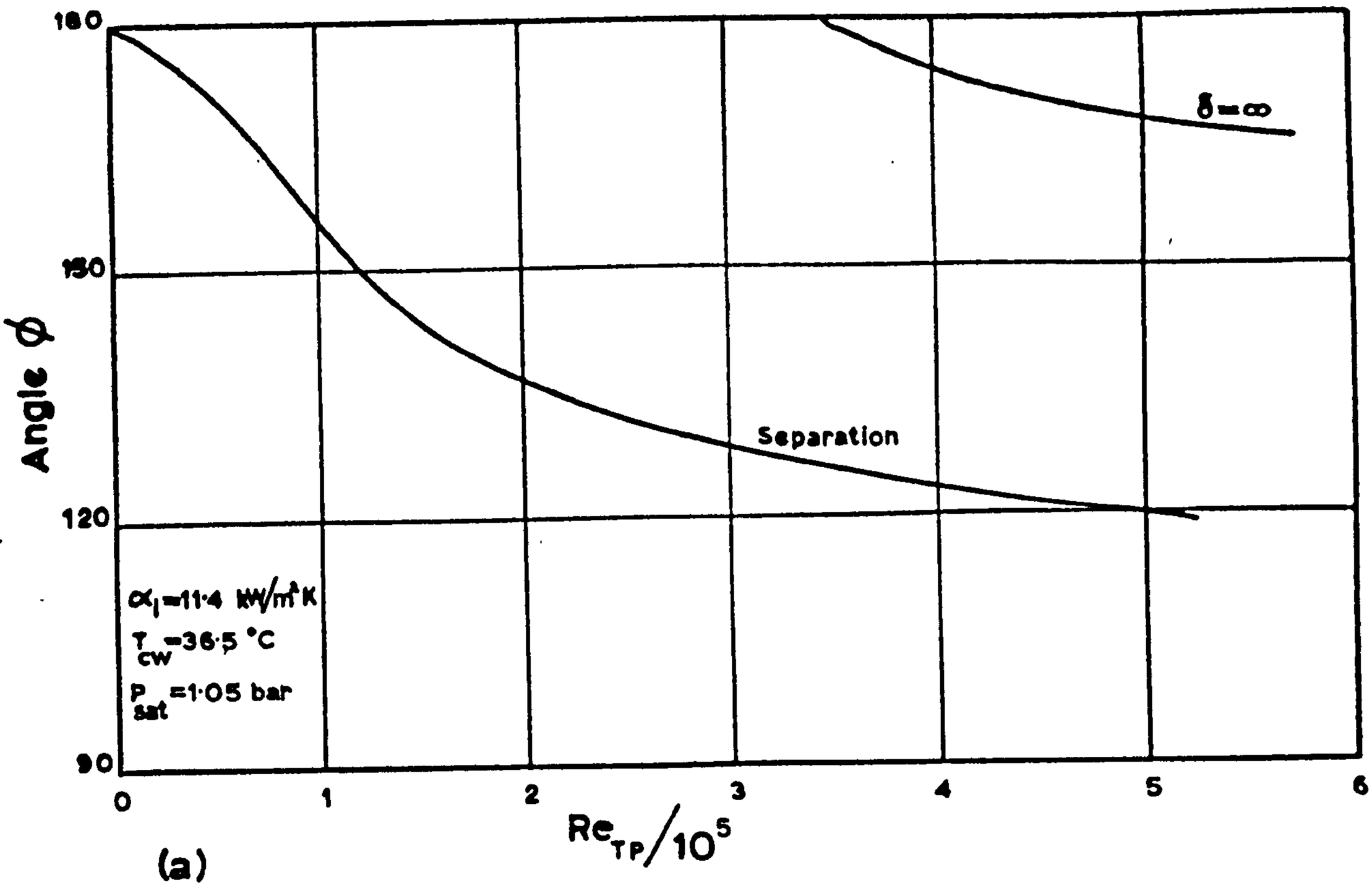

(a)

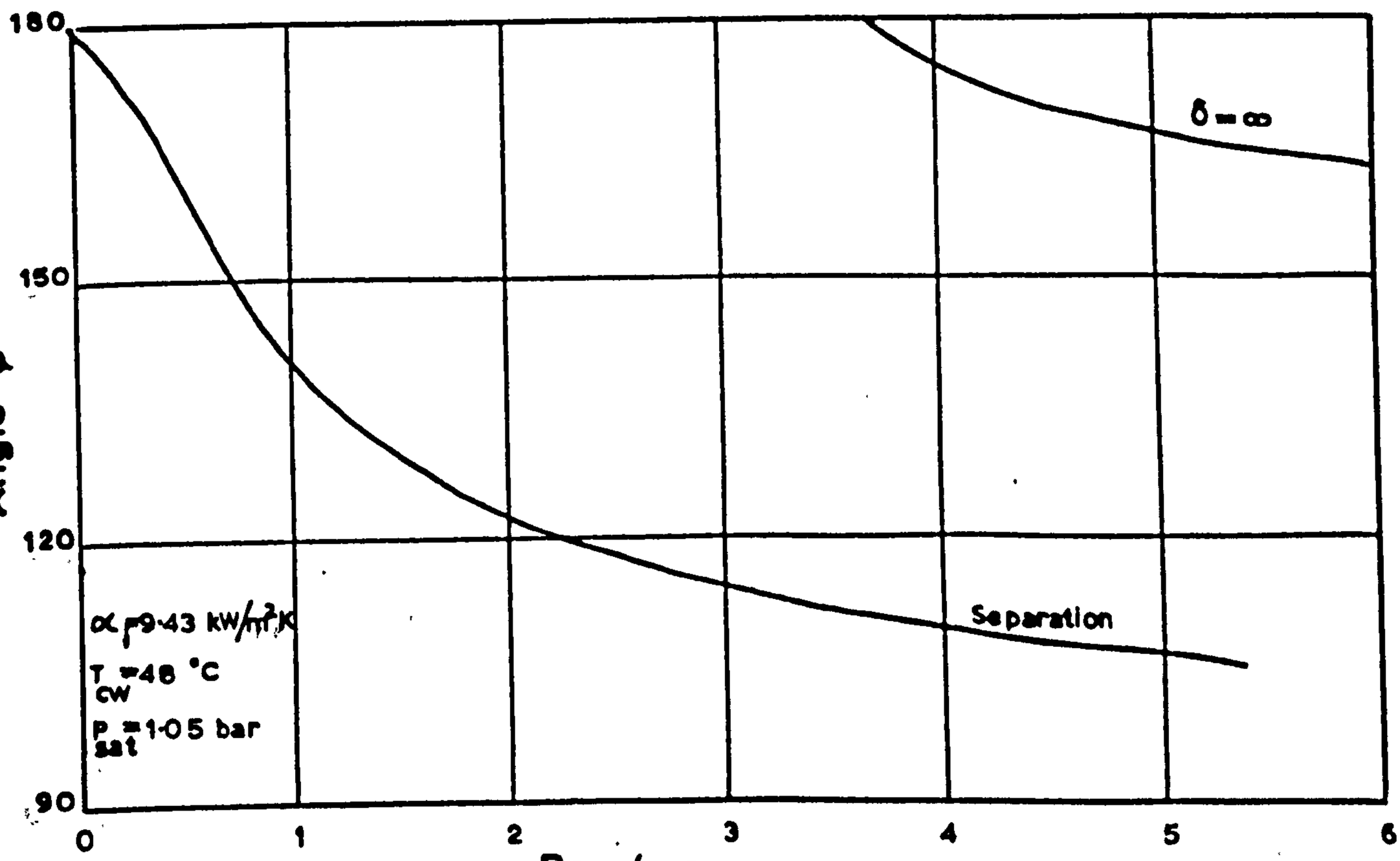

(b)

FIG. 8 VARIATION OF ANGLES OF SEPARATION AND INFINITE CONDENSATE THICKNESS PREDICTED BY THE M•G•F•P THEORY

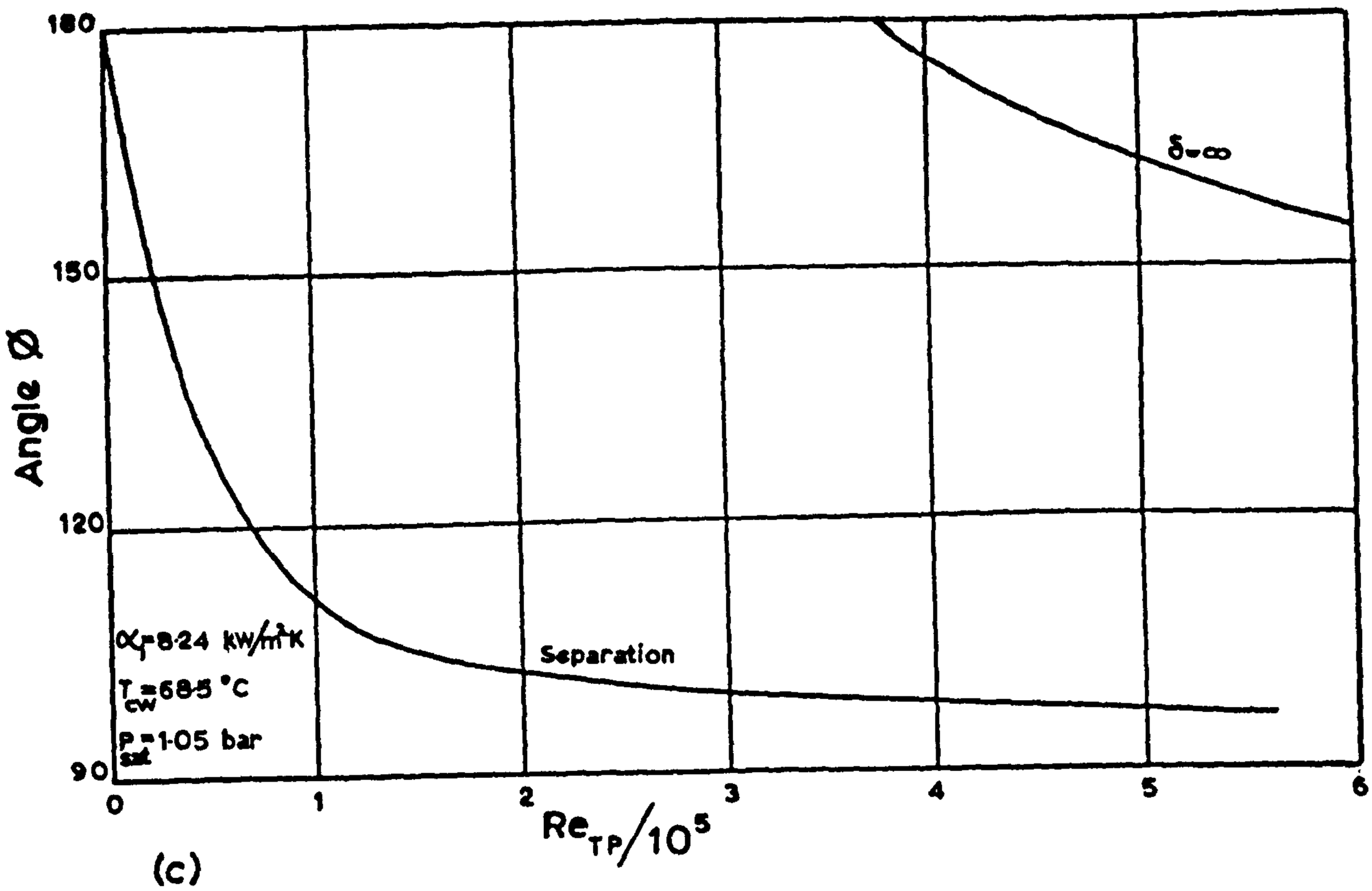

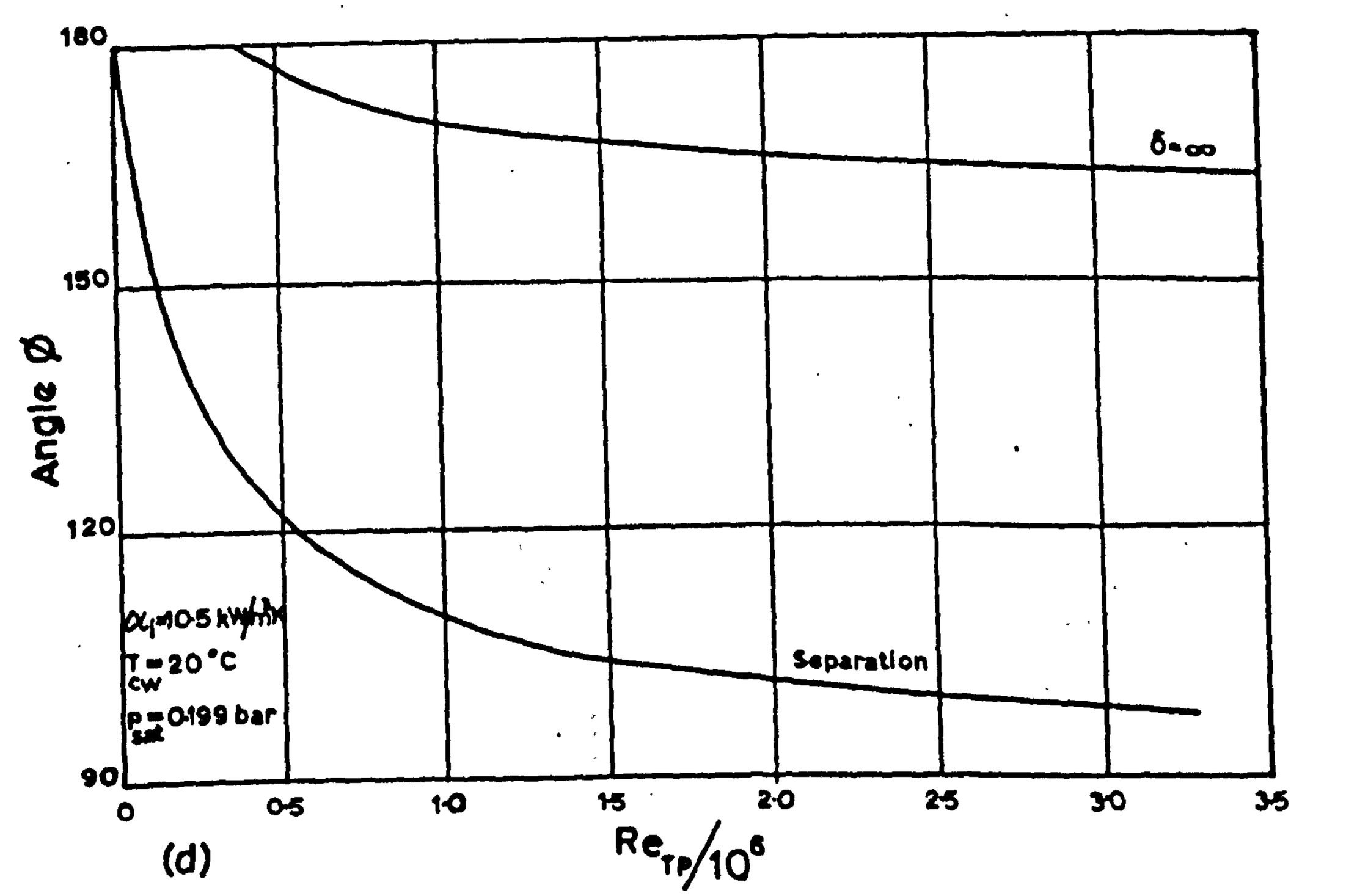

FIG. 8 VARIATION OF ANGLES OF SEPARATION AND INFINITE CONDENSATE THICKNESS PREDICTED BY THE M+G+F+P THEORY

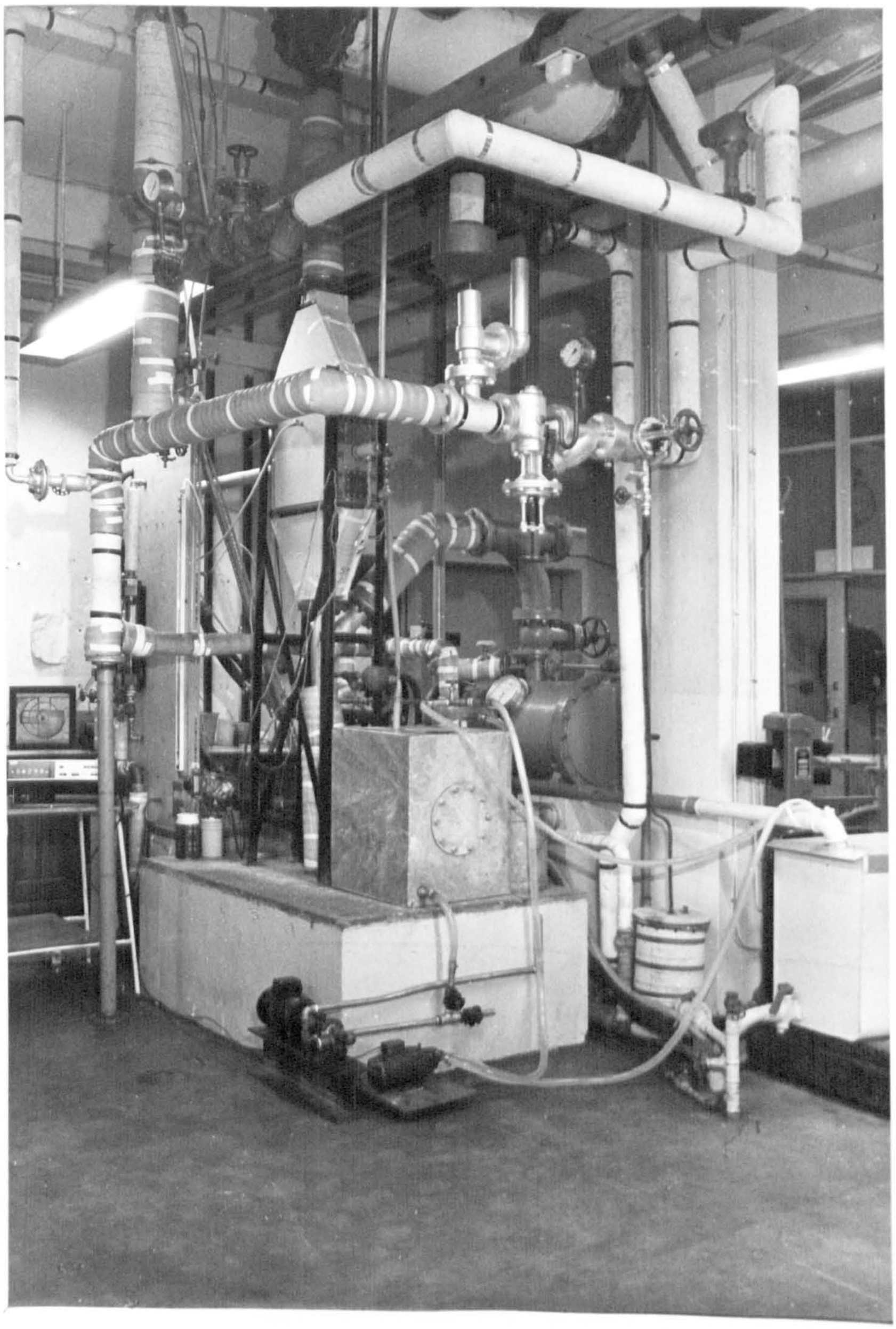

FIG 9 PHOTOGRAPH OF EXPERIMENTAL APPARATUS

FIG. 10

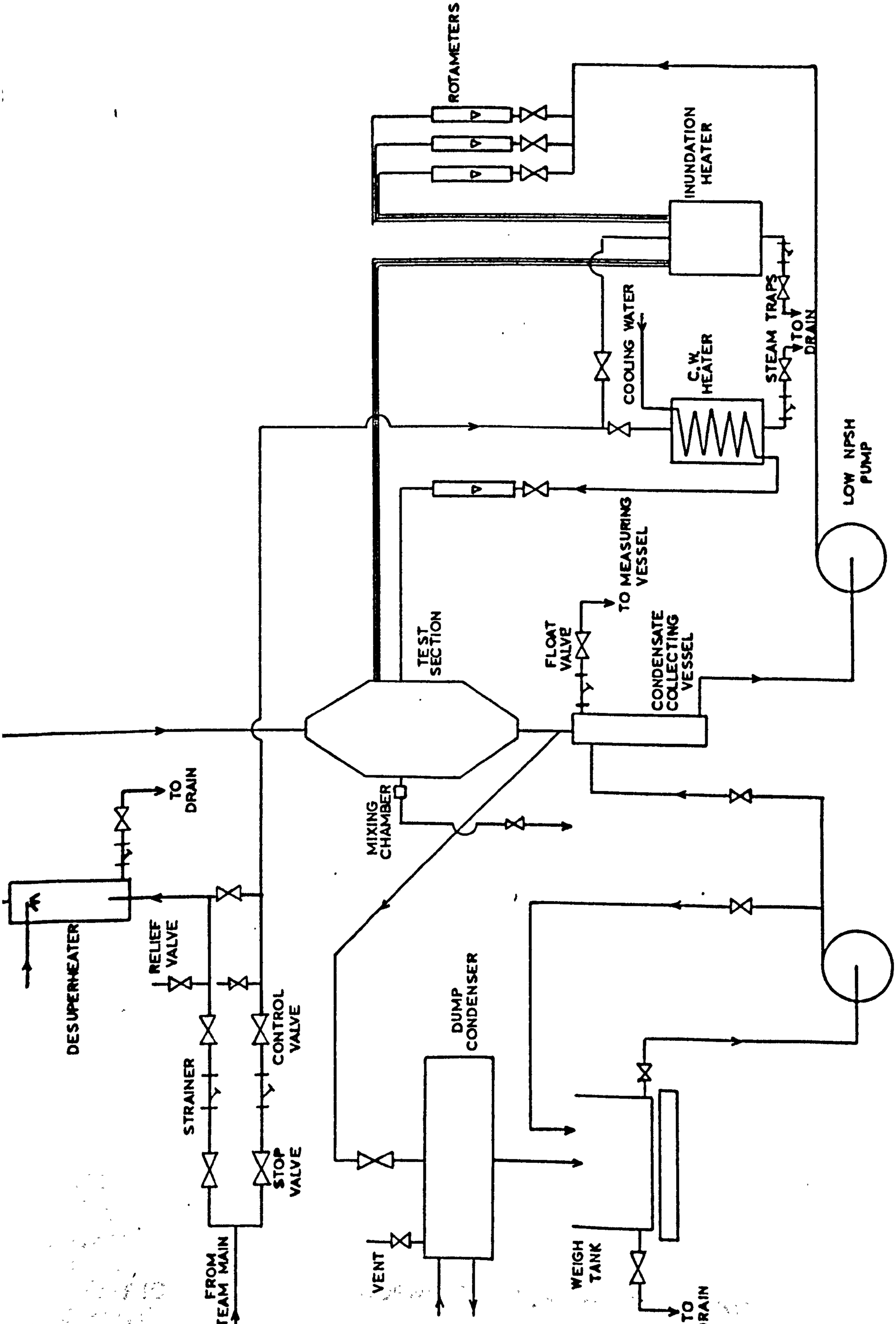

FIG.10 LINE DIAGRAM OF RIG

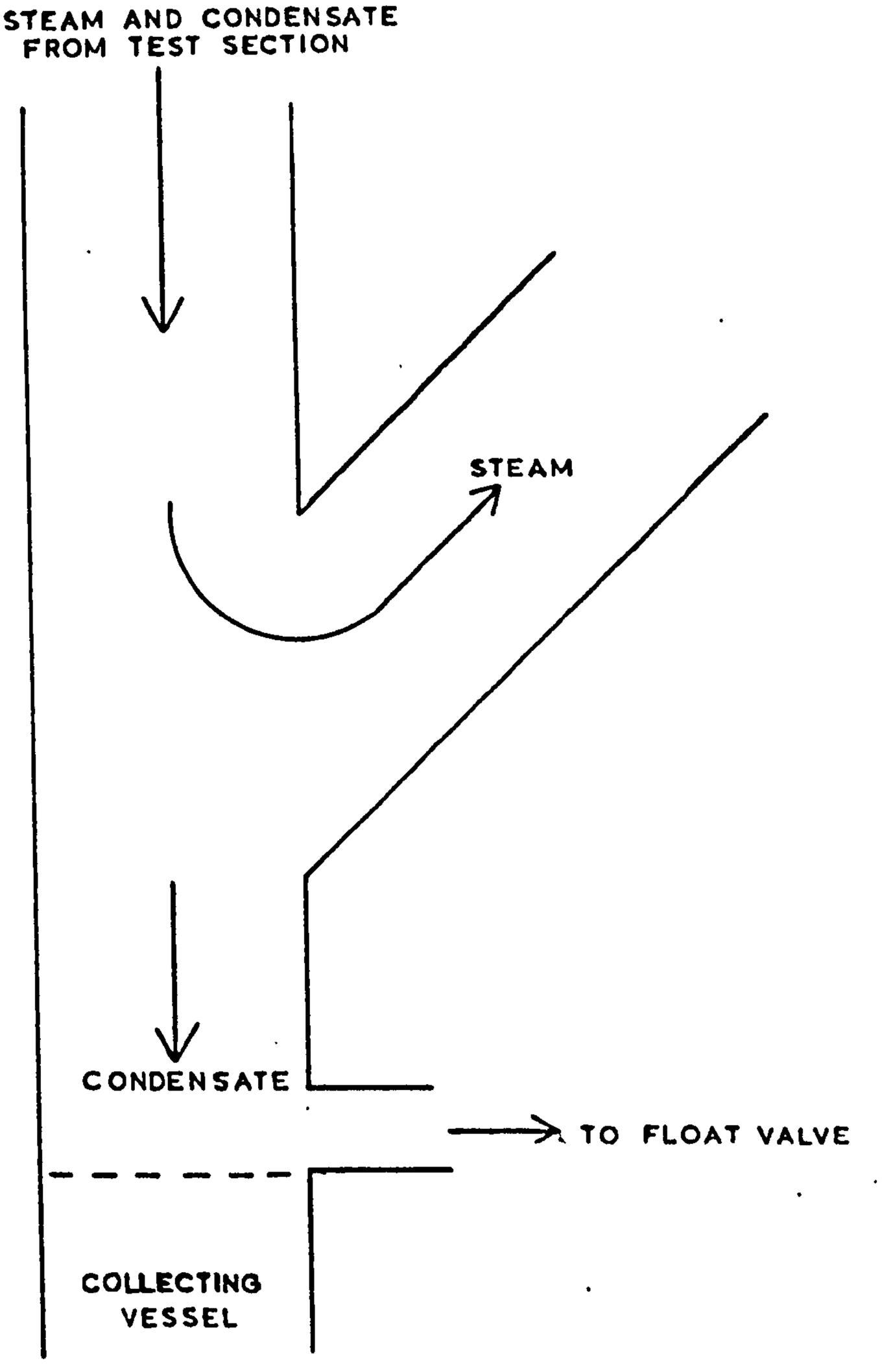

FIG. 11 STEAM/CONDENSATE SEPARATING BEND

FIG. 12

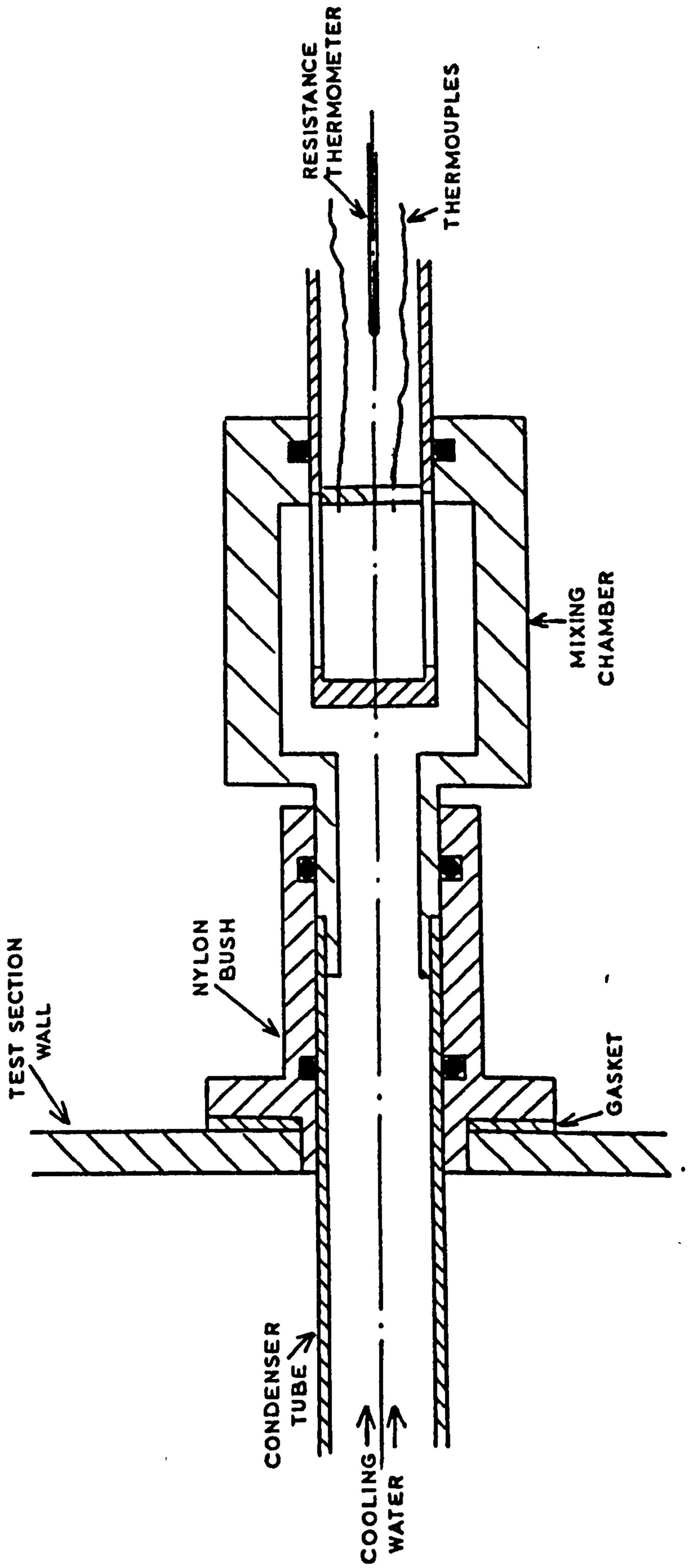

FIG. 12 MIXING CHAMBER

FIG. 13

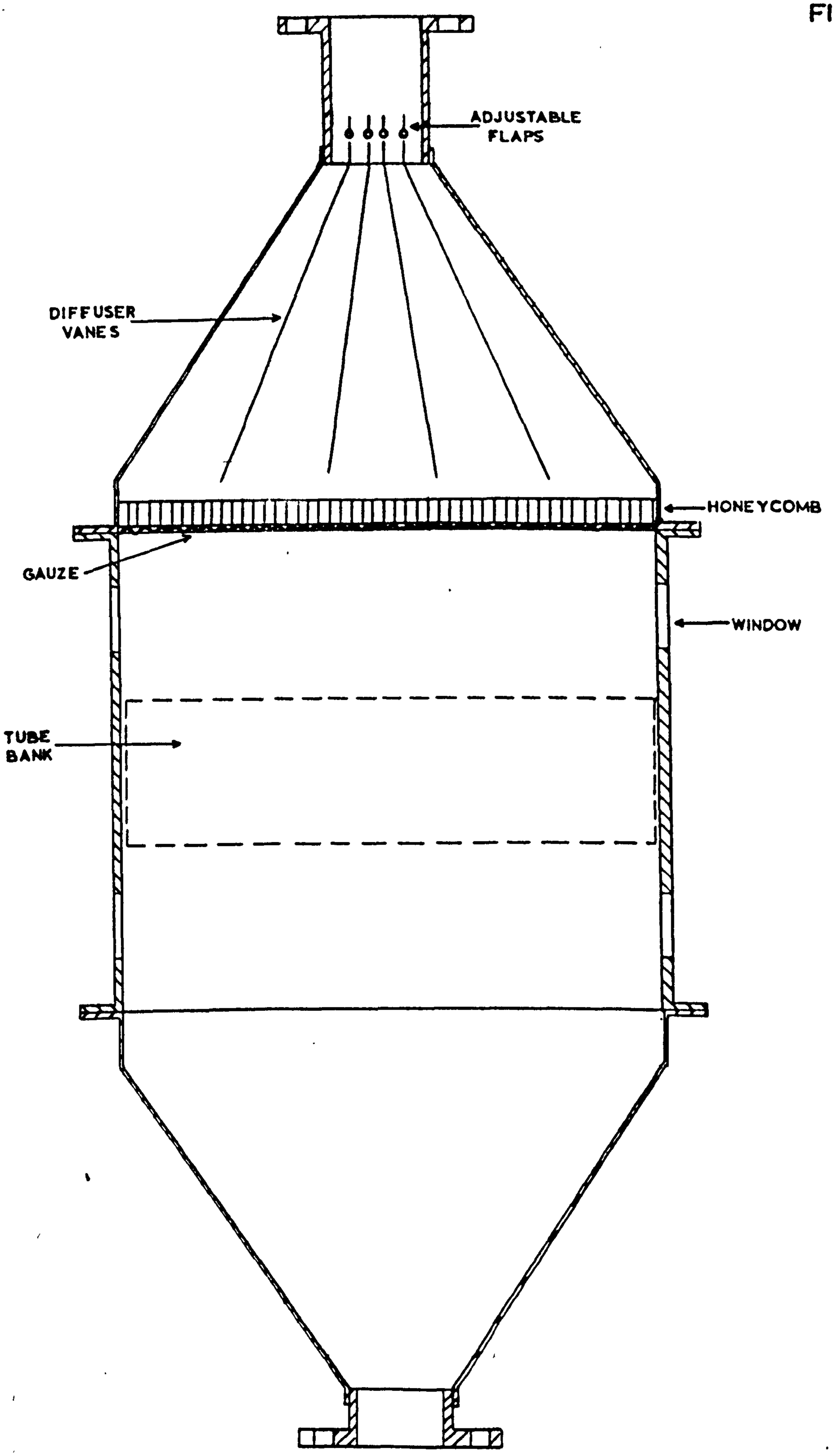

FIG.13 TEST SECTION

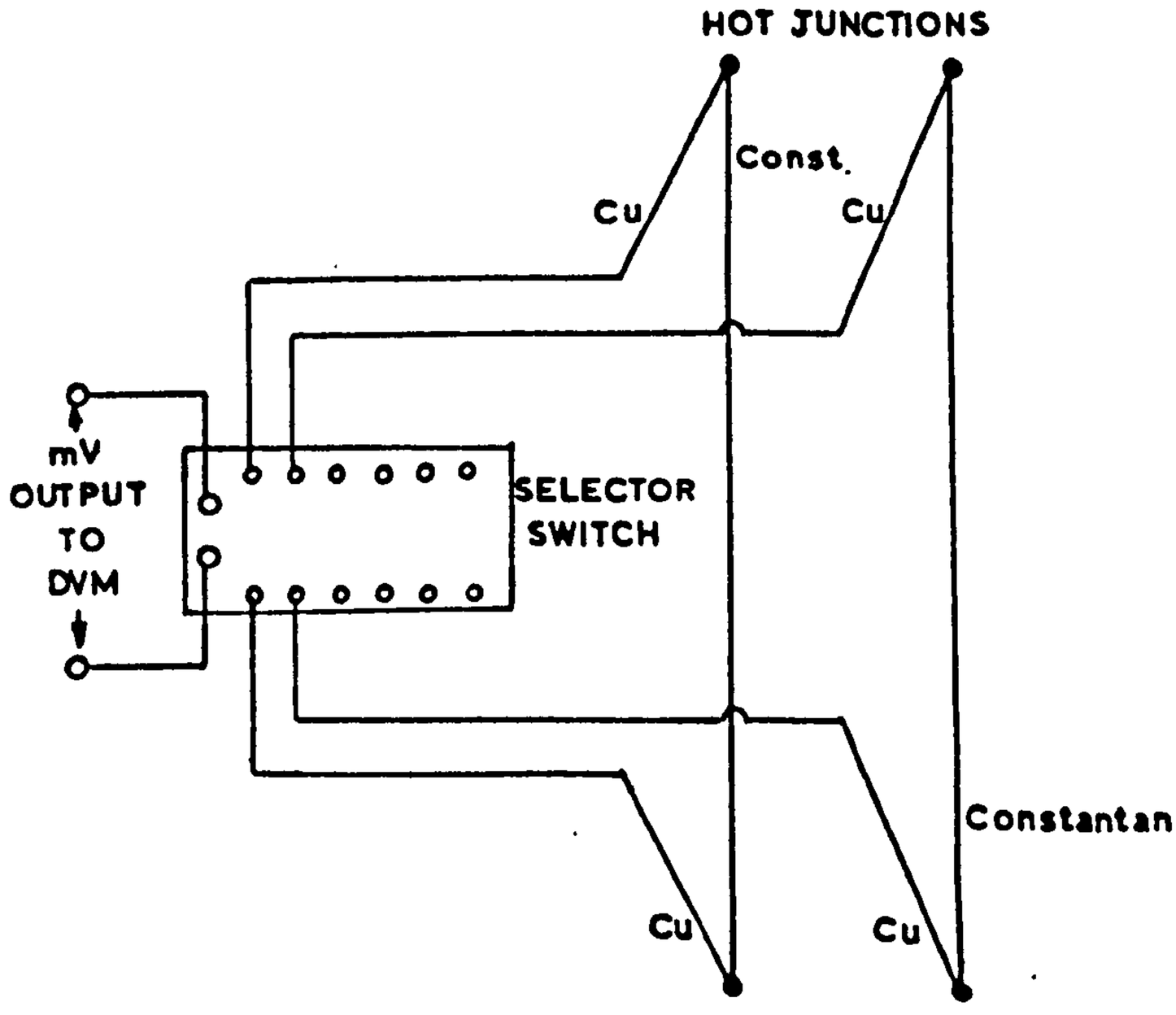

FIG.14 METHOD OF CONNECTING THERMOCOUPLES

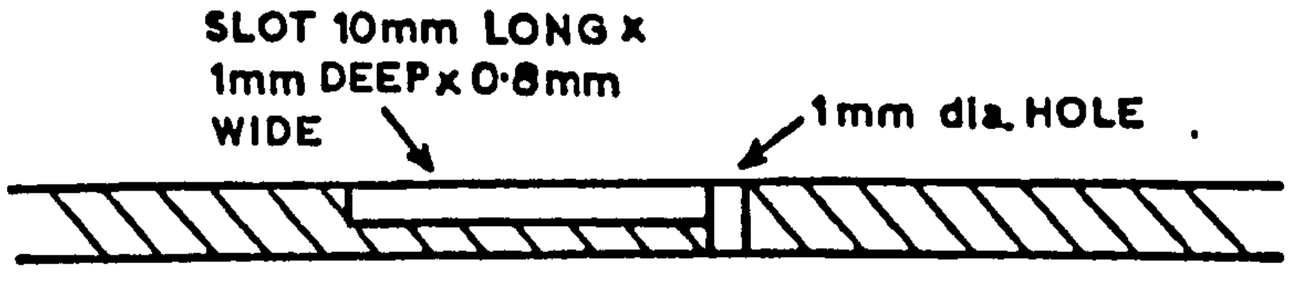

FIG. 15 SLOT FOR WALL THERMOCOUPLES

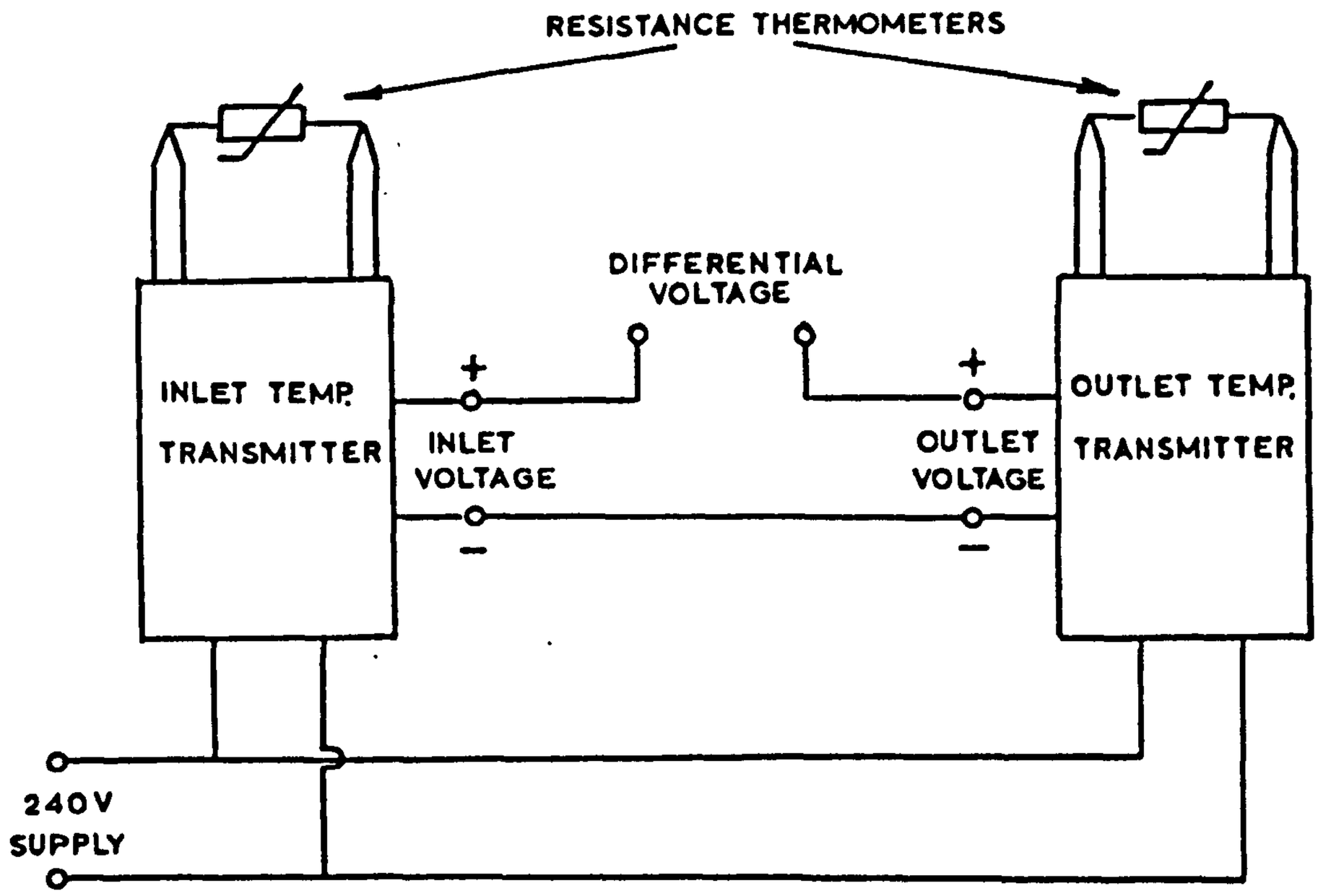

FIG. 16 RESISTANCE THERMOMETER CONNECTIONS

FIG. 17

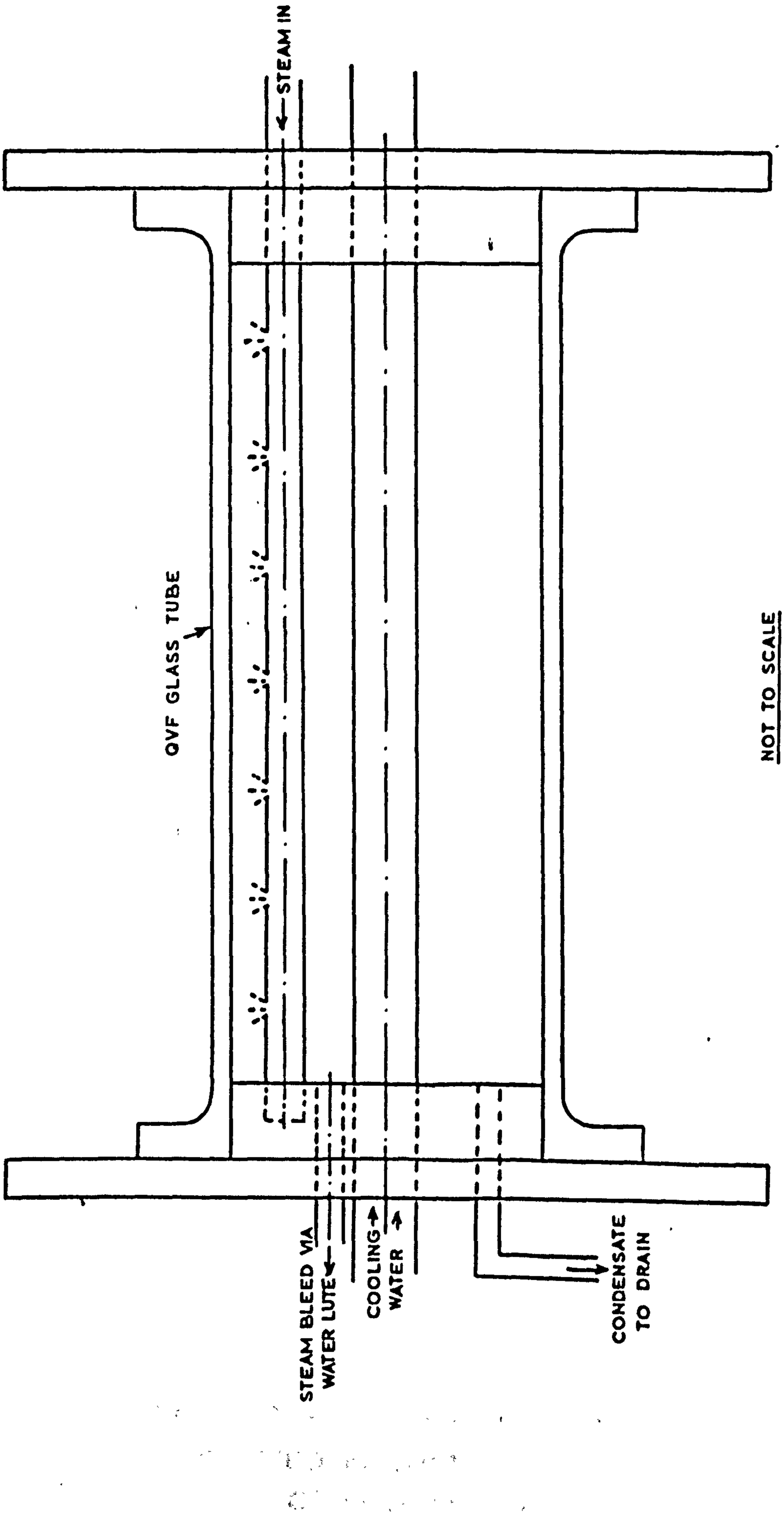

NOT TO SCALE

FIG. 17. TEST RIG FOR EXAMINING DROPWISE CONDENSATION

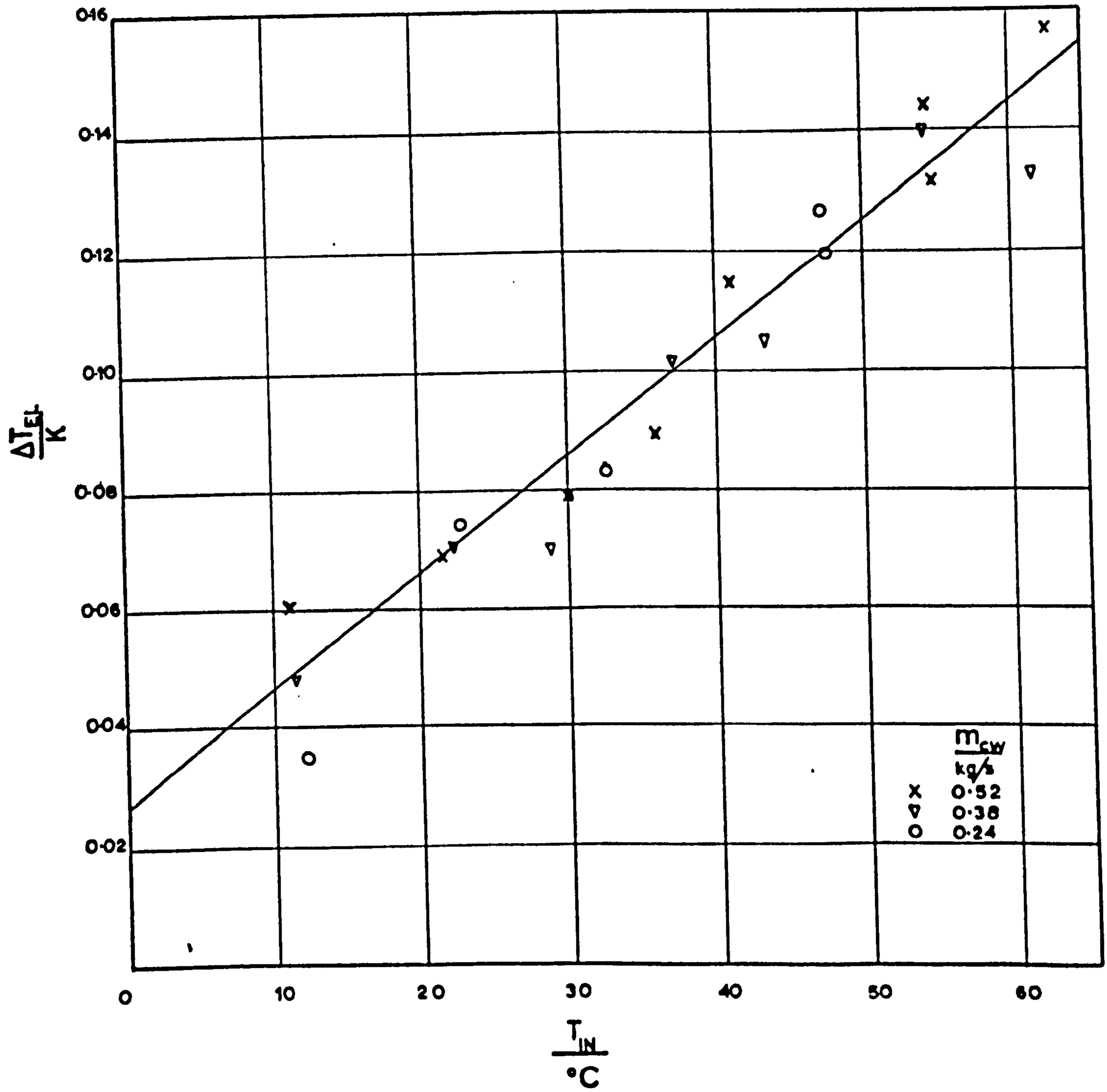

FIG. 18 TEMPERATURE DROP ALONG ENTRY LENGTH PLOTTED AGAINST INLET TEMPERATURE OF COOLING WATER

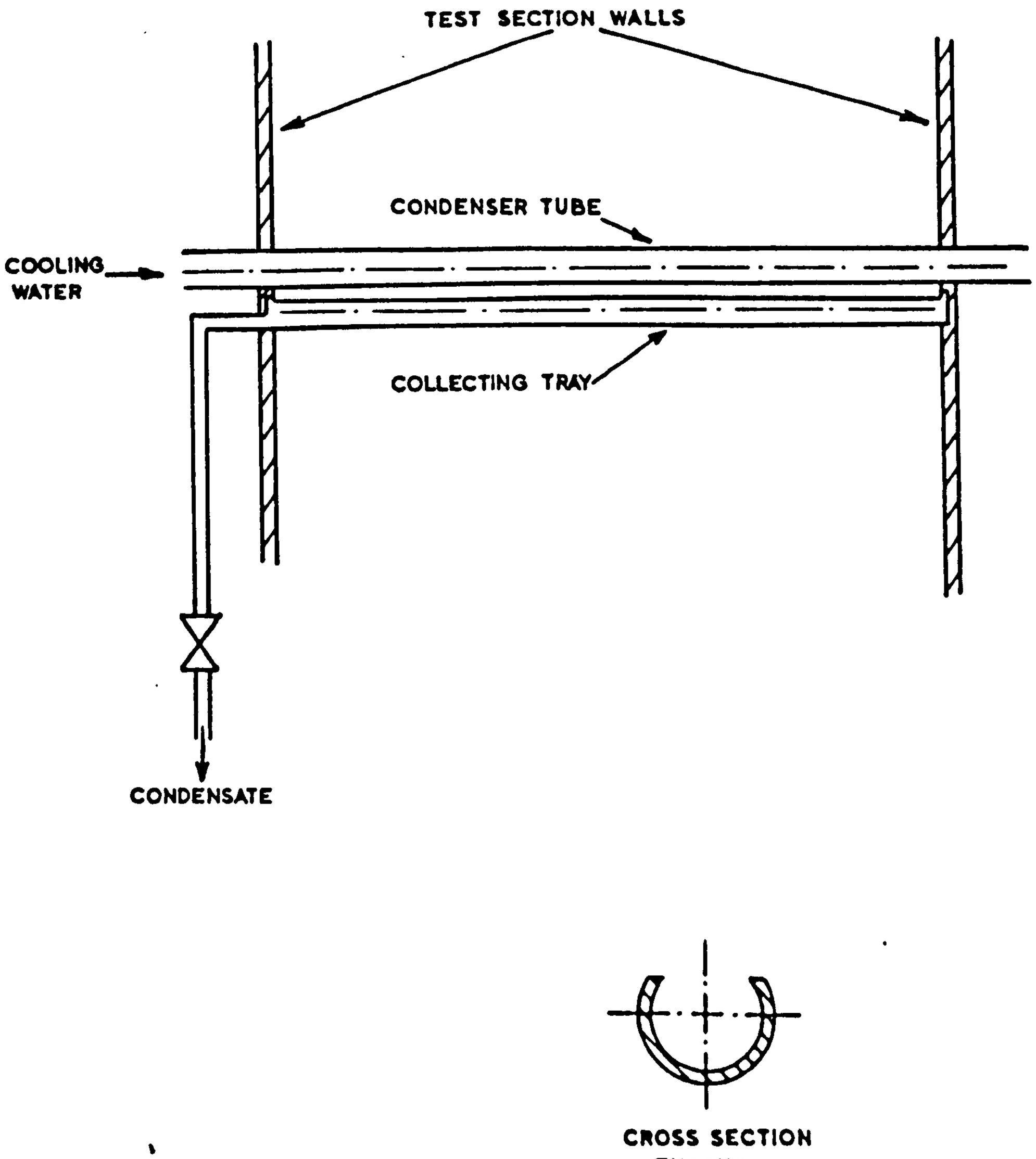

CROSS SECTION THROUGH COLLECTING TRAY

FIG. 19 MODIFICATIONS TO TEST RIG FOR ENERGY BALANCE TESTS

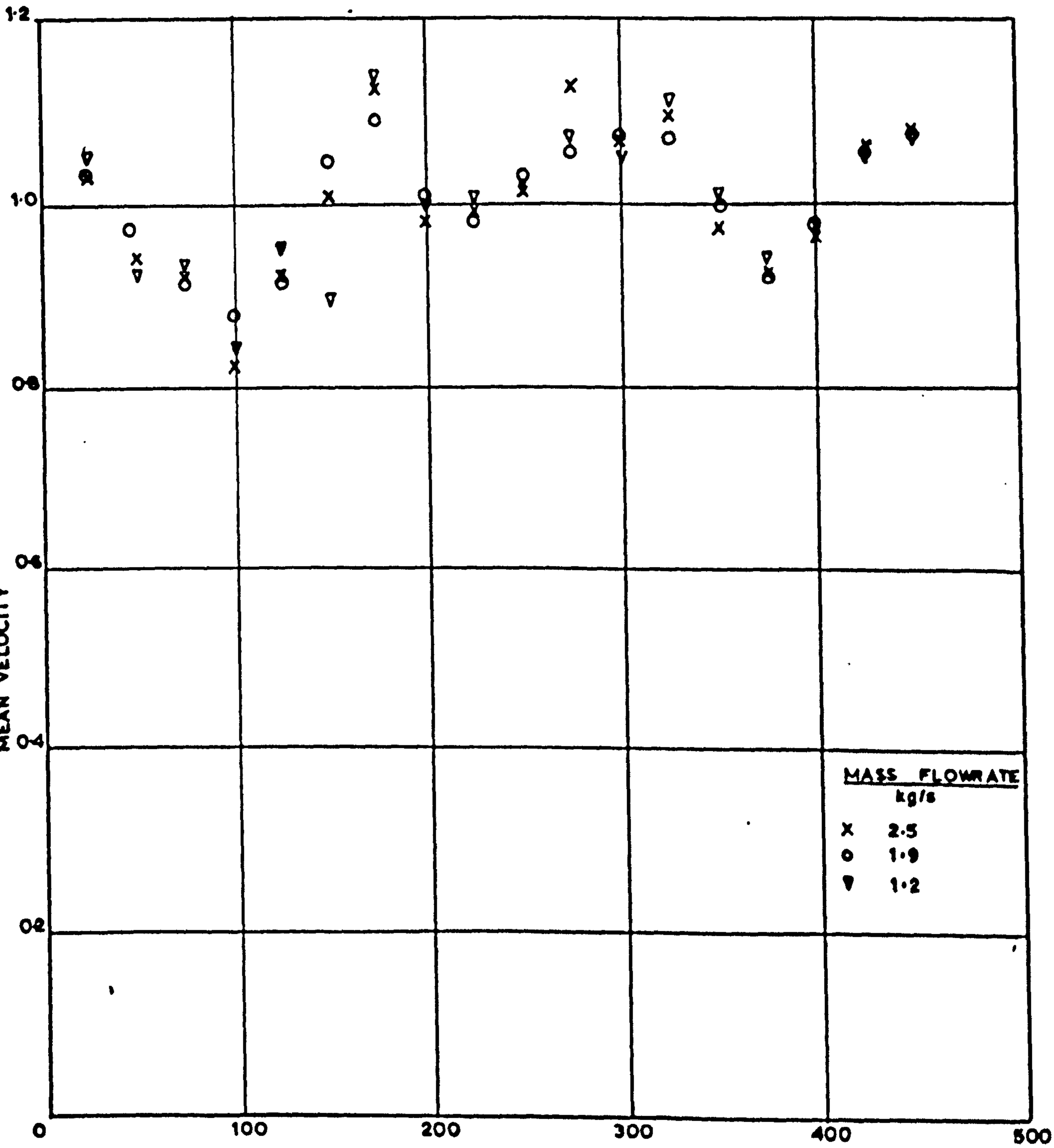

FIG. 20 NON-DIMENSIONAL VELOCITY PROFILE OF STEAM ACROSS TEST SECTION

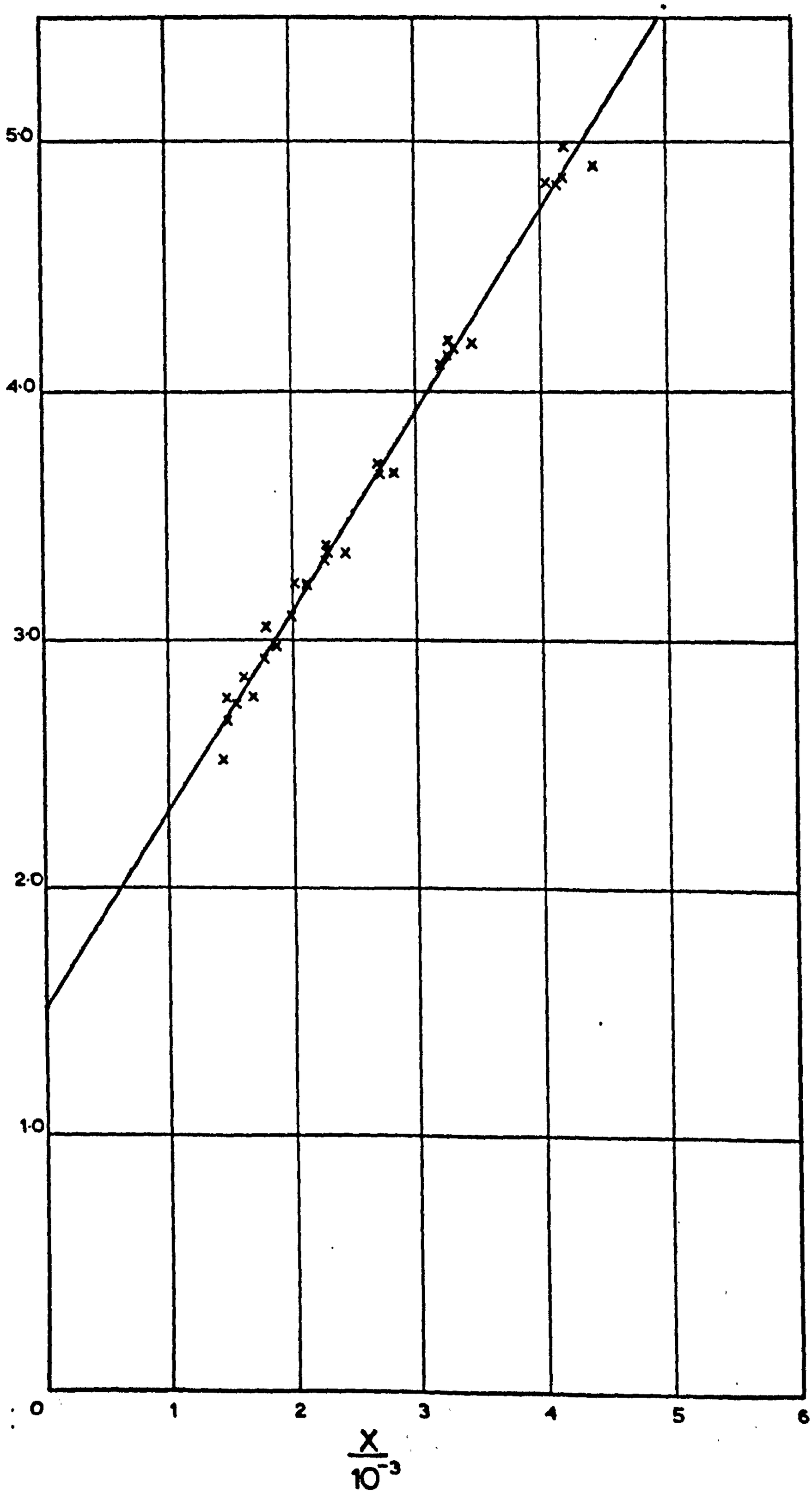

FIG. 21 ORIGINAL MODIFIED WILSON PLOT

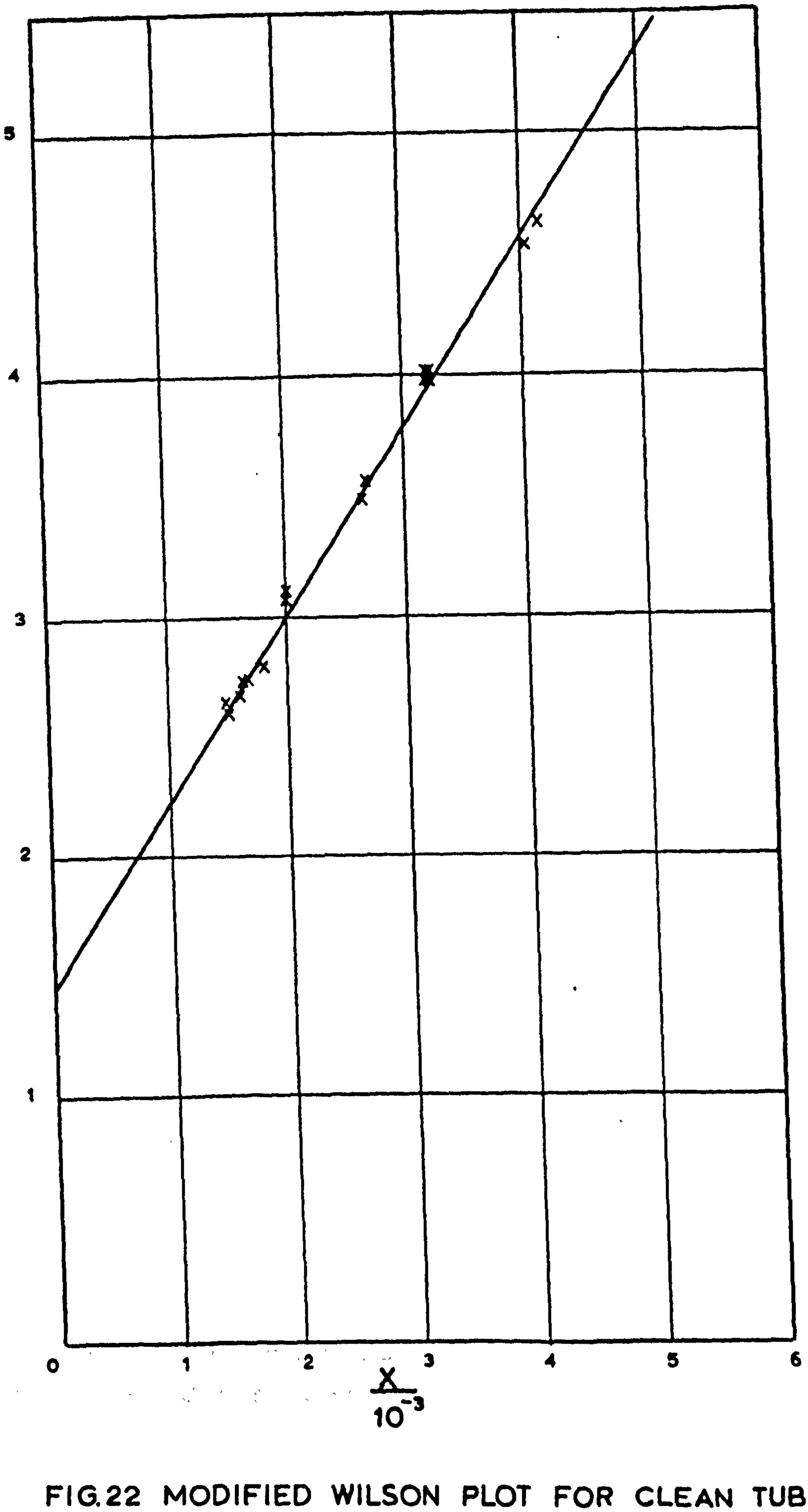

FIG. 22 MODIFIED WILSON PLOT FOR CLEAN TUBE

FIG. 23

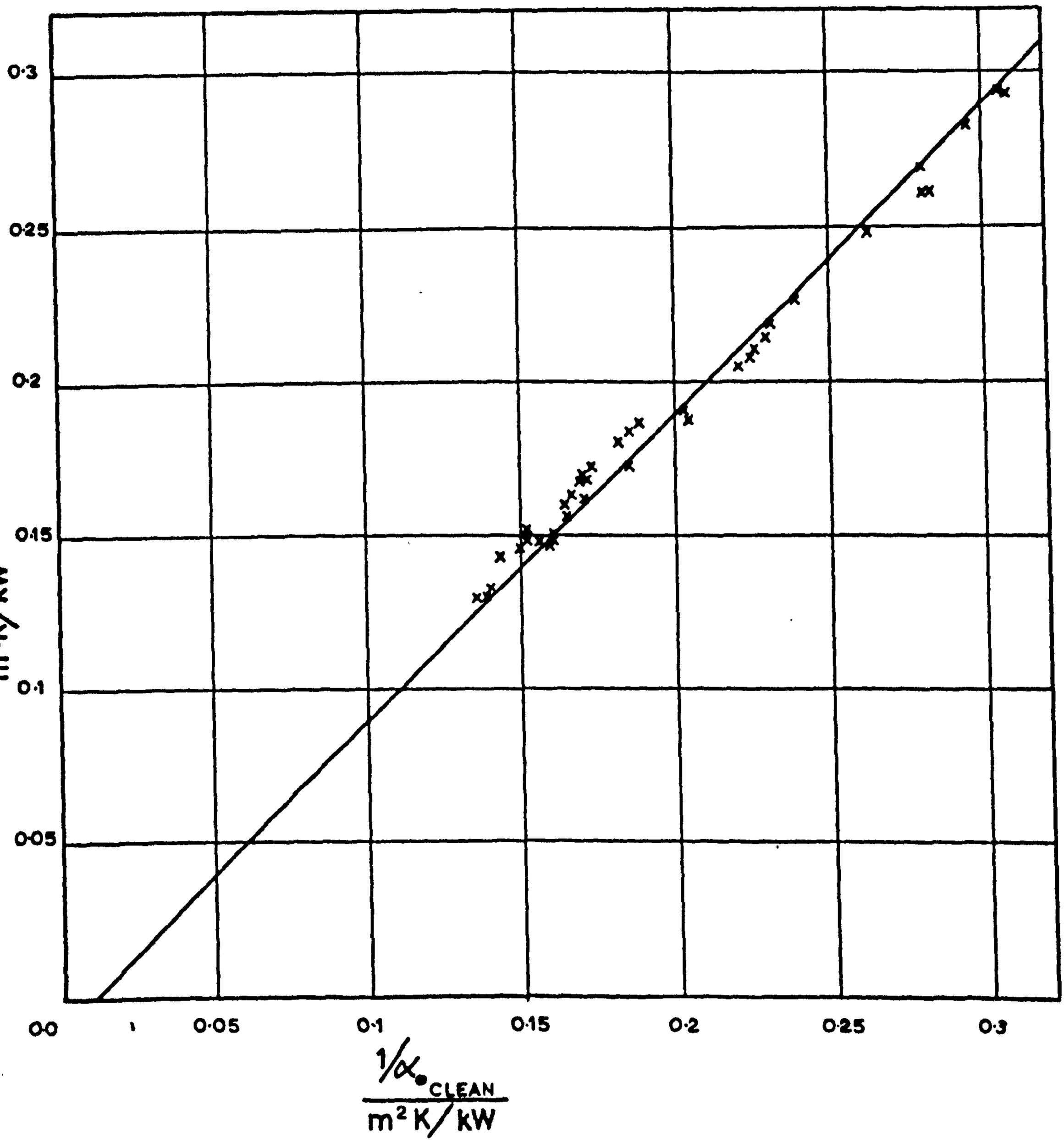

FIG. 23 COMPARISON OF RECIPROCAL OF OVERALL H.T.C. FOR CLEAN AND DIRTY TUBE UNDER SIMILAR TEST CONDITIONS

FIG. 24

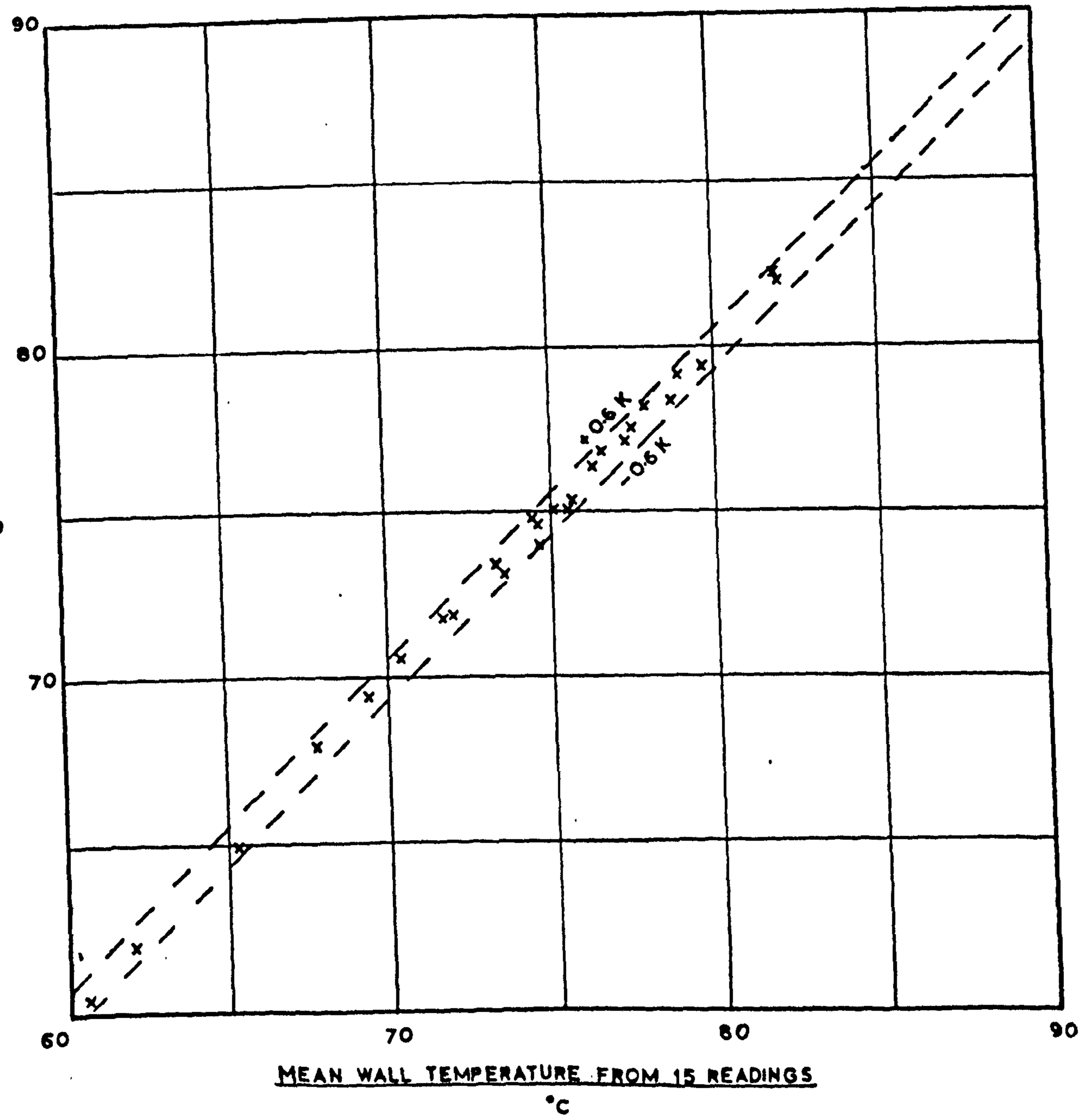

FIG.24 COMPARISON OF MEAN WALL TEMPERATURE CALCULATED FROM 21 THERMOCOUPLE READINGS WITH THAT FROM 15 READINGS

FIG. 25

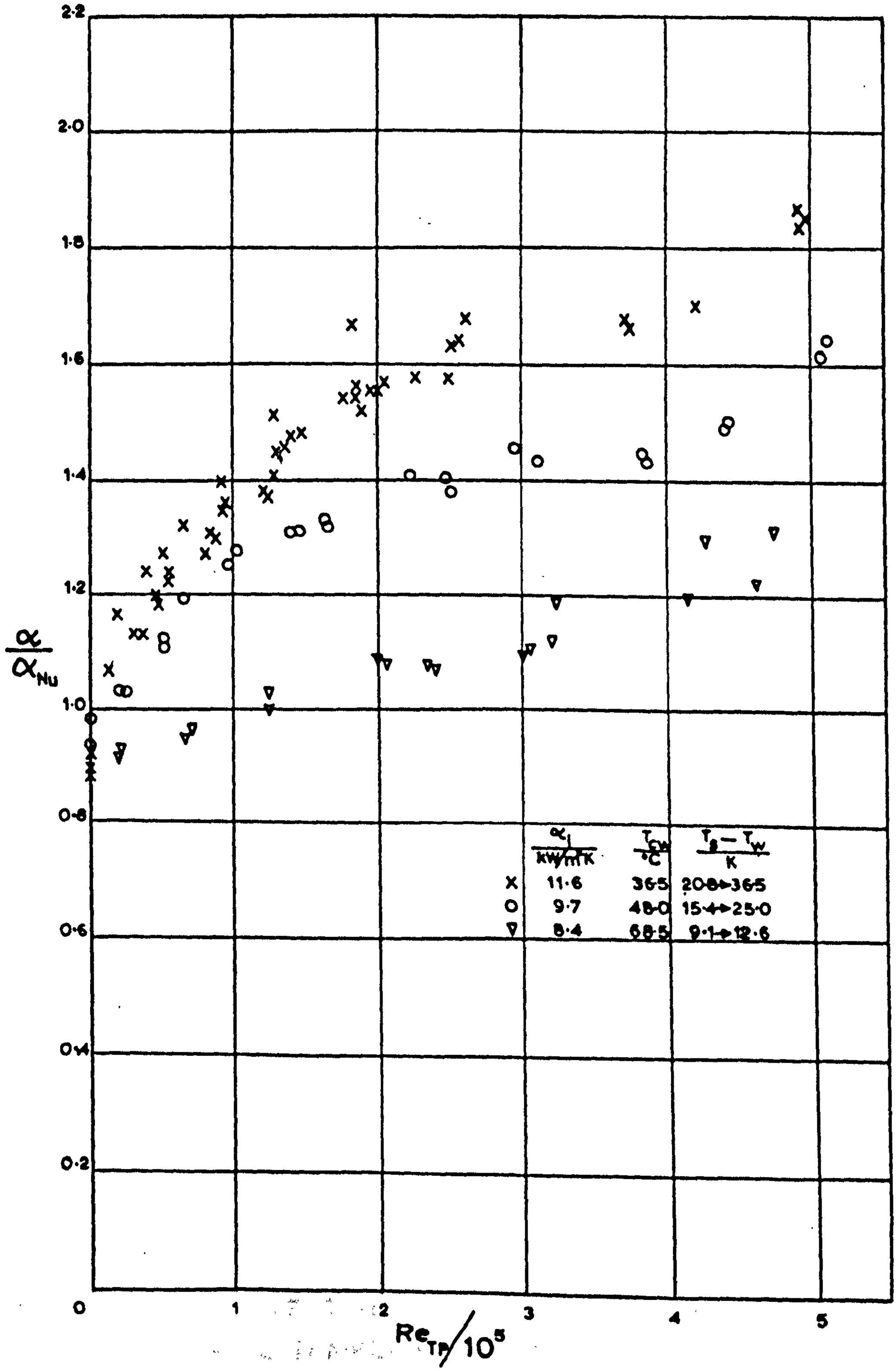

FIG. 25 SINGLE TUBE TESTS WITH CONSTANT COOLING WATER CONDITIONS

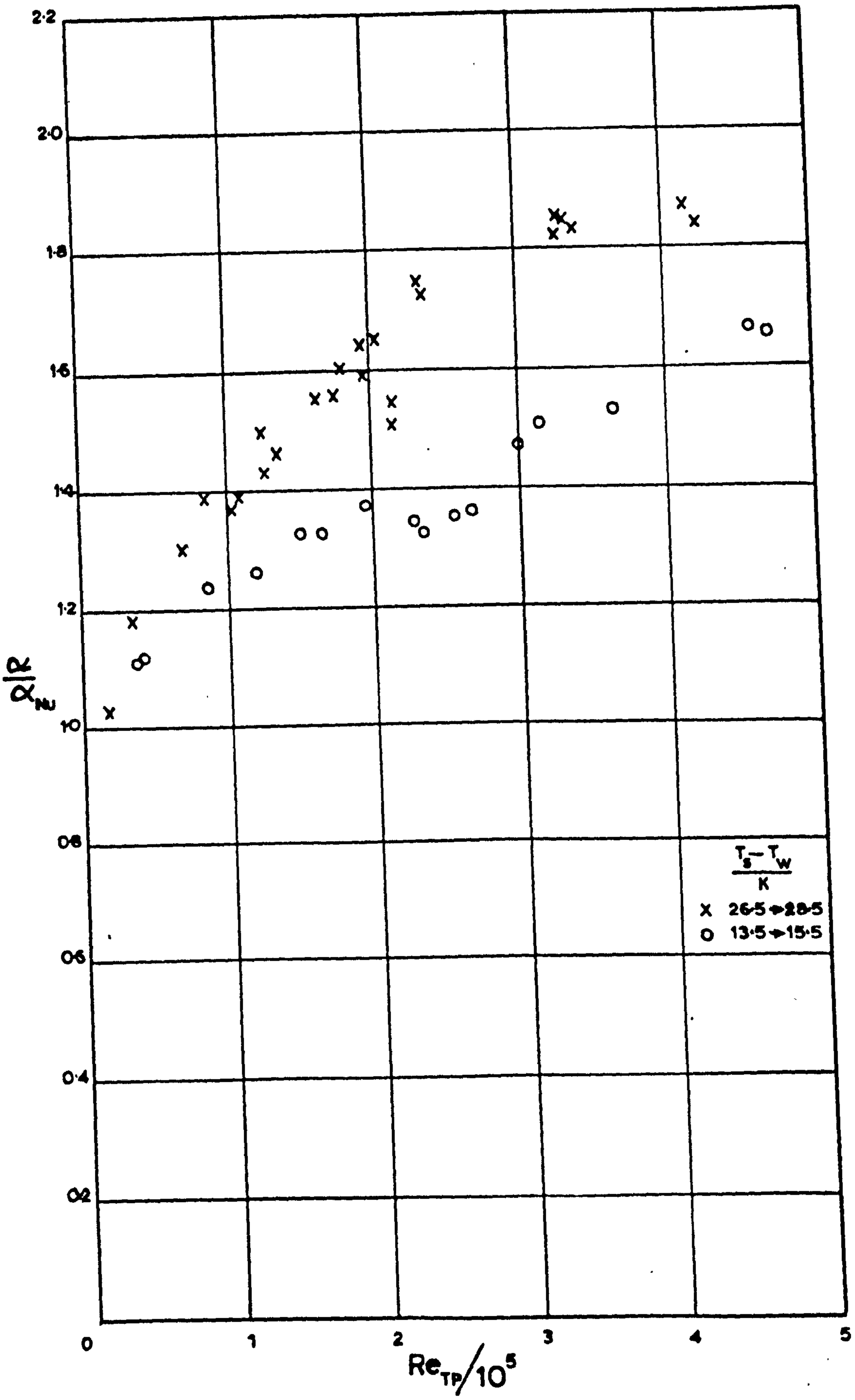

FIG. 26 SINGLE TUBE TESTS AT CONSTANT MEAN WALL TEMPERATURE USING WALL THERMOCOUPLES

FIG. 27

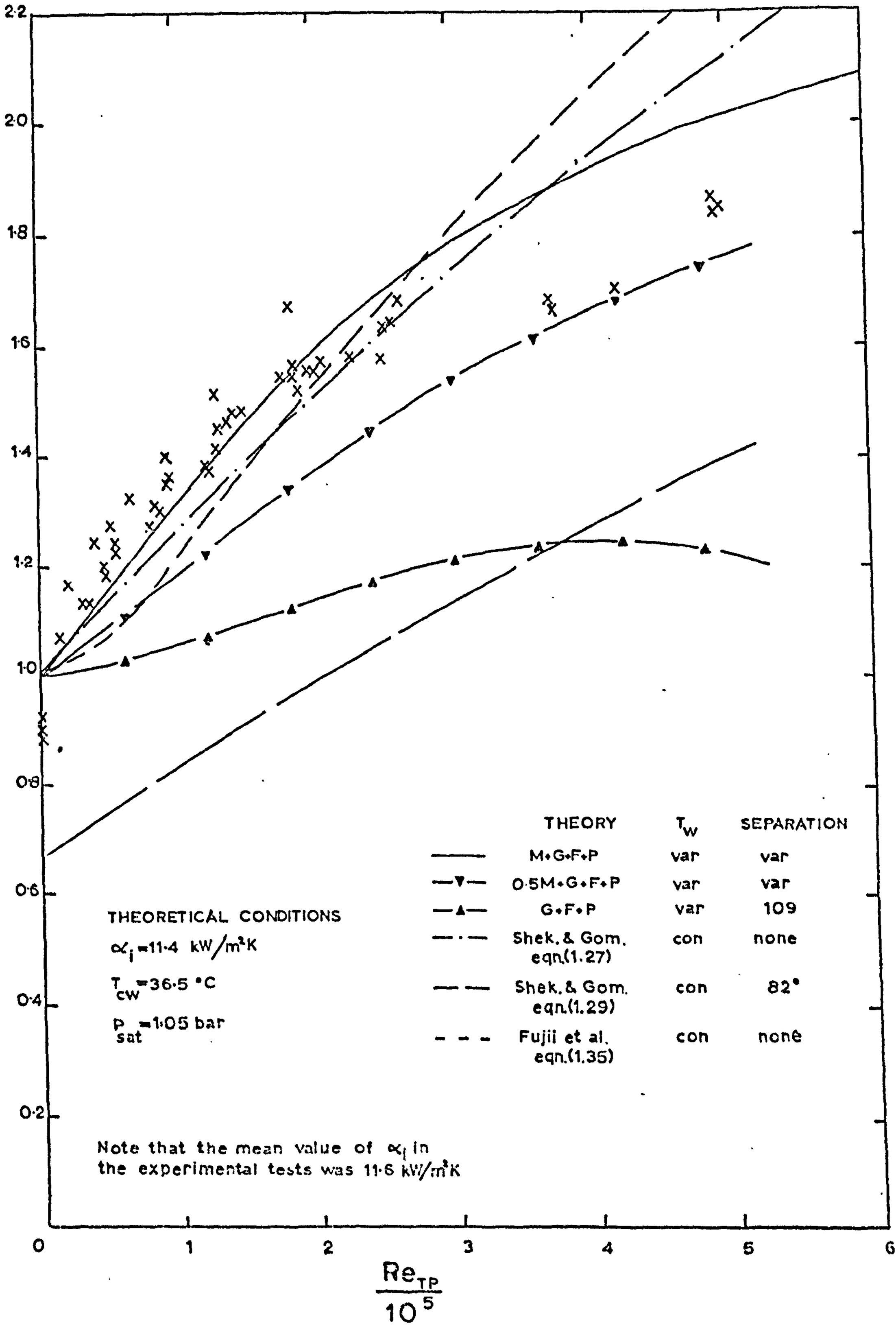

FIG. 27 COMPARISON OF EXPERIMENTAL RESULTS WITH PREDICTED SOLUTIONS FOR SINGLE TUBE (HIGH HEAT FLUX)

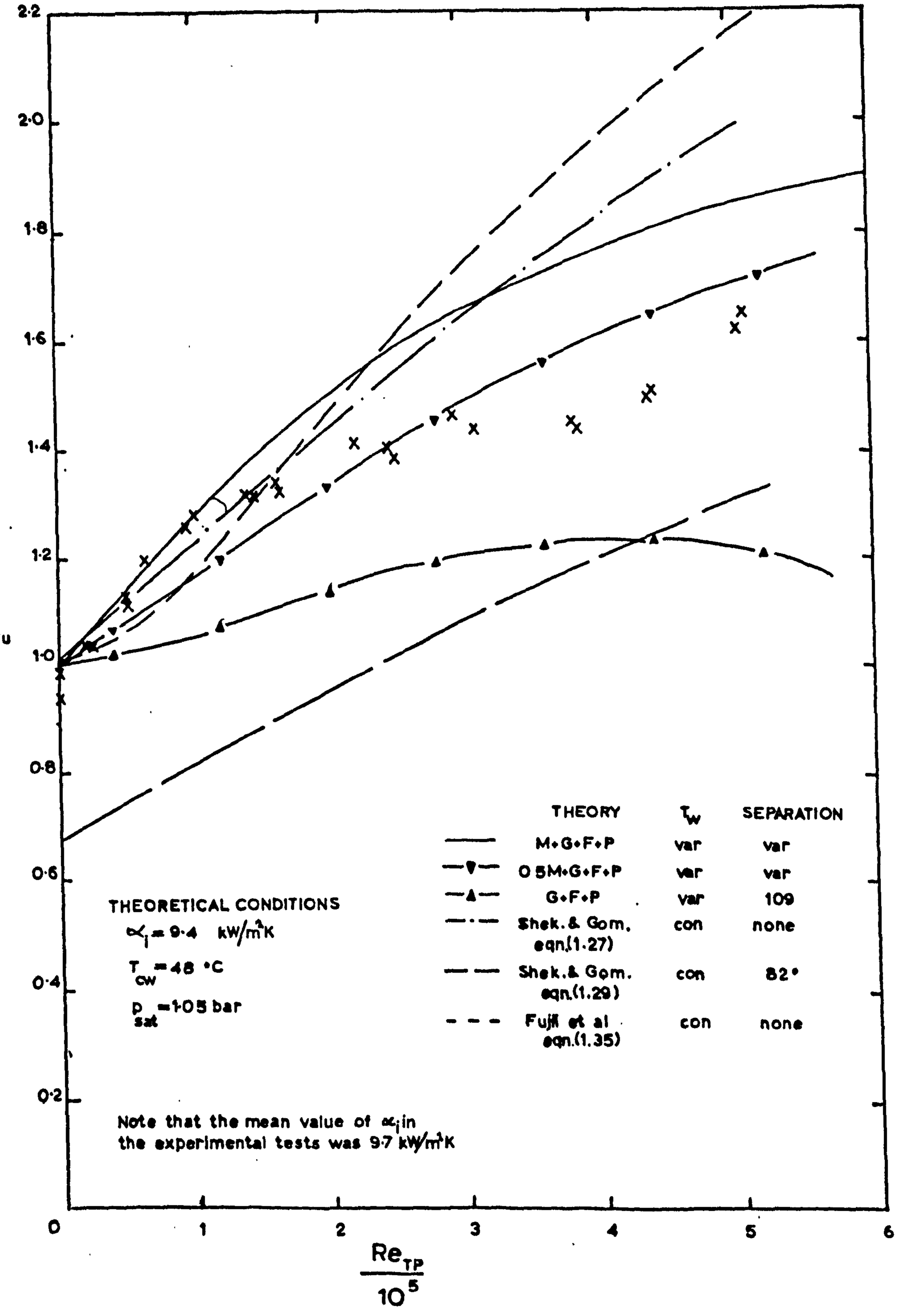

FIG 28 COMPARISON OF EXPERIMENTAL RESULTS WITH PREDICTED SOLUTIONS FOR SINGLE TUBE (MEDIUM HEAT FLUX)

FIG. 29

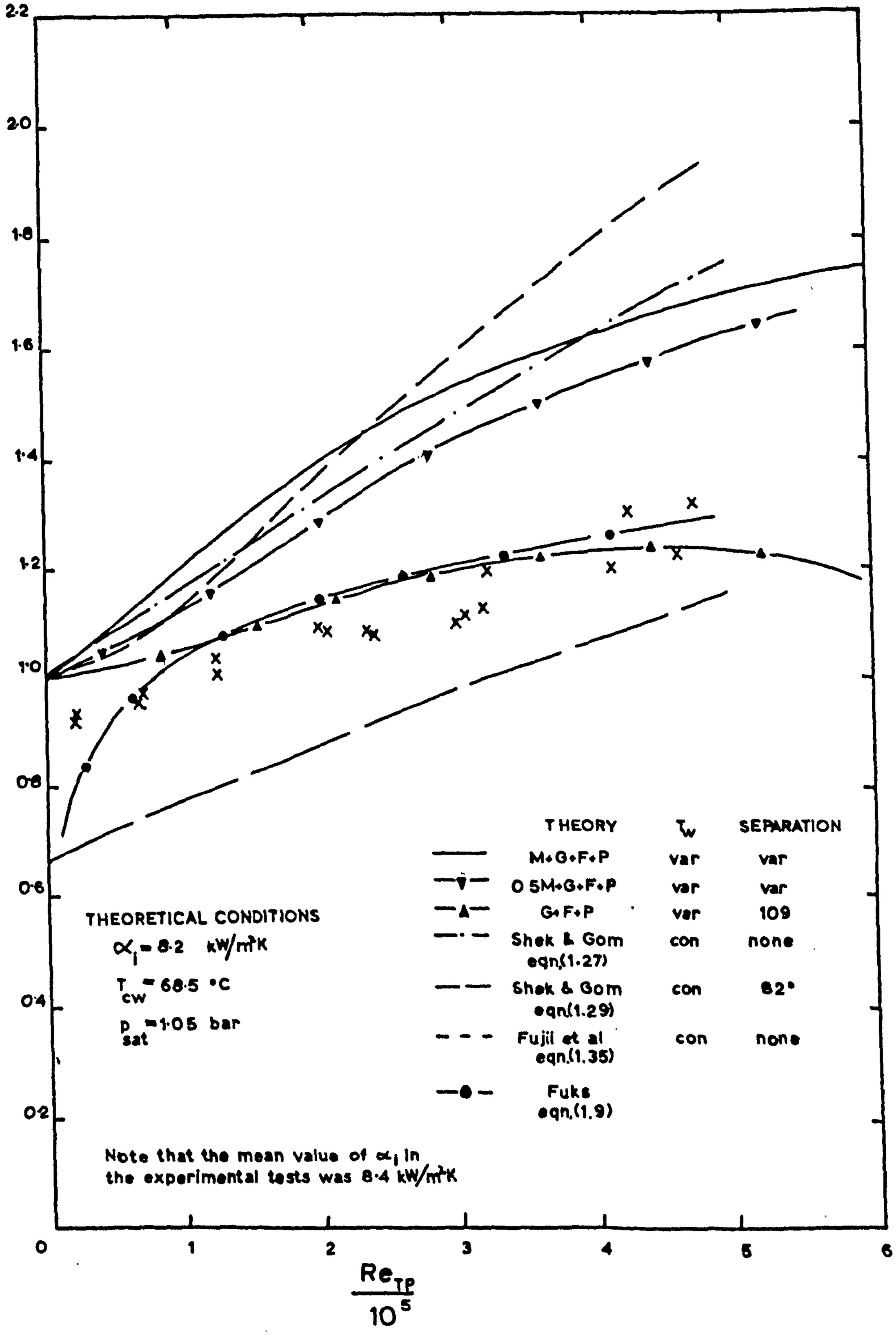

FIG 29 COMPARISON OF EXPERIMENTAL RESULTS WITH PREDICTED SOLUTIONS FOR SINGLE TUBE (LOW HEAT FLUX)

FIG. 30

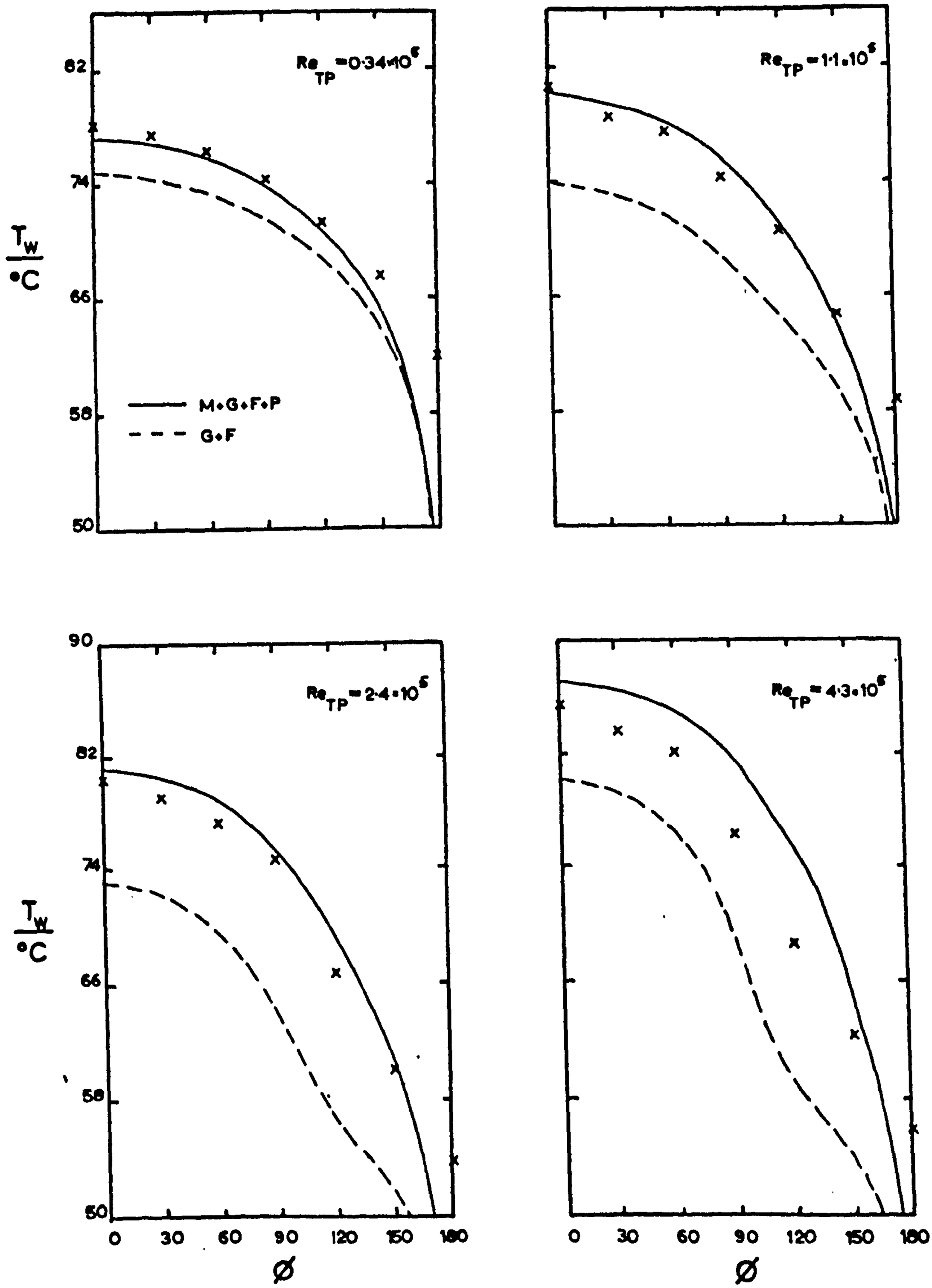

FIG. 30 COMPARISON OF MEASURED AND PREDICTED TEMPERATURE PROFILES FOR $(T_s - T_w) = 27.5K$

FIG. 31

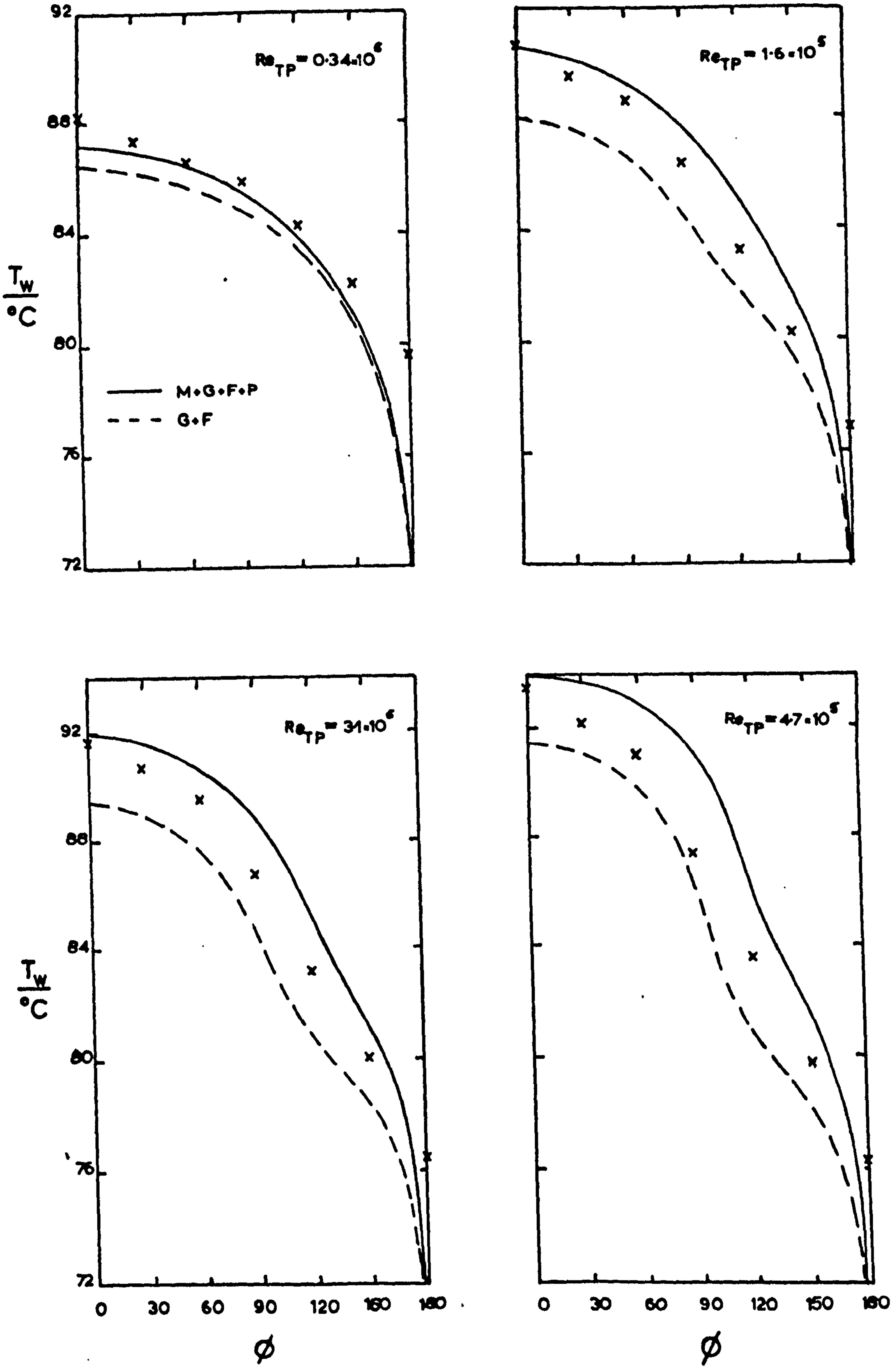

FIG. 31 COMPARISON OF MEASURED AND PREDICTED TEMPERATURE PROFILES FOR $(T_s - T_w) = 14.5\,K$

FIG. 32

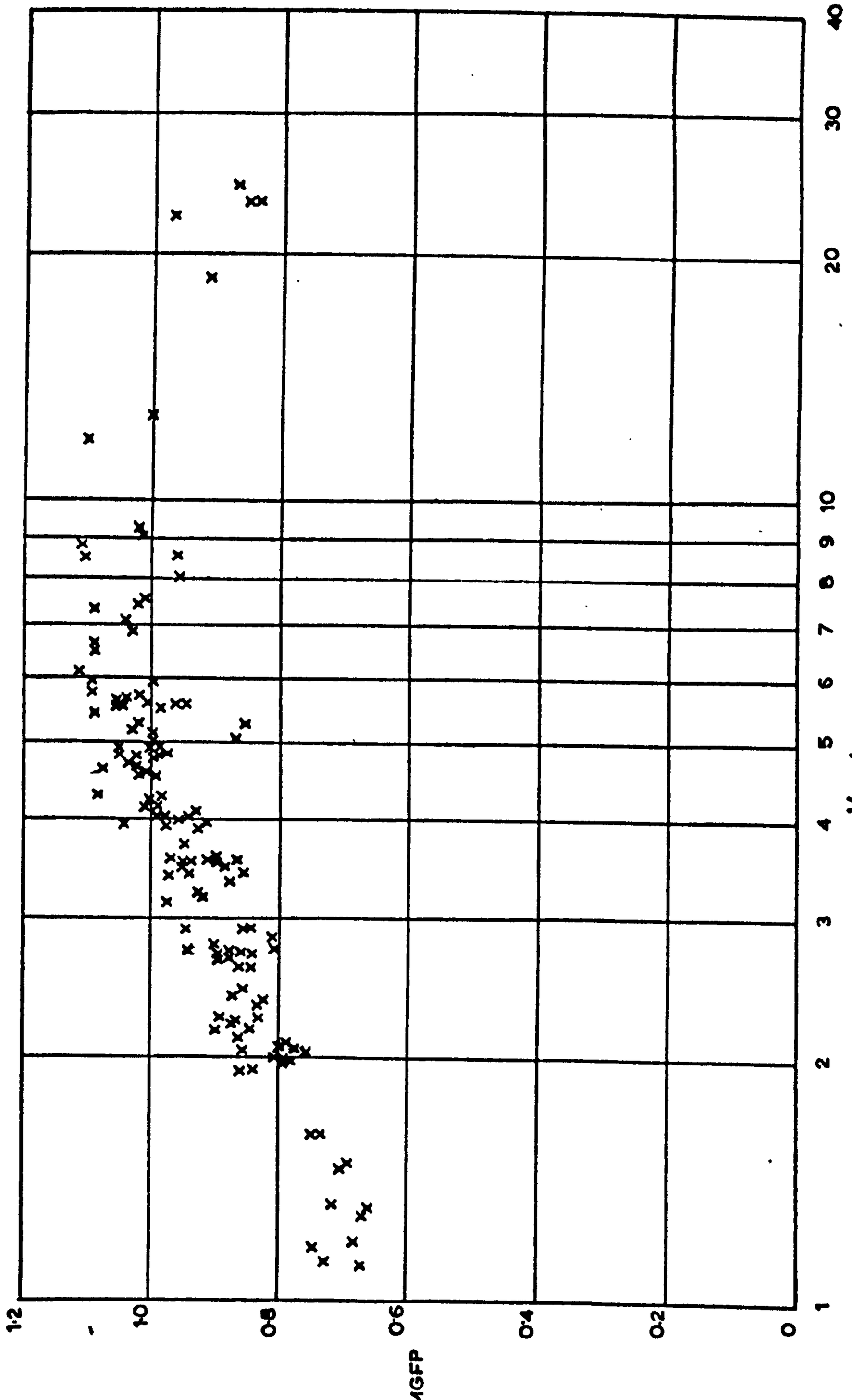

FIG. 32 PLOT OF RATIO OF EXPERIMENTAL H.T.C. TO THAT PREDICTED BY THE M•G•F•P THEORY VERSUS THE SUCTION PARAMETER FOR THE SINGLE TUBE

FIG. 33

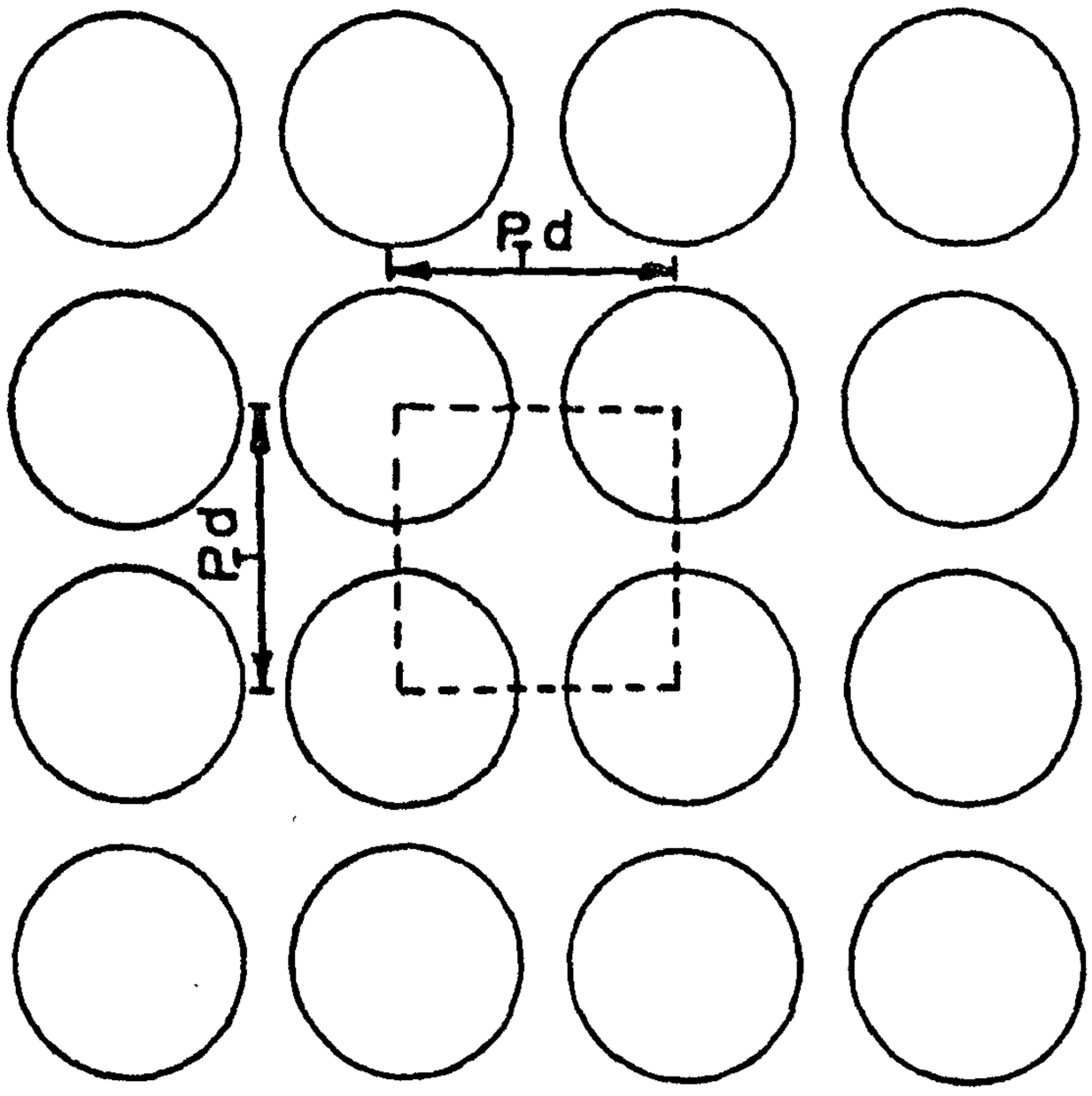

AREA OF UNIT CELL = $(P_T d)^2$
FREE AREA OF CELL = $d^2(P_T^2 - \pi/4)$
MEAN FLOW WIDTH = $d(P_T - \pi/4P_T)$ (=FREE AREA/HEIGHT OF CELL)

(a) SQUARE PITCH TUBE BANK

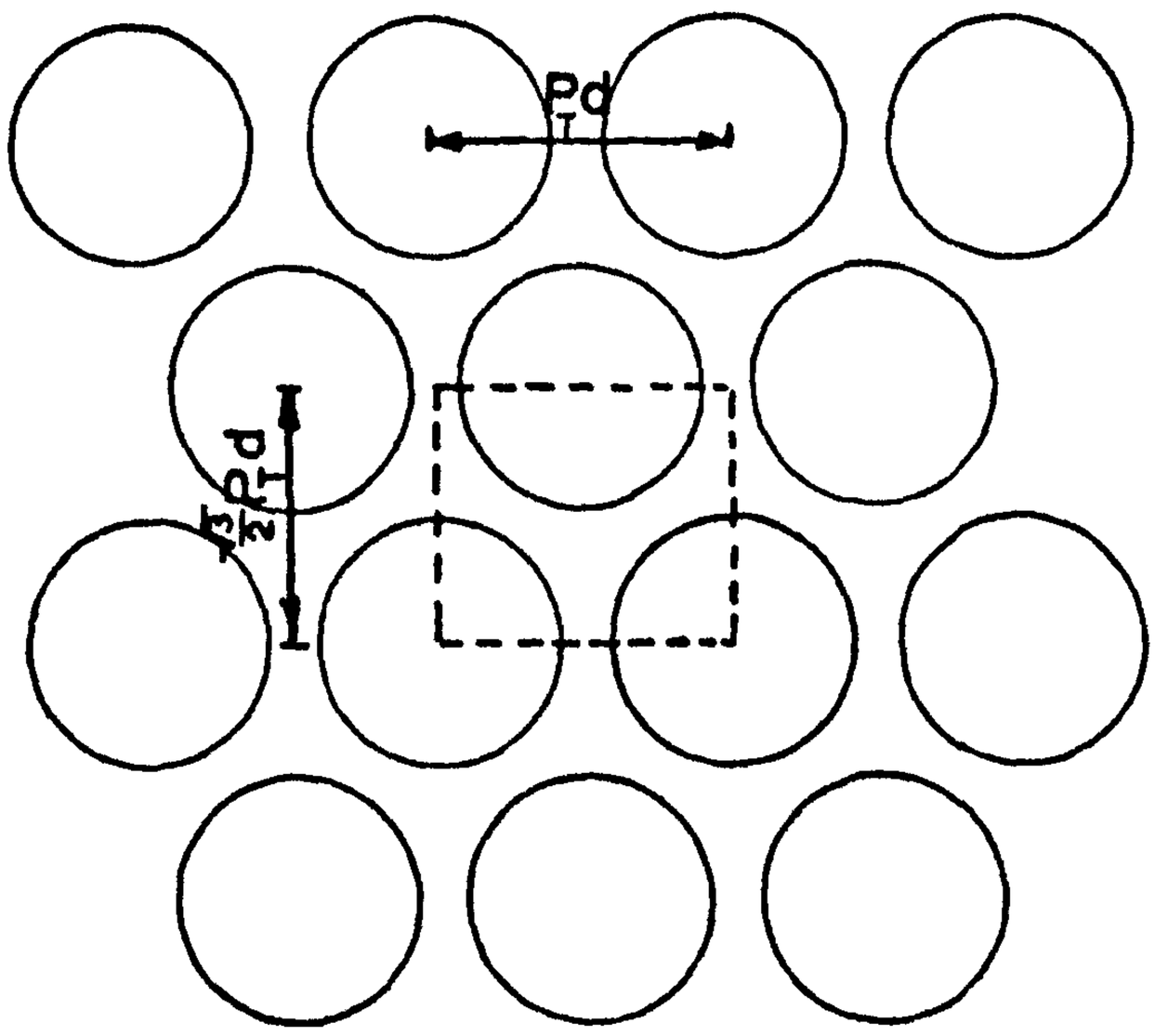

AREA OF UNIT CELL = $\sqrt{3}(P_T d)^2/2$
FREE AREA OF CELL = $d^2(\sqrt{3}P_T^2/2 - \pi/4)$
MEAN FLOW WIDTH = $d(P_T - \pi/2\sqrt{3}P_T)$ (=FREE AREA/HEIGHT OF CELL)

(b) EQUILATERAL TRIANGLE TUBE BANK

FIG. 33 CALCULATION OF MEAN FLOW WIDTHS

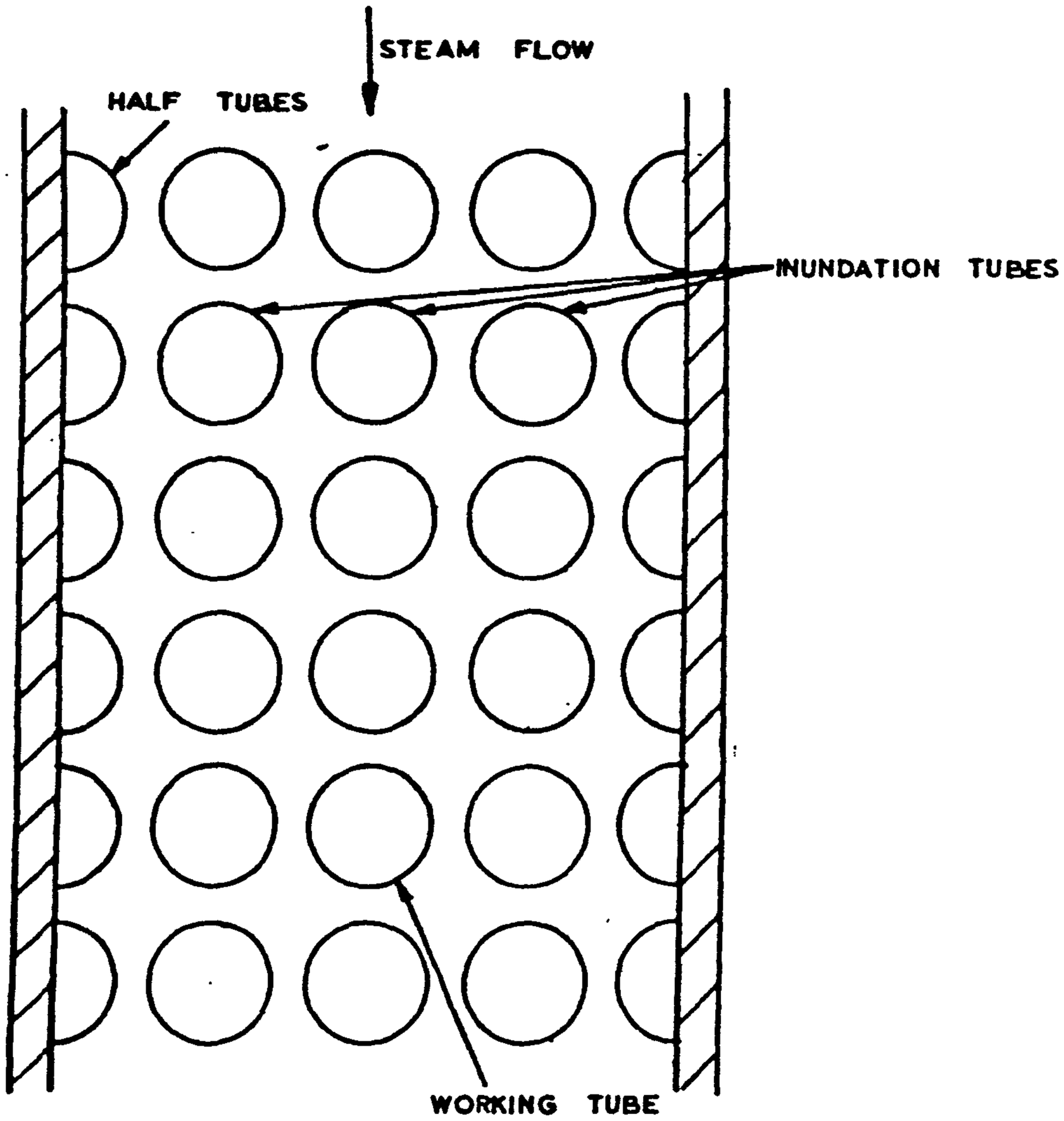

(a)

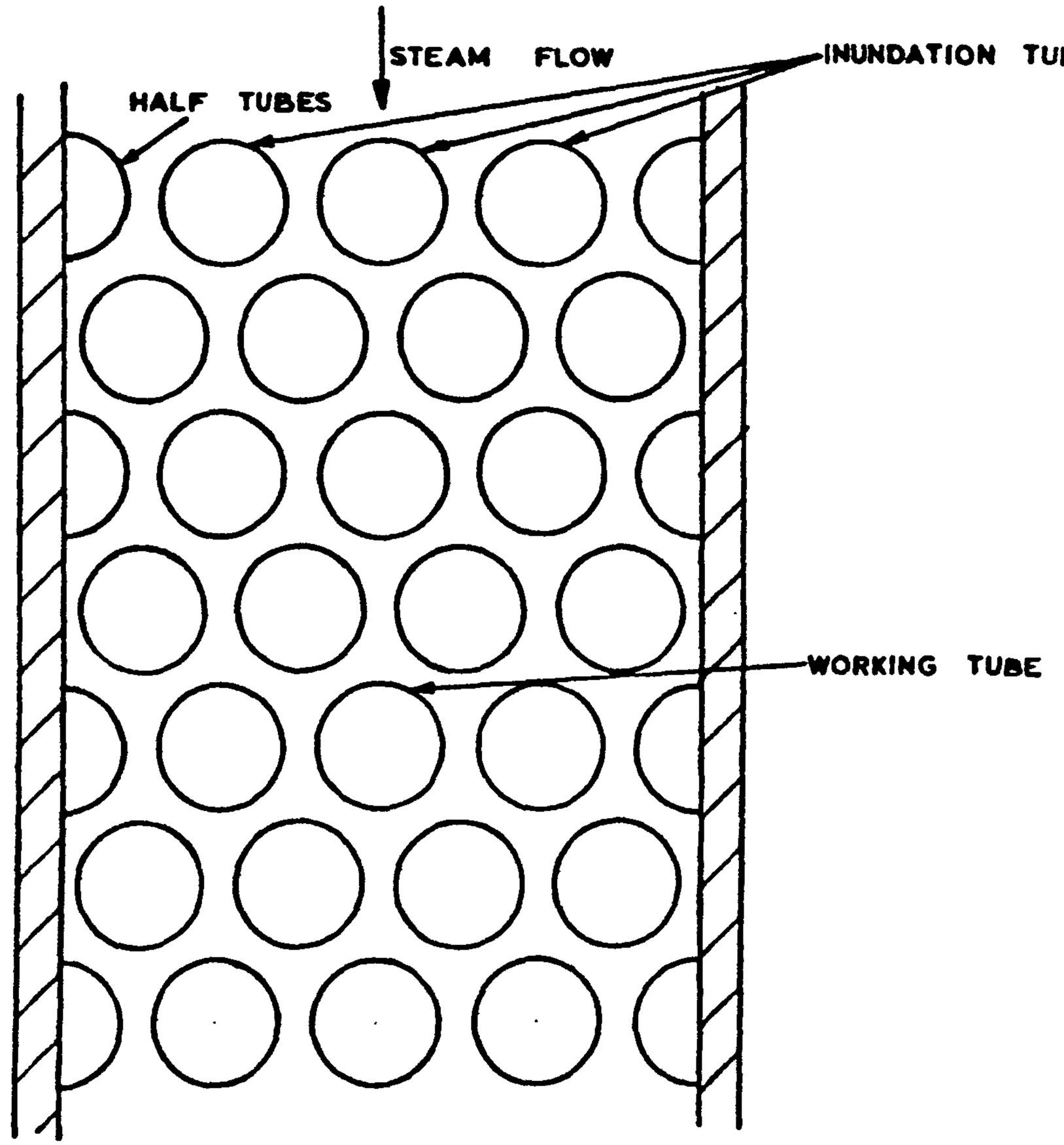

(b)

FIG. 34 SQUARE AND EQUILATERAL - TRIANGLE TUBE BANKS.

FIG. 34

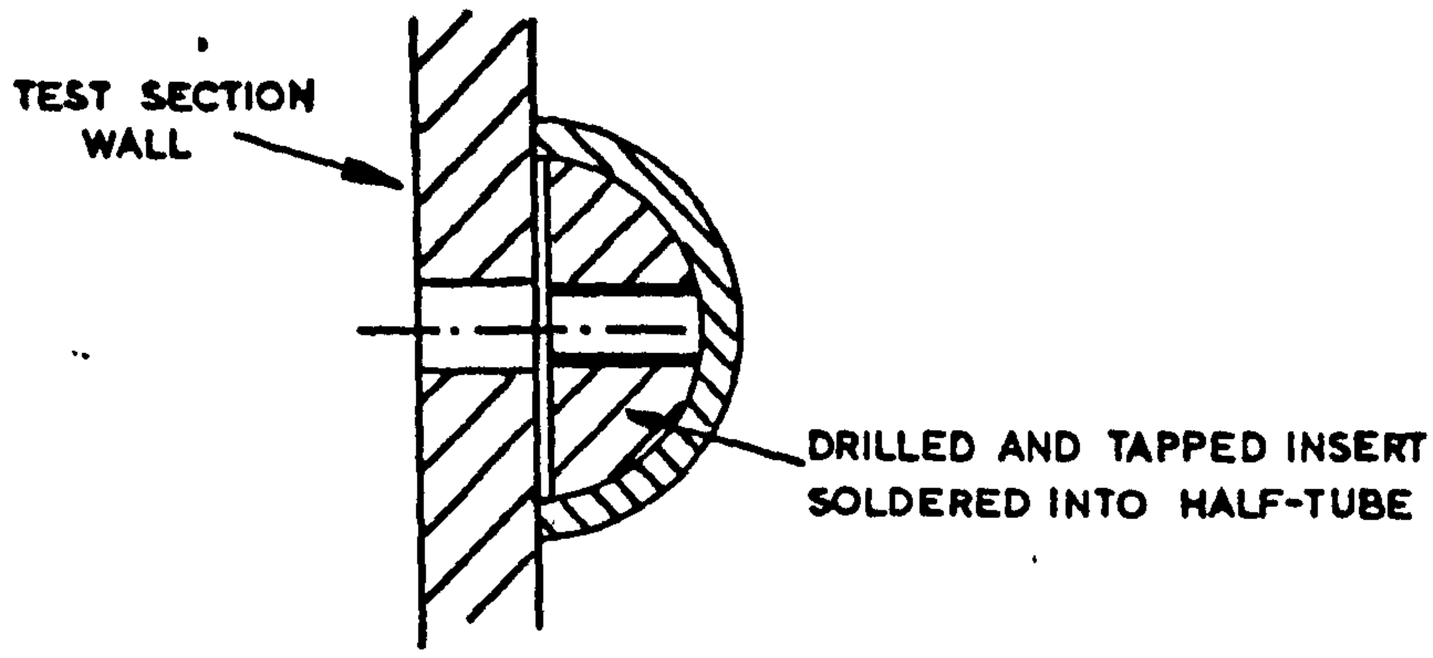

FIG. 35 HALF-TUBE CONNECTIONS

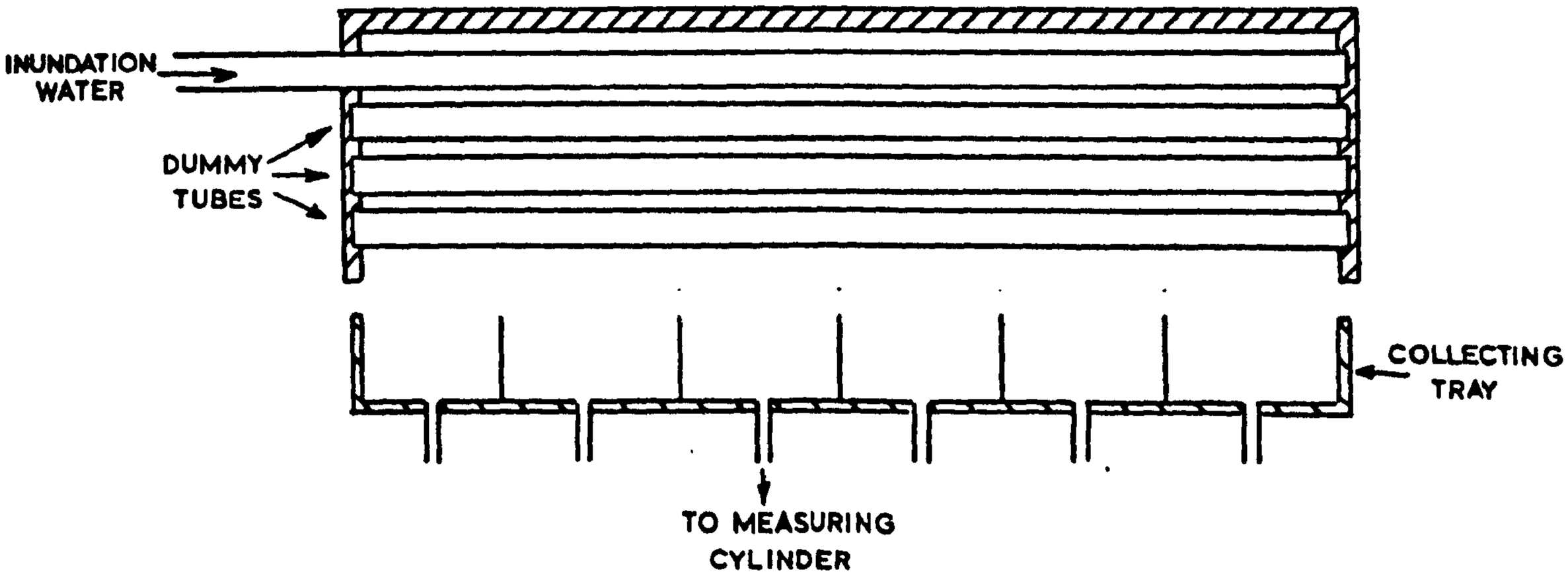

FIG. 36 APPARATUS FOR MEASURING INUNDATION DISTRIBUTION

FIG. 37

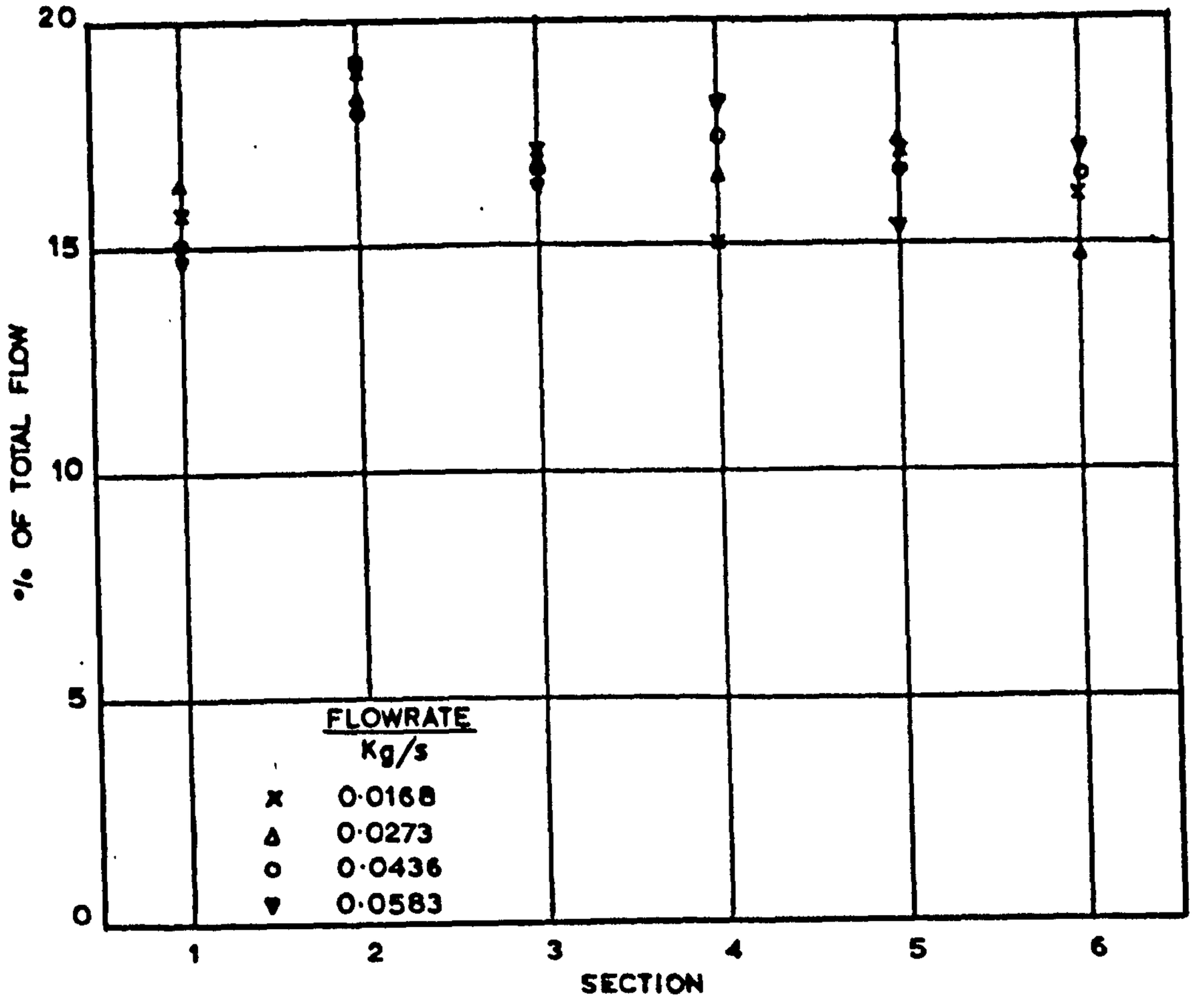

(a) TUBE FOR LOW INUNDATION RATES

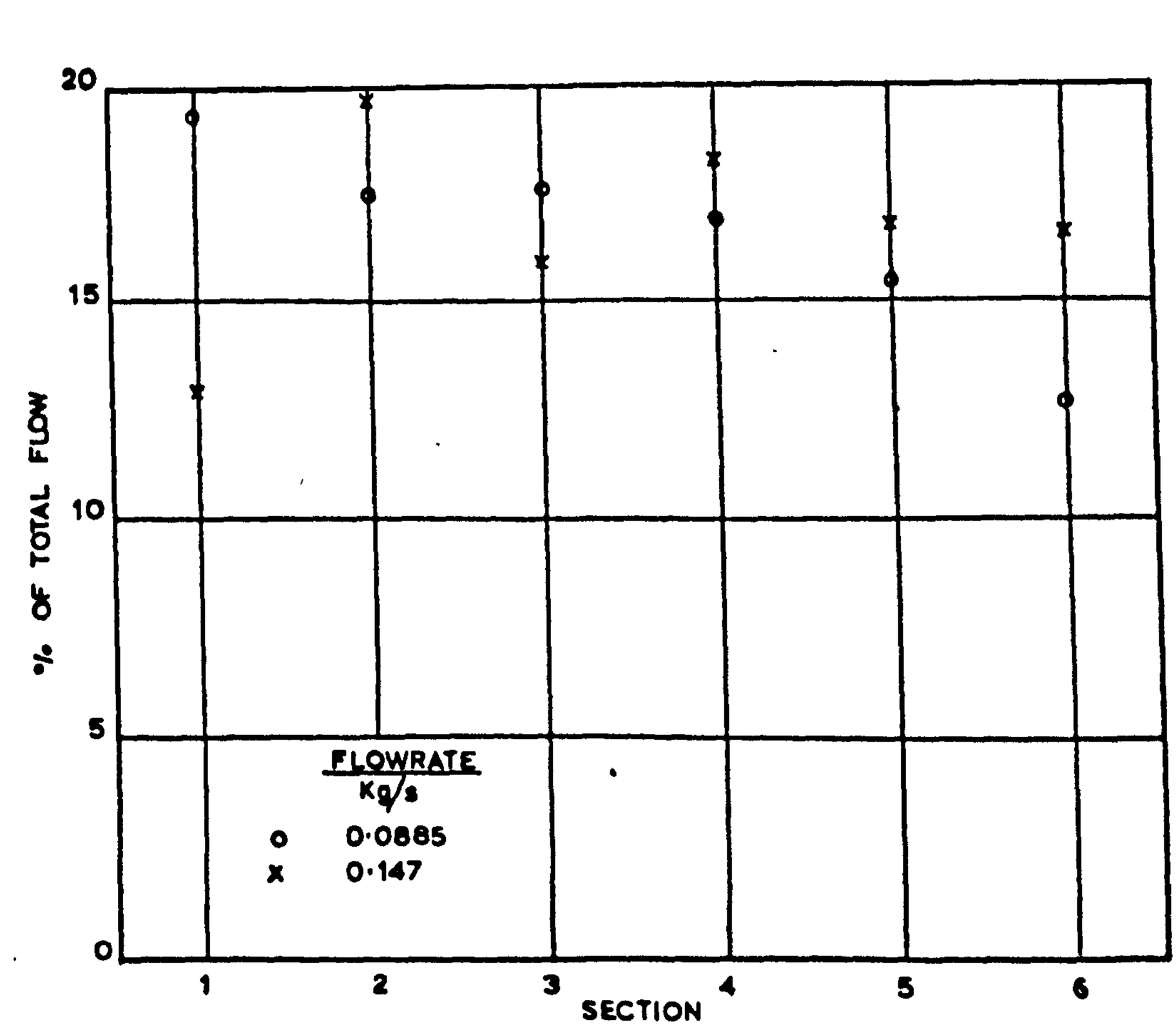

(b) TUBE FOR HIGH INUNDATION RATES

FIG 37 DISTRIBUTION OF INUNDATION FROM INUNDATION TUBES

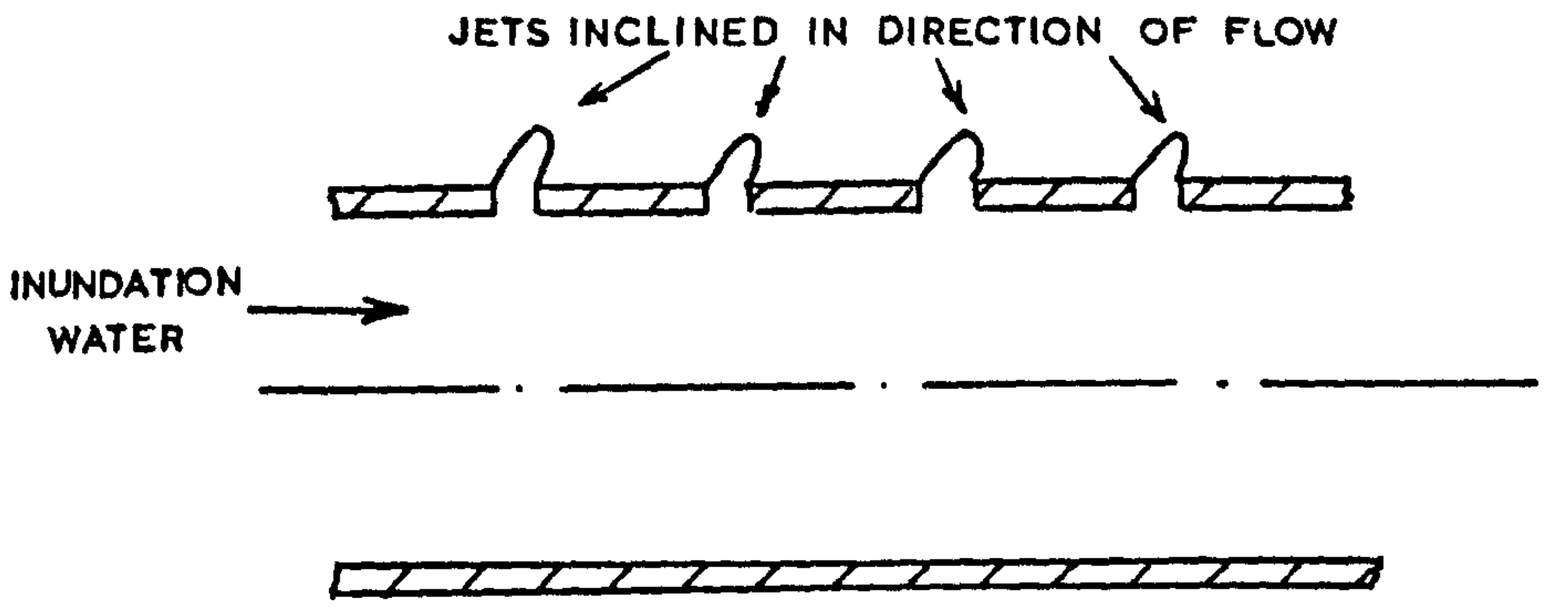

FIG. 38 WATER JET FROM INUNDATION TUBE

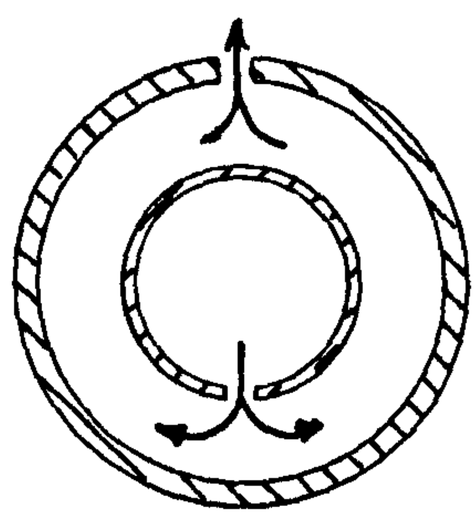

FIG. 39 INUNDATION TUBE WITH INNER TUBE

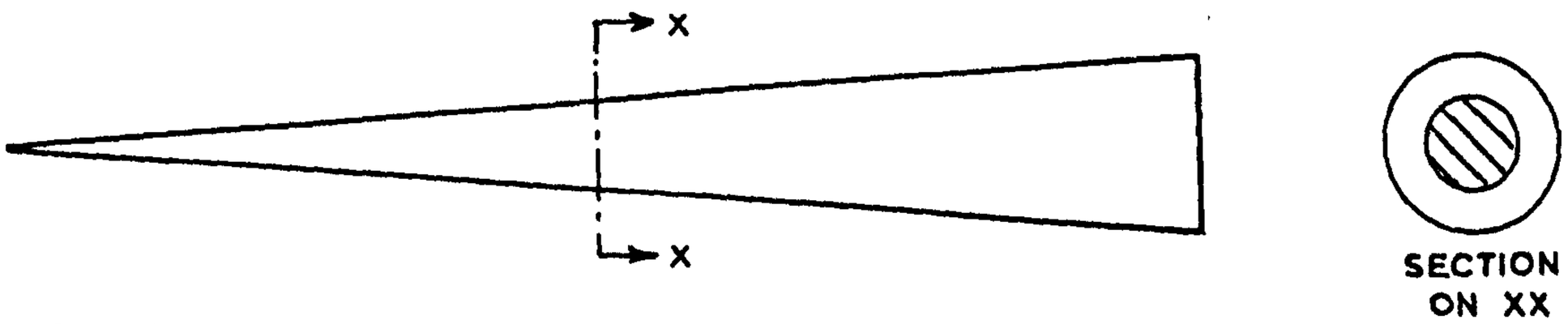

(a) Tapered cone

(b) Diagonally cut cylinder

FIG. 40 INUNDATION TUBE INSERTS

FIG. 41

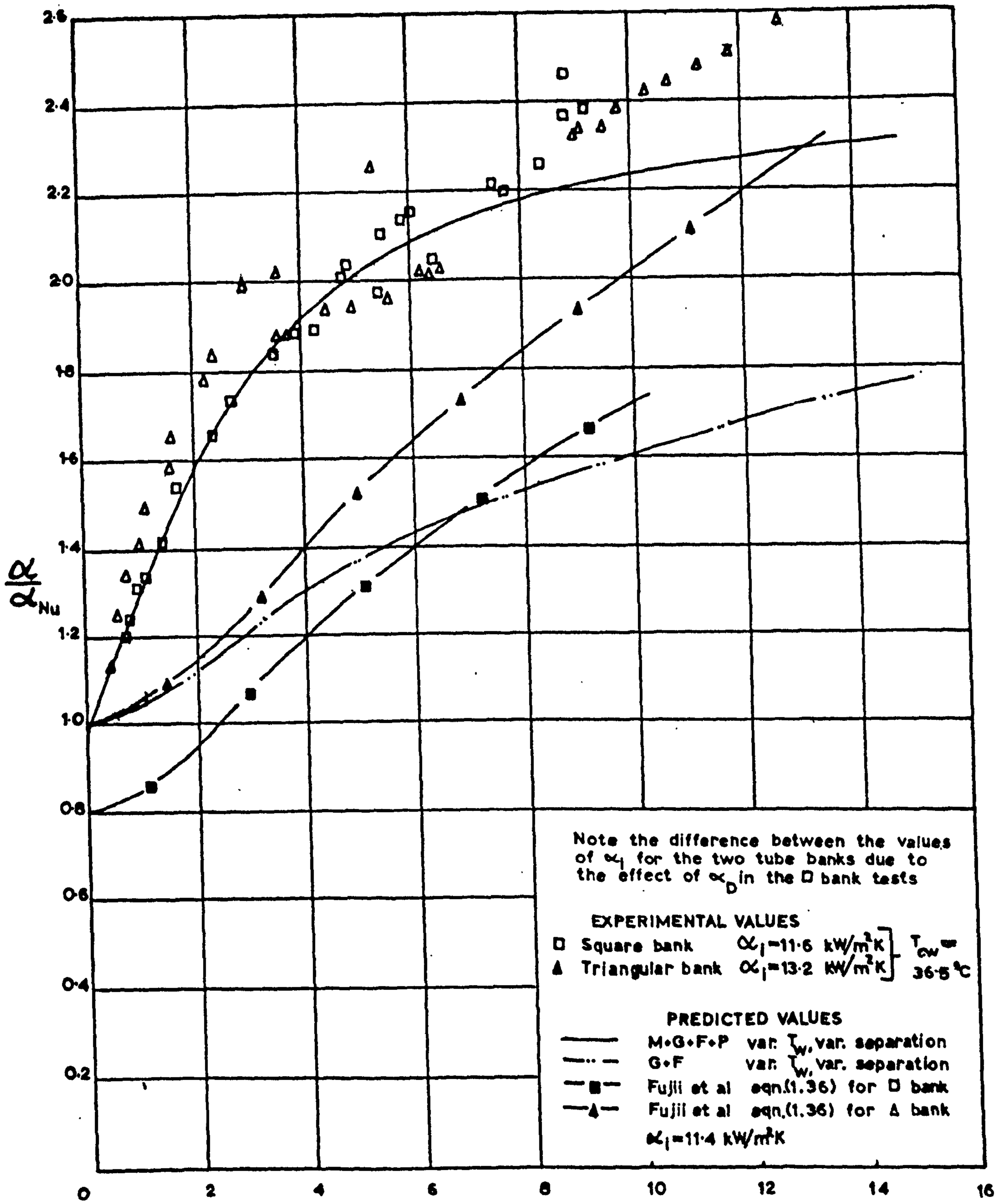

FIG. 41 COMPARISON OF EXPERIMENTAL DATA ON UNINUNDATED TUBE BANKS WITH PREDICTED SOLUTIONS (HIGH HEAT FLUX)

FIG. 42

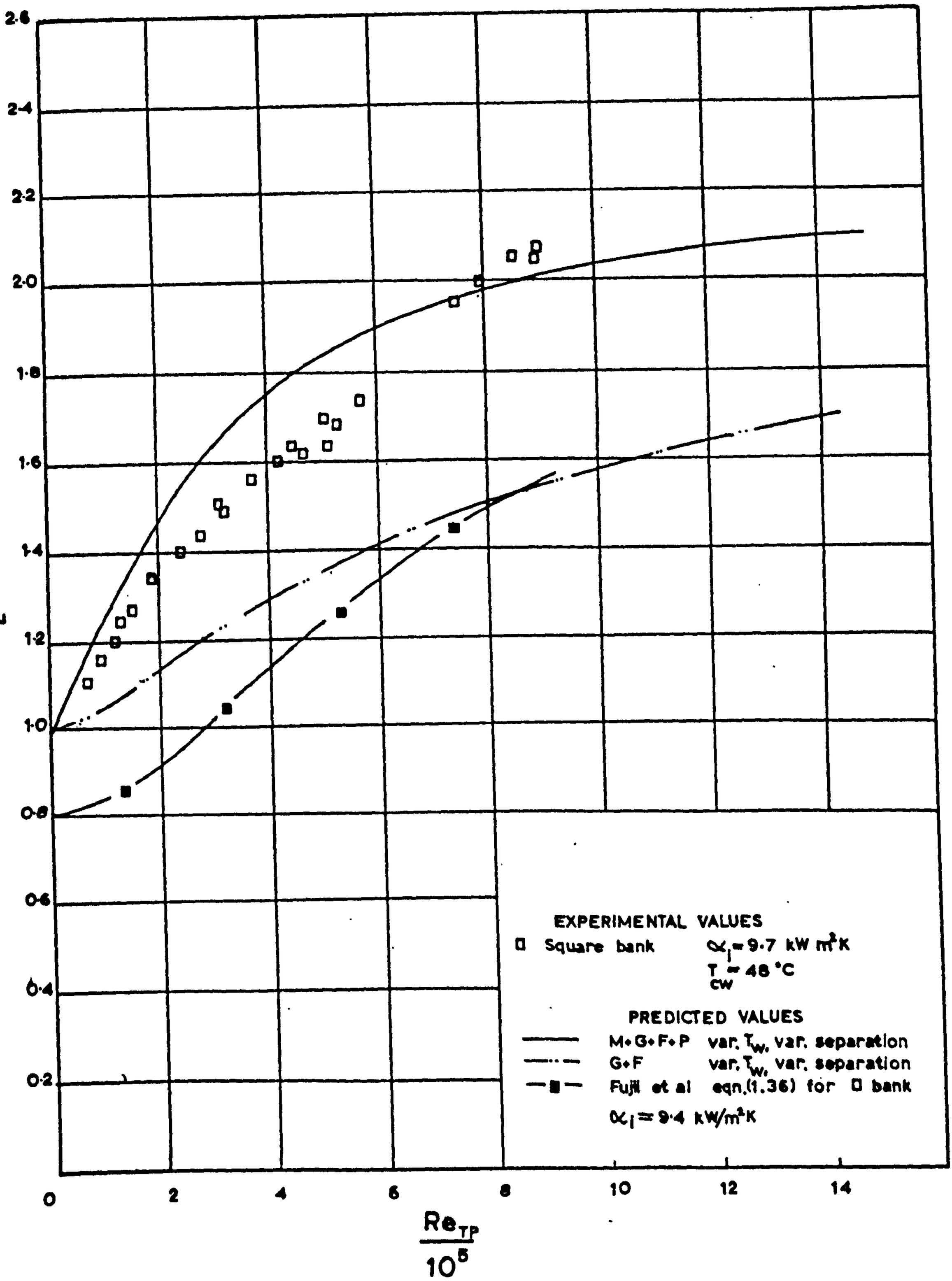

FIG. 42 COMPARISON OF EXPERIMENTAL DATA ON UNINUNDATED TUBE BANKS WITH PREDICTED SOLUTIONS (MEDIUM HEAT FLUX)

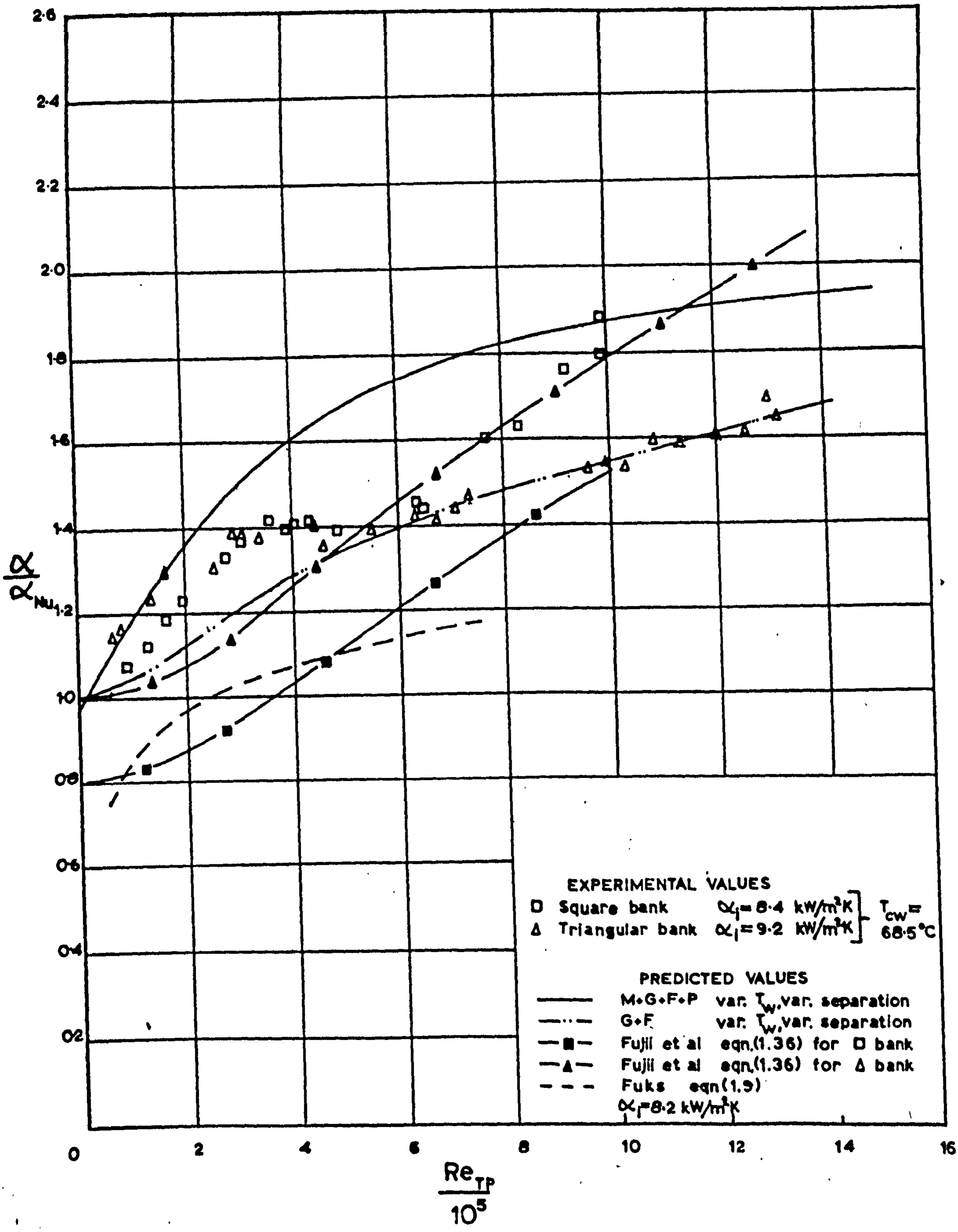

FIG. 43 COMPARISON OF EXPERIMENTAL DATA ON UNINUNDATED TUBE BANKS WITH PREDICTED SOLUTIONS (LOW HEAT FLUX)

FIG. 44

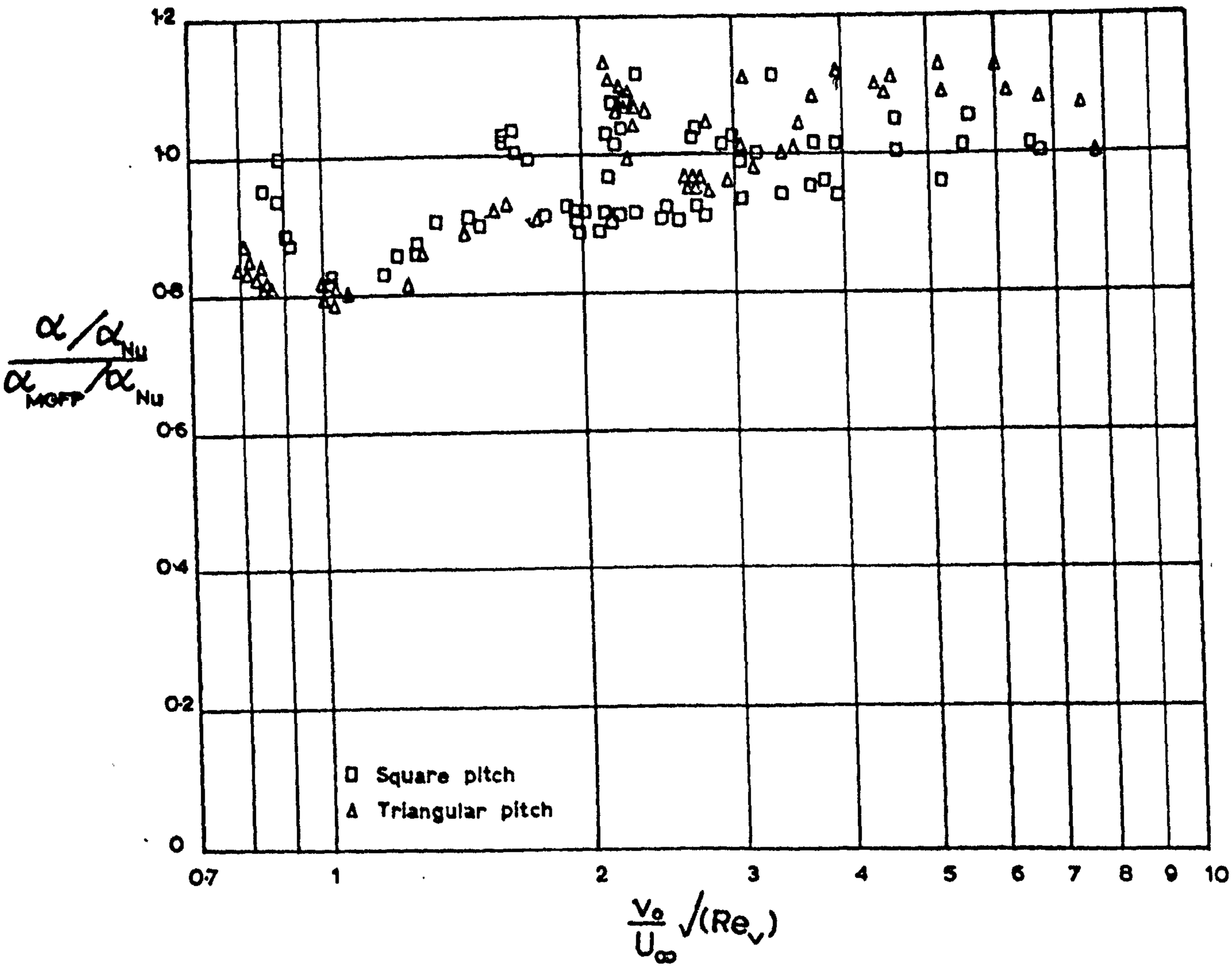

FIG. 44 PLOT OF RATIO OF EXPERIMENTAL H.T.C. TO THAT PREDICTED BY THE M·G·F·P THEORY AGAINST THE SUCTION PARAMETER FOR UNINUNDATED TUBE BANKS

FIG. 45

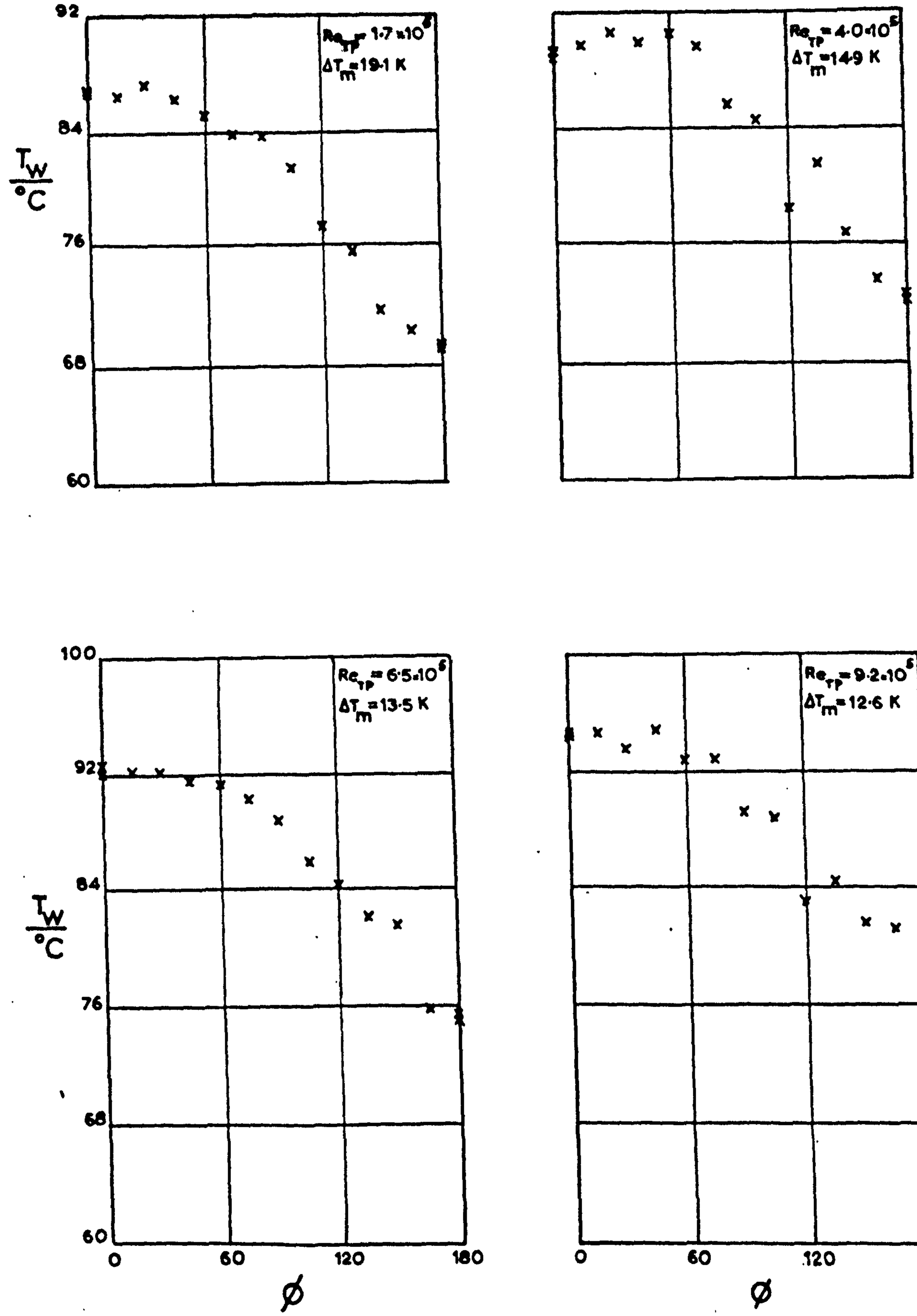

FIG. 45 TEMPERATURE PROFILE ON AN UNINUNDATED TUBE IN A SQUARE PITCH TUBE BANK α_i=10·7 kW/m^{2}K

T_{CW} = 41 °C

FIG. 46

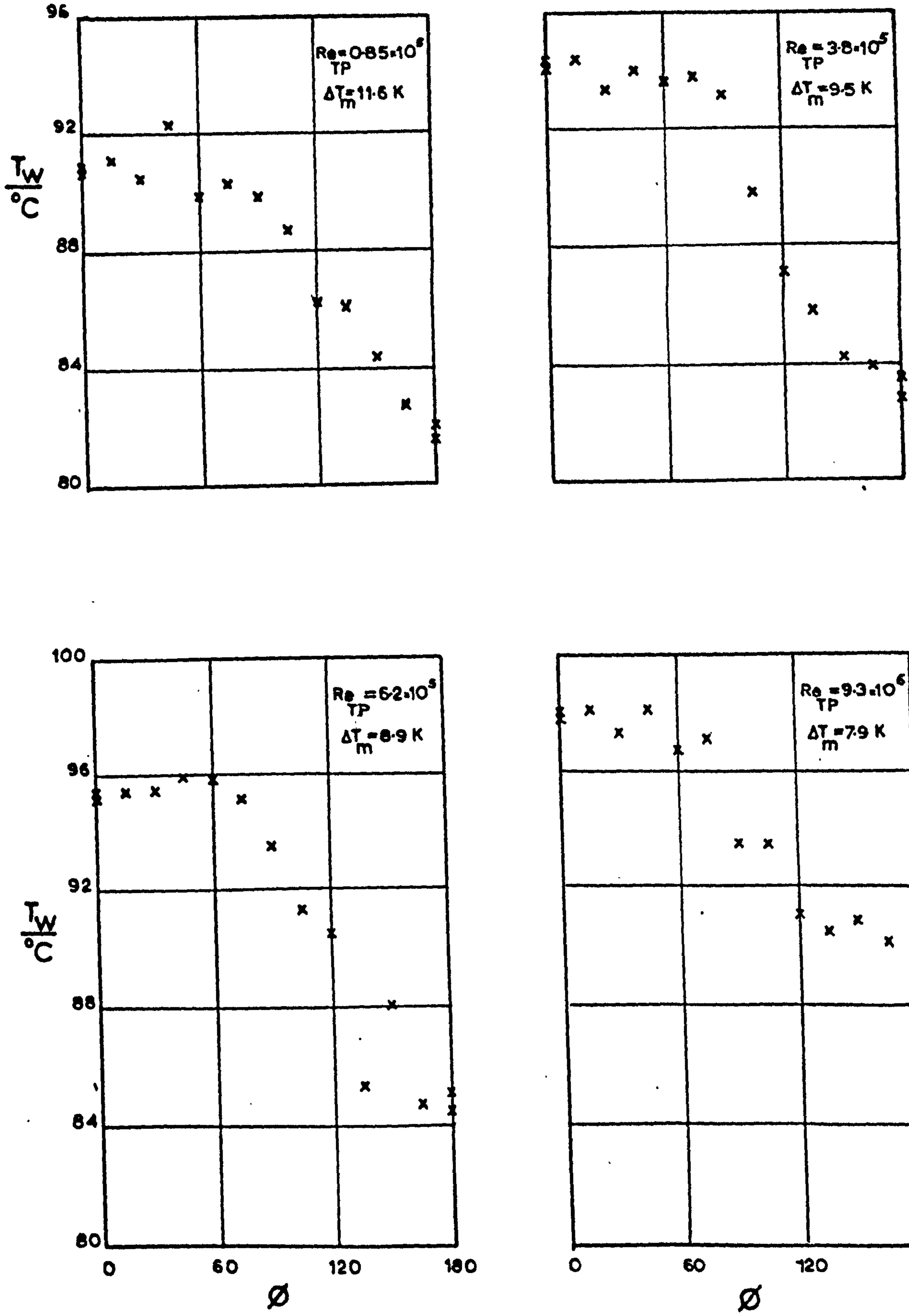

FIG. 46 TEMPERATURE PROFILE ON AN UNINUNDATED TUBE IN A SQUARE PITCH TUBE BANK $\alpha_i = 8.6$ kW/m²K

$T_{cw} = 60$ °C

FIG. 47

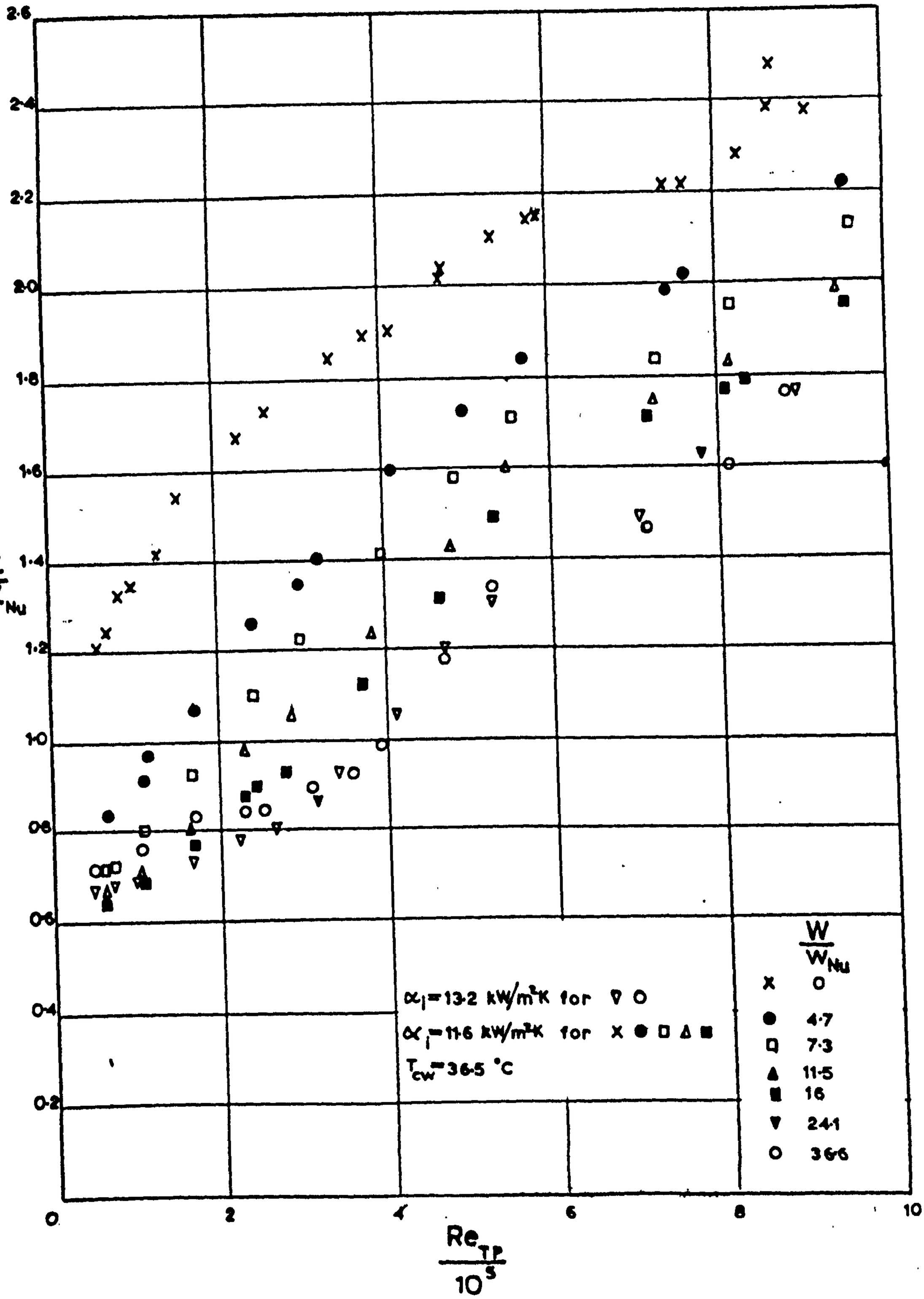

FIG. 47 INUNDATION TESTS ON SQUARE PITCH TUBE BANK (HIGH HEAT FLUX)

FIG. 48

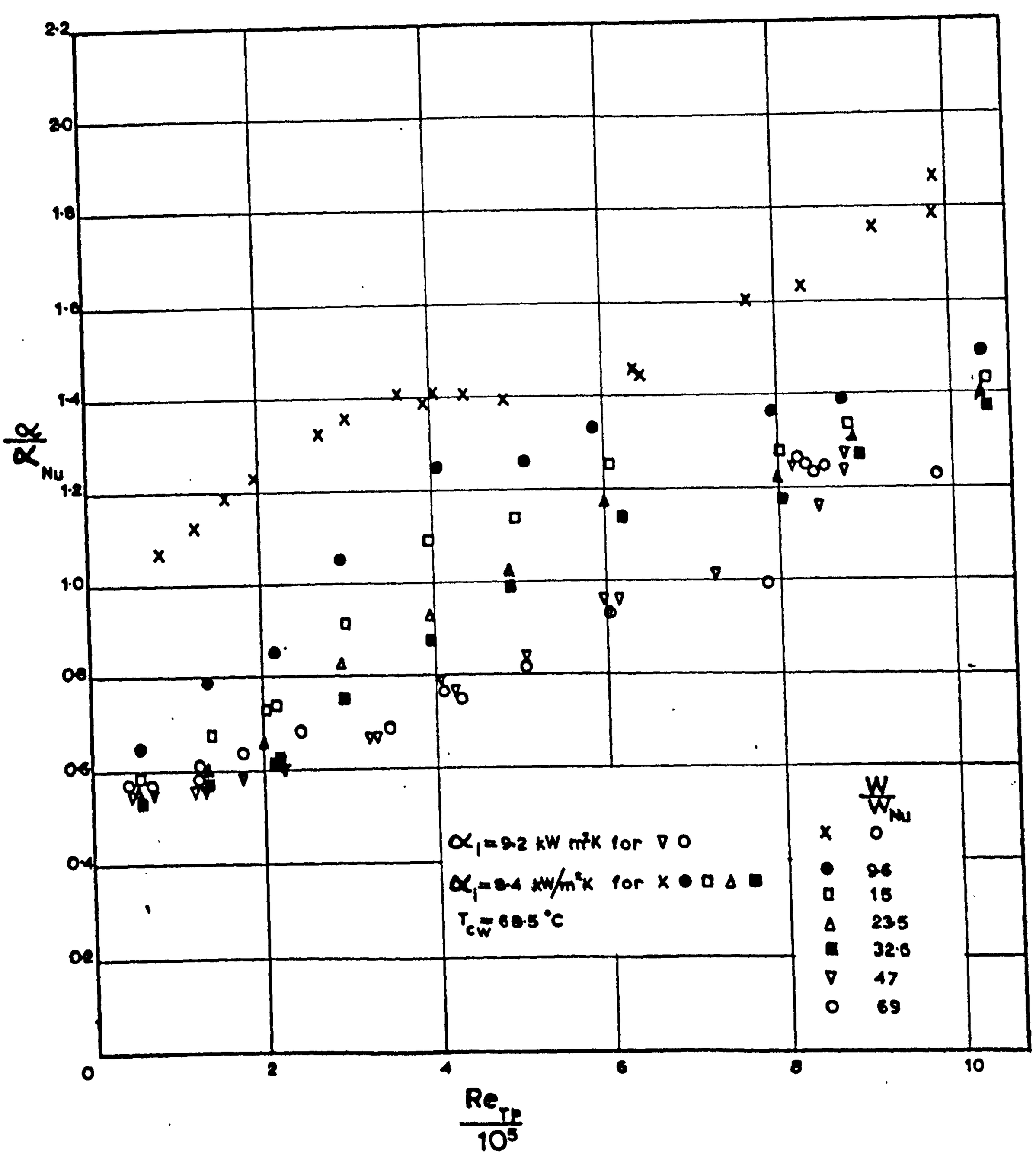

FIG. 48 INUNDATION TESTS ON SQUARE PITCH TUBE BANK (LOW HEAT FLUX)

FIG. 49

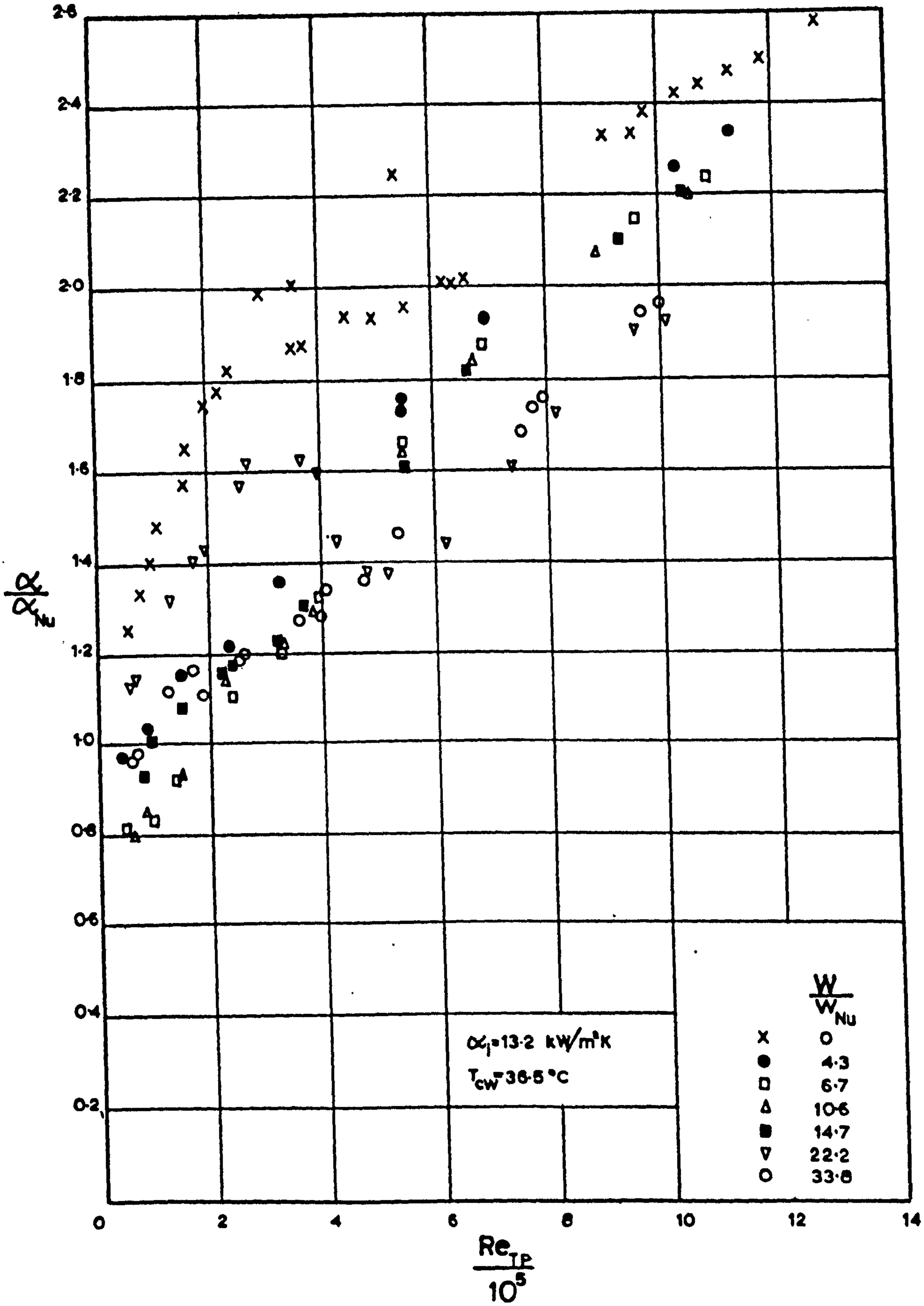

FIG. 49 INUNDATION TESTS ON TRIANGULAR PITCH TUBE BANK (HIGH HEAT FLUX)

FIG. 50

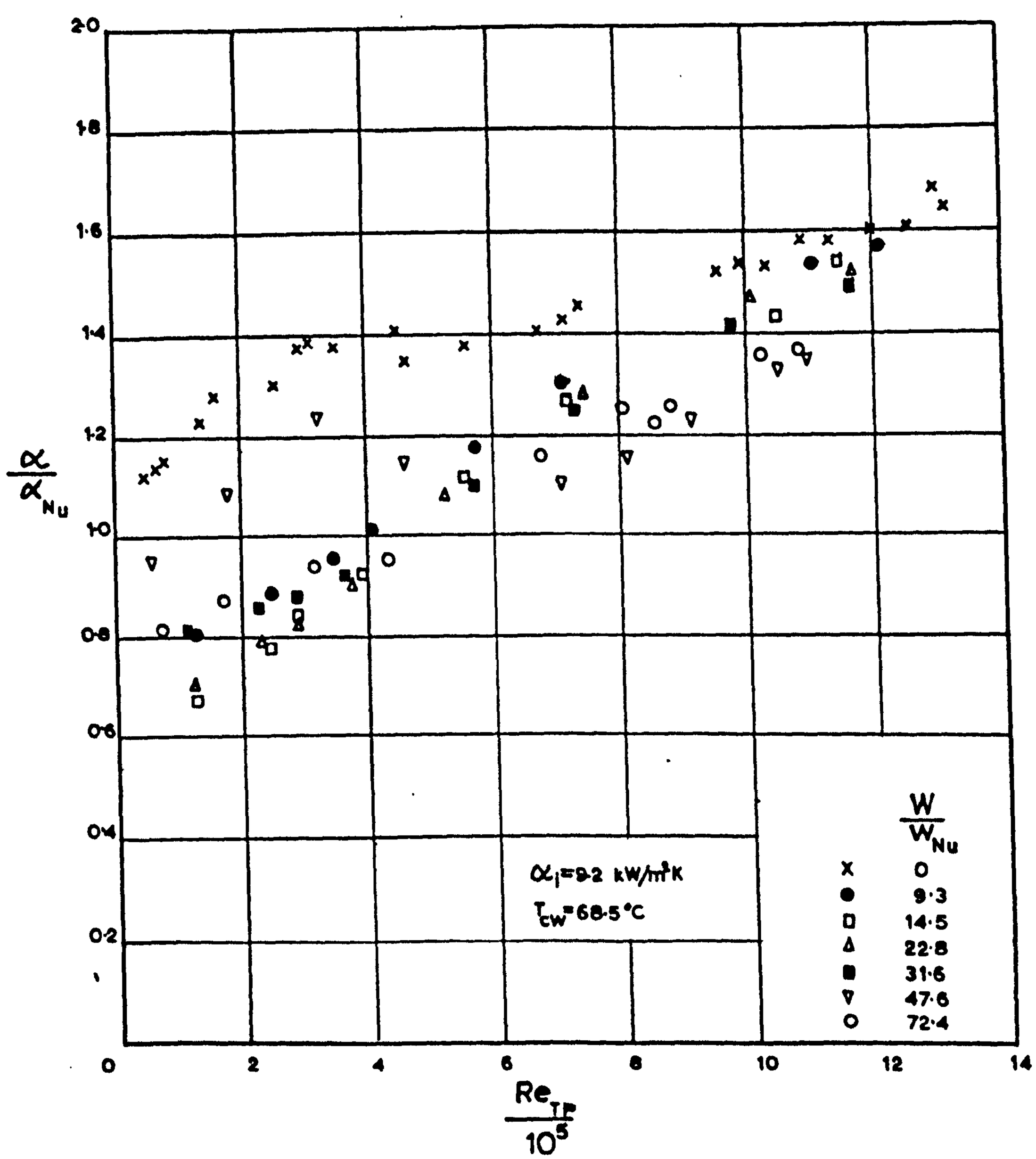

FIG. 50 INUNDATION TESTS ON TRIANGULAR PITCH TUBE BANK (LOW HEAT FLUX)

FIG. 51

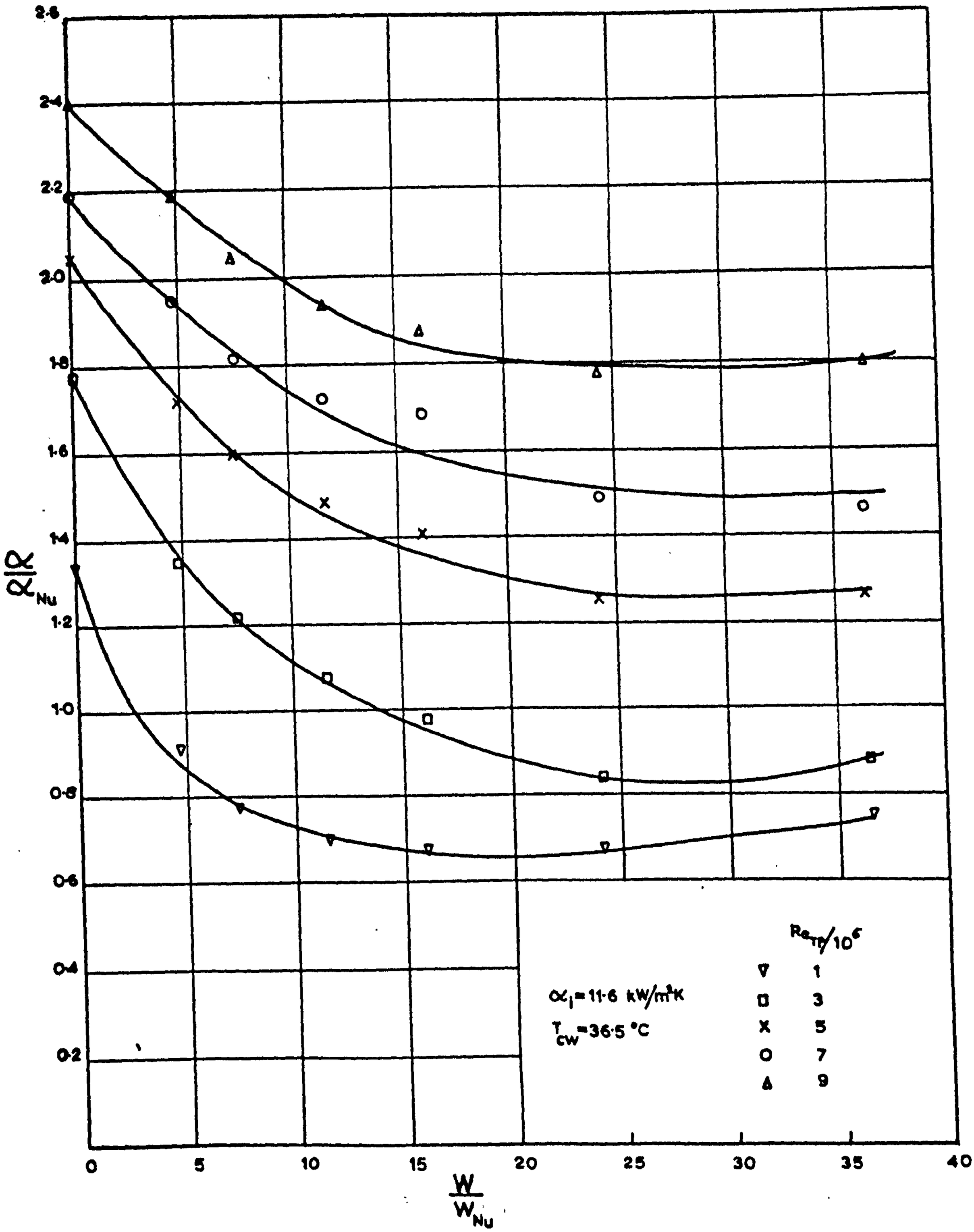

FIG 51 VARIATION OF DIMENSIONLESS H.T.C. WITH DIMENSIONLESS INUNDATION RATE FOR SQUARE PITCH TUBE BANK (HIGH HEAT FLUX)

FIG. 52

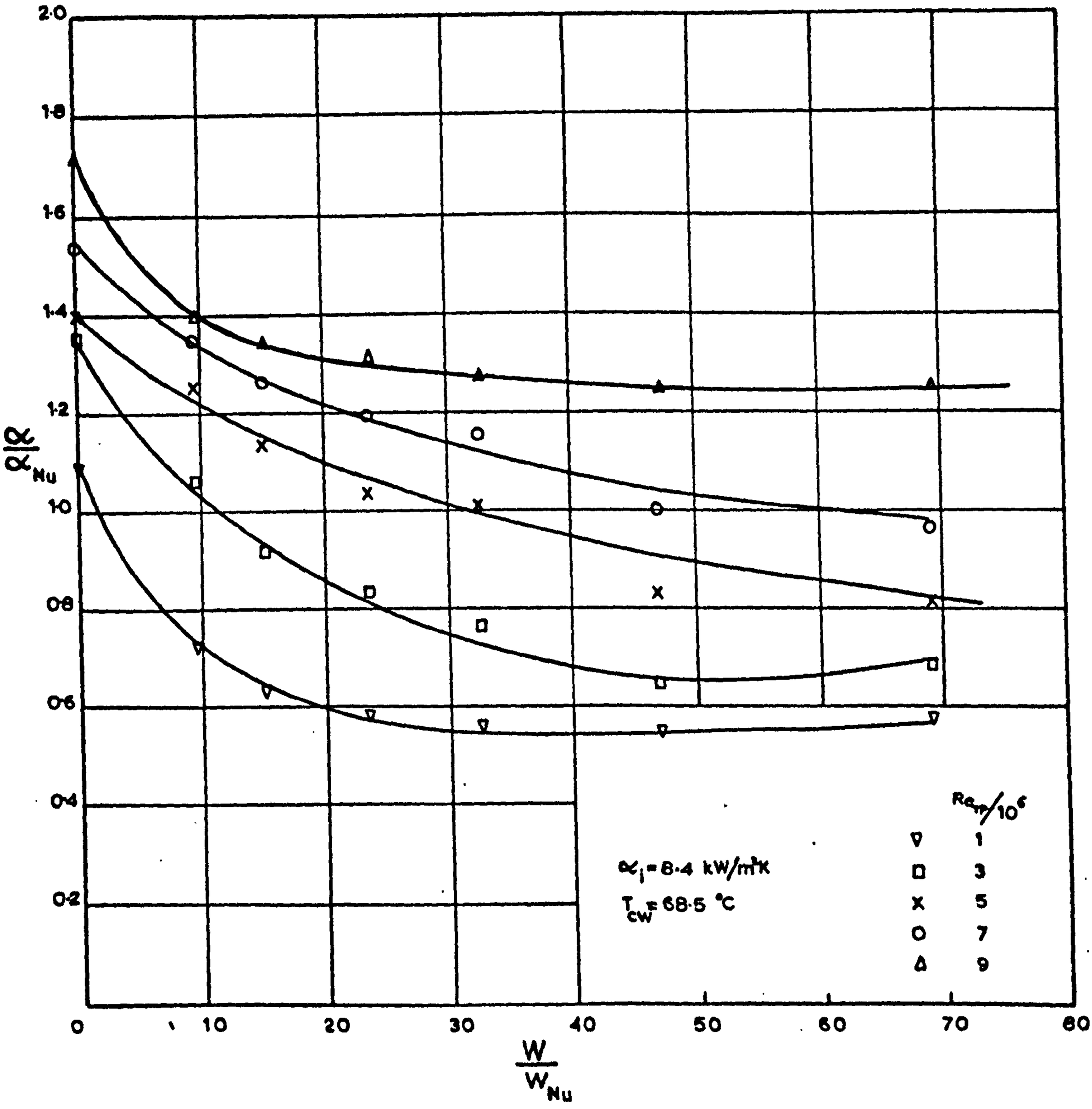

FIG. 52 VARIATION OF DIMENSIONLESS H.T.C. WITH DIMENSIONLESS INUNDATION RATE FOR SQUARE PITCH TUBE BANK (LOW HEAT FLUX)

FIG. 53

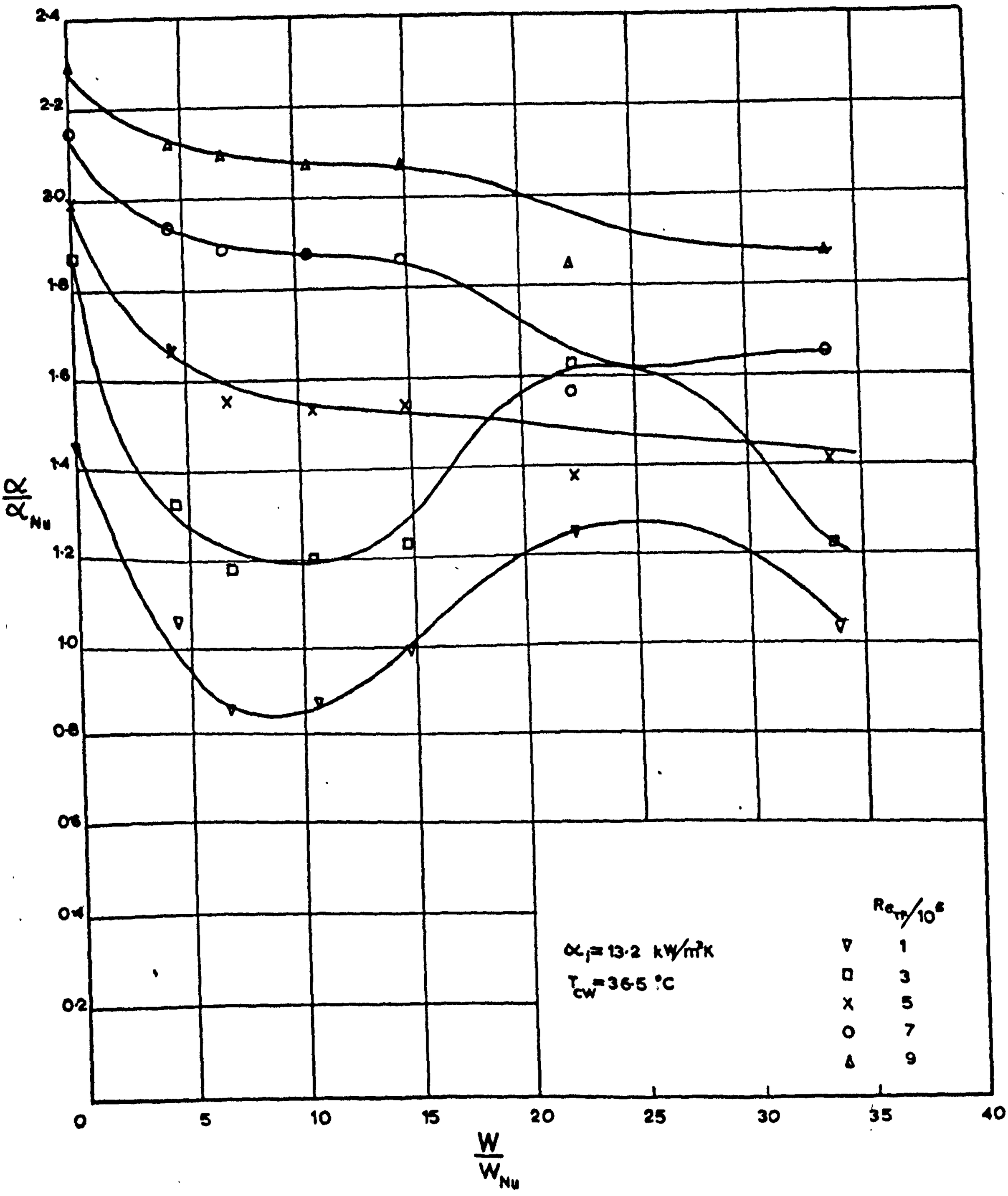

FIG. 53 VARIATION OF DIMENSIONLESS H.T.C. WITH DIMENSIONLESS INUNDATION RATE FOR TRIANGULAR PITCH TUBE BANK (HIGH HEAT FLUX)

FIG. 54

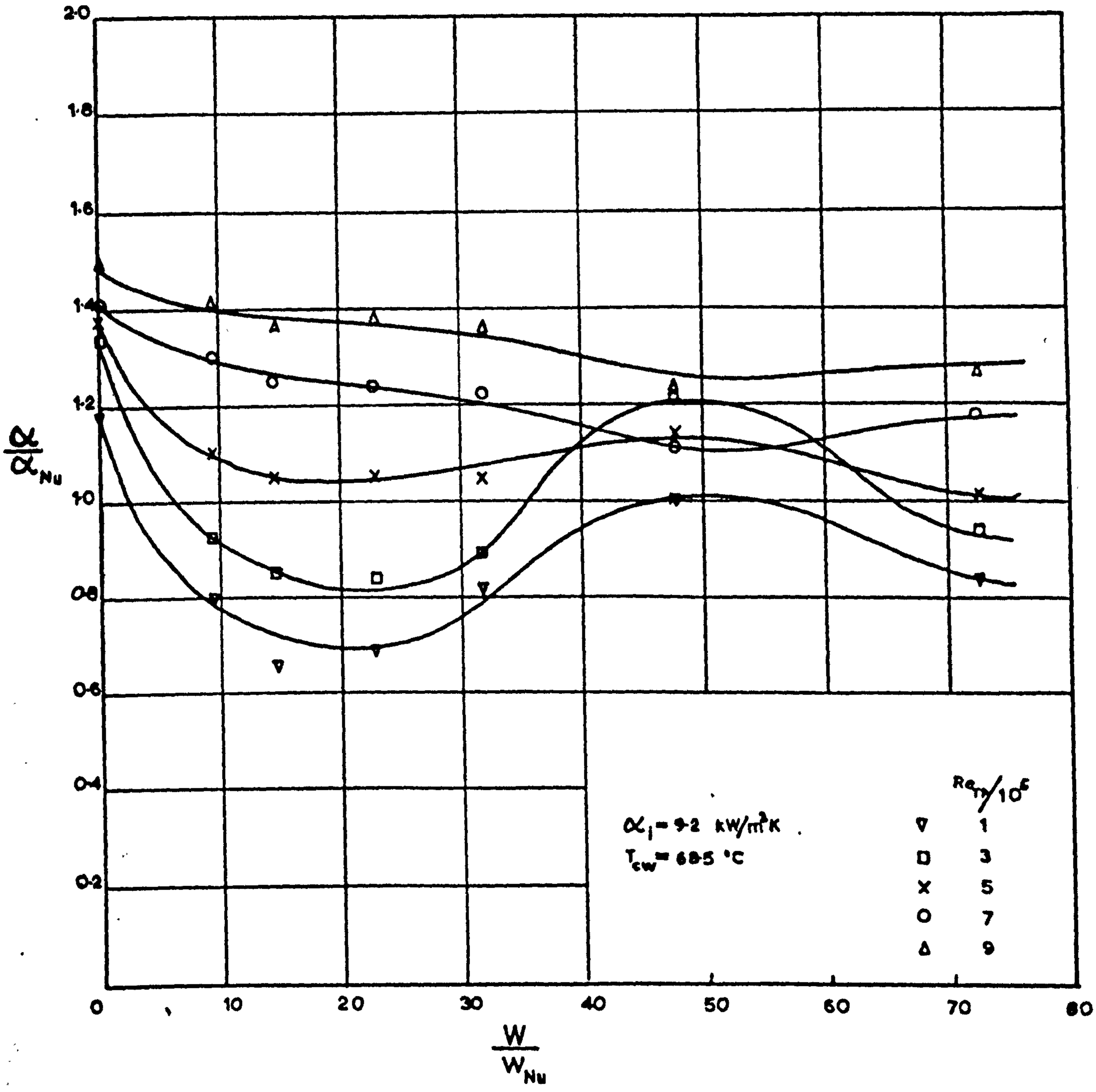

FIG. 54 VARIATION OF DIMENSIONLESS H.T.C. WITH DIMENSIONLESS INUNDATION RATE FOR TRIANGULAR PITCH TUBE BANK (LOW HEAT FLUX)

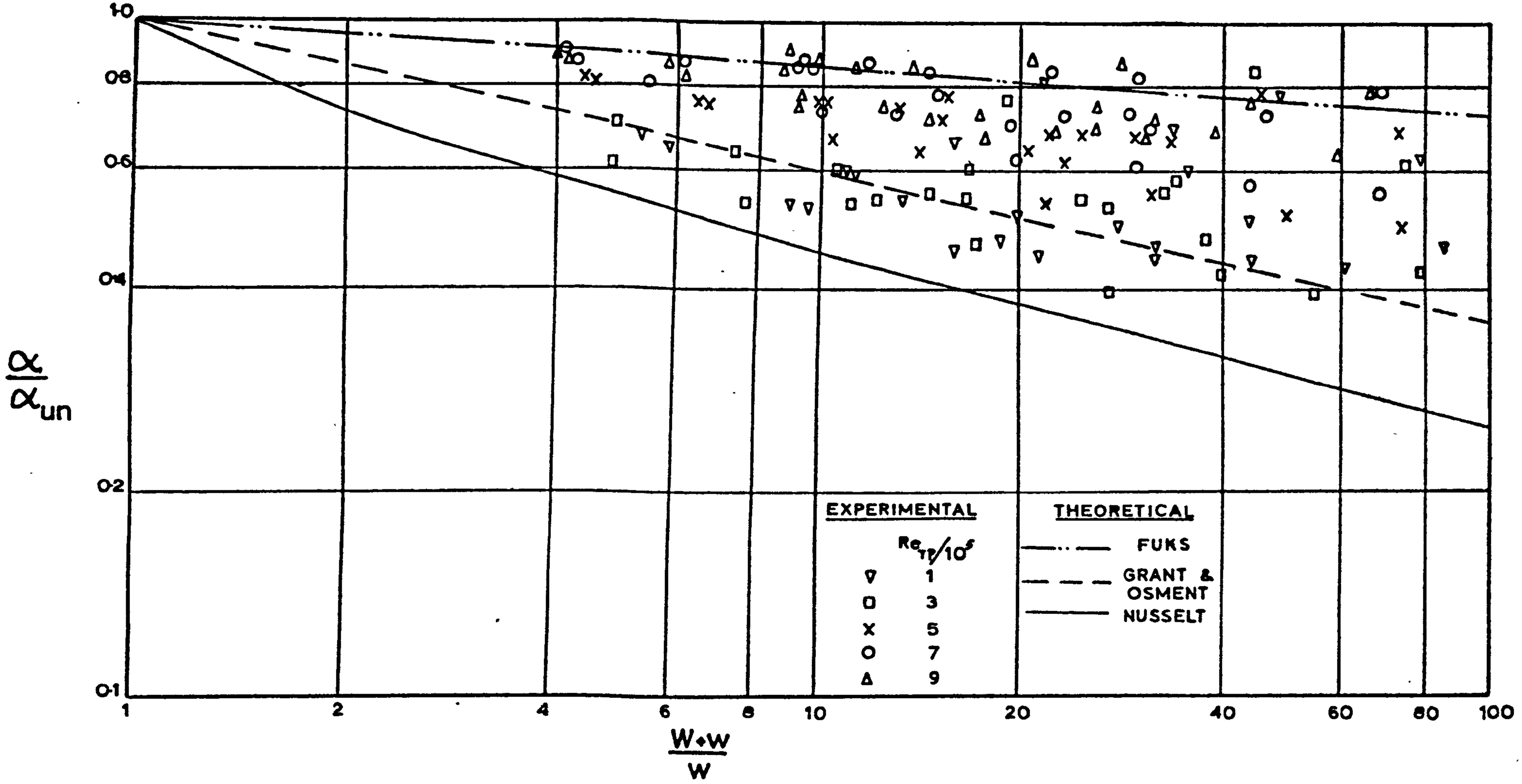

FIG. 55 COMPARISON OF EXPERIMENTAL H.T.C. FOR INUNDATED TUBE WITH THAT FOR UNINUNDATED TUBE AS A FUNCTION OF DIMENSIONLESS INUNDATION RATE

FIG. 55

FIG. 56

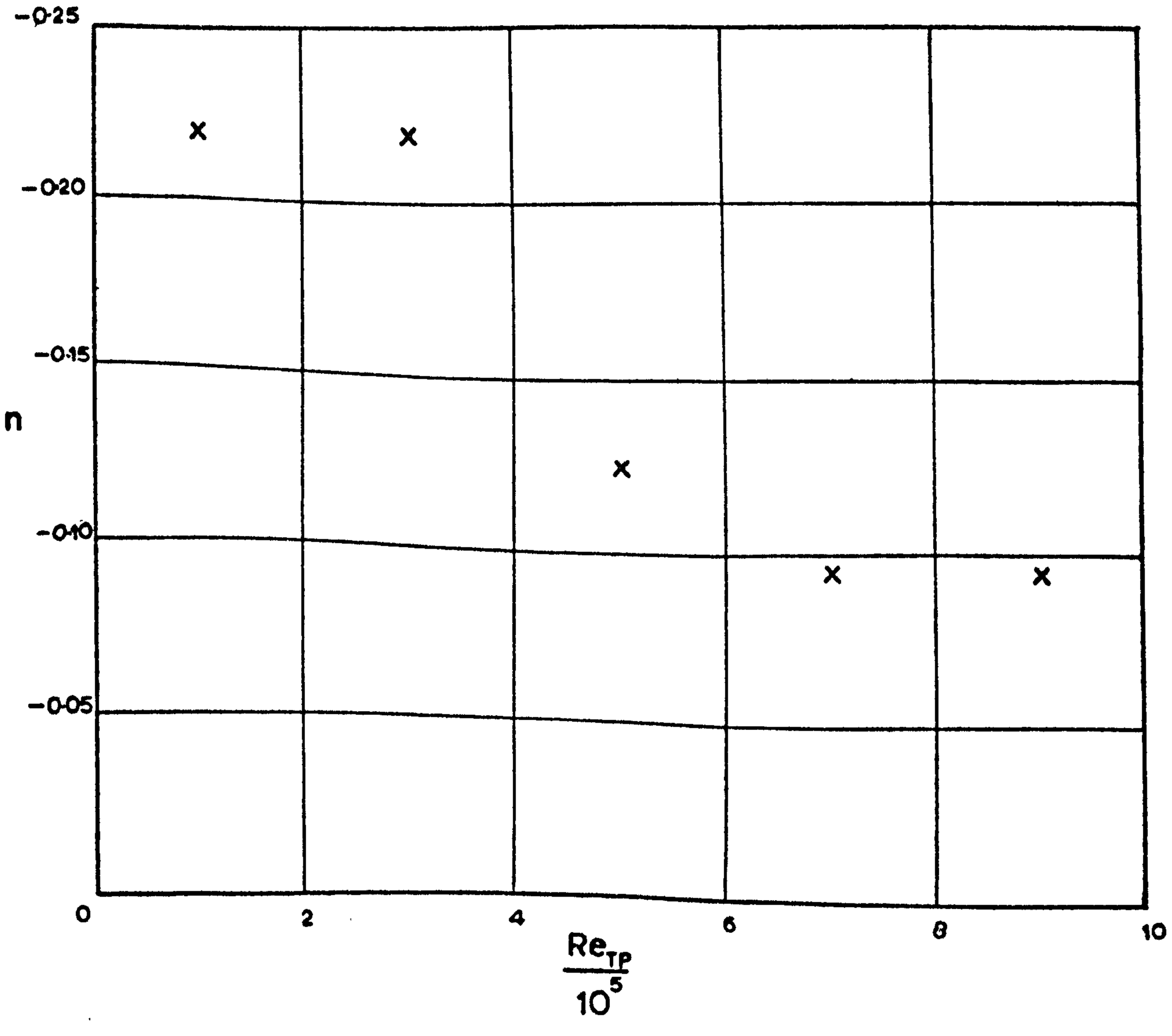

FIG. 56 VARIATION OF EXPONENT n WITH TWO-PHASE REYNOLDS NUMBER